

**Molecular models for drug permeation
across phospholipid membranes**

Inaugural-Dissertation
zur Erlangung des Doktorgrades
der Mathematisch-Naturwissenschaftlichen Fakultät
der Heinrich-Heine-Universität Düsseldorf

vorgelegt von
Céline Anézo
aus Guérande

Düsseldorf 2003

Gedruckt mit der Genehmigung der Mathematisch-Naturwissenschaftlichen Fakultät der Heinrich-Heine-Universität Düsseldorf

Referent:	Prof. Dr. H.-D. Höltje
1. Korreferentin:	Prof. Dr. C. Marian
2. Korreferent:	Prof. Dr. M. Wiese
Tag der mündlichen Prüfung:	25.07.2003

Diese Arbeit ist als elektronische Dissertation veröffentlicht.
URL: <http://www.ulb.uni-duesseldorf.de/diss/mathnat/2003/anezo.html>

Die vorliegende Arbeit wurde von August 1999 bis Juni 2003 am Institut für Pharmazeutische Chemie der Heinrich-Heine-Universität Düsseldorf unter Anleitung von Herrn Prof. Dr. H.-D. Höltje angefertigt.

Mein besonderer Dank gilt Herrn Prof. Dr. H.-D. Höltje für die Überlassung des interessanten Themas, die idealen Arbeitsbedingungen und die stetige Unterstützung.

Frau Prof. Dr. C. Marian und Herrn Prof. Dr. M. Wiese danke ich herzlich für die Anfertigung der Gutachten.

Bei meinen Kooperationspartnern, Herrn Dr. D. P. Tieleman, Universität Calgary, und Herrn Dr. S.-J. Marrink und Herrn Dr. A. H. de Vries, Universität Groningen, möchte ich mich für die konstruktive und freundschaftliche Zusammenarbeit bedanken. Ohne die Rechenkapazitäten dieser beiden Universitäten wäre die vorliegende Arbeit nicht möglich gewesen.

Ein ganz besonderes Dankeschön geht an allen Kolleginnen und Kollegen des Arbeitskreises für das angenehme Arbeitsklima und die ständige Hilfsbereitschaft.

Contents

1	Introduction	9
1.1	Biomembranes	9
1.1.1	Organization, structure, and functions	9
1.1.1.1	Organization	9
1.1.1.2	Structure	10
1.1.1.3	Functions	11
1.1.2	Composition	12
1.1.2.1	Membrane lipids	13
1.1.2.2	Membrane proteins	21
1.1.3	Asymmetry	22
1.1.4	Roles of lipids	23
1.1.5	Membrane models	24
1.1.6	Model membranes	26
1.2	Phospholipid properties relevant to biomembranes	28
1.2.1	The hydrophobic effect	28
1.2.2	Phase structures	29
1.2.2.1	Crystalline phases	29
1.2.2.2	Gel phases	29
1.2.2.3	Fluid phases	30
1.2.3	Phase transitions	33
1.2.4	Motional properties and membrane fluidity	36
1.2.4.1	Motional order	36
1.2.4.2	Motional rates	37
1.2.4.3	Membrane fluidity	39
1.3	Biomembrane transport	40
1.3.1	Transport pathways and mechanisms	40
1.3.2	Drug transport	45
1.3.2.1	Drug absorption	45

1.3.2.2	Physicochemical determinants in drug absorption	46
1.3.2.3	Membrane permeability	48
2	Scope of the thesis	51
3	Molecular dynamics simulations of lipid bilayers	53
3.1	Computer simulations of lipid bilayers	53
3.1.1	Mean field versus atomistic simulations	54
3.1.2	Monte Carlo simulations	55
3.1.3	Molecular dynamics simulations	56
3.1.4	Hybrid simulations	57
3.1.5	Coarse grain models	58
3.1.6	Applications of computer simulations	59
3.2	Molecular dynamics studies of lipid bilayers	60
3.2.1	Review	60
3.2.2	Strategic issues	61
3.2.2.1	Force fields	62
3.2.2.2	System size and boundary conditions	63
3.2.2.3	Macroscopic ensembles	64
3.2.2.4	Starting structures and equilibration procedures	68
3.2.2.5	Simulation time steps	69
3.2.2.6	Treatment of long-range interactions	70
3.2.3	Simulations and experiments	73
3.2.4	Limitations of the MD technique	74
4	A phospholipid bilayer model	77
4.1	Introduction	77
4.2	Method of simulation	78
4.2.1	Membrane system	78
4.2.2	Structural parameters	78
4.2.3	Setup of the bilayer membrane	81
4.2.4	Force field parameters and partial atomic charges	84
4.2.5	Macroscopic boundary conditions	87
4.2.6	Treatment of electrostatics	88
4.2.7	Simulation conditions	91
4.3	Results	92
4.3.1	Equilibration time and equilibrium structural parameters	92
4.3.2	Overall bilayer organization	96

4.3.3	Headgroup region	98
4.3.3.1	Interfacial atom distributions	98
4.3.3.2	Headgroup hydration and water ordering	101
4.3.3.3	Headgroup orientation	105
4.3.3.4	Hydrogen bonding	106
4.3.3.5	Headgroup-headgroup interactions	109
4.3.4	Hydrocarbon region	114
4.3.4.1	Atom distributions	114
4.3.4.2	<i>Trans-gauche</i> isomerization	116
4.3.4.3	Hydrocarbon chain order parameters	118
4.3.5	Electron density distribution	122
4.3.6	Membrane dipole potential	123
4.3.7	Lipid mobility and lateral diffusion	126
4.3.8	Summary	130
4.4	Discussion	131
4.5	Conclusion	136
5	Solute permeation across a phospholipid bilayer	137
5.1	Introduction	137
5.2	Theory	139
5.2.1	Permeation models	139
5.2.1.1	Homogeneous solubility-diffusion model	139
5.2.1.2	Inhomogeneous solubility-diffusion model	140
5.2.1.3	Defect model	142
5.2.2	Simulation of permeation processes	143
5.2.2.1	Equilibrium MD simulations	143
5.2.2.2	Non-equilibrium MD simulations	144
5.3	Review	150
5.4	Method of simulation	153
5.4.1	Choice of penetrants	153
5.4.2	Force field parameters and partial atomic charges	155
5.4.3	Equilibrium MD simulations	156
5.4.4	Umbrella sampling MD simulations	157
5.4.5	Constrained MD simulations	158
5.5	Results	158
5.5.1	Equilibrium MD simulations	158
5.5.1.1	Time course of solute position	158

5.5.1.2	Solute distribution	165
5.5.1.3	Hydrogen bonding	169
5.5.2	Umbrella sampling MD simulations	170
5.5.2.1	Free energy profiles	170
5.5.2.2	Hydrogen bonding	174
5.5.2.3	Water penetration	174
5.5.2.4	Solute orientation	174
5.5.3	Constrained MD simulations	180
5.6	Discussion	182
5.7	Conclusion	183
6	Summary	185
	Bibliography	187
A	List of abbreviations	199
B	Methodological issues in lipid bilayer simulations	201
B.1	Introduction	201
B.2	Method of simulation	204
B.2.1	Simulated systems	204
B.2.2	Force field	204
B.2.3	Electrostatics	204
B.2.4	Macroscopic boundary conditions and pressure coupling	206
B.2.5	Simulation conditions	206
B.3	Results	208
B.3.1	Equilibration and fluctuations of structural properties	208
B.3.2	Area per lipid	211
B.3.3	Area compressibility	214
B.3.4	Hydrocarbon chain order parameters	214
B.3.5	Dipole potential and dipole moments	215
B.3.6	Radial distribution functions	217
B.3.7	Diffusion coefficients	218
B.4	Discussion	219
B.5	Conclusion	223

Chapter 1

Introduction

In 1884, Thudichum already stated: “Phospholipids are the centre, life, and chemical soul of all bioplasm whatsoever, that of plants as well as animals” [1]. If the fluid lipid bilayer, representing the core of the membrane, is now well established as the fundamental structure of most biomembranes, it took however a long time to really appreciate the role of lipids in membrane structure and function and to realize the importance of solute-lipid interactions in membranes for cell functioning.

This introductory chapter presents first the main features of biomembranes, underlines then properties of phospholipids relevant to biomembranes, and focuses finally on transport processes across biomembranes and, more precisely, on drug absorption.

1.1 Biomembranes

1.1.1 Organization, structure, and functions

1.1.1.1 Organization

Each biological cell is enclosed by its outer plasma membrane which provides a barrier between intracellular and extracellular domains and controls interactions between the cell and its surroundings. This description applies both to the relatively small prokaryotic cells, which have no cell nucleus, and to the much larger eukaryotic cells, which do have such a nucleus. Bacteria have prokaryotic cells, while animals, plants, as well as single-celled microorganisms such as yeasts have eukaryotic cells.

Prokaryotic cells Prokaryotes exhibit the most simple organization of cell membranes, containing no nucleus and no organelles. The plasma membrane determines the boundary of the cytoplasm and forms a semipermeable barrier between the intracellular and extracellular environments. Some prokaryotes possess an extracellular matrix. The plasma membrane is then surrounded by a cell wall, which is not a membrane and represents a relatively rigid structure held together essentially by covalent forces. Outside the cell wall of bacteria is the outer membrane of the cell. Its structure is not as rigid as that of the cell wall, but its composition differs from that of the plasma membrane.

Eukaryotic cells The organization of nucleated cells is more complex. In addition to the plasma membrane, eukaryotic cells contain an impressive array of cytoplasmic organelles, each surrounded by its own membrane. These intracellular compartments ensure various cellular activities and allow more diverse and specialized functions than are possible in prokaryotic cells. To the internal organelles belongs the nucleus, the endoplasmic reticulum (ER), Golgi complexes, mitochondria, lysosomes, and chloroplasts. Their functional specialization arises from distinctive characteristics of their membranes: each of these organelle membranes exhibits a unique lipid and protein composition, which is directly related to a typical function. In the case of plant cells, the plasma membrane may in addition be surrounded by a cell wall.

1.1.1.2 Structure

On the molecular level, biological membranes are quite complex: they are composed of specific mixtures of lipids and proteins, which account for their diverse functions. Despite their complex composition, all biomembranes exhibit a universal construction principle. They essentially consist of a two-dimensional matrix made up of a lipid bilayer, interrupted and coated by proteins. The hydrocarbon chains of the lipids confer a hydrophobic character on the membrane interior, whereas the polar headgroups found in the interfacial region have hydrophilic properties. This structural pattern results directly from the so-called *hydrophobic effect* (see Section 1.2.1, page 28, for more details), whereby the apolar lipid chains and the hydrophobic side-chains of amino acid residues in proteins tend to minimize contacts with the aqueous phase. Figure 1.1 provides a simplified but informative picture of membrane structure.

The components of the bilayer matrix are held together largely by non-covalent forces. Thus, biomembranes are not rigid structures, but are rather deformable. The hydrophobic effect accounts for most of the interaction energy that stabilizes the bilayer organization. Hydrogen bonding and electrostatic interactions, however, contribute significantly to the consolidation of this assembly in the interfacial region, while dispersive forces between the lipid hydrocarbon chains stabilize the core of the membrane.

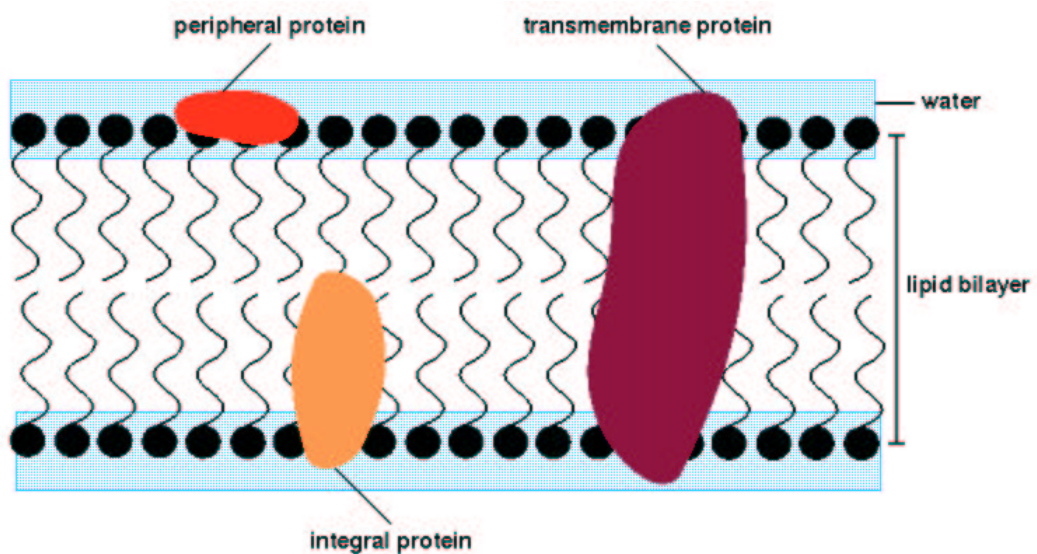


Figure 1.1: Schematic representation of a typical biomembrane.

1.1.1.3 Functions

Even though each membrane exhibits functions unique to that membrane, general functions, common to all membranes, can be distinguished.

The first basic function of biomembranes is to provide different spatial compartments in living organisms. Compartmentalization, *i.e.* the physical separation of one compartment from another, supplies morphological identity to the cell and its organelles.

Biomembranes act as selective barriers for the exchange of molecules between the different compartments, and ultimately, protect the internal microenvironments from the variability and fluctuations of their surroundings. They sustain concentration gradients of chemical species from one side to the other and the cell makes use of the membrane to create, maintain, or utilize the energy stored in these concentration gradients.

The bilayer matrix provides a two-dimensional network in which various functional molecules such as enzymes are specifically distributed and oriented. Lipids act not only as solvent but also as anchors, activators, and conformational stabilizers for proteins which carry out specific catalytic and translocation functions.

Another important aspect is the transduction of molecular information across and along membranes. For instance, receptors located on the cell surface receive extracellular signals that are conveyed to the cell interior which alters its behavior in response.

The plasma membrane defines the cell boundary and delineates intracellular from extracellular domains. This outer membrane plays an important regulatory role in the metabolism of the cell, controlling the entrance and exit of solutes. Due to these protective functions, the plasma membrane constitutes a fundamental ingredient for life: cell components could not probably survive without the enclosure by a membrane. The plasma membrane together with the cytoskeleton is responsible for the unique combination of flexibility and mechanical stability of cells. In the plasma membrane are also embedded various proteins which fulfill a great number of vital functions such as energy-driven transport of ions and metabolites, receptor-mediated events, synthesis of membrane components, secretion, ATP synthesis... Another function of the plasma membrane is to control cell-cell interactions. During their development, cells differentiate and organize into tissues. In this process, cells have to recognize the right matrix and aggregate together according to the pattern dictated by their genome. Cell-cell and cell-matrix recognition processes are mediated by the plasma membrane through receptors [2].

The intracellular membranes found in eukaryotic cells not only enclose the different organelles but are also involved in a series of cellular processes such as biosynthesis, transport, recycling, energy metabolism, and degradation.

1.1.2 Composition

The major components of membranes are lipids and proteins. Depending on the type of membrane, their relative amounts vary significantly, ranging from about 20% protein (dry weight) in myelin to 80% protein in mitochondria.

1.1.2.1 Membrane lipids

The most striking feature of membrane lipids is their very large diversity. Considering the possible number of structural and conformational lipid isomers, a hundred of components is involved in eukaryotic cells. In spite of this diversity, only a few classes of lipids predominate in membranes of a given type of organisms. In this section, the main classes of lipids are described with regard to their molecular characteristics.

Glycerophospholipids The glycerophospholipids are the predominant phospholipids found in biological membranes. They are derivatives of glycerol phosphate and contain an asymmetric carbon atom. Two glycerol hydroxyls are linked to hydrophobic hydrocarbon chains. A stereospecific numbering (*sn*) of the glycerol carbon atoms is commonly used in the nomenclature of glycerophospholipids, as indicated in Figure 1.2. In this nomenclature, the two hydrocarbon chains can be differentiated as *sn*-1 and *sn*-2 chains, the phosphate group being usually at the *sn*-3 position of the glycerol. In biological membranes, most of the glycerophospholipids are derivatives of *sn*-glycero-3-phosphatidic acid, the R-stereoisomer. The various glycerophospholipid types depend on the organic base, amino acid, or alcohol (the X-group in Figure 1.3) to which the phosphate is esterified and on the hydrocarbon chains which can be attached to the glycerol moiety through ester or ether linkages and vary widely in terms of length, branching, or degree of unsaturation.

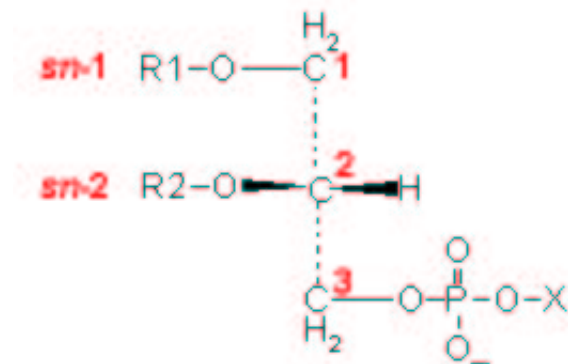


Figure 1.2: General structure of glycerophospholipids with the glycerol backbone drawn in a Fischer projection. The stereospecific numbering (*sn*) of the glycerol carbon atoms, with the distinction between the *sn*-1 and *sn*-2 chains, is indicated.

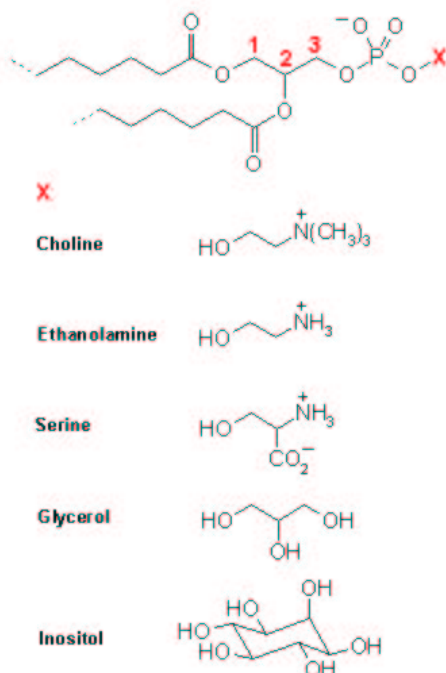


Figure 1.3: Generic structure of phospholipids. The phosphate can be esterified to the various X-groups listed to form the different classes of phospholipids.

- 1,2-Diacylglycerophospholipids or phospholipids** These fatty acid esters of glycerol are the predominant lipids in most biomembranes. The phosphate is usually linked to one of the several groups listed in Figure 1.3, including choline, ethanolamine, the S-amino acid serine, and polyalcohols such as glycerol or inositol. The corresponding phospholipids are called phosphatidylcholines (commonly abbreviated PC), phosphatidylethanolamines (PE), phosphatidylserines (PS), phosphatidylglycerols (PG), and phosphatidylinositols (PI). PC and PE constitute the major components of biological membranes. The chemical structure of these polar headgroups determines what charge the phospholipid as a whole may carry. At physiological pH values, PC and PE carry a full negative charge on the phosphate and a full positive charge on the quaternary ammonium: they are thus zwitterionic but electrically neutral. PS contain, in addition to the negatively charged phosphate and the positively charged amino group, a negatively charged carboxyl group. At neutral pH, PS exhibit an overall negative charge. PG and PI carry a net negative charge, since the alcoholic moiety does not carry any positive charge to counterbalance the negative charge on the phosphate. The headgroup charges are held at the interface between the aqueous and hydropho-

bic phases by the organization of the membrane bilayer. Phospholipids play therefore an important role in the determination of the surface charge of the membrane. The division of phospholipids into classes according to the structure of their headgroup represents only one level of complexity. On a second level, each phospholipid class exhibits various fatty acid chain compositions. The acyl chain lengths vary usually between 12 and 26 carbon atoms and may be saturated or unsaturated. The number of carbon-carbon double bonds can reach as many as six per chain. The most abundant saturated chains contain 16 or 18 carbon atoms and the major unsaturated species are C18:1, C18:2, and C20:4. In this notation, the first figure refers to the chain length, while the second one indicates the number of double bonds. Nearly all naturally occurring double bonds are *cis* rather than *trans*. A *cis* double bond introduces a kink or bend in the molecule, so that *cis* isomers disrupt the ordered packing of the lipid chains, perturbing the membrane structure. Some branched fatty acids such as isomyristate or isopalmitate may also occur in the lipid chain composition. Another variation is for instance the inclusion of a cyclopropane ring in the fatty acid chain.

- ***Diphosphatidylglycerols or cardiolipins*** These are essentially dimeric phospholipids, containing two diester phosphates linked by a glycerol molecule. Their structure is depicted in Figure 1.4. They are significant components of mitochondrial and chloroplast membranes; they also occur in some bacterial membranes, but are rather rare in other membranes.

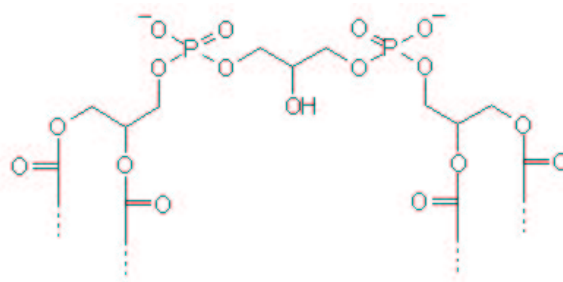


Figure 1.4: Structure of cardiolipins.

- ***Plasmalogens*** Their structure is analogous to that of the phospholipids, with a variation occurring at position 2 of the glycerol: the *sn*-2 hydrocarbon chain is attached via a vinyl ether linkage. Ethanolamine plasmalogens constitute an important class of polar lipids in the brain (myelin) and heart (cardiac sarcoplasmic reticulum) membranes

of some species. Choline headgroups may also be found in plasmalogens (see Figure 1.5).

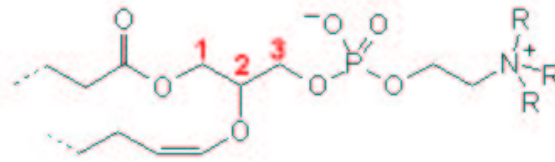


Figure 1.5: Generic structure of plasmalogens. R = H in ethanolamine plasmalogens and R = CH₃ in choline plasmalogens.

- **Phosphonolipids** They are found as major components in molluscs and protozoa, and in trace amounts in certain tissues (brain, heart) in humans. As shown in Figure 1.6, they contain a phosphorus-carbon bond which may influence the headgroup hydration at the bilayer interface. Phosphonolipids, like plasmalogens, contain an ether linkage at the *sn*-2 position.

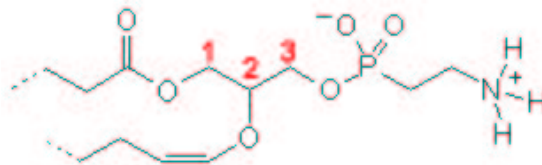


Figure 1.6: Example for a phosphonolipid. The bonding between the phosphate and ethanolamine found in PE is now replaced by a direct phosphorus-carbon bond.

Phosphosphingolipids Phosphosphingolipids contain the same kind of polar substituents (e.g. phosphorylcholine) as do the glycerophospholipids, but the glycerol part is now sphingosine (see Figure 1.7). The most common form of sphingosine contains 18 carbon atoms; some variation in the chain length is however possible. Sphingomyelin (SPHM) is widely found in animal cell plasma membranes. In the human erythrocyte membrane, it appears in approximately equal frequency to phosphatidylcholine. In sphingomyelin, the amino group of sphingosine is esterified to a fatty acid whose length varies between 16 and 25 carbon atoms in most cases.

Glycosphingolipids Glycosphingolipids have a glycosidic linkage to the terminal hydroxyl of ceramide. They are classified with respect to the carbohydrate moiety which can

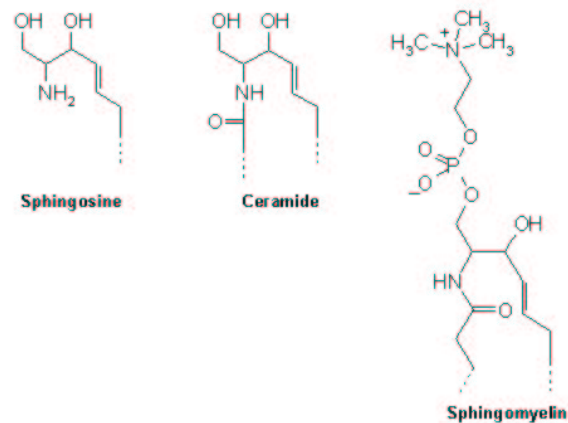


Figure 1.7: Structures of sphingosine, ceramide, and sphingomyelin.

range from a single sugar to very complex polymers. Glycosphingolipids are usually found as minor components on the outer surface of animal cell plasma membranes but constitute, occasionally, an important component of the membrane lipids. In the erythrocyte membrane, for instance, they carry blood group antigens.

- **Cerebrosides** Monoglycosyl ceramides are generally known as cerebrosides. The most frequent sugar moieties found in cerebrosides are glucose and galactose.
- **Gangliosides** Gangliosides are anionic derivatives of the ceramides with multiple addition of sugars ending with N-acetylneuraminic acid (sialic acid), a sugar acid carrying a negative charge.

Glycoglycerolipids In glycoglycerolipids, the *sn*-3 position of glycerol forms a glycosidic link to a carbohydrate such as galactose. These lipids are more closely related to the phospholipid structure than the sphingolipid one, a sugar replacing the phosphate moiety. Through alterations in the structure of the headgroups or the fatty acid chains, a large number of derivatives can be obtained. Glycoglycerolipids are predominant in the chloroplast membrane and are also found in substantial quantity in bacterial membranes.

Sterols Sterols are found in many plant, animal, and microbial membranes. Cholesterol is, by far, the most commonly found sterol in mammalian plasma membranes and constitutes about 30% of the lipid mass of these membranes. This molecule is a rigid and compact hydrophobic entity – consisting of a fused-ring nucleus and a hydrocarbon tail – with a polar

hydroxyl group. Cholesterol is thus quite different in structure from the other membrane lipids that have been described before. If cholesterol is the major sterol component in animal cells, other sterols, notably sitosterol and stigmasterol, are found in plants. The structure of these three sterol is given in Figure 1.8.



Figure 1.8: Structures of three sterols. Cholesterol occurs predominantly in animal cells, while sitosterol and stigmasterol are found in plants.

Lipid composition of a few membranes An overview of the lipid composition of mammalian plasma and intracellular organelle membranes, stemming from the work of Jamieson and Robinson, is given in Table 1.1 [3]. Although these various membranes exhibit characteristic differences in their composition, some common features emerge. With a few exceptions, PC, PE, and cholesterol appear to be the main components. Mammalian plasma membranes contain also an important quantity of sphingomyelin. Each of these four constituents represents roughly 20% by mass of the overall lipid amount. The cholesterol content is much lower in the internal organelles than in the plasma membrane, excepted in lysosomes. Myelin membranes, like plasma membranes, exhibit a high cholesterol content (28 weight%). The lipid composition of mitochondrial membranes is significantly different from that of the other organelles and is characterized by a large amount of cardiolipin. This difference may result from the partial genetic and biosynthetic independence of this organelles.

The distribution of the most abundant fatty acids found in the phospholipids of human erythrocytes is summarized in Table 1.2 [3]. The most common chain lengths and degrees of unsaturation can be deduced. More interesting is the distribution of fatty acids peculiar to each type of lipids. PC are mainly composed of short chains and dipalmitoylphosphatidylcholine (DPPC), with saturated chains of 16 carbon atoms, is one of the principal component of this class of phospholipids. The principal unsaturated chains found in PC are 18:1 and 18:2. Sphingomyelin, in contrast, contains a great amount of long chains with 24 C-atoms with one double bond at the most. In PE, a relatively high proportion of polyunsaturated chains are found, especially 20:4 chains.

Table 1.1: Lipid composition of various cellular organelles of mammalian liver cells and mammalian plasma membranes. Values are given in percentages by mass of total lipids.

	Plasma membrane		ER	Golgi	Lysosome
	Human erythrocyte	Rat liver			
PC	20	18	48	25	23
PE	18	12	19	9	13
PS	7	7	4	3	
PI	3	3	8	5	6
SPHM	18	12	5	7	23
Cardiolipins	–	–	–	–	≈ 5
Glycolipids	3	8	traces	0	
Cholesterol	20	19	6	8	14
Others ^a	11	21	10	43	16

	Nuclear membrane	Mitochondria	Nerve cells	
			Neurons	Myelin
PC	44	38	48	11
PE	17	29	21	17
PS	4	0	5	9
PI	6	3	7	1
SPHM	3	0	4	8
Cardiolipins	1	14	–	–
Glycolipids	traces	traces	3	20
Cholesterol	10	3	11	28
Others ^a	15	13	1	6

^aInclude free fatty acids, cholesterol esters, and triglycerides.

Table 1.2: Distribution in mole% of most abundant fatty acids among phospholipids of human erythrocytes. Amounts smaller than 1 mole% are indicated by dashes. Chains with a total relative abundance inferior to 1 mole% are left out. Therefore, the numbers do not add up to 100%.

	C16:0	C18:0	C18:1	C18:2	C20:3	C20:4
PC	31	12	19	22	2	7
PE	13	12	18	7	2	24
PS + PI	3	37	8	–	3	24
SPHM	24	6	–	3	–	1.4
Total	20	17	13	9	1.5	13

	C22:0	C22:4	C22:5	C22:6	C24:0	C24:1
PC	–	–	2	–	–	–
PE	2	8	4	8	–	–
PS + PI	3	4	3.5	10	–	–
SPHM	9.5	–	–	–	23	24
Total	2	3	2	4	5	4

Concluding remarks The lipids found as membrane components are very diverse but have the same fundamental property in common: they are all amphipathic molecules, presenting separate polar and apolar regions and, for this reason, have a natural propensity to form bilayer structures in an aqueous environment. They can be differentiated by two main features: the size and electrical property of the headgroups which may be charged, zwitterionic, or neutral, and the structure of the hydrocarbon chains which may have various lengths and different degrees of unsaturation. It should be emphasized that lipids having the same polar headgroup but different hydrocarbon chains, or vice versa, exhibit different physical and metabolic properties.

The various membranes present in different organisms show characteristic patterns of lipid composition. To a first approximation, the specific functions exhibited by these membranes may arise from qualitative and quantitative differences in their composition. Many of these functions, however, might be appreciated in terms of the properties of the membrane in specific environments and not on the basis of the structure or the reactivity of its components *per se* [4].

1.1.2.2 Membrane proteins

Membranes contain between 20 and 80 weight% protein. Just as each membrane can be characterized by its lipid composition, each membrane can be also characterized by its protein content. Thousands of different proteins are found as constituents of biological membranes. Whereas the primary role of membrane lipids is to provide the structural framework of the membrane in the form of a stable bilayer, proteins provide the diversity of enzymes, transporters, receptors, and pores, *i.e.* the principal active components of the membrane.

The covalent structure of membrane proteins is similar to that of soluble proteins. Membrane proteins can be distinguished from non-membranous proteins by the nature of their association with the lipid bilayer. This association may be loose or tight. The proteins may be incorporated into the bilayer structure or simply associated to a lipid or protein component on the surface of the membrane. Membrane proteins are generally bound to the membrane through non-covalent forces, such as the hydrophobic force or electrostatic interactions. They may fold so as to present both a non-polar hydrophobic surface which can interact with the apolar regions of the lipid bilayer, and polar or charged regions which can interact with the polar lipid headgroups at the interface of the membrane. There is also a certain number of membrane proteins which are covalently bound to the membrane via lipid anchors.

Operationally, membrane proteins have been divided into two major classes: peripheral (or extrinsic) proteins and integral (or intrinsic) proteins. This classification is based on the nature of their association with the lipid bilayer. The distinction between peripheral and integral proteins does not clearly define the mode of attachment to the bilayer, but rather the relative strength of the attachment, or the harshness of the treatment required to release the protein from the membrane.

- ***Peripheral membrane proteins*** Peripheral membrane proteins generally interact with the surface of the membrane only and are not integrated into the hydrophobic core of the lipid bilayer. They are thought to be weakly bound to the membrane surface by electrostatic interactions, either with the lipid headgroups or with other proteins. Such an association is rather loose and peripheral membrane proteins can be readily removed by washing the membrane, changing the ionic strength or the pH.
- ***Integral membrane proteins*** Integral membrane proteins extend deeply into or completely through the lipid bilayer and are thus integrated into the bilayer structure.

Generally, they can be removed from the membrane only with detergents or stronger agents that disrupt the membrane structure. The portion of the protein integrated into the membrane is thus thermodynamically compatible with the hydrophobic core of the bilayer: one expects a preponderance of hydrophobic amino acid residues in the intramembranous portion of the protein. Integral membrane proteins can be further divided into two subclasses. Transmembrane proteins constitute one of these subclasses and, as their name implies, span the lipid bilayer of the membrane. The other subclass refers to anchored proteins. A portion of these proteins is embedded in the hydrophobic interior of the bilayer, without passing completely through the membrane. In most cases, the lipids provide a hydrophobic anchor by which the protein is attached to the membrane.

1.1.3 Asymmetry

All biomembranes present a transverse asymmetry and some of them may also exhibit a lateral asymmetry.

Transverse asymmetry, implying transversal composition differences, can be easily rationalized by the fact that membranes consist of two leaflets which are exposed to different environments, e.g. cytoplasmic and extracytoplasmic. Membrane protein asymmetry clearly results from the way proteins have been inserted into the membrane. Once membrane proteins are in place within the bilayer, they do not flip their orientation anymore with regard to the two bilayer leaflets and remain kinetically trapped in the bilayer in their original orientation for the rest of their life time. Membrane lipids are also asymmetrically distributed throughout the bilayer. The origin and the maintenance of this lipid asymmetry is not entirely clear. However, in contrast to membrane proteins, membrane lipids exhibit relatively rapid transbilayer motions, called “flip-flop”, which may explain, at least in part, the differences in lipid composition between the two halves of the bilayer observed in a number of biomembranes. An important asymmetry has been found in the plasma membrane of eukaryotic cells: PS, PE and phosphoinositides are principally located in the inner leaflet of the membrane, whereas PC, sphingomyelin, and glycolipids are rather distributed in the outer leaflet [5]. Specific enzymes, phospholipid translocases or “flipases”, seem to play a major role in maintaining this asymmetry. A well-studied membrane is the mammalian erythrocyte membrane. The asymmetric lipid distribution has clearly been demonstrated in human red blood cells for instance: the outside leaflet of the plasma membrane consists primarily of PC

and sphingomyelin, while the inside leaflet is enriched in PE and PS [6]. The aminophospholipid translocase has first been discovered in these cells and is responsible for the selective transport of aminophospholipids from the outer to the inner leaflet of the membrane through interactions between the phospholipid headgroup and the enzyme [7, 8]. An important observation was that the rapid transbilayer movement of aminophospholipids such as PE or PS is significantly slowed down in ATP-depleted cells. It was then speculated that enzymes catalyze this ATP-dependent process.

In addition to transverse asymmetry, biomembranes may also exhibit lateral inhomogeneities. Distinct macroscopic domains are often observed at the cell surface and may be maintained by specific protein-protein or lipid-protein interactions, by protein aggregation, or by specific interactions between the membrane components and the cytoskeletal elements.

Compositional asymmetry gives rise to morphological and functional asymmetry. Transverse and lateral asymmetry also imply a real communication between both sides of the membrane and within the membrane plane, respectively.

1.1.4 Roles of lipids

Membrane lipids form a two-dimensional matrix in which proteins are embedded. On a morphological level, the primary roles of this matrix are to define a permeability barrier and to provide a lattice for diffusion of various substrates and vectorial organization of functional molecules. On a molecular level, lipids are important regulatory agents and are involved in many biosynthetic pathways. Lipids also modulate the structure and functions of proteins. This last statement has largely been demonstrated by numerous experiences, in which the removal or degradation of membrane lipids by appropriate phospholipases leads to the loss of most of the protein functions.

In the first class of lipid-protein interactions, protein functions can be affected by the bulk properties of the membrane lipids which provide a specific microenvironment to the proteins. In a membrane containing proteins, a population of lipids is temporally confined at the interface between the protein and the lipid bilayer. The number of lipid molecules in direct contact with the protein is well defined at any instant of time. From the activation of a delipidated protein, it is possible to calculate the number of lipid molecules required to activate or functionally reconstitute the protein. This corresponds to the number of lipids necessary to form a monomolecular ring around the periphery of the protein embedded in the bilayer [4]. A conformational change of a protein embedded in a membrane requires a

transient adjustment of the lipid molecules surrounding the protein or, in other words, a protein conformational change is related to a modification of the volume occupied by the protein within the bilayer. Depending on the packing properties of the lipids, more or less free volume elements can be recruited from the lipid assembly, allowing or preventing the protein conformational change. The effects of some lipid environments on membrane proteins have successfully been explained in the context of “free volume” [2]. For instance, an increase in the membrane cholesterol content may give rise to an inhibition of membrane proteins, which would be directly related to the condensing effect of cholesterol. The presence of unsaturated lipids around a membrane protein, however, proved to favor the activated state of the protein: unsaturation, indeed, increases free volume in the bilayer by introducing kinks and packing defects into the bilayer [9].

The second class of lipid-protein interactions involves lipids that bind tightly and specifically to sites on the protein surface. In such interactions, the lipid headgroups commonly provide the ligands for binding to the protein and affect the protein functions through allosteric mechanisms. A few examples of regulation of membrane protein functions by bound lipids can be mentioned. Phosphatidylcholine is required for proper activity of α -hydroxybutyrate dehydrogenase, the choline moiety binding to the enzyme [10]. Cardiolipin supports the activity of the mitochondrial ADP-ATP exchange protein. Six cardiolipin molecules are tightly bound to the protein, stabilizing the active form [11]. Phosphatidylinositol plays also a functional role in human erythrocyte glycophorin, three or four PI molecules being bound to the protein [12].

1.1.5 Membrane models

This section gives a brief historical overview of the main stages that have contributed to the actual conception of membrane model.

At the turn of the nineteenth century, Overton speculated on the lipid nature of biomembranes by observing a correlation between the rates at which various small molecules penetrate plant cells and their partition coefficients in an oil/water system [13].

In 1925, Gorter and Grendel introduced for the first time the concept of lipid bilayer as structural basis of biomembranes [14]. They postulated that lipids in the human erythrocyte membrane are organized in the form of a bimolecular leaflet or lipid bilayer.

In 1935, Davson and Danielli made a major contribution to the development of membrane models [15]. They found that a membrane such as the erythrocyte contains, besides lipids, a significant amount of proteins and included, therefore, proteins in their model. They suggested that proteins coat the surface of the lipid bilayer. This description was motivated by the new (at that time) knowledge of the β -sheet structure. In this model, the protein was thus not allowed to penetrate into the lipid bilayer.

In the 1960's and 1970's, new molecular insights into biological membranes were gained by the emergence of more sophisticated experimental techniques. Freeze-fracture electron microscopy revealed the existence of globular particles embedded within the lipid bilayer. Spectroscopic methods indicated that membrane proteins had an appreciable amount of α -helixes and that they were likely globular. The characterization of hydrophobic domains in membrane proteins also stimulated the integration of proteins into the membrane interior. At the same time, nuclear magnetic resonance measurements pointed out the fluid character of the lipid bilayer.

In 1966, Green and co-workers attempted to integrate the protein structure into the membrane in a model built around lipid-protein complexes as the fundamental structural pattern [16]. Although this model did not give prominence to the lipid bilayer as the basic structure of the membrane, it did incorporate proteins inside the membrane structure, introducing the concept of integral membrane proteins.

In 1970, Frye and Edidin performed a series of experiments on cell membrane fusion and suggested that membrane components can move laterally in the plane of the membrane [17].

In 1972, Singer and Nicolson amalgamated all these experimental observations and conceived a new model for the membrane structure, the so-called *fluid mosaic model* [18]. This model described the biological membrane as a two-dimensional fluid or liquid crystal in which lipid as well as protein components are constrained within the plane of the membrane, but are free to diffuse laterally. The notions of integral and peripheral membrane proteins were asserted and it was also suggested that some proteins may pass completely through the membrane.

The fluid mosaic model has constituted the most important step in the development of our current understanding of biomembranes. Although the model contains little structural detail, it summarizes the essential features of biological membranes. This model has undergone modifications and refinements are still expected in the future. In particular, it is now clear that membrane proteins do not all diffuse freely in the plane of the bilayer: their mobility varies

in morphologically distinct membranes from highly mobile arrangements to rigid structures whose molecular motion is more or less constrained. The existence of differentiated lateral domains within the membrane is also now known. Some regions of biological membranes are not arranged in the traditional bilayer; hexagonal or cubic phases, for instance, may also occur. Nevertheless, the fluid mosaic model still provides the conceptual backdrop for all current models which just represent refined versions.

1.1.6 Model membranes

Various model membrane systems have been developed for studying biomembrane properties. The simplest model systems are provided by pure lipids or lipid mixtures forming a bilayer. Since these systems do not contain membrane proteins and usually exhibit a simple lipid composition, they are not able to reproduce all the properties found in real membranes, but the main biophysical and biochemical features are nevertheless preserved. More complex systems reconstitute lipid-protein mixtures and provide insight into lipid-protein interactions.

Liposomes Liposomes are probably the most commonly used model membrane systems. The term “liposome” refers to any lipid bilayer structure which encloses a volume. The primary uses of liposomes are to encapsulate solutes for transport studies and to provide model membranes in which proteins can be incorporated. Multilamellar vesicles (MLV) were the first liposomes to be characterized and consist of multiple bilayers forming a series of concentric shells with a diameter ranging from 5 to 50 μm . MLV are easy to prepare, can be made in large quantities and high concentrations, and exhibit reproducible properties. They are thus suitable for a wide variety of biophysical studies. Drawbacks of MLV include the inhomogeneity in size and number of layers, the limited aqueous space for trapping solutes, and the close apposition of bilayers which may affect membrane properties. The heterogeneity problem has been overcome by the introduction of small unilamellar vesicles (SUV), usually prepared by sonification of aqueous phospholipid dispersions. These vesicles have diameters from 10 to 50 nm and consist of a hollow sphere whose surface is a single lipid bilayer. SUV are rather unsuitable for transport studies because of the too small size of the internal aqueous space. The radius of curvature of these vesicles is also much smaller than that usually observed in cell membranes, resulting in packing constraints in the bilayer. The vesicle size was thus increased and large unilamellar vesicles (LUV), with diameters ranging from 50 to 500 nm, were produced. These vesicles are large enough to trap a significant

amount of solute, necessary for transport experiments, and provide interesting drug delivery systems.

Planar bilayer membranes Planar bilayer membranes are traditionally created by painting a concentrated solution of phospholipid in a solvent like hexane or decane over a small hole (about 1 mm diameter) immersed in an aqueous solution. Under appropriate conditions, the lipids spontaneously form a bilayer across the hole. Because of their optical properties (lack of light reflectance), they are called black lipid membranes (BLM). The major advantages of planar membranes over vesicle preparations are their suitability for electrical measurements and for the study of membrane proteins. These systems are particularly appropriate for studying pores, channels, or carriers that catalyze the transfer of charges across the bilayer. The unknown amount of residual solvent they contain as well as their relative instability may, however, generate some problems.

Monolayers Lipids can be spread in a monolayer at an air/water interface: the polar head-groups are in contact with the aqueous phase, while the hydrocarbon chains extend in the gas phase. From the aqueous phase, the monolayer surface is similar to that of an entire membrane and surface properties can be investigated under variation of the surface density and the lateral surface pressure. Monolayers are especially useful for examining the behavior of molecules like lipases, known as being active at the membrane surface. The main disadvantages of monolayers as membrane models are twofold: some of the monolayer properties might differ from those of a bilayer; a second difficulty resides in the choice of the lateral surface pressure to apply to mimic the properties of a real membrane.

Membrane computer models Membrane computer models have a short history compared to experimental models. In the last decade, computer simulations such as Monte Carlo (MC) or molecular dynamics (MD) simulations emerged as a powerful tool to gain detailed insights into the molecular structure and dynamics of biomembranes. Various lipid bilayer systems have been simulated, incorporating or not membrane proteins. The two major limitations of such membrane simulations involve the system size and the accessible time scale. However, computer simulations constitute an irreplaceable technique to probe membrane properties at the atomic level. Strong and weak points of the MD approach will be extensively discussed in the next chapters.

Each of the membrane model systems described above presents advantages and disadvantages, the one providing insight into membrane regions to which the other does not have access. Information from each kind of systems turns out to be very useful for the better understanding of specific membrane properties and can be combined to refine the fluid mosaic model.

1.2 Phospholipid properties relevant to biomembranes

In spite of their complexity and their specific differences in composition, all biomembranes have the same universal structure: the basic structural element is provided by a lipid bilayer. Among membrane lipids, phospholipids constitute an important class (see Section 1.1.2.1, page 13) with regard to their occurrence in cell membranes and their ability to form bilayer vesicles spontaneously when dispersed in water. The understanding of their physical and chemical behavior is essential in order to appreciate many of the properties of biological membranes.

1.2.1 The hydrophobic effect

The *hydrophobic effect* is one of the most important concepts necessary for the understanding of membrane structure. The major driving force stabilizing hydrated phospholipid aggregates is the *hydrophobic force*, which is not an attractive force but rather a force representing the relative inability of water to accommodate non-polar species. The three other stabilizing factors are hydrogen bonding and electrostatic interactions between polar headgroups and between headgroups and water, and van der Waals dispersion forces between adjacent hydrocarbon chains, which are short-range and weak attractive forces resulting from interactions between induced dipoles. Compared to the hydrophobic force, however, they are relatively minor stabilizing factors.

The hydrophobic force is the thermodynamic drive for the system to adopt a conformation in which contact between the non-polar portions of the lipids and water is minimized [19]. This so-called “force” is entropic in origin. Hydrophobic molecules aggregate in water so as to maximize orientational and configurational entropy. The larger the surface area of the hydrophobic molecule, the larger the water cage that must be built around that

molecule, and the larger the unfavorable entropy contribution to the transfer of that molecule into the water phase [2].

The hydrophobic effect drives phospholipids to aggregate into the fundamental structural element of biological membranes, the phospholipid bilayer.

1.2.2 Phase structures

Phospholipid molecules aggregate in an aqueous solution to form a variety of assemblies, which correspond to structurally distinct phases. Which phase predominates in a given system depends on environmental factors such as temperature, pressure, pH, and ionic strength, on the composition and water content of the system, and on the structure and conformation of the individual phospholipid components. The various morphologies of phospholipid assemblies are reviewed below (see also reference [20]). Each morphology is stabilized by a balance between favorable and unfavorable interactions, resulting directly from an optimization of the hydrophobic effect, with a variety of intramolecular and intermolecular interactions.

1.2.2.1 Crystalline phases

At low temperatures and/or hydration levels, most phospholipids form crystalline lamellar phases, denoted L_C . These phases are true crystals, exhibiting both long-range and short-range order in the three dimensions. They may be anhydrous, or may contain a certain number of water molecules of co-crystallization. The phospholipid hydrocarbon chains are in an all-*trans* conformation.

1.2.2.2 Gel phases

Gel phases are ordered lamellar phases in which phospholipid molecules undergo hindered long-axis rotation on a time scale of 100 ns and in which the hydrocarbon chains adopt essentially an all-*trans* conformation. Such gel phases are formed at low temperatures in the presence of water, although the water content is often relatively low.

In the L_β gel phase, the hydrocarbon chains are arranged parallel to the bilayer normal. In the $L_{\beta'}$ phase, the chains are tilted with respect to the bilayer normal. The tilting occurs when the cross-sectional area required by the headgroup exceeds about twice that required by the acyl chains. The chain tilt increases the cross-sectional area of the acyl chains, and

allows thus the packing mismatch to be accommodated. When the tilting becomes too great, the (untilted) interdigitated $L_{\beta I}$ phase may occur.

An intermediate phase $P_{\beta'}$ between the gel phase L_{β} and the liquid crystalline phase L_{α} (see next section) is found in the gel phase of a few phospholipids. This is a rippled phase in which the lamellae are deformed by a periodic modulation, with the chains being essentially in a tilted conformation.

The different gel phases are depicted in Figure 1.9.

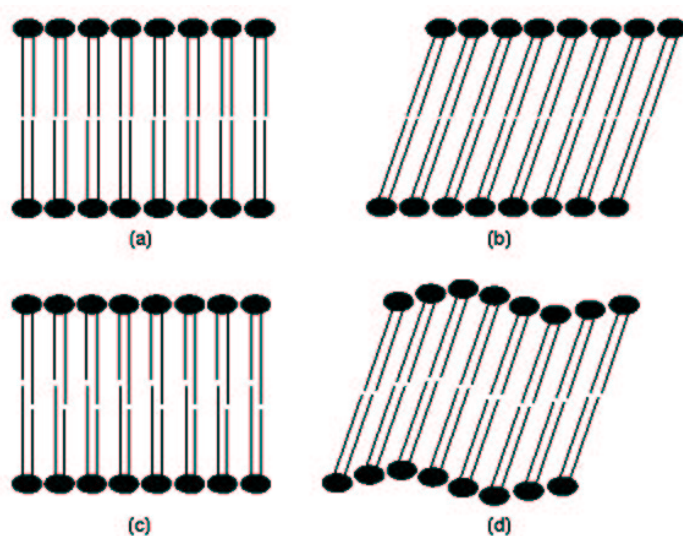


Figure 1.9: Gel phases of phospholipids: (a): L_{β} untilted phase; (b): $L_{\beta'}$ tilted phase; (c): $L_{\beta I}$ interdigitated phase; (d): $P_{\beta'}$ rippled phase.

1.2.2.3 Fluid phases

Lamellar liquid crystalline phase L_{α} Upon heating a gel phase, the phospholipid chains melt to a liquid-like conformation, transforming usually to the lamellar L_{α} phase. The rate of lateral diffusion of the lipids increases by at least two orders of magnitude and the hydrocarbon chains exhibit a high tendency to isomerize, alternating conformations about the carbon-carbon bonds. In this disordered fluid state, phospholipid movements are still inhibited by some organizational constraints: for instance, the phospholipid molecules cannot translate extensively in the direction normal to the bilayer surface but remain rather confined within the bilayer, in accordance with the hydrophobic effect. The phospholipids are therefore neither in a true liquid state, in which their movement would be isotropic, nor in a solid

state, but in a so-called *liquid crystalline* state. A liquid crystal retains at least one dimension of order relative to the solid state. Under usual physiological conditions, the lipid bilayer of biological membranes most closely resembles the lamellar liquid crystalline phase.

Hexagonal and cubic phases For some phospholipid systems, the gel phase melts directly to a fluid non-lamellar phase with a hexagonal or cubic symmetry. In the hexagonal I phase H_I , the phospholipids are organized in the form of cylinders with the polar headgroups facing out and the hydrocarbon chains facing the interior. The cylinders are packed onto a hexagonal lattice and the volume between the cylinders is filled with a continuous water phase. These long tubes can be thought of as many micelles fused together. This phase structure is only formed under specific conditions and is not particularly relevant to biological membranes. In the inverse hexagonal II phase H_{II} , the phospholipids also aggregate into cylinders, but with the headgroups facing the inside and the hydrocarbon chains the outside. The polar groups contact water and surround an aqueous channel located at the center of the cylinder. These tubes also form a hexagonal array in cross section. The H_{II} phase is very common in phospholipids such as PE having small weakly hydrated headgroups and attractive headgroup-headgroup interactions [21]. Phospholipids can also exhibit cubic phases, which almost behave as isotropic phases. The cubic phase structure consists of short tubes connected in a hexagonal array. In this structure, the phospholipid molecules experience all possible orientations, which accounts for its isotropic character. Cubic-like phases are observed in mitochondrial and ER membranes [22,23]. The reasons why biological membranes incorporate into their structure lipids that destabilize the bilayer organization can be found in many physiological processes. For instance, such lipids facilitate membrane fusion and stabilize regions of high curvature.

The fluid phases described above are schematically represented in Figure 1.10.

In biological membranes, lipid assemblies essentially form a bilayer structure, corresponding to the lamellar liquid crystalline phase L_α . The bilayer pattern is essential to the structure and proper function of biomembranes. The membrane matrix can be however interrupted by non-lamellar phases within the overall constraints of the bilayer organization. Such non-lamellar phases are for instance observed as intermediate phases in common biological processes such as cell-cell adhesion and fusion.

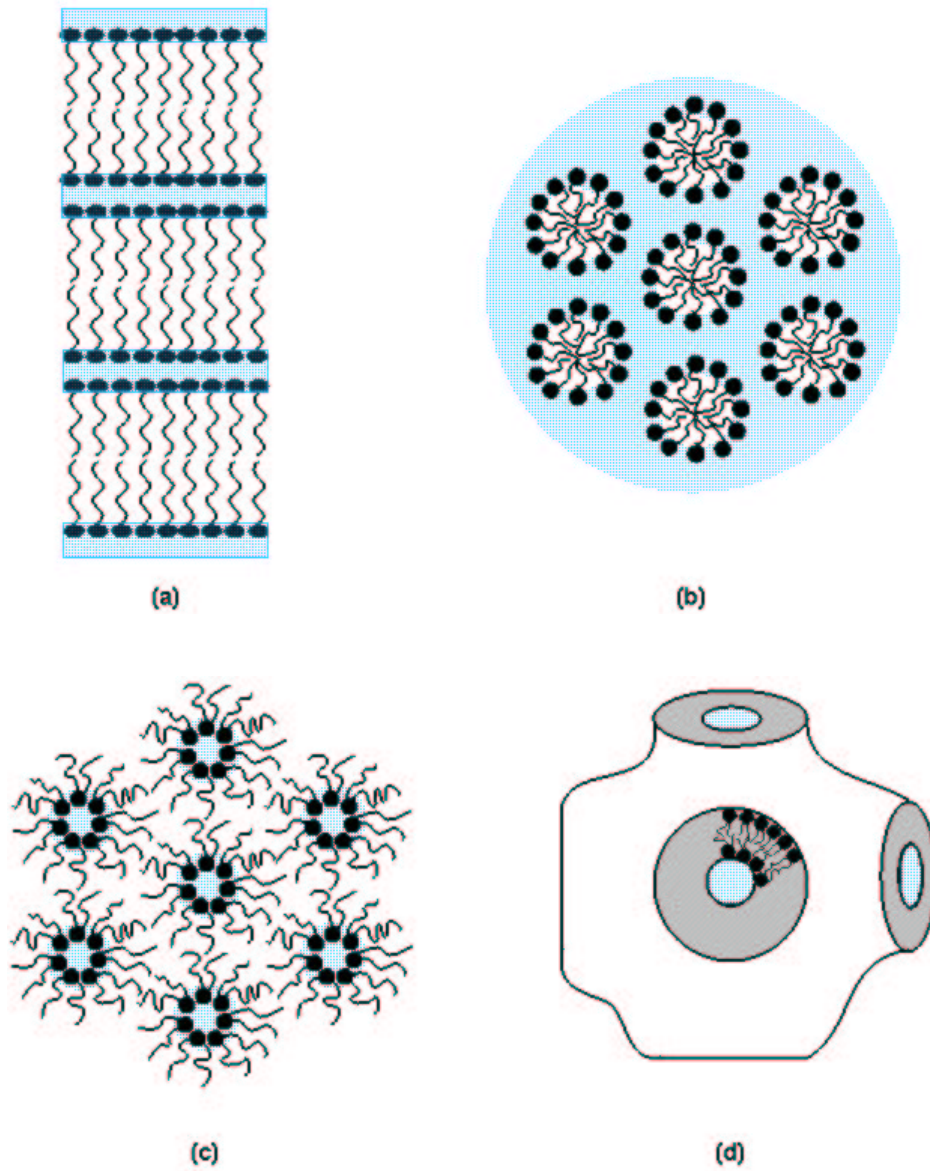


Figure 1.10: Fluid phases of phospholipids. (a): L_{α} lamellar liquid crystalline phase. (b): H_I hexagonal I phase. (c): H_{II} inverted hexagonal II phase. (d): Example for a cubic phase.

1.2.3 Phase transitions

A phase transition is an abrupt change in the macroscopic properties of a system, involving a modification of the symmetry and/or topology of the system. Phase transitions are driven predominantly by two system variables which are temperature and water content. There is thus a “natural” sequence in which the various possible phases occur. At low temperatures and hydration degrees, phospholipids tend to adopt an ordered conformation leading to crystalline or gel phases, while, at higher temperatures and hydration levels, fluid phases rather occur. At a given temperature and water content, transitions can be also induced by changes in the lipid composition or by additives. A study of the factors affecting or inducing a phase transition and of the changes taking place at the phase transition provides a very valuable method of characterizing the properties of the fluid state, which is the more relevant to biological membranes (see also reference [20]).

Effect of phospholipid hydration The effect of water on the thermotropic behavior of phospholipid assemblies is complex. A certain amount of water molecules is bound to the polar headgroups and behaves differently from bulk water. Bound water appears to represent about 20% of the phospholipid-water system. Usually, the addition of water causes a general loosening of the lipid packing density, leading to a decrease of the transition temperature. The decrease in temperature can reach as much as 50°C. This can be explained by a growing mobility of all phospholipid molecules with increasing hydration, due to a diminishing intermolecular steric hindrance. More precisely, increasing hydration gives rise to a softening of the interfacial region, which enhances headgroup mobility; the enhanced headgroup mobility leads in turn to an increased mobility of the hydrocarbon chains.

Effect of phospholipid chemical structure Within a particular class of phospholipids, the length of the hydrocarbon chains has a direct influence on the transition temperature, e.g. from the gel state L_{β} to the liquid crystalline state L_{α} . Increasing the chain length has the effect of increasing the chain-chain interactions, stabilizing the phospholipid bilayer in the gel state and thus increasing the chain-melting temperature. The L_{α} -H_{II} transition temperature falls also steeply with increasing the chain length. The hydrophobicity of longer chains is indeed more pronounced, which tends to favor the formation of inversed non-lamellar phases. The presence of double bonds in the phospholipid hydrocarbon chains has a more powerful effect on the transition temperature than the chain length. Chain unsaturation dras-

tically lowers the gel-fluid transition temperature (typically by approximately 60°C for a *cis*-unsaturated bond) as well as any transitions to inverse non-lamellar phases. A *cis*-double bond generates the formation of a permanent kink in the hydrocarbon chains, which inhibits a tight packing of the chains. Unsaturation destabilizes the bilayer structure, especially in the gel state, and the phase transition occurs therefore at a lower temperature. The effect on the phospholipid phase behavior depends strongly upon the position of the double bond along the chain, the maximal effect occurring when the double bond is located close to the middle of the chain [24]. Monounsaturated fatty acids commonly found in phospholipids from cell membranes exhibit a double bond between carbons 9 and 10: the double bond is thus located precisely where the maximal effect on the phase behavior can be achieved. For diacylphospholipids, increasing asymmetry between the lengths of the two chains also tends to lower the chain-melting temperature [25]. The chemical structure of the phospholipid headgroups plays also a major role in determining the phase transition behavior. The effective polarity of the headgroups, defined by their intrinsic hydrophilicity but also depending on their accessibility to water or their possibility for hydrogen bonding, constitutes a crucial factor. Minor modifications, such as the replacement of a single proton by a methyl group, can profoundly alter the phase behavior. Striking differences are for instance observed between the polymorphism of PE and PC. The transition temperature from the gel to liquid crystalline states is about 20°C higher in PE than in PC. For the former phospholipid species, intermolecular hydrogen bonds between the amino group of one headgroup and the phosphate moiety of the neighboring headgroup are possible. Such hydrogen bonds intensify headgroup interactions but weaken the interactions between headgroups and water. Hydrogen bonding and poor hydration of the PE headgroups result in a stabilization of the gel state relative to the liquid crystalline state. For PC, the possibility of direct hydrogen bonds between the headgroups is missing, so that the PC headgroups interact much more strongly with water. This increases the hydration of the bilayer, modifies its structure, and lowers the gel-fluid transition.

Effect of phospholipid mixtures Mixing phospholipids together alters the phase behavior of each phospholipid component in a complex way. The study of lipid mixtures is of great interest since biological membranes contain a variety of lipid species. The fact that biomembranes are generally in a lamellar liquid crystalline phase under physiological temperatures shows that a well-defined balance in the lipid composition is necessary to maintain such a fluid morphology.

Effect of cholesterol Cholesterol tends to fluidize the gel phase L_{β} and to order the lamellar liquid crystalline phase L_{α} , thereby broadening or even eliminating the transition between the two phases. Cholesterol can induce a liquid crystalline state in phospholipids that would otherwise adopt a gel state, enhancing thus the stability of fluid bilayers. However, maintaining a fluid state in biological membranes is likely not the major role of cholesterol in cell biology. Most plasma membranes would be indeed in a fluid state at 37°C without cholesterol. The introduction of a double bond in the hydrocarbon chains of membrane phospholipids, for example, would be sufficient to keep the bilayer in a liquid crystalline state [2]. Cholesterol is, nonetheless, essential for the normal growth and functioning of cells (e.g. by modulating the function of membrane proteins through direct binding to sterol-specific sites on membrane proteins). The ordering effect of cholesterol observed in fluid bilayers can be explained by the rigid structure of cholesterol. The portion of the phospholipid hydrocarbon chains encountering the rigid steroid nucleus is indeed hindered in its motion and *trans-gauche* isomerization about the carbon-carbon bonds is diminished. The effects of cholesterol on the phospholipid phase behavior are however much more complex than described above and are strongly dependent on the cholesterol concentration. Cholesterol can induce domain formation in membranes in the liquid crystalline state and tends to promote the transition towards inverse phases such as H_{II} [26].

Effect of solutes The incorporation of solutes into a phospholipid assembly can modify the phase equilibria in a great number of ways. Polar solutes generally cause an osmotic dehydration of phospholipid systems, since they are in competition with the phospholipid headgroups to interact with water [27]. The dehydration effect is enhanced if the solute directly binds to the phospholipid headgroup, replacing bound water molecules. The introduction of polar solutes tends to favor the formation of ordered phases and inverse non-lamellar phases. Amphiphilic solutes preferentially adsorb with their polar moiety near the phospholipid headgroups and their hydrophobic part embedded within the phospholipid hydrocarbon region. Their effects are closely related to their chemical structure and cannot be generalized. Non-polar solutes tend to reduce chain packing constraints by partitioning into the interstices within the hydrocarbon regions of the phospholipid phase. They facilitate thereby the formation of inverse phases such as H_{II} , where there is a significant degree of chain stress due to the necessity to fill the hydrophobic region at a uniform density [20].

1.2.4 Motional properties and membrane fluidity

The dynamic properties of a phospholipid membrane in the biologically relevant liquid crystalline state arise from the conformational flexibility of its components. Conformational flexibility implying motion, the determination of the rate and extent of phospholipid motions is essential for understanding dynamic properties of membranes. The major motivation for studying membrane dynamics is its relevance to biological functions. At first, it is important to make a distinction between motional order and motional rates. The two concepts are independent, even if changes in motional rates often parallel changes in motional order. Motional order on one hand, and motional rates on the other hand, provide different insights into the membrane dynamics which can be combined to obtain an overall vision of the complex dynamic properties. Both concepts will be clarified in the next sections. The notion of membrane fluidity will be then redefined and emphasis will be laid on its biological relevance.

1.2.4.1 Motional order

The motional or orientational order of a phospholipid molecule or a portion of the molecule refers to the number of degrees of freedom expressed by the motion experienced by the molecule or a part from it [2]. The order of motion is usually described by an order parameter. Depending on the method of measurement, different order parameters can be defined and calculated (see Chapter 4, Section 4.3.4.3, page 118, for more details). Generally, small values of the order parameters correspond to a high degree of freedom, *i.e.* a disordered state.

In a phospholipid bilayer, the region between the carbonyl groups and the middle of the hydrocarbon chains is usually characterized by relatively high order parameters, which are roughly constant independently on the position considered. Beyond the middle of the chains, the order parameters drop significantly towards the chain termini. The motions of the phospholipid molecules are thus restricted in the region of the hydrocarbon chains near the glycerol backbone, while the molecules exhibit more motional freedom towards the chain extremities. The motional order profile across the bilayer is characteristic of the physical state of the membrane.

1.2.4.2 Motional rates

Phospholipid motions occur on different time scales. The rates of motion are characterized by correlation times – the motion being described by an exponential correlation function – and are not directly related to the motional order.

Phospholipids exhibit various motional modes, which all account for the dynamic properties of the membrane. The different types of motion are illustrated in Figure 1.11. Intramolecular reorientational motions comprise torsional oscillations around single bonds and free or slightly hindered rotations of certain groups or segments (such as methyl groups or fragments of the headgroup). The rotational motion of the phospholipids constitutes an important contribution to the membrane dynamics. The overall rotational motion can be characterized by a spinning motion, which is a rotation around the long molecular axis parallel to the bilayer normal, and by a so-called wobbling motion, in which the long axis changes its orientation – the molecule describing thereby a cone of finite dimensions. “Wobble” is a restricted motion, since all possible orientations of the long axis are not allowed within the bilayer structure and large deviations from the bilayer normal are unlikely. Brownian translational diffusion or jump diffusion of the phospholipid molecules within the plane of the membrane is called lateral diffusion: the in-plane motion of the whole phospholipids consists of a local diffusion within their solvent cage and of long-range diffusional jumps between adjacent sites [28]. Transbilayer “flip-flop” processes, in which phospholipid molecules are translocated from one side of the bilayer to the other, are also of importance, although they occur more rarely. At last, patches of phospholipid molecules exhibit collective motions, leading to undulations of the bilayer surface and resulting in relatively slow fluctuations.

The anisotropic nature of the phospholipid bilayer implies strong anisotropic constraints upon the orientation, conformation, and motion of the phospholipid molecules. The reorientational motions about different molecular axes occur thus on vastly different time scales [29]. For instance, rotation is much more facilitated around the long axis of the phospholipid molecule than around other axes. Another important point to mention is the different motional behavior of the headgroup compared with the hydrocarbon chains. A certain independence of motion is observed and some particular motions may occur on different time scales.

The most rapid of the motions described above is rotation about single bonds, characterized by correlation times inferior to 100 ps. Rotation about single bonds is usually slower in the headgroup region than in the hydrocarbon chains. *Trans-gauche* isomerizations in

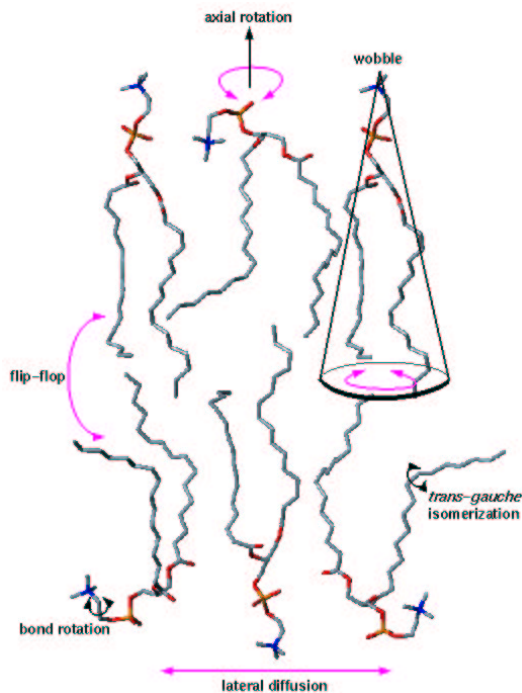


Figure 1.11: Schematic representation of the various motional modes observed in a phospholipid bilayer in the liquid crystalline state.

the fatty acid chains are very rapid, with correlation times τ_J from 1 to 10 ps in the liquid crystalline state. The values of τ_J are relatively long near the glycerol backbone but become shorter towards the chain termini. The rotation of the terminal methyl groups in the chains is about one order of magnitude shorter than τ_J . In the headgroups, the dynamics of the dihedrals is slower, with correlation times up to a few hundred of picoseconds. This can be explained by the strong interactions within and between the headgroups. The time scales become significantly longer when the whole phospholipid molecule is considered. Rotation of the molecule around its long axis involves a correlation time $\tau_{||}$ of a few nanoseconds. The wobbling motion, however, happens on a larger time scale and is characterized by a correlation time τ_{\perp} of the order of tens of nanoseconds or more. The wobbling motions in a cone are indeed only possible within a restricted angular range determined by the neighboring molecules. Translational motion of the phospholipid molecules in the plane occurs with a lateral diffusion coefficient of the order of 10^{-7} cm²/s [28]. The transmembrane movement of phospholipids or “flip-flop” is very slow and takes place on a typical time scale of minutes to hours or even days [29]. The dynamic properties of a phospholipid membrane are

therefore characterized by a very wide range of motional modes, which makes their study particularly challenging.

1.2.4.3 Membrane fluidity

Now that the motional properties of the phospholipid components in a membrane have been examined, the concept of “fluidity” in membrane biology can be redefined and its involvement in many biological functions can be better understood.

The term “fluidity” is imprecise and elusive in its physical meaning, especially when applied in the context of membrane structure. For an isotropic liquid such as water, fluidity represents the inverse of viscosity, which is a well-defined and easily measured bulk thermodynamic property. Viscosity is essentially a measure of the frictional resistance encountered when adjacent layers of fluid are moving with different velocities [19]. However, biological membranes as well as pure phospholipid bilayers are highly anisotropic and the above definition of fluidity cannot be applied directly. The membrane components are principally confined to two dimensions, *i.e.* the surface of the membrane, with only a limited third dimension available, being the bilayer normal. The phospholipid behavior is not only anisotropic but also strongly dependent on the location considered along the bilayer normal. If the hydrophobic membrane interior, characterized by highly disordered chains experiencing considerable freedom, can be modeled by any isotropic hydrocarbon phase, the glycerol region is much more ordered and static, and the interfacial region, composed of the head-groups facing the water phase, exhibits specific order and dynamic properties. As applied to membrane, the term “fluidity” has to be considered both as a dynamic property related to the motion of the individual components and as a static feature related to the arrangement or order of the molecules in the membrane. Generally, fluidity is measured by observing the motion of fluorescent probes incorporated into the membrane. Since fluorescence depolarization is sensitive to molecular motion, information concerning the environment in which the probe resides can be collected. Fluidity represents then the ability of a foreign molecule to move in the membrane and to experience internal conformational flexibility. However, such measurements are sensitive to both the rate of motion and any constraints to that motion, so that information about dynamics and molecular order gets intermixed [19]. Fluidity can be also quantified by the rotational correlation time of spin probes, by the order parameter, also derived from spin or fluorescent probes, or by the partition coefficient describing the distribution of certain probes between the membrane and the aqueous medium. Membrane

fluidity cannot be characterized by a single parameter: multiple parameters are needed to describe the physical state of the bilayer.

The fluidity of biomembranes is essential to many biological functions. Biomembranes apparently adjust their lipid composition in such a way that they remain in a fluid state irrespective of the ambient temperature or other external conditions. The rate of lateral diffusion of membrane components plays a pertinent role, for instance, in enzyme reactions involving multiple membrane-bound components: some enzymatic functions require the membrane-bound components to be freely diffusing within the plane of the bilayer, whereas other processes clearly rely on constraints imposed on the mobility of membrane components. The rate with which lipids adjacent to proteins exchange with bulk lipid is also essential to protein properties and functions. The most dramatic evidence that membrane fluidity is critical to physiological functions comes probably from studies showing adaption of various organisms to environmental stress [30]. This is most often observed in microorganisms, plants, or hibernating animals, which are able to sustain low temperatures. In response to thermal stress, they alter their membrane lipid composition, usually by increasing the degree of lipid unsaturation or by decreasing the average lipid chain length, to maintain optimal membrane fluidity.

1.3 Biomembrane transport

1.3.1 Transport pathways and mechanisms

One of the most important roles of biomembranes is to moderate the passage of substances between compartments of organisms. Epithelia and endothelia represent the main physiological barriers to be crossed by solutes like nutrients or drugs. Epithelia cover the surface of the body and line all internal organs. In spite of their chemical and structural differences, they all act as highly selective permeability barriers, separating internal and external fluids. Endothelia line blood capillaries and regulate the distribution of compounds between the blood and the interstitial fluids. The transport processes that have evolved to overcome these barriers are at least as important as the barrier functions of biomembranes. Solute transport can occur via a transcellular pathway (across the cell) or via a paracellular pathway (between the cells). The lipid matrix, structural framework of all biological membranes, constitutes the main permeation barrier to transcellular transport. The adhesion of adjacent cells is ensured

by junctions, whose structure influences paracellular transport. Epithelial cells are linked by tight junctions, whereas endothelial cells have rather loose junctions. In the latter case, the paracellular pathway is thus favored. The lipoidal surface of a membrane is however much greater than the aqueous one – in the small intestine for instance, tight junctions represent only 0.1% of the whole membrane surface [31] – so that the transcellular pathway accounts for most transport processes in the body. Paracellular diffusion is, by definition, solely passive, while transcellular transport involves various mechanisms. These mechanisms can be divided in two main classes. In the first class, the solute moves from a region of relatively high chemical potential to a region of lower chemical potential by passive or facilitated diffusion. For this type of transport, no cellular energy, such as that in the form of ATP, is required. The second form of transport involves active processes, which do require an input of energy and generally occur against a concentration gradient. These processes are all protein-mediated. In each class of transport, a wide variety of mechanisms elucidates how solute flux across membranes is achieved. The principal transport mechanisms are briefly described in this section.

Passive diffusion across the lipid matrix Passive diffusion across the lipid matrix represents the simplest form of transport and refers to the movement of a molecule by random processes through the lipid bilayer portion of a membrane without an expenditure of energy. A net flux of the transported species across the membrane is only achieved when a difference in chemical potential of the species is observed between both sides of the membrane. This chemical potential difference usually results from a difference in concentration (or activity) of the species on one side versus the other. The solute diffuses down the concentration gradient, *i.e.* from a region of relatively high concentration to a region of relatively low concentration. Energy is obtained from the downhill flow; the amount of energy, also known as the free energy change ΔG , is directly proportional to the concentration difference. In the case of charged species, *i.e.* ions, an additional factor has to be taken into consideration. Indeed, many biological membranes are electrically positive on one side and negative on the other side, exhibiting a potential difference or voltage gradient across them. This arises from differences in the distribution of positive and negative ions on the two sides of the membranes. The diffusion of a charged species is considerably influenced by this transmembrane electrical potential. The inside of many cells is electrically negative compared with the outside: inward fluxes of positive ions and outward fluxes of negative ions are thus favored. For the transport of charged solutes, a concentration gradient as well as an electrical gradient

have to be taken into account: both notions can be combined with the electrochemical gradient. The rate of diffusion of an uncharged species across a membrane is well described by Fick's law:

$$J = P \cdot A \cdot \Delta C \quad (1.1)$$

This states that the flux J , or amount of solute passing through the membrane per unit time, is directly proportional to the solute concentration gradient ΔC , to the area A of membrane absorptive surface, and depends on the permeability coefficient P of the solute in the membrane. The permeability coefficient is both characteristic of the solute and the membrane, and is defined as follows:

$$P = \frac{K \cdot D}{h} \quad (1.2)$$

K is the partition coefficient of the diffusing species between the membrane and the aqueous phase and describes the relative solubility of the species in both media. D is the diffusion coefficient of the solute in the membrane and represents the speed with which the solute can move through the membrane. D depends on the size and shape of the solute but also on the viscosity and density of the membrane. h is the thickness of the membrane. The partition coefficient is the most important determinant of the permeation rate (see Section 1.3.2.2, page 46). Hydrophobic substances are viewed as being able to permeate the lipid bilayer of a membrane more easily than hydrophilic ones, owing in part to their ability to dissolve in and subsequently diffuse through the hydrophobic core of the bilayer. The generally high hydration degree of a polar species also constitutes a barrier to its transport across the lipid bilayer. Usually, this hydration shell must be stripped away before the solute can enter the membrane bilayer, which is often accompanied by a high energy of dehydration. Smaller solutes diffuse more rapidly than larger ones, so that better correlations between permeability and hydrophobicity are obtained when applying a correction for the size of the solute. The structural properties of the membrane as well as its dynamic state are also an important component of diffusion processes. Anything enhancing the occurrence of defects in the bilayer, for instance an increase in unsaturation in the lipid chains or packing defects at lipid-protein interfaces due to transient mismatches between the rough protein surface and the lipid bilayer, will enhance passive diffusion. Transit of the hydrophobic interior of the lipid bilayer is not the only barrier to passive diffusion through a membrane. Before encountering the membrane interior, a solute must get through the interfacial region which exhibits properties very different from those of the bulk solution. Study of the passive diffusion of a solute

across the lipoidal matrix implies therefore a good knowledge of both solute and membrane properties.

Passive diffusion through pores and channels One of the great barriers to passage of polar and/or ionic substances across a membrane is their incompatibility with the hydrophobic core of the lipid bilayer. Pores and channels, formed by proteins, provide a water-filled pathway through the membrane and are capable of supporting great fluxes of polar and ionic solutes. This form of transport implies passive diffusion of the solute in an aqueous medium and is also driven by an electrochemical gradient between the two sides of the membrane. The terms of *pore* and *channel* are generally used interchangeably, but *pore* is used most frequently to describe structures that discriminate between solutes primarily on the basis of size, allowing the passage of molecules that are sufficiently small to fit. The term *channel* is mostly reserved to describe ion channels [19]. Pore and channel proteins do not require any conformational alteration in order for the solute entering from one side of the membrane to exit on the other side. They may undergo conformational changes, but these regulate whether they are open or closed to solute traffic and play no role in the mechanism of translocation per se. Two major groups of channels distinguish “voltage-gated” from “ligand-gated” channels. Channels are said to be voltage-gated if they open or close in response to a change in the transmembrane potential. The open or closed state of ligand-gated channels is related to the binding of specific signal molecules. The channel formed by gramicidin A is a well-known example of channel. In a hydrophobic environment, gramicidin A forms a helical structure, leaving a pore of about 4 Å in diameter in the center of the helix. All the side chains of the amino acid residues of gramicidin A are hydrophobic. In the helical conformation, these hydrophobic side chains are oriented towards the outside of the helix, which makes the helical gramicidin structure compatible with the hydrophobic interior of the membrane. The selectivity of ions transported by a gramicidin channel is determined by both size and dehydration energies: to enter the channel, the ion cannot be too large and must be stripped of its bound water molecules. Aquaporins are a specialized class of proteins that promote the diffusion of water across membranes. Although water has a rather high permeability across lipid bilayers and can also pass through ion channels, aquaporins are found in most membranes involved in homeostasis, salt (electrolyte) metabolism, and water retention and secretion (kidney and lung epithelia for example).

Facilitated diffusion Facilitated diffusion designates the carrier-mediated diffusion of solutes through the membrane. A carrier is a species that binds specific solutes and translocates them across the membrane. The role of carriers is usually to ensure the transport of polar or ionic substances that could not occur by simple diffusion across the lipid membrane. A carrier often presents a polar interior as binding site for the solute and exhibits a hydrophobic exterior compatible with the hydrocarbon region of the membrane. The carrier masks the hydrophilic nature of the polar solute and the complex thus formed can passively diffuse through the membrane. Like traditional passive diffusion processes, carrier-mediated transport can be driven either by a concentration or an electrochemical gradient of the transported species across the membrane. In all cases, the transport is down the gradient and thus does not require an energy input. This process is however saturable, since it is limited by the number of carriers, and usually exhibits specificity for solute structure. In some cases, it can also be inhibited by structural analogs to the transported solutes. Antibiotics provide examples of carrier-mediated transport. Valinomycin, for instance, is a ionophore that ensures the transport of cations, especially potassium ions, across membranes. This carrier is a cyclic dodecamer: all the polar carbonyls of the amide and ester functions face the inside of the cyclic structure, while the hydrophobic side chains dominate the outside. The cation, usually K^+ , binds to the interior of valinomycin and generates a conformational change in the ionophore: the ring closes in and arranges itself such that the side chains point towards the outside. This conformation allows the translocation of the complex across the membrane by passive diffusion. A dissociation of the complex finally occurs on the other side of the membrane.

Active transport Cells also have transport proteins that transfer solutes across the membrane against their electrochemical gradient. This process is called active transport because an input of energy is needed to bring it about. It is a saturable process and can be affected by competitive inhibitors. The energy to drive active transport may come from a number of sources. The most common source is the hydrolysis of ATP. Others include light energy or the energy stored in ion gradients. Primary active transport processes, which use a direct source of energy, can be distinguished from secondary active transport processes, which are generally coupled with ion gradients (that have been generated by a primary active transport) to achieve for instance the transport of metabolites. Most of the chemical energy in the body is used up to reestablish ion gradients, gradients that keep metabolic processes going, including signaling mechanisms. Primary active transporters are mostly ion pumps, where ion

translocation is mechanistically coupled to an energy-yielding chemical or photochemical reaction. Na^+/K^+ -ATPase, also called sodium pump, is one of the most important enzymes in the plasma membranes of animal cells. This enzyme pumps sodium ions out of the cell and potassium ions into the cell, both against their respective concentration gradients, catalyzing the hydrolysis of ATP and making use of the released energy. Primary active transporters are used to generate voltage and ion gradients across the membrane and secondary active transporters utilize such gradients to drive solute transport. One example is found in the co-transport of glucose and sodium in the intestinal brush border membrane. In this system, glucose transport is coupled with the sodium gradient established by Na^+/K^+ -ATPase. The transport system allows sodium to flow down its concentration gradient, which in turn allows the flux of glucose against its concentration gradient.

1.3.2 Drug transport

1.3.2.1 Drug absorption

The preferred route of drug administration is peroral: about 90% of marketed drugs are administered orally. To reach their target organ, drugs must enter the systemic circulation. Therefore, they have first to be absorbed from the gastrointestinal tract, which requires the passage through barrier membranes. Drug bioavailability is largely determined by the extent of absorption and is also influenced by presystemic metabolism. The ability of a drug to cross membranes will thus affect all aspects of its disposition in the body. The rate of absorption depends both on the physicochemical properties of the drug and on the properties of the membrane. Drugs are predominantly absorbed by passive diffusion across the gastrointestinal membranes. Diffusion can occur transcellularly or paracellularly. However, the paracellular route is negligible for compounds having a molecular weight greater than 200 g/mol, which includes the vast majority of drugs. In the search of new drug candidates, the optimization of delivery processes is essential. The number of newly discovered active compounds does not cease increasing with the continuous advances in rational drug design, combinatorial chemistry, and high-throughput screening techniques, often making delivery problems the rate-limiting step in drug research. A good knowledge of the molecular and physicochemical properties of the drug candidates and a full understanding of the nature of the barriers they may encounter are required to overcome these problems.

1.3.2.2 Physicochemical determinants in drug absorption

In order to predict and evaluate passive drug absorption, it is essential to understand the factors that may limit or enhance absorption. Drug candidates can be characterized by a series of physicochemical properties that is strongly related to their ability to pass through biological membranes and thus to their rate of absorption. The main physicochemical determinants are reviewed in this section.

Lipophilicity Lipophilicity is widely used as a predictor of membrane permeability, since drug partitioning into the lipid bilayer is generally the rate-limiting step for passive diffusion. The most common expression of lipophilicity is the logarithm of the n-octanol/water partition coefficient ($\log P_{\text{Oct/wat}}$). Octanol, with its long alkyl chain and its polar hydroxyl group, presents certain analogies with the amphiphilic lipid components of biological membranes. More or less linear relationships between the logarithm of the permeability coefficients of various solutes in different model membranes and their $\log P_{\text{Oct/wat}}$ values have been found. Nevertheless, the octanol/water system fails into mimicking the highly hydrophobic region of membranes and better correlations are often found using solvents like hexadecane or olive oil. The mentioned solvent systems are however largely isotropic and cannot adequately reproduce the anisotropic features of biomembranes. Anisotropic systems formed from natural or artificial phospholipids have been developed for lipophilicity determination. Drug-liposome partitioning for instance revealed to be a valuable tool to predict drug absorption in the human intestinal tract [32]. Such liposomal systems are generally less discriminating than octanol, and compounds with low $\log P_{\text{Oct/wat}}$ values may show higher partitioning in these systems. Whatever the system selected, the ionization state of the compound has also to be considered. Many drugs are indeed organic acids or bases, which might be ionized depending on the ambient pH. Most commonly utilized approaches calculate $\log P$ values (partition coefficients) for the neutral form of the compound. The estimation of $\log D$ values (distribution coefficients), with explicit consideration of the ionization state of the compound at physiological pH, is often more pertinent for QSAR studies. The general rule stating that only non-ionized (*i.e.* lipid soluble) drugs permeate membranes [33] is questioned by experimental investigations underlining ion partitioning and showing that the behavior of ionizable drugs in the body is controlled by the interactions of both the neutral and ionic forms with the membranes [34, 35].

Hydrogen-bonding capacity A correlation between the hydrogen-bonding properties of a drug and its permeation rate across a membrane is usually observed. In order to enter the hydrophobic core of a membrane, a drug containing polar functional groups has first to break the hydrogen bonds that it may have formed with the water molecules and/or the polar lipid headgroups located at the interfacial region. Depending on the amount of energy required to break these hydrogen bonds, this step might be rate-limiting in the permeation process of the drug molecule through the membrane. The introduction of a descriptor characterizing the H-bond ability of a compound facilitates the prediction of its permeability properties. Numerous studies have shown that the difference between two different logP scales, generally octanol/water minus alkane/water ($\Delta\log P_{\text{oct-alk}}$), is a measure of the hydrogen-bonding capacity [36]. Raevsky and co-workers [37, 38] introduced a new descriptor called “Cad”, corresponding to the sum of absolute values of free energy H-bond factors, and obtained a sigmoidal correlation between the logarithm of the permeability coefficients and the Cad values for a series of structural heterogeneous compounds.

Molecular size Permeability coefficients across biomembranes have been shown to be highly dependent on the molecular size of the permeants [39, 40]. The larger the permeating compound, the lower the permeability coefficient. When the molecular size of the permeant is used to adjust the value of the permeability coefficient, a better correlation is usually found between the logarithmic values of permeability and partition coefficients.

Aqueous solubility Aqueous solubility is another important parameter related to drug absorption and determines the amount of drug in solution available for gastrointestinal absorption. Poorly soluble compounds may suffer from dissolution-rate-limited absorption, which might ultimately lead to incomplete absorption. A relationship between poor solubility and poor absorption can be thus expected and is often verified. Compounds showing a balance between lipophilicity and aqueous solubility represent the best drug candidates for oral absorption.

Conformational variability and molecular surface properties The physicochemical properties of a compound described previously may vary among the possible conformations adopted by the compound. Its molecular flexibility and potential conformational variability have thus to be taken into account when evaluating its ability to permeate biological membranes: the conformational space should be systematically explored to evaluate the contri-

bution of the different conformers to permeation [36]. For instance, conformations favoring internal hydrogen bonds increase the lipophilicity of the solute by reducing its hydrogen-bonding donor capacity and, as a result, enhance its permeation through the hydrocarbon region of the membrane. It is often interesting to determine the solvent-accessible surface area (SASA), which is related to the three-dimensional geometry of the compound and fluctuates with its conformational changes. Hence, the notion of lipophilicity should not be viewed as a static property: the variation of lipophilicity within the conformational space of a molecule is often more pertinent in terms of drug absorption and permeation.

The absorption of compounds by passive diffusion can be reasonably well predicted on the basis of their physicochemical properties. The presence of polar and charged functional groups, low octanol/water partitioning, a substantial number of hydrogen-bonding sites, high molecular weight, and large polar surface area are generally associated with poor membrane permeability. In many cases, however, the consideration of drug properties alone proves to be not sufficient for a proper evaluation of permeation data: permeability coefficients may be overestimated or, on the contrary, underestimated. Another important factor to take into account is, indeed, the nature and the permeability of the membranes that have to be crossed by the drug.

1.3.2.3 Membrane permeability

Depending on the route selected for drug administration, the different physiological barriers encountered by drug molecules have to be identified and their structural, biochemical, and dynamic properties investigated. In the case of oral administration, for instance, the principal physiological barrier that drugs have to pass through is the intestinal mucosa; in the case of transdermal drug delivery, the barrier is the skin. The various membranes found in the body exhibit specific compositions and organizations which have to be known before permeation studies are undertaken.

Independently on the type of membranes, membrane fluidity is generally correlated with membrane permeability and the degree of fluidity influences largely the ability of a solute to pass through the membrane. All factors increasing membrane fluidity (see Section 1.2.4.3, page 39) may also enhance membrane permeability. The formation of structural discontinuities in the bilayer, even only transiently, increases membrane permeability, especially in the case of small permeants which can jump from one discontinuity to another. Such disconti-

nities are for instance observed in the presence of unsaturated lipid chains which generate packing defects in the bilayer interior. Phase separation phenomena within the membrane can also increase permeation processes. Under certain conditions, indeed, the bilayer organization can be interrupted by non-bilayer phases as well as by bilayer phases of different compositions. The regions of mismatch between these coexisting phases can be viewed as fractures within the membrane. Such topological discontinuities may promote solute permeation through the membrane. Drug bioavailability can be improved by absorption-enhancing formulations that increase membrane permeability. The mechanisms by which permeation enhancers increase membrane permeability are various: some enhancers seem to affect membranes by solubilizing membrane components, others induce a dilatation of the cellular tight junctions. Membrane permeability is also particularly sensitive to cholesterol content. A high cholesterol concentration reduces membrane permeability by decreasing the ability of hydrocarbon chains to undergo *trans-gauche* isomerizations and thus increasing ordering of the membrane lipids.

During the diffusion process, drug molecules may exhibit a well-defined orientation with respect to the bilayer normal and adopt specific conformations, different from those generally found in an aqueous medium. This can be related to the highly structured environment of the bilayer and to its difference in polarity compared with water. Because of the anisotropic properties of membranes, their complex structural organization and chemical composition, and their asymmetry, drug transport cannot be correctly described by single parameters such as octanol/water partition coefficients. A detailed knowledge of membrane characteristics is fundamental for a proper estimation of permeation rates. This is especially true for amphiphilic drugs, having a hydrophobic and a hydrophilic gravity center: their orientation within the membrane may be strongly affected by the structural organization of the bilayer as well as by the possible electrostatic and van der Waals interactions with the membrane components.

Chapter 2

Scope of the thesis

Prediction of human intestinal absorption is a major goal in the design, optimization, and selection of candidates for development as oral drugs. Characteristics of the transport of drugs across biological membranes are of crucial importance for the ability of drugs to reach their target and action sites, but are still not well understood at a molecular level.

The description of transport processes first requires a good knowledge of the nature of the permeation barriers. Biological membranes contain a large number of lipid species as well as integral and peripheral proteins. The fluid lipid bilayer represents the core of the membrane and acts as permeation barrier. In spite of their complex and heterogeneous character, biological membranes can be modeled by simple phospholipid bilayers which reproduce the main membrane properties.

Most drugs permeate passively across the lipid part of membranes and their permeation rates depend on their own chemical and physical properties as well as on the macroscopic properties of the considered membrane. Since all macroscopic properties of membranes are determined by the microscopic behavior of the lipid components, a detailed knowledge of the membrane features at a molecular level forms the necessary basis for understanding permeation mechanisms.

The aim of this thesis was to investigate the permeation of small drug-like molecules through a phospholipid membrane at a molecular level using the molecular dynamics simulation technique. This technique is of particular relevance for such a study since all properties of interest can be computed with full atomic detail. As a first step, a realistic model for a phospholipid membrane had to be developed and validated by comparison with available experimental data. The simulation of lipid bilayers is not a straightforward procedure and

requires a systematic search of the optimal simulation conditions. As a second step, interactions of different solute molecules with the phospholipid membrane had to be thoroughly followed to gain insight both into the solute partitioning into the membrane and into the permeation process across the membrane. However, as permeation processes are too slow on the time scale accessible to the molecular dynamics technique, innovative methods had to be introduced.

Chapter 3

Molecular dynamics simulations of lipid bilayers

The simulation of lipid bilayers is not an easy task: a long series of parameters needs to be taken into consideration to ensure the reliability and the stability of the simulations. Methodological aspects are of crucial importance and have to be handled with care. The aim of this chapter is to introduce the main features of the molecular dynamics technique applied to the simulation of membranes. First, the molecular dynamics technique is briefly compared to other computational methods to give an overview of the different possibilities as well as their associated advantages and inconveniences. Second, emphasis is laid on molecular dynamics of lipid bilayers, with the principal strategic issues.

3.1 Computer simulations of lipid bilayers

In recent years, powerful experimental tools such as X-ray crystallography, electron microscopy, infrared and Raman spectroscopy, nuclear magnetic resonance and especially magic angle spinning (MAS) NMR techniques have been developed to characterize membrane properties and have produced detailed pictures of the structure of fluid phase lipid bilayers [41–43]. Despite this progress, some structural and dynamical aspects are still obscure. The high variability of the physiologically relevant fluid crystalline phase makes indeed experimental determinations particularly difficult and available experimental data are not always interpretable in terms of positions, conformations, and motions of constituent molecular groups. Currently, the only complementary theoretical approach which can com-

pete with the degree of resolution reached by modern experimental techniques is computer simulations. The increased computational power and the introduction of efficient algorithms in the last decade have opened new ways to study lipid bilayers. The motivation underlying computer simulations is the amount of information which can be gained at the atomic level and which greatly exceeds the information that may be obtained from the necessarily more coarse experiments. Various computer simulation techniques have been developed in order to assess specific properties of the system studied. A distinction can be made between *static equilibrium properties*, such as average structural parameters or the average potential energy of the system, and *dynamic or non-equilibrium properties*, such as viscosity or diffusion coefficients. The choice of the technique used depends on the question asked, on the degree of precision sought, and on the capacity of the method to yield reliable results. The main computational techniques and molecular representations employed for the study of lipid bilayers are presented in this section. Emphasis is laid on the molecular dynamics technique which was selected for the investigations described later on in this thesis.

3.1.1 Mean field versus atomistic simulations

A system can be simulated using two types of representation: a mean field representation or an atomistic one. The choice of the one or the other approach defines the degree of accuracy with which the lipid bilayer is modeled.

In mean field simulations, the lipid bilayer is generally represented by a simple hydrophobic slab, oriented in the x,y -plane and separating two hydrophilic phases. In this bilayer model, lipid and water molecules are not explicitly included. An empirical potential energy function describes the partitioning of hydrophilic and hydrophobic parts of a given molecule into the lipid bilayer. This function consists of bonded and non-bonded terms to which a hydrophobic interaction term is added [44]. This mean field representation has been further refined by introducing a dipole potential that accounts for the decrease in dielectricity across the water/lipid interfacial region from the water phase to the hydrocarbon interior [45].

Atomistic simulations treat lipid and water molecules explicitly, providing a more detailed insight into the lipid bilayer at the atomic level. The level of detail may vary depending on the type of the atomic representation used. In an all-atom representation, all hydrogens are included explicitly; in a united-atom representation, non-polar hydrogens (e.g. hydrogens of methylene and methyl groups) are merged into the central carbon atoms, polar hydrogens only are treated explicitly. All-atom representations give in principle better results for stud-

ies on diffusion and relaxation phenomena, but are computationally expensive and become unsuitable for large systems. The reduced number of non-bonded interactions in a united-atom model makes this representation very attractive, since the calculations are considerably speeded up.

3.1.2 Monte Carlo simulations

Monte Carlo (MC) simulations are based on statistical thermodynamics: samples are drawn from a probability distribution, often the classical Boltzmann distribution, to obtain thermodynamic properties, minimum-energy structures, or just to sample conformers as part of a global conformer search algorithm. According to this theory, a system can be fully described by a weighted sum of all possible configurations. As it is impossible to sample the whole configurational space, approximations which converge to the exact solution after a finite number of sampling steps are needed. Such an approximation has been developed by Metropolis and co-workers [46]. The initial configuration of the system is described by a set of atomic coordinates defining the starting point. The energy of the system is then computed, based on the underlying force field. A random perturbation, called MC move, is applied to the system. After comparison of the energy before and after the perturbation, the move may be accepted or rejected. The move is accepted if the energy after perturbation is lower. In the case of no energy change, the probability of acceptance is calculated according to the Boltzmann distribution. In systems with mean field approximation of the surrounding environment, MC calculations are particularly effective to sample the configurational space since non-physical moves, such as translation or rotation of whole lipids within the bilayer, are allowed. In systems with an atomistic description of the environment, non-physical moves would lead to high energies due to unfavorable steric interactions occurring in the dense particle ensemble [44].

MC points belonging to the same distribution are in principle independent and can come from very different regions of configurational space. In contrast to a molecular dynamics (MD) simulation (see next section), there is no equation of motion, *i.e.* no physical time connecting the sampled configurations. In MC simulations, average static properties of the system are thus obtained by ensemble averaging (*i.e.* by averaging the properties of interest over the sampled configurations) and not by time averaging as it is the case in MD simulations.

3.1.3 Molecular dynamics simulations

The basic principle of molecular dynamics is to reproduce the motional behavior of a system in time. More precisely, the time evolution of a set of interacting atoms is followed by integrating their equations of motion. MD follows the laws of classical mechanics and most notably Newton's law. For a system consisting of N interacting atoms, atomic trajectories are calculated from Newton's equations of motion:

$$F_i(t) = m_i a_i(t) = m_i \frac{d^2 r_i(t)}{dt^2} \quad (3.1)$$

r_i are the position vectors of the atom i , $a_i = \frac{d^2 r_i(t)}{dt^2}$ its acceleration, and F_i the force acting upon it due to its interaction with the other atoms of the system. The required force is obtained by derivating the interaction potential V between the atoms:

$$F_i = -\frac{\partial V(r_i)}{\partial r_i} \quad (3.2)$$

Given a set of initial coordinates of the atoms in the system at time $t = t_0$, the position of an atom at time $t = t_0 + \Delta t$ is obtained by solving Equation 3.1 for all atoms – Δt being the integration time step. The atom coordinates as a function of time constitute a trajectory of the system. The form of the potential function and the type of algorithm used for integration then dictates the time step. This one must be small enough to avoid integration errors which can lead to an unacceptable drift in the energy. Owing to the fast vibrational motion of the atoms, a time step of 1 fs is usually used. Integration of Equation 3.1 cannot be done analytically for a multibody system, so that numerical integration methods have to be employed. The Verlet-Leap-Frog algorithm is generally adopted to update the time step with Δt and requires that the velocities at $t = t_0 - \frac{\Delta t}{2}$ are known. If the corresponding velocities are not available, they are typically obtained from a Maxwell-Boltzmann distribution and are scaled (or rerandomized) until kinetic and potential energies are in equipartition and the target temperature is reached.

Hence, a starting configuration of the system has first to be chosen, the system is then heated until the desired temperature is reached and simulated for a while to allow relaxation. After the system has reached an equilibrium state, the “productive” trajectory starts, over which macroscopic properties of the system can be averaged.

All the information necessary to describe the system simulated is contained in the interaction potential V , which is a function of the underlying force field. A force field can be

defined as a set of equations (potential functions) on the one hand, and parameters on the other hand, characterizing the strength of the various interactions within the system. Both components – potential functions and parameters used in these functions – are however interdependent and are combined to form a consistent set. The potential functions can be divided into a non-bonded term, describing interactions between any pair of non-bonded atoms, and a bonded term, describing interactions between atoms connected by chemical bonds. Non-bonded interactions are subdivided into electrostatic and van der Waals interactions. Bonded interactions consist of bond, angle, and dihedral terms. In the MD simulations performed in this thesis, the non-bonded potential V_{nb} between atoms i and j contains repulsion and dispersion terms combined in the Lennard-Jones (LJ) 12-6 potential V_{LJ} (the repulsive part falls off as $1/r^{12}$ and the attractive part as $1/r^6$), and an electrostatic term described by the Coulomb potential V_C :

$$\begin{aligned} V_{nb}(r_{ij}) &= V_{LJ}(r_{ij}) + V_C(r_{ij}) \\ &= \frac{C_{ij}^{(12)}}{r_{ij}^{12}} - \frac{C_{ij}^{(6)}}{r_{ij}^6} + f \frac{q_i q_j}{\epsilon_r r_{ij}} \end{aligned} \quad (3.3)$$

r_{ij} is the distance separating atoms i and j , $C_{ij}^{(12)}$ and $C_{ij}^{(6)}$ are the LJ parameters, q_i and q_j are the partial charges carried by atoms i and j , f is equal to $1/4\pi\epsilon_0$, where ϵ_0 is the vacuum permittivity, and ϵ_r is the relative dielectric constant. Concerning the bonded interactions, bonds and angles are described as harmonic oscillators and dihedral angles by a cosine expansion. The bonded potential V_{bd} used is of the form:

$$\begin{aligned} V_{bd} &= V_b(r_{ij}) + V_a(\theta_{ijk}) + V_d(\phi_{ijkl}) \\ &= \frac{1}{2}k_{ij}^b (r_{ij} - b_{ij}^0)^2 + \frac{1}{2}k_{ijk}^\theta (\theta_{ijk} - \theta_{ijk}^0)^2 + k_{ijkl}^\phi \left(1 + \cos(n\phi_{ijkl} - \phi_{ijkl}^0) \right) \end{aligned} \quad (3.4)$$

V_b describes bond stretching, V_a bond angle vibration, and V_d dihedral angle potential. k^b , k^θ , and k^ϕ are force constants for bonds, angles, and dihedrals; n is the dihedral multiplicity; b^0 , θ^0 , and ϕ^0 are equilibrium values for bond lengths, angles, and dihedral angles.

3.1.4 Hybrid simulations

Hybrid simulation procedures, mixing MC and MD techniques, may be used to accelerate the equilibration phase of the simulated system. Chiu *et al.* reported an equilibration pro-

cedure consisting of alternating MD trajectory calculations (in a constant surface tension and temperature ensemble) with configurational bias MC moves to different regions of the configurational space of a hydrated lipid bilayer (in a constant volume and temperature ensemble) [47]. Applying this procedure, equilibration was reached three times as fast in CPU time as with a pure MD simulation. The configurational bias Monte Carlo approach (CBMC) was originally developed by Siepmann and Frenkel [48, 49]. CBMC moves across energy barriers more readily and efficiently than MD or conventional MC. Efficiency is achieved via reduced degrees of freedom, focusing on important transitions in configurational space. MD, on the other hand, replicating the continuous motions of the system, explores local regions of the configurational space more thoroughly than CBMC. When these procedures are alternated, the CBMC technique allows the system to experience substantial conformational changes (provided these changes are energetically favorable), while the subsequent MD calculation explores the region of conformational space which was perturbed by the CBMC move.

3.1.5 Coarse grain models

The study of collective molecular behaviors found in lipid membranes is currently of great interest. Indeed, many key biological processes occur at the membrane level and include, for instance, membrane fusion, membrane-protein interactions, formation of micron size domains in membranes (called “rafts”)... A broader understanding of lipid interactions at a mesoscopic level is therefore desired. Atomistic simulation techniques provide accurate lipid membrane models, but current algorithms and computer power limit such studies to domain sizes of 5-10 nm and time scales of about 10 ns, making the investigation of collective phenomena difficult or even impossible. Simplified models of the coarse grain (CG) type have been introduced with the ambition to bridge the gap between full atomistic detail and the mesoscopic regime. In coarse grain models, solute and solvent sites are usually represented as a group of atoms that interact in an effective way, reducing in this way the computational time needed for the calculations. Coarse grain models can be adjusted to mimic a specific system instead of a general phenomena [50]. Lopez *et al.* constructed a dimyristoylphosphatidylcholine (DMPC) lipid membrane using simplified representations for water, hydrocarbon chains, and phospholipid headgroups [51]. Each type of molecules was modeled so as to reproduce some key physical or structural features known from experiment or atomistic simulations. Single spherically symmetric sites were used to represent the choline,

phosphate, glycerol, and ester groups. In the lipid tails, triplets of methylene groups (CH₂)₃ were also fused to single spheres and linked together to form chains using stretching and bending potentials. Simulation of the DMPC bilayer using this coarse grain model revealed to be about four orders of magnitude less time demanding than an all-atom simulation.

3.1.6 Applications of computer simulations

In the biomolecular area, three types of applications of computer simulations may be distinguished. Firstly, simulations can be simply used to sample the configurational space of a system and to explore which conformations of a molecule are thermally accessible. Structural data obtained from experiments, for instance crystal data from X-ray diffraction, can be thus refined by a simulation protocol. Secondly, simulations enable one to determine equilibrium averages, which can include structural as well as thermodynamic characteristics of the system. Sufficient sampling of the configurational space is a necessary condition for obtaining reliable averages from a simulation. Thirdly, the natural dynamics of a system can be studied by simulations and motional properties can be assessed. Depending on the approach employed, insights into various time scales of the thermodynamic behavior of the considered system may be collected.

Concerning the two first application areas, MD as well as MC simulations are appropriate. The MD technique only is however relevant to follow the motions of a molecule and their time development. Indeed, in contrast to the MC method, MD is a deterministic technique: given an initial set of positions and velocities, the subsequent time evolution is in principle completely determined. Thus, if both simulation methods can be theoretically used to generate a representative equilibrium ensemble, the MD technique only is adapted for the analysis of dynamic events. Furthermore, although MC simulations are more simple than MD ones – they do not require the computation of forces – they generally do not give better statistics than MD in a given amount of computational time. The MD technique is for these reasons often preferred to MC. If the starting configuration is far from equilibrium, hybrid procedures (see Section 3.1.4, page 57) combining both techniques can be helpful to achieve a complete relaxation of the system.

In the current work, the MD technique, in association with a united-atom representation of the system, has been selected in order to investigate the properties of a lipid bilayer. This choice can be justified by the importance of the dynamic aspect in the study and the modeling of lipid membranes (see Chapter 1, Section 1.2.4, page 36). If the use of coarse

grain models enables one to describe collective phenomena occurring at mesoscopic scales, such phenomena are unfortunately out of reach for atomistic models. The latter models offer, however, more detailed information on the structure of the system and more closely reproduce the properties of real lipid bilayers, whereas much of the molecular complexity of the lipid bilayer environment is ignored in the CG models which only give a simplified view. Moreover, coarse grain models cannot be truly predictive in the absence of sufficient data for careful parameterization.

3.2 Molecular dynamics studies of lipid bilayers

3.2.1 Review

MD simulations provide a powerful tool to analyze biomolecular systems from an atomic perspective with a level of detail missing in any other approach. This technique has been widely used in studies of proteins and nucleic acids, but has been less applied to the analysis of biological membranes for several reasons. Biomembranes are indeed very complex in terms of both structural and dynamic properties. Unlike proteins or nucleic acids which have well-defined three-dimensional structures, membrane components derive a large majority of their properties and functions from their fluid nature. The fluid character of the physiologically relevant fluid crystalline phase makes experimental studies particularly difficult and only limited atomic-level data from X-ray or neutron diffraction have been for long accessible, compared with the amount of data available on proteins and nucleic acids. As structures from X-ray crystallography are usually taken as starting configurations for MD calculations, the difficulty in obtaining such data for lipid bilayers may have slowed down the development of the MD technique in the biomembrane field. Another reason may be the difficulty in developing force fields able to reproduce the dynamic properties of lipid molecules. Since the fluidity of lipid bilayers determines to a great extent their structural and functional properties, reliable computer models have to include the flexible nature of the lipid molecules, static models being unrealistic. The occurrence of complex hydrophilic and hydrophobic interactions within membranes also poses formidable modeling challenges. For all these reasons, simulations of lipid membranes have attracted in the past far less attention than the molecular modeling of small molecules and proteins. More recently, however, with the increasing computational capacities and the awareness of the biological importance of membranes, the modeling of lipid bilayers has emerged as a growing research field [44].

In order to begin to understand membrane properties, simple model systems have first been investigated. The earliest studies of lipid systems appeared in the literature in the 1980's. Monolayer [52] and bilayer [53] membrane simulations were performed on simplified models, in which the lipid headgroups and/or hydrocarbon tails were stylized and the solvent disregarded. The application of MD simulations to lipid bilayers with explicit solvent was pioneered by Egberts and Berendsen in 1988 [54]. They proceeded to an all-atom simulation of a system consisting of a mixture of water, soap (sodium decanoate), and alcohol (decanol). Such ternary systems form stable multilamellar phases and provide good models for the study of the general behavior of lipid membranes, although they often exhibit a denser packing and a higher ordering degree than phospholipid membranes. Egberts published in a PhD-thesis in 1988 [55] and in an article in 1994 [56] the first simulation of a phospholipid-water bilayer system in full atomic detail. In 1992 and 1993, several research groups reported simulation studies of single component membranes consisting, for instance, of dipalmitoylphosphatidylcholine (DPPC), dilauroylphosphatidylethanolamine (DLPE), or palmitoyloleoylphosphatidylcholine (POPC) molecules, demonstrating that the MD technique applied to patches of a few phospholipids in water has enormous potential and can give detailed insights into lipid motions and interactions.

During the past ten years, computer hardware has become faster and cheaper, software problems have found innovative solutions, so that impressive improvements in the size and complexity of the simulated systems as well as in calculation time have been achieved. These improvements enable one nowadays to simulate mixed lipid systems (mixing for instance two type of phospholipids [57] or introducing a certain amount of cholesterol [58–64]), to include small molecules like drugs into the bilayer [65–73], or to insert peptides or even membrane proteins to study their interactions with the lipid components [61, 74–85]. These new applications have been performed with more or less success and the simulation of lipid-protein systems in particular still remains a very challenging area, which can only benefit in the next years from the increase in simulation time scale and system size.

3.2.2 Strategic issues

The numerous MD simulations of lipid bilayers which have been reported vary in different aspects. At first sight, they may be distinguished by different microscopic interaction parameters (*i.e.* force fields) and by different macroscopic boundary conditions (*i.e.* different ensembles). In addition, more technical issues like the choice of the method used for the

computation of van der Waals and electrostatic interactions or the length of the time step may differ. This introduces the problem of combining the right conditions and parameters in order to obtain a correct bilayer model system, such simulation conditions being indeed an integral part of the model.

3.2.2.1 Force fields

The choice of interatomic force fields and related parameters is of crucial importance for the simulation of a biomolecular system. The ability of a model membrane to reproduce realistic static and dynamic features depends strongly on the balance between attractive and repulsive forces, which directly results from the force field employed. A force field is indeed required to compute the potential energy of the system as a function of the instantaneous atomic coordinates. Various force fields have been developed to simulate proteins and nucleic acids; no special force fields have however been designed for the modeling of lipid bilayers [44]. With the exception of charges, which are often derived from *ab initio* quantum chemical calculations on lipid fragments, the parameters in the potential functions are thus usually taken from pre-existing force fields for proteins or nucleic acids. The most popular force fields used in membrane simulation studies are the AMBER [86], the CHARMM [87], and the GROMOS [88] force fields. One of these force fields is often applied in combination with the OPLS (Optimized Potentials for Liquid Simulations) parameter set [89] for the computation of the non-bonded interactions.

Over the last decade, effort has been spent to adapt charges and/or force field parameters in order to obtain results consistent with experimental data. In 1996, Schlenkrich *et al.* developed, within the CHARMM force field, a set of potential functions for saturated phospholipids that better reproduced experimental results [90]. Feller *et al.* extended this set in 1997 [91] to include unsaturated hydrocarbon chains and refined it in 2000 [92]. Berger and co-workers modified in 1997 the Lennard-Jones parameters of the methylene and methyl groups in the lipid chains and, together with the GROMOS force field for the calculation of the bonded interactions and the OPLS force field for the computation of the non-bonded interactions, could reproduce the experimental density of a DPPC bilayer within a few percents [93]. In 1999, Smondyrev and Berkowitz redefined the torsional parameters implemented in the AMBER force field for the DPPC molecule to fit geometry and energy profiles with *ab initio* calculations of phospholipid fragments [94]. The resulting force field led to excellent agreement with experimental data.

Even if the force fields used in membrane simulations have not been originally derived specially for lipids, the refinements that have recently been undertaken yield lipid bilayer models whose properties are rather in good agreement with available experimental data [44]. It should be however noted that details in simulation protocols may influence the force field parameters, so that an adjustment of the parameters may be necessary when simulation conditions or algorithms are changed.

3.2.2.2 System size and boundary conditions

According to the size scale of a MD simulation, a real lipid membrane is of infinite size. Only patches of a few lipid molecules can be generally simulated. This corresponds to a truncation of the system and can introduce possible artifacts. Indeed, a lipid membrane in the fluid state behaves like a smectic liquid crystal, exhibiting a continuous spectrum of normal mode frequencies and wavelengths for thermally induced fluctuations in thickness and curvature. A truncation of the system eliminates all wavelengths longer than the simulation box. Another problem induced by truncation is that the simulation system is surrounded by a vacuum, leading to so-called “edge effects”: the behavior of the molecules located at the boundaries deviates from that of the molecules in the center. In the case of a very large system, the number of boundary molecules would be small enough to be neglected. The simulation of such large systems is unfortunately not feasible presently, so that membrane models are usually restricted to relatively small samples consisting of a few hundreds of lipid molecules. In this case, about 40% of the lipids belong to the border region.

The commonly used method to eliminate edge effects is the implementation of periodic boundary conditions (PBC), which ensure that the system does not have an abrupt border with vacuum. It is assumed that the simulated system is surrounded on all sides by an exact replica of itself to form an infinite lattice. Thus, when a molecule leaves one side of the system, an identical molecule enters through the opposite side at the same time and at the corresponding position. Interactions of a molecule with its surroundings is calculated from both the original box and the neighboring cells. PBC are generally employed in liquid state simulations for systems presenting a homogeneous character in terms of chemical or structural composition. PBC have been widely used in membrane simulations, as they naturally emulate the effectively infinite extent of the membrane. PBC present nonetheless a few disadvantages. The use of PBC inhibits the occurrence of long wavelength fluctuations in the simulated membrane: for a box side L , the periodicity will suppress any fluctuations with

a wavelength greater than L [95]. The membrane simulated with PBC is indeed precluded from exhibiting bending or splay modes, because such modes would prevent the matching of the membrane with its image at the lateral boundaries of the central unit cell [96]. It was also shown that PBC can induce some artifacts, such as the occurrence of spurious collective motions or orientations, e.g. an excessive collective tilt of the hydrocarbon chains [97] or the introduction of anisotropies into the membrane structure. Such effects can be alleviated by enlarging the simulation box: if the box is large enough, the boundaries have little effect on the interior of the box. This is of course at the cost of computational speed. It should be mentioned that, after the equilibration phase of the simulation has been reached, doing a sampling run on a large membrane patch is almost as economical as on a small one. A larger system gives indeed more information per picosecond of simulation time than a smaller one, since it provides data sampling not only temporally but also spatially. After equilibration of the system, a membrane consisting of 100 lipid molecules will provide as much data in a 100 ps simulation as a membrane of 50 lipids in 200 ps; the data collected with the larger membrane will be furthermore less affected by boundary artifacts.

The competing method to face edge effects is to enclose the system in a sphere, with restraints and often stochastic forces acting at the boundary to mimic an extended system. One possibility consists in surrounding the system with repulsive walls. Another possibility consists in constraining the outermost atoms to their initial position by a harmonic force [44]. Stochastic boundary conditions fail, however, into generating an effectively infinite bilayer system and the restraints applied to the molecules located at the boundaries may influence the behavior of the rest of the system.

Although computationally more expensive, PBC are generally preferred to stochastic boundary conditions for the simulation of bilayer systems. It should be however pointed out that a small system infinitely replicated cannot be completely compared with the macroscopic system that it is supposed to represent.

3.2.2.3 Macroscopic ensembles

The sensitivity of lipid bilayers to the macroscopic boundary conditions applied in a simulation has been shown in several studies [98, 99]. Several macroscopic ensembles can be distinguished and the choice of a specific ensemble may influence the results obtained from the simulation. While the temperature T and the number N of atoms are generally kept constant, the volume V of the simulation box, the external pressure P , or the applied sur-

face tension γ may be kept constant or not. The most commonly ensembles applied to lipid bilayer simulations are described and commented below.

***NVT* ensemble** A certain number of membrane simulations have been performed with the so-called canonical ensemble *NVT*, in which the volume of the unit cell is kept constant [100, 101]. Assumptions about the total molecular density of the simulated system have to be made in order to be able to fix the volume of the unit cell. Experimental values for the area per lipid and the bilayer lamellar spacing (*i.e.* bilayer repeat distance) are usually used to determine the box size. Depending on the accuracy of the available experimental data, the model system will restore with more or less success the features of membrane structure and properties. The density of the system is directly related to the physical state of the membrane and has to be finely adjusted so as to reproduce a liquid crystalline state. If the density is too high, the chain packing becomes too tight, the global ordering increases, and a gel-like state may be simulated. If the density is too low, a gap might be observed between the two monolayers. If the estimation of the density is correct, the main membrane properties will be well replicated. The principal danger of the *NVT* ensemble is that the results might look promising even if there are underlying flaws in the calculation procedure or in the force field. As long as the system density is right, the simulation will produce a rather good looking fluid phase membrane irrespective of the quality of the force field or other computational parameters, since the constraints applied on the box volume prevent the system from going to an incorrect density. Furthermore, accurate experimental data about structural membrane parameters are often limited to a few single lipid component bilayers and, in the case of membranes made up of mixture of lipids, experiments provide only indirect guidance for assigning the appropriate simulation cell dimensions, making membrane simulations using constant volume algorithms difficult.

***NPT* ensemble** The constant pressure and temperature or isobaric-isothermal ensemble *NPT* is most often applied to the simulation of membranes. After specification of the pressure tensor P , the size and shape of the simulation box adjust to maintain the pressure along each box dimension. Or, in other words, the computed pressure is fed back as a control on the size of the system. If the instantaneous pressure is higher (lower) than the set point, the system is expanded (contracted) slowly as the simulation proceeds. Thus, using this method, the initial dimensions of the system do not need to be approximated, since the system finds its size by itself, based on the force field employed. This ensemble opens up the possibility for

validating simulations by checking their ability to reproduce important structural parameters like the area per lipid or the bilayer thickness when they are known and for predicting these parameters when they have not been determined experimentally. Generally, an isotropic pressure tensor ($P_{xx} = P_{yy} = P_{zz}$) is applied, with both lateral and perpendicular components usually equal to 1 bar (it should be noted that, within the numerical accuracy of pressure algorithms, a pressure of 1 bar is equivalent to a pressure of zero). An isotropic pressure implies that there is no surface tension in the bilayer. The greatest advantage of the *NPT* ensemble is that it provides a stringent test of the potential energy parameters implemented in the force field: the system adjusts its density according to the force field *i.e.*, if the latter is appropriate, the right density will be naturally reached during the simulation.

***N γ T* ensemble** The constant surface tension and temperature ensemble is a variant of the *NPT* ensemble and corresponds to a constant anisotropic pressure tensor. Anisotropic pressures along and perpendicular to the membrane plane give rise to a surface tension in the plane of the bilayer. The surface tension γ is defined by the relation $\delta W = \gamma dA$, where δW represents the work required to change the surface area by dA . This also means that the surface tension is equal to the derivative of the free energy with respect to the area at constant temperature and volume: $\gamma = \left(\frac{\partial F}{\partial A}\right)_{T,V}$. Unstressed lipid bilayers are free to adjust their surface area to attain an equilibrium with the surroundings. In terms of energy, the bilayer tends to adjust its surface area so as to minimize its free energy. Owing to the hydrophobic effect, an increase of the area leads to an increase in free energy. If this were the only parameter to consider, a membrane would minimize its area, going into an ordered gel phase whatever the temperature. The entropic contribution to the free energy has also to be considered: the entropy of the system grows upon increasing the area, which reduces the free energy. A small surface area forces the chains into a more ordered state, reducing the entropy of the system and thus increasing the free energy. To reach its thermodynamic equilibrium, the membrane has thus to find a balance between the enthalpic and entropic terms. When the minimum in free energy is attained, the surface tension is then, per definition, equal to zero [102]. In 1995, Chiu *et al.* introduced a surface tension into the simulation of a DPPC membrane, arguing that the surface tension of a bilayer is twice that of the corresponding monolayer [97]. This assumption was however doubtful since the main contribution to the surface tension in an air-monolayer-water system comes from the interface between the air and the hydrocarbon chains and not between the headgroups and water. The explicit inclusion of a surface tension was also adopted by Feller and Pastor in a series of DPPC bilayer simulations [99].

They recognized that the surface tension of a bilayer patch is surely zero on a large length scale (microns), but put forward that a bilayer on the typical length scale of a MD simulation (nanometers) may exhibit a finite surface tension at the surface area that minimizes its free energy. They claimed that the application of a nonzero surface tension may be appropriate to compensate for the absence of long wavelength undulations in the small systems used in simulations, the applied surface tension being then considered as a correction for a finite-size effect. As the suppression of undulations is even reinforced by the confining effect of PBC, a nonzero surface tension would be only the expression of the suppressed undulations. Or, in other words, a tension would be required to remove the undulations which are normally present in real membranes, but absent in simulated ones. Marrink and Mark however showed in an extensive series of glycerolmonoolein (GMO) bilayer simulations that, at stress free conditions, the equilibrium area per lipid does not strongly depend on the system size and concluded that the application of an external surface tension to compensate for suppressed fluctuations is not necessary [103].

Discussions are still ongoing to answer the question: “what are the appropriate ensembles for simulating hydrated lipid membranes?”. While the *NVT* ensemble is the standard condition to simulate a protein in a crystal lattice, simulating a lipid bilayer at constant volume is rather not recommended, because the dimensions of the simulation unit cell are then determined by the area per lipid and the bilayer repeat spacing which are experimentally often not well known. Furthermore, even if the system density is correct, the *NVT* ensemble may dissimulate shortcomings in the force field. Performing simulations with the *NPT* ensemble has the advantage to let the implemented interaction potential determine the optimal system dimensions and then to assess the quality of the simulation by comparing the properties that one is interested in with available experimental data. Employing an isotropic pressure tensor is equivalent to imposing a condition of zero surface tension on the lipid interface. In the case of an unstressed bilayer, the surface tension is equal to zero at the free energy minimum. In the bilayer patches simulated, it has been argued that it is necessary to apply a finite surface tension to compensate the fact that longwave undulations are suppressed in smaller systems, especially under PBC. There is unfortunately little guide from experiment on the precise value to adopt for the surface tension. Lindahl and Edholm attempted to split up the surface stresses in a DPPC bilayer into several components and to determine each of them using local virial calculations [104]. They showed that the tension in the bilayer is the sum of two large opposing tensions: an attractive energy in the headgroup region and

a repulsive one in the hydrocarbon region. For the overall surface tension to vanish, these two contributions must exactly balance. This is effectively what they found despite a large uncertainty. Such calculations are indeed very sensitive to the force field employed, the treatment of long-range electrostatics, and other technical parameters of the simulation protocol. Consequently, it is still not clear whether a surface tension has to be applied or not in lipid membrane simulations. But, insofar as it is very difficult to assign a concrete value to the surface tension and it is quite possible that the required tension is equal to zero, the majority of lipid simulations are performed using the *NPT* ensemble which seems to provide reliable macroscopic conditions.

3.2.2.4 Starting structures and equilibration procedures

Developing suitable initial conditions for the MD simulation of a lipid bilayer in the liquid crystalline phase is not straightforward. The major problem is reaching equilibrium in finite computational time scales. Several approaches have been reported in the literature to construct starting structures.

One basic approach is to start with ordered lipid conformations based on the few available X-ray structures of phospholipids in the crystalline state. Crystal structure data are then used to build a membrane lattice. While this procedure is standard for the simulation of less heterogeneous systems such as proteins, it can require very long equilibration times in the case of lipid systems, unless special techniques are applied. Crystal structure configurations of proteins for instance are indeed similar to configurations found in natural environments and rapidly evolve to an equilibrated state. Lipid crystal structures are highly ordered with all-*trans* conformations of the alkyl chains and are therefore far from equilibrium relative to the fluid-like physiological state. Starting from a lipid crystal structure, simulated annealing techniques are often employed in order to save equilibration time. The system is heated up to such a temperature that energy barriers are easily overcome and lipid conformations with disordered hydrocarbon tails are generated. The system is then cooled down, often using a multistep procedure. The use of high-temperature MD to achieve disordering of the system suffers, however, from the inability of MD to rapidly evolve the disorder towards an equilibrium configuration, so that the generated disordered structure may be far from an equilibrium state [47].

Another approach consists in assembling the bilayer with conformationally averaged lipids designed to be representative of a fluid phase. The various conformations are taken

from a library of structures obtained, for instance, by sampling from a mean field. The lipids are then put on a grid to build up the bilayer system, using programs for the placement of adjacent molecules at energetically feasible positions and orientations. Starting from these randomized configurations, a MD simulation is subsequently performed to drive the system to equilibrium. This method was introduced by Venable and Pastor and appears to speed up equilibration times [105]. The main difficulty is the selection of the initial configurations: considering the large number of degrees of freedom, a rational choice of configurations representing equilibrium states is delicate. Since MD trajectories sample a very small configurational space in subnanosecond time scales, the equilibration phase will be really speeded up provided that the initial random configurations are fortuitously near equilibrium.

An alternative method based on hybrid MC/MD simulations, developed by Siepmann and Frenkel, was already described in Section 3.1.4, page 57 [48,49]. This approach, called configurational bias Monte Carlo (CBMC), proves to be particularly efficient for the sampling of flexible-chain torsion space. The ability of CBMC to sample “allowed” configurational space rapidly leads, in conjunction with MD, to a quick equilibration of bilayer systems consisting of either ordered or random configurations.

Equilibration times required for MD lipid bilayer simulations are often long, of the order of a few nanoseconds or more, depending on the starting structure and the simulation conditions. The construction of a suitable initial configuration for the membrane system is therefore critical to the success of simulations covering less than several nanoseconds: although the precise distribution of tail dihedrals equilibrates reasonably fast, a strong correlation of the orientation of entire lipids with the starting structure persists in short simulations [106]. In principle, simulation times should be extended until the system variables no longer change. The most commonly used factors to judge the status of a membrane simulation include the potential energy or the temperature of the system as well as the area per lipid. Ideally, the converged structure of the lipid membrane should be completely independent of the initial conditions, *i.e.* should not be trapped in a local energy minimum. In other words, MD simulations starting from different initial conditions should present the same statistically averaged quantities [107].

3.2.2.5 Simulation time steps

Owing to the long equilibration times needed and to the presence of a very wide range of time scales in the dynamics of lipid membranes, the simulation of such systems is a

rather computationally intensive undertaking. To be able to extend the simulation time, a time step as long as possible has to be used to integrate the equations of motion. Usually, the motions of principal interest, associated with typical biological processes, occur at a relatively long time scale. The limiting factors that govern the size of the time step are the fastest vibrations, like bond stretching and angle bending. These fast motions are not interesting *per se*, but need to be properly sampled to generate an accurate trajectory and keep the large-scale dynamics correct. The time step has thus to be small enough so that these fast degrees of freedom are evolved reasonably, thereby ensuring numerical stability. To deal with this problem, several types of time-saving schemes have been proposed.

An attractive solution is to remove the fast vibrations in bonds and/or angles by performing constraint dynamics. Constraint algorithms are applied to keep bond lengths and/or angles equal to their constant equilibrium values. A longer time step can be thus used: errors when integrating bond and angle oscillations are avoided, and slow and large scale dynamics is not affected much. The most popular algorithm is SHAKE: for each bond or angle, the force necessary to restore it to its equilibrium value is computed [108]. Since bonds/angles in molecules are coupled, the procedure has to be iterated until convergence is reached. For time steps above 2–3 fs and when displacements are too large, convergence is not always achieved. The iterative nature of SHAKE makes moreover its parallelization difficult. A non-iterative method based on matrices, called LINCS (LINEar Constraint Solver), has been developed by Hess and co-workers [109]. LINCS is a more stable and efficient constraint algorithm which allows time steps of at least 3–4 fs. LINCS can be easily parallelized and is three or four times faster than SHAKE at the same accuracy.

Another alternative to relieve the limitation related to the sampling of the fast degrees of freedom is the implementation of multiple time step (MTS) integrators [110]. The various forces present in the system are separated into several components according to their characteristic time scales. The equations of motion involving the fast components are integrated with a small time step, whereas a longer time step is used to handle slow motions. This results in a significant decrease of CPU time in the simulation.

3.2.2.6 Treatment of long-range interactions

The membrane system is a very large and flexible system in which all components are tightly packed together and the bilayer structure is maintained only by the non-bonded interactions. The treatment of these non-bonded interactions in a simulation requires thus special care.

While van der Waals interactions rapidly decrease with increasing distance (fast decline of the Lennard-Jones potential), Coulomb interactions are quite long-ranged. The correct handling of long-range electrostatic interactions in phospholipid bilayers is of particular concern since the headgroups of many phospholipids are highly charged or contain strongly polar groups. The most straightforward way of calculating electrostatic interactions would be to simply evaluate the Coulomb interactions between each pair of charged atoms in the system. In the simulation of large systems like membranes, the computation of electrostatics constitutes one of the most expensive tasks and the computational cost to include all atom pair interactions is prohibitive. To reduce computational effort, approximations have to be introduced into the calculation of the long-range electrostatic contribution. Since these approximations often belong to the most drastic ones in a simulation procedure, they are expected to have a significant influence on the system structure and dynamics and, for this reason, need to be applied with care. The most common techniques used for the treatment of electrostatics are briefly surveyed below. Advantages and drawbacks of each technique when applied to the simulation of lipid bilayers will be examined in detail in Appendix B.

Truncation techniques One of the most frequently used techniques applied in biomolecular simulations to speed up the computations is truncation of the long-range electrostatic forces. These so-called cutoff methods are also widely used in membrane simulations. Interactions beyond a predefined maximum, the cutoff distance R_C , are neglected to reduce the amount of time spent computing the large number of pairwise electrostatic interactions present in the simulated system. Such spherical cutoffs can be implemented in different ways, depending on whether the distance is calculated between the interacting atoms (atom-based) or between groups of atoms (group-based). In the case of atom-based truncation, electrostatic interactions are computed for each atom pair within the cutoff sphere. Substantial distortions can however occur when the cutoff distance from an atom A includes one atom of a dipole B–C (*i.e.* B or C), but not the other. This gives rise to an exaggerated attraction between A and B–C and an artificial charge-dipole orientation of B–C relative to A. To eliminate such effects, the use of group-based cutoffs is recommended. Neighboring atoms are clustered into bonded charge groups, usually with no net charge. For any atom pair within the cutoff distance, all pair interactions between the corresponding charge groups are included in the electrostatic computation. This group-based method enables one to avoid the artificial creation of charges cutting through dipoles. When periodic boundary conditions are used, the minimum-image convention is generally applied to prevent double

counting of the interactions between the atoms in the central simulation cell and those in the images: only one image of each particle (the nearest one) is considered for a pair interaction. To avoid that an atom interacts with its own image, the cutoff radius used to truncate the non-bonded interactions must not exceed half the box size (considering the shortest box vector in the case of non-cubic simulation boxes). To circumvent the abrupt truncation of the electrostatic interactions by a straight cutoff, “shift” or “switch” functions can be applied to smooth the interaction energy or force to zero, either within the whole cutoff range or over a limited region. The truncated forces are thus replaced by continuous forces which have continuous derivatives at the cutoff radius. A shift function increases the magnitude of the force or potential before it is smoothed to zero (*i.e.* adds a function to the force or potential), while a switch function multiplies the force or potential by a function. There is actually no fundamental difference between both functions and the switch function can be considered as a special case of the shift function. Truncation of the long-range electrostatic interactions may introduce serious artifacts into computer simulations. The artifacts caused by the use of cutoffs have generally been attributed to a net ordering in the vicinity of the cutoff radius.

Ewald summation techniques One way to eliminate truncation effects is to include all the electrostatic interactions in the infinite array of periodic replicas of the central simulation cell by using Ewald summation techniques. Applying such techniques, electrostatic interactions are in principle considered with an infinite cutoff. The Ewald summation has originally been developed to handle long-range electrostatic interactions in simulations carried out with periodic boundary conditions and has traditionally been used to compute electrostatics in crystals. This method can be however applied to other systems, provided the charges in the system are distributed over a fine grid. The Ewald summation technique is nonetheless very costly from a computational point of view and has rarely been used for systems as large as lipid bilayers. Improved algorithms based on simplifications of the Ewald sum, like the Particle-Particle Particle-Mesh (P^3M) method [111] or the Particle-Mesh Ewald (PME) method [112, 113], have been developed for a more rapid and efficient convergence of the Ewald equations, and have been applied with success in numerous membrane simulations. The current trend to take long-range electrostatic interactions explicitly into account via Ewald techniques is certainly done in an exact but periodical manner, so that artificial periodicity may be enhanced. While periodic boundary conditions already introduce a factitious periodicity into the system, Ewald summation techniques include this periodicity at all

times in the long-range electrostatic interactions. Whether or not such effects are significant is obviously dependent on the system size and the properties of interest (see Appendix B).

Reaction field approach An alternative method that incorporates the full electrostatic interactions is the reaction field (RF) approach, in which the Coulomb potential is corrected for the effect of the polarizable surroundings beyond the cutoff radius [114]. This method has been developed for homogeneous systems, for instance for liquid simulations, or for a small solute immersed in a solvent. Within the cutoff sphere, solute and solvent are simulated in atomic detail, whereas the solvent outside the sphere is treated as a dielectric continuum. Tang *et al.* used this approach for the simulation of the gramicidin A channel in a fully hydrated DMPC bilayer and concluded that the inclusion of a reaction field has a significant improvement on the correction of the long-range calculation of the electrostatic interactions [78].

The selection of methodologies for the simulation of lipid bilayer membranes is particularly complex: many choices must be made concerning force fields, boundary conditions, treatment of long-range interactions, and other technical parameters. The fact that so many simulations carried out under different conditions lead to similar results is certainly a consequence of favorable combinations of parameters, one shortcoming compensating for another one. No choice is in any case perfect and every decision involves trade-offs. Compromises have to be made between accuracy and efficiency or more exactly, owing to the enormous computational intensiveness of membrane simulations, between accuracy and feasibility [96].

3.2.3 Simulations and experiments

The major drawback of simulations with regard to experiments is that simulations are based on theoretical models and are thus not as “real”. The question to ask is then: “what can be learned from simulations that cannot be learned from experiments?”. One striking result from simulations is the ability to make pictures of fluid membranes on an atomic scale of resolution, at a level of detail far beyond that achievable experimentally. In a sense, simulations provide a “computational microscope” that transcends the limitations of other visualization techniques [115] and can address relevant details which are experimentally inaccessible. Beyond the visualization aspect, MD simulations have a certain predictive power: the prediction of a simulation is represented by a set of atomic coordinates and velocities, namely

a trajectory, deriving from interaction potentials. From the predicted coordinates and velocities, averaged over many simulation steps, a plenitude of microscopic and macroscopic properties can be obtained, some of which are not available experimentally.

Of particular interest is the interplay between simulations and experiments. The wealth of predicted information gained by simulations can be used to guide experimental investigations, to complement and assist in the interpretation of experimental results, and to refine the experimentally derived microscopic picture of the structure and dynamics of model membranes. The refined experimental data will in turn help to tune the force field parameters used in the simulations. If simulations give a much more detailed view than any experiments on lipid bilayers, they are not better than the models that are simulated, and sometimes worse given the uncertainties in the force fields, the restriction to the nanosecond time scale, and the limitation to small systems [42]. Models need therefore to be tested against available experimental data whenever possible to validate the simulation results. When simulations yield good agreement with experiments, one can have some degree of confidence in the model and further trust the simulation results which are not available experimentally. Thus, a narrow interconnection exists between simulations and experiments, and the continuous progress in the comparison of simulation results with experiments, both to validate the simulation algorithms and to guide the interpretation and the design of new experiments, is very promising for the development of the two research areas.

3.2.4 Limitations of the MD technique

Although a powerful technique in many aspects, molecular dynamics presents a number of important limitations which must be kept in mind when using this technique and analyzing the results.

One obvious limitation is the length of the simulated time scale. Most trajectories to date are confined to the 10 ns regime, which does not allow the investigation of many biologically relevant processes. Another limitation is the size of the simulated system: the largest system that can be currently handled contains about tens of thousands of atoms, which corresponds to system sizes of the order of 5–10 nm. Such systems are still very small and do not enable one to study phenomena only present over longer distances. To circumvent this size problem, periodic boundary conditions are used to extend the system in a periodical manner. This approximation can however introduce some artifacts into the molecular behavior of the lipids, especially when the simulation box is not large enough. Both limitations have their

origins in the available computer power. With the continuous increase in computer speed and the improvement of the actual computational algorithms, time scales and system sizes will be enhanced by at least one order of magnitude in the near future and one can expect that MD simulations of lipid bilayers will reach microsecond capabilities in the next five years.

The accuracy of a MD simulation is also limited by the accuracy of the underlying force field. The potential function used to describe the interactions in the simulated system is a simplified approximation of the “real” function and involves uncertain parameters like partial charges, Lennard-Jones constants, equilibrium values for bonds, angles and dihedrals, and force constants. In the commonly used force fields, atomic polarizability is furthermore omitted: average effects of polarizability are retained in the force field parameters, but detailed effects are not properly represented [116]. Another crude approximation done in MD simulations is to compute only forces between pairs of atoms: three or four particle interactions are indeed neglected. To speed up calculations, long-range electrostatic interactions are often truncated beyond a given cutoff distance, which may have significant effects on the final results. Other methods have been implemented to include the long-range contribution, like Ewald summation or reaction field approaches. Each method has, however, some drawbacks which have to be taken into account.

An extension of present computational algorithms and methodologies as well as a refinement of current force fields represent thus an important challenge in the MD field to gain both in efficiency and accuracy. Nevertheless, molecular dynamics still constitutes a very reliable technique to study structural and motional properties of biomolecular systems, as long as the limitations and approximations described above are not ignored and their influence on the results carefully is considered.

Chapter 4

A phospholipid bilayer model

4.1 Introduction

In order to simulate the permeation of drug molecules across a lipid membrane and to study their interactions with the lipid environment, a realistic model for the membrane itself is required. The first task consists thus in the choice and setup of a membrane system reproducing the principal physicochemical properties of real membranes. Pure phospholipid bilayers in the liquid crystalline phase represent simple but very informative models. While phospholipids are responsible for the extreme flexibility of the membrane, they also provide, paradoxically, its basic barrier functionality, so that phospholipid bilayers have often been adopted to model biomembranes.

This chapter reports the elaboration of a dipalmitoylphosphatidylcholine (DPPC) bilayer model. DPPC has been chosen in reason of its prevalence in mammalian plasma membranes (see Chapter 1, Section 1.1.2.1, page 13) and of the large amount of experimental data available on DPPC and related phospholipids. Details of the simulation protocol are described, followed by a thorough analysis of the membrane characteristics. Emphasis is laid on properties that are thought to play a decisive role in permeation processes. Note that the choice of the various simulation conditions reported in this chapter derives from a series of test simulations described in Appendix B.

4.2 Method of simulation

4.2.1 Membrane system

The membrane system consists of 128 DPPC molecules – each monolayer containing 64 lipid molecules – surrounded by 3726 water molecules. The total number of atoms amounts to 17578 with a united-atom representation of the methylene and methyl groups in DPPC. The system size is large enough to allow, in a next step (see Chapter 5), the addition of drug molecules into the membrane. The water to DPPC ratio is of 29.1 (42% water by weight), which corresponds to a fully hydrated state of the bilayer. X-ray experiments on the structure of DPPC bilayers have shown that the main physical characteristics remain conserved between a hydration degree of 15.3 and 29.1 waters per lipid [117].

The chemical structure of DPPC is depicted in Figure 4.1. The lecithin headgroup is a zwitterion, overall neutral, with a positive charge distributed over the choline group and a negative charge on the phosphate group. The biologically relevant enantiomer is R-configured, the carbon atom GC2 of the glycerol moiety being the chiral center.

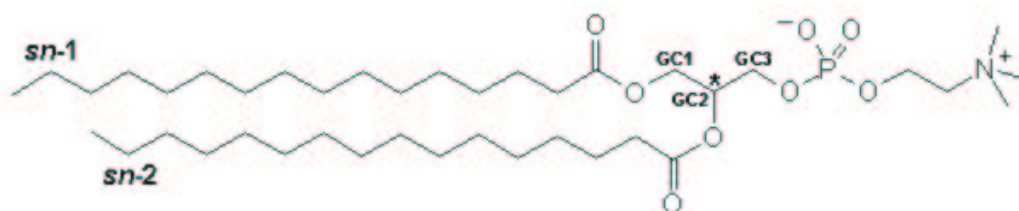


Figure 4.1: Chemical structure of DPPC. The stereospecific numbering of the glycerol moiety is indicated. The chiral center is denoted by an asterisk.

4.2.2 Structural parameters

Lipid bilayer membranes can be characterized by a series of structural parameters. The precise value of these parameters is determined by the interactions between the lipid constituents and their measurement provides a practical way to acquire information on the intermolecular interactions. Before going into the details of the simulation procedure, it is first important to define the main structural parameters.

The biologically relevant liquid crystalline state of lipid membranes is characterized by an inherent disorder, precluding the possibility of an atomic-level structural determination, as

is routinely obtained for proteins from X-ray diffraction. The resolution of X-ray diffraction is indeed limited by the lack of long-range order in liquid crystals compared to real ones. Diffraction (X-ray or neutron) measurements can be however performed on multilamellar dispersions consisting in regular arrangements of stacked bilayers to achieve a periodicity similar to that of crystals. Such experiments essentially give information on atomic positions along the bilayer normal. Information on the structure in the lateral direction (*i.e.* in the plane of the bilayer) is generally determined through a combination of experimental data (diffraction, NMR) and model interpretation [118].

The key structural quantity is the average interfacial area A per lipid molecule, which describes the bilayer microstructure with regard to molecular packing and which is modulated by the lateral interactions within the bilayer. The optimal value of the area per lipid is determined by a balance between the hydrophobic effect and any attractive interactions (e.g. hydrogen bonding in the headgroup region, dispersion forces in the hydrophobic core), tending to minimize the area, and repulsive chain and headgroup interactions, tending to expand it. The type of headgroup has the greatest influence on the equilibrium area, while different acyl chains provide for a fine tuning, generating a rich spectrum of values. The interfacial area per lipid cannot be directly obtained from experiments. Nevertheless, it can be indirectly derived from gravimetric X-ray methods or from approaches based on either electron density profiles, or NMR order parameters, or MAS measurements [42]. The volume V_L occupied by each individual lipid characterizes the density of the bilayer. Unlike the area per lipid, the volume per lipid can be accurately determined using a variety of experimental techniques, all based on specific volume measurements (e.g. neutral flotation combined with dilatometry measurements) [42]. Various distances within the membrane can also be accurately determined via diffraction methods. The most direct result from diffraction measurements performed on multilamellar stacks of bilayers is the distance D from the center of one bilayer to the next in the stack, namely the lamellar repeat spacing. This distance D increases with the amount of water added, until it becomes constant when water is added in excess. Determining the amount of water at the point where D becomes constant yields the number of water molecules n_W per lipid for the fully hydrated system. Another interesting distance, particularly relevant to the hydrophobic matching of membrane proteins, is the thickness $2D_C$ of the hydrophobic core. The hydrophobic thickness includes all hydrocarbon chain carbons with the exception of the carbonyl carbon which exhibits a substantial hydrophilic character.

All these structural parameters can be straightforwardly determined from MD simulations. Figure 4.2 schematically represents a lipid bilayer packed into a simulation box and enables one to visualize the different quantities described above. The interfacial area per lipid corresponds to the average area occupied by a lipid molecule projected onto the plane of the bilayer (*i.e.* the x,y -plane). If L_x , L_y , and L_z denote the simulation cell lengths in the x , y , and z directions, respectively, the area per lipid can be calculated by simply dividing $L_x L_y$ by the number N of lipids per leaflet:

$$A = \frac{L_x L_y}{N} \quad (4.1)$$

Since the simulation box contains a single bilayer surrounded by the experimentally determined amount of water for a full hydration of the lipid headgroups, L_z can be assimilated to the lamellar repeat spacing D . The volume per lipid V_L can be calculated from the following relation:

$$V_{box} = L_x L_y L_z = N_L V_L + N_W V_W \quad (4.2)$$

where V_{box} is the volume of the simulation box, N_L and N_W the total number of lipid and water molecules, and V_W the volume per water molecule. V_{box} , N_L , and N_W are known, while V_W can be determined from separate simulations of pure water under appropriate conditions.

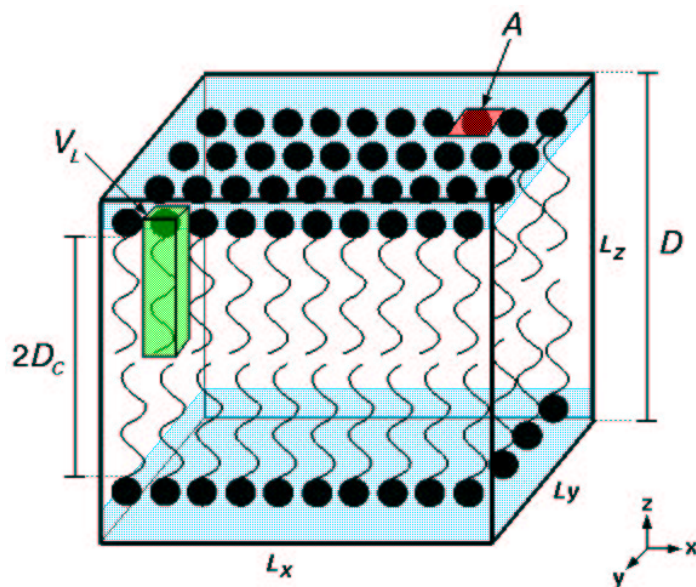


Figure 4.2: Definition of a few structural parameters. A is the area per lipid, V_L the volume per lipid, D the lamellar repeat spacing, and $2D_C$ the hydrophobic thickness. L_x , L_y , and L_z represent the simulation box dimensions.

Owing to large improvements achieved in the last few years in both methodologies and force fields, membrane simulations are now reasonably accurate in reproducing many experimental structural parameters. They often fail, however, into reproducing all parameters simultaneously. For instance, the average interfacial area per lipid has usually been quite problematic to reproduce. Variations of the area strongly affect the orientational order as well as the dynamics of the lipid molecules within the bilayer, so that discrepancies larger than 5% with respect to the experimental value cannot be tolerated.

4.2.3 Setup of the bilayer membrane

The initial conformation chosen for the DPPC unit stems from a crystal structure of DMPC. The only difference in chemical composition between both phospholipids is the chain length, DPPC having two more methylene groups in each chain than DMPC. The crystal structure of DMPC was primarily determined by Pearson and Pascher [119], and then energy minimized by Vanderkooi [120]. Minimization removed the acyl chain disorder present in the initial crystal structure, so that the carbon planes of the acyl chains became mutually parallel. The asymmetric unit cell of the DMPC crystal contains two non-identical DMPC molecules (DMPC A and B) and four water molecules which are hydrogen-bonded to DMPC and form bridges between neighboring molecules [119]. The overall conformations of the A and B molecules are rather similar. The main difference lies in the orientation of the polar groups with respect to the hydrophobic parts and essentially arises from different torsion angles about the GC1-GC2 bond of the glycerol moiety. To build up the DPPC membrane, the minimized structure of DMPC B was used. The most salient features of this crystal structure can be deduced from Figure 4.3. The area per lipid is about 0.39 nm^2 . The phosphodiester group has a double-*gauche* conformation that gives rise to a 90° kink at the phosphate group. As a result, the phosphatidylcholine headgroup is oriented approximately parallel to the bilayer surface, the P-N dipole making an angle of about 27° with respect to the x,y -plane. The glycerol group is essentially oriented normal to the plane of the bilayer. The two fatty acid chains are not equivalent. The *sn*-1 chain extends directly into the bilayer, continuing the line of the glycerol backbone. The *sn*-2 chain extends parallel to the plane of the bilayer for the first two carbons and then makes a bend at the C2-atom to become aligned parallel to the *sn*-1 chain, thus achieving closer packing than would be the case if the chains extended from their original conformations with respect to the headgroup. This conformation displaces the methyl end of the *sn*-2 chain by three methylene groups. Apart from the bend

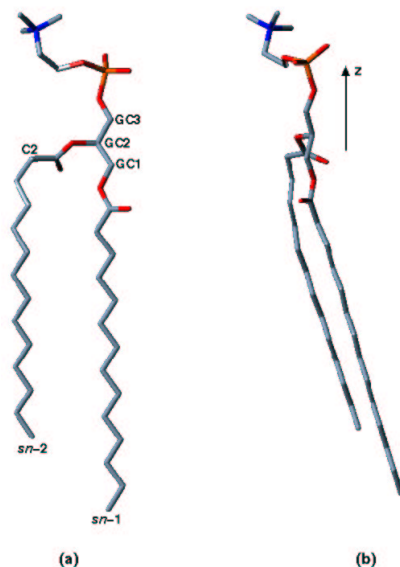


Figure 4.3: Energy-minimized conformation B of DMPC in the crystalline state. The nitrogen atom is blue; the phosphorus atom is orange; oxygen and (united) carbon atoms are red and grey, respectively. **(a):** Front view. **(b):** Side view (tilt of the hydrocarbon chains).

in the *sn-2* chain, both chains are in an all-*trans* configuration. The chains are tilted about 12° away from the bilayer normal. The chain tilt is rationalized as being due to a simple packing problem: the chain tilt allows for stabilizing interactions between the acyl chains of adjacent molecules, while maintaining the large molecular area due to the bulky headgroup. A “crystal-like” structure of DPPC was generated from the crystal structure of DMPC by simply expanding both chains by two methylene groups. The resulting structure was slightly rotated to achieve an orientation of the acyl chains approximately parallel to the *z*-axis or bilayer normal. Indeed, NMR measurements [121] as well as previous simulation studies [107] suggested the absence of a collective tilt in lipid bilayers in the liquid crystalline phase. A monolayer of 8×8 DPPC molecules was first generated by applying lattice translations of the crystal and then duplicated to form a bilayer. The bilayer was packed into a parallelepipedic simulation box – the *x,y*-plane defining the bilayer surface and the *z*-axis the bilayer normal – and energy minimized to relax the structure from non-physical contacts between the lipid components. Two slabs of water molecules were finally added and an energy minimization was again performed, this time to allow water molecules to adapt themselves to the lipid environment. The “pseudo-crystalline” DPPC bilayer can be seen in Figure 4.4.

In order to break the crystalline arrangement – introducing some disorder into the head-groups and hydrocarbon tails – and to obtain an area per lipid consistent with experimental determinations, two MD simulations were carried out at 323 K, above the main transition temperature of 315 K from gel to liquid crystalline states for DPPC. In the first simulation, a surface tension of 14.5 mN/m per lipid/water interface and a pressure of 1 bar along the bilayer normal were applied. After 450 ps, the dimensions of the resulting simulation box were $6.38 \times 6.38 \times 6.66 \text{ nm}^3$: this corresponds to an area per lipid of 0.636 nm^2 that lies within the experimental range $0.63\text{--}0.64 \text{ nm}^2$ [41,42]. The system was then simulated at constant volume for 1 ns to ensure its stability. In both simulations, a time step of 1 fs was used. The bilayer finally obtained, represented in Figure 4.5, is taken as starting structure for the simulation study of the DPPC membrane.

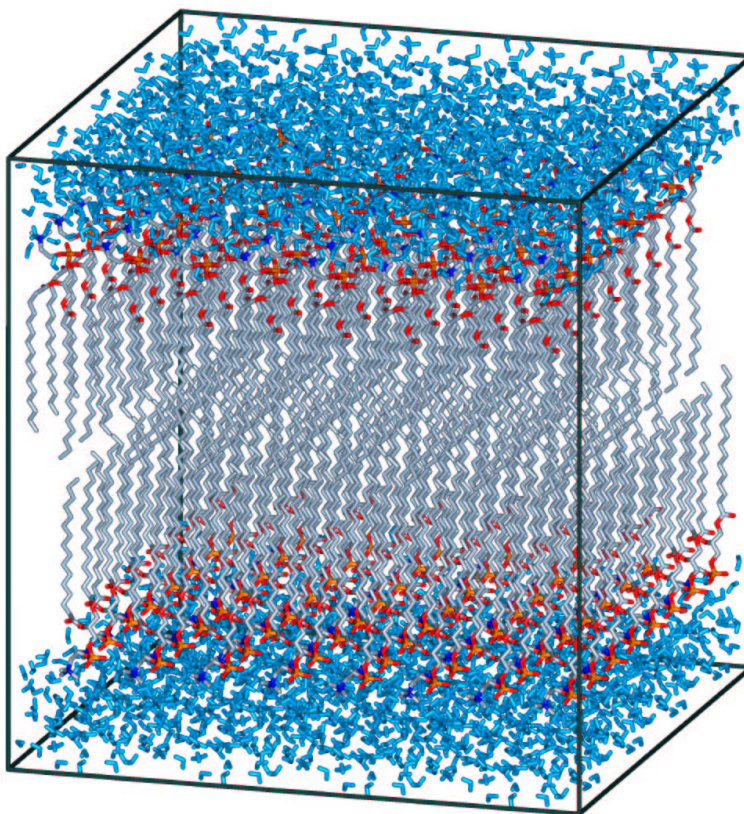


Figure 4.4: “Pseudo-crystalline” DPPC bilayer. Water molecules are light blue.

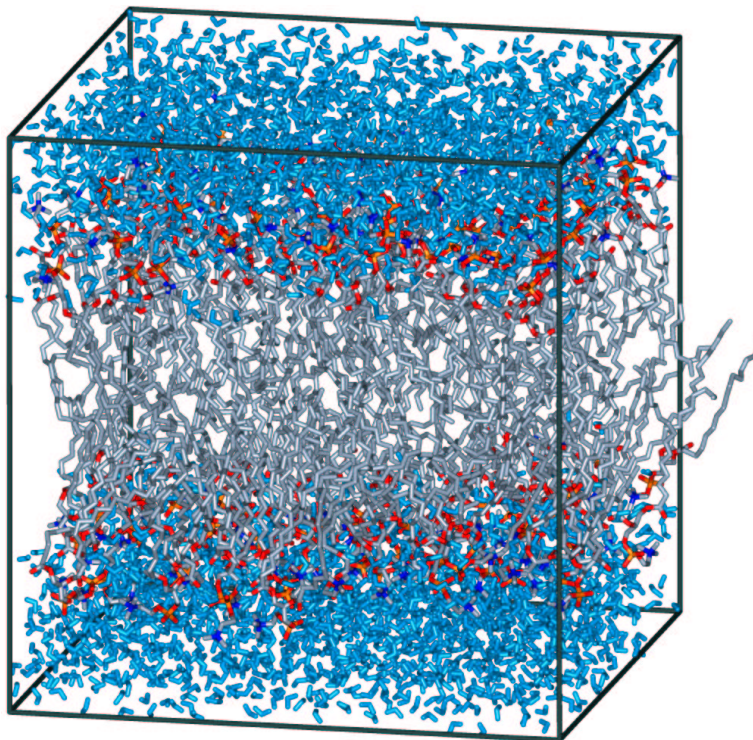


Figure 4.5: Starting structure for the MD simulation of the DPPC bilayer membrane.

4.2.4 Force field parameters and partial atomic charges

Bonded parameters The set of bonded parameters used for DPPC is based on the AMBER force field [86], refined for phosphatidylcholine lipids by Smondyrev and Berkowitz [94]. They essentially focused their efforts on developing an accurate set of torsional parameters for the polar groups of DPPC. Torsional parameters were fitted to reproduce geometry and energy profiles obtained from *ab initio* calculations of model compounds. To optimize the torsional parameters of the PC headgroup, three model compounds were considered: ethyltrimethylammonium, choline, and dimethylphosphate. Torsional parameters for the two ester groups were obtained by modeling methylacetate, ethylacetate, and methylpropionate. The robustness of the resulting force field parameters was confirmed by a MD simulation on a DPPC/water system showing a good agreement with experimental data. Dihedrals in the hydrocarbon chains are modeled by the Ryckaert-Bellemans potential which has proved to be more realistic for liquid alkanes, giving better statistics on *trans-gauche* behavior:

$$V_{RB}(\phi_{ijkl}) = \sum_{n=0}^5 C_n (\cos(\phi))^n \quad (4.3)$$

where $\phi = \phi - 180^\circ$, $C_0 = 9.28$ kJ/mol, $C_1 = 12.16$ kJ/mol, $C_2 = -13.2$ kJ/mol, $C_3 = -3.06$ kJ/mol, $C_4 = 26.24$ kJ/mol, and $C_5 = -31.5$ kJ/mol [122]. The use of this potential implies the exclusion of Lennard-Jones interactions between the first and last atom of the dihedral; the corresponding “1,4 interactions” are thus removed.

Non-bonded parameters The Lennard-Jones (LJ) parameters for the DPPC headgroup are taken from the OPLS force field [89] and the tail parameters are those determined by Berger *et al.* [93]. When using standard LJ parameters from united-atom force fields for the description of tail interactions, the density of the membrane tends to be much too high: deviations of the volume per lipid from the experimental value by more than 10% have been observed in many simulations. In order to obtain correct densities for lipid systems, Berger and co-workers adjusted the hydrocarbon LJ parameters of the OPLS force field to reproduce the density and heat of vaporization of pentadecane. Their optimized LJ parameters led to a density matching within 1% the experimental value found for DPPC. As recommended for the OPLS parameter set, all 1,4 LJ interactions are scaled by a factor of 8 to avoid possible distortions of the molecule.

Partial atomic charges The choice of partial atomic charges for the strongly polar phosphatidylcholine headgroup of DPPC is crucial for a correct description of electrostatic interactions within the interfacial region. In an earlier simulation of Egberts *et al.*, for instance, the simulated DPPC bilayer behaved as if it was in a gel state, with a much smaller area per lipid and higher chain order parameters than experimentally determined, although the system was simulated at a temperature of 335 K, well above the phase transition temperature (315 K) [56]. The initial atomic charges on DPPC, taken from the GROMOS force field [88], had to be reduced by a factor of two to lower the headgroup-headgroup attraction, allowing thereby a lateral expansion of the membrane and destabilizing the gel phase. However, such a scaling down of the charges is obviously not the most elegant solution to achieve the expected liquid crystalline state. In the present DPPC simulation, charges are those determined by Chiu *et al.* [97]. The charges were calculated by *ab initio* electronic structure computations with the GAUSSIAN program at Hartree-Fock self-consistent field (SCF) level with the 6-31G* basis set. When simulating neutral lipids like DPPC, it is recommended for the submolecular charge groups to be neutral or, at least, to exhibit charges as small as possible. This can be generally done with minor adjustments of the computed partial charges, well within their inherent range of uncertainty. Figure 4.6 shows the partial atomic charges used

q_H and q_O , and the LJ parameters employed. In simulations performed with the GROMACS molecular dynamics package [126], which has been used for the present study, SPC and SPC/E models have traditionally been preferred. Several authors pointed out the superiority of the SPC model with regard to the extended model for simulations at interfaces [98, 127]. SPC/E includes a self-energy term due to polarization and has better bulk properties than SPC, which makes it a logical choice in MD simulations of bulk water. However, the thermodynamic potential of SPC/E water is only correct if the proper polarization self-energy correction is applied. In the case of interfacial systems, where water is in equilibrium with different environments, such corrections cannot be applied and the uncorrected value for the chemical potential is too high, resulting in a too low solubility of SPC/E compared to SPC water at interfaces. Since the chemical potential of the original SPC model is closer to the experimental value, this model is expected to better reproduce equilibrium distributions at the lipid/water interface and is therefore adopted for the current DPPC/water simulation. The geometric and electrostatic characteristics of the SPC water model are given in Figure 4.7. In MD simulations with a large number of water molecules, as it is the case here, holonomic constraints are usually employed to keep the bond lengths of water at their equilibrium values. The analytical SETTLE algorithm is used for resetting the positions and velocities to satisfy the holonomic constraints on the SPC water molecules [128]. This algorithm has been developed to constrain rigid water molecules in a quick and effective way. Indeed, reducing the computational time spent on the satisfaction of bond constraints significantly speeds up the simulations. In the case of the rigid SPC water model, SETTLE constrains three bonds: two real O–H bonds of equal length and one fictitious H–H bond.

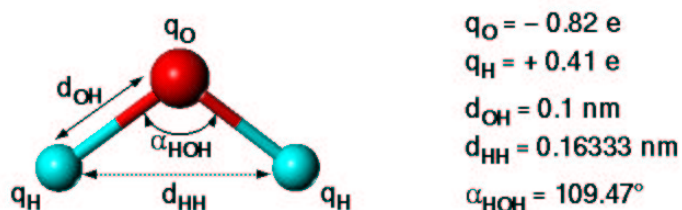


Figure 4.7: SPC water model.

4.2.5 Macroscopic boundary conditions

The simulation is carried out under constant pressure and temperature conditions with the *NPT* ensemble, in which the size and the shape of the simulation box are free to adjust

(see Chapter 3, Section 3.2.2.3, page 64). The correct ensemble for the bilayer system would be actually $N\gamma P_N T$, in which the surface tension γ and the pressure P_N in the direction normal to the bilayer are explicitly specified [129]. The surface tension is defined by $\gamma = \int_{-\infty}^{+\infty} (P_N(z) - P_L(z)) dz$, with P_N and P_L the normal and lateral pressures, respectively. In the present simulation, the applied pressure is controlled anisotropically, *i.e.* the three unit cell dimensions fluctuate independently from each other, while the total pressure remains constant. This corresponds to an $NP_x P_y P_z T$ ensemble, which is not rigorously defined and only stable when at least two of the pressure components are equal. The three pressure components are kept constant at 1 bar on average in the simulation, which corresponds to an average surface tension equal to zero. At constant box lengths, specifying a lateral and normal pressure of 1 bar is the same as specifying zero surface tension and a normal pressure of 1 bar. The effect of the fluctuating box lengths was ignored and it was assumed that the $NP_x P_y P_z T$ ensemble, with $P_x = P_y = P_z = 1$ bar, is equivalent to the $N\gamma P_N T$ ensemble, with $\gamma = 0$ mN/m and $P_N = 1$ bar.

4.2.6 Treatment of electrostatics

Serious artifacts can be introduced into MD simulations if all the electrostatic interactions are not taken into account. A correct treatment of long-range electrostatics is of crucial importance for the reliability of the results and this statement is especially verified in lipid bilayer simulations.

When using periodic boundary conditions, the total electrostatic energy of a system of N particles in a simulation cell and their periodic images is given by the following equation:

$$V_{Coulomb} = \frac{f}{2} \sum_{n_x} \sum_{n_y} \sum_{n_z^*} \sum_i^N \sum_j^N \frac{q_i q_j}{\mathbf{r}_{ij, \mathbf{n}}} \quad (4.4)$$

The cell-coordinate vector is $\mathbf{n} = (n_x, n_y, n_z)$. The original cell is located at $\mathbf{n} = (0, 0, 0)$ where terms with $i = j$ are omitted, as indicated by the asterisk. The distance $\mathbf{r}_{ij, \mathbf{n}}$ represents the real distance between the charges q_i and q_j and not the minimum-image (see Chapter 3, Section 3.2.2.6, page 70). f is equal to $1/4\pi\epsilon_0$, where ϵ_0 is the vacuum permittivity. Unfortunately, the above sum converges very slowly, so that its use in MD simulations for the computation of electrostatics is far too much time consuming.

The Ewald summation was introduced in 1921 to calculate long-range interactions between particles and their infinite images in an efficient way [130]. The method was originally used in crystals. In this approach, the single slowly converging series (Equation 4.4) is converted into the sum of two rapidly converging series plus a constant term:

$$V_{Ewald} = V_{dir} + V_{rec} + V_0 \quad (4.5)$$

The total Coulomb energy is divided into a short-ranged “direct” part (V_{dir}), a long-ranged “reciprocal” part (V_{rec}), and a correction term (V_0), also called “self-term”, that cancels out the interaction of each particle with itself:

$$V_{dir} = \frac{f}{2} \sum_{i,j}^N \sum_{n_x} \sum_{n_y} \sum_{n_z^*} q_i q_j \frac{\text{erfc}(\beta \mathbf{r}_{ij,\mathbf{n}})}{\mathbf{r}_{ij,\mathbf{n}}} \quad (4.6)$$

$$V_{rec} = \frac{f}{2\pi V} \sum_{i,j}^N q_i q_j \sum_{m_x} \sum_{m_y} \sum_{m_z^*} \frac{\exp\left(-(\pi \mathbf{m}/\beta)^2 + 2\pi i \mathbf{m} \cdot (\mathbf{r}_i - \mathbf{r}_j)\right)}{\mathbf{m}^2} \quad (4.7)$$

$$V_0 = -\frac{f\beta}{\sqrt{\pi}} \sum_i^N q_i^2 \quad (4.8)$$

β is the Ewald convergence parameter, which determines the relative rate of convergence between the direct and reciprocal sums (*i.e.* the relative weight between both sums). V is the volume of the simulation cell. $\mathbf{m} = (m_x, m_y, m_z)$ is the reciprocal-space vector. The complementary error function erfc is defined by $\text{erfc}(x) = 1 - \text{erf}(x) = 1 - \frac{2}{\sqrt{\pi}} \int_0^x \exp(-u^2) du$, and decreases monotonically as x increases. The Ewald method permits, in principle, the exact evaluation of electrostatic interactions in systems with infinite periodic boundary conditions. However, the computational cost of the reciprocal sum increases as N^2 , which makes the use of the Ewald summation unrealistic for large systems.

The performance of the Ewald reciprocal sum has significantly been improved by the introduction of Fast Fourier Transform (FFT) techniques. In the present DPPC simulation, the Particle-Mesh Ewald (PME) algorithm [112, 113] is used, which scales as $N \log(N)$ and performs significantly faster than the standard Ewald summation. Instead of computing the traditional reciprocal sum over reciprocal vectors, the charges are first assigned to a 3D-grid that fills the simulation space. The grid is then Fourier transformed using a 3D-FFT algorithm and the reciprocal energy term is evaluated by a single sum over the grid. The potential energy at the grid points is finally calculated by applying the inverse Fourier Transform, and

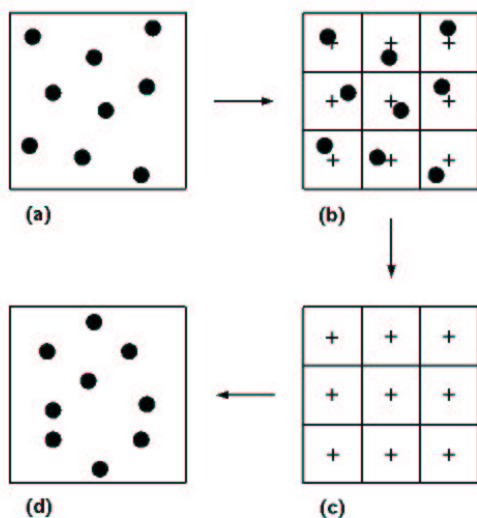


Figure 4.8: A 2D schematic description of the PME method. **(a):** A system of N particles. **(b):** Projection of the charges onto a grid using cardinal B-spline interpolation. **(c):** Computation of the potential energies and forces at grid points using FFT. **(d):** Interpolation of the forces from the grid to particle locations (using the same function as the one in step (b)), and update of the coordinates.

forces are obtained by an analytical differentiation of the energies. Figure 4.8, inspired by the review article of Toukmaji and Board [131], summarizes the different steps for the computation of the long-range potential. In the direct sum, the choice of a large value for the Ewald parameter β allows the use of a short cutoff radius beyond which the interactions can be neglected, which reduces the complexity of the direct sum from $\mathcal{O}(N^2)$ to $\mathcal{O}(N)$. In the reciprocal sum, the number of reciprocal vectors is increased to compensate for the truncation made in the direct sum. In the MD simulation of the DPPC system, a cutoff of 1 nm is applied in the direct space sum for short-range interactions. For the calculation of long-range interactions in the reciprocal space, the charges are projected onto a grid using cardinal B-spline interpolation [100]. The grid is then Fourier transformed with a 3D-FFT algorithm using a maximum spacing of 1.2 Å for the FFT grid. This method, even with a moderate grid size, should give an accuracy of about 5×10^{-3} for the calculated electrostatic interactions.

4.2.7 Simulation conditions

Software and hardware The simulation is carried out with the GROMACS molecular dynamics package [126], version 2.1, on a dual processor Pentium PIII 1 GHz node achieving a rate of about 20 CPU hours per nanosecond of simulation.

Time step and simulation time All bond lengths in the DPPC molecule are kept constant using the LINCS routine [109] (see Chapter 3, Section 3.2.2.5, page 69) and the water geometry is maintained with the SETTLE algorithm [128]. The efficiency and stability of both algorithms allow a time step of 5 fs [132]. Owing to this relatively large time step, the simulation could be extended up to 150 ns to cover a broad spectrum of modes of motion.

Pressure and temperature The bilayer system is simulated at a constant pressure of 1 bar, corresponding to the atmospheric pressure, and at a constant temperature of 323 K. The choice of this temperature can be justified by two reasons: first, it is a few degrees above the main transition temperature of 315 K, so that the system should be in the expected fluid crystalline state; second, it enables one a direct comparison of the simulation results with experimental data which have mostly been determined at 323 K. In a simulation, the temperature is given by the total kinetic energy of the system, while the pressure is calculated from the difference between the kinetic energy and the virial tensor. For several reasons (numerical inaccuracy due to force truncation or integration errors, heating caused by external or frictional forces, etc...), the pressure and temperature in the system tend to drift away from their initial values. To avoid such drift phenomena, it is necessary to control both the pressure and the temperature. To this end, the so-called “weak coupling” scheme developed by Berendsen is used, in which the membrane is coupled to a “bath” of constant pressure and temperature via some suitable coupling parameters [133]. DPPC and water are coupled independently to the heat bath and the coupling times for pressure and temperature are set at 1 and 0.1 ps, respectively.

Boundary conditions As it is common in liquid state simulations, periodic boundary conditions are applied in all three dimensions, so that actually a multilamellar system is simulated. In addition to eliminating edge effects in the membrane patch simulated, PBC are natural since most of the model membranes studied experimentally are in the form of mul-

tilamellar arrays with a regular spacing (e.g. multilamellar vesicles: see Chapter 1, Section 1.1.6, page 26).

4.3 Results

4.3.1 Equilibration time and equilibrium structural parameters

To ensure that the bilayer system is at equilibrium and behaves properly throughout the simulation, one has to take great care that conserved quantities fluctuate around a constant value, without any noticeable drift during the simulation.

Energy and temperature As seen in Figure 4.9 (a), the equilibration of the total energy of the system requires about 25 ns. After this equilibration time, the energy is conserved, does not drift. Furthermore, the temperature, proportional to the average kinetic energy, remains constant at about 323 K (see Figure 4.9 (b)). The trajectory is thus stable throughout the entire simulation.

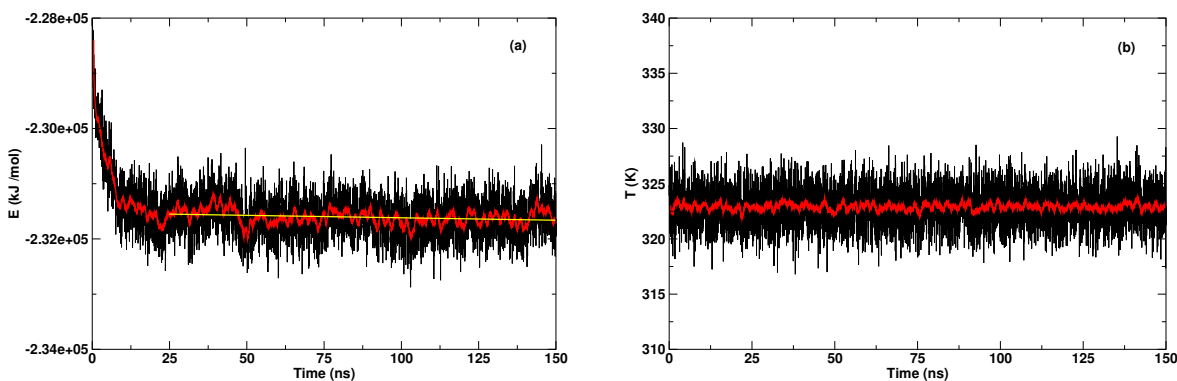


Figure 4.9: (a): Total energy of the system: the yellow line is a linear regression from 25 to 150 ns. (b): Temperature of the system. The red curves represents running averages.

Area per lipid The interfacial area A per DPPC is calculated using Equation 4.1, page 80, with $N = 64$. Figure 4.10 displays its time evolution throughout the simulation. The area decreases during the first 13 ns, after which it fluctuates around an average value of 0.635

nm^2 with a standard deviation of 0.010 nm^2 (*i.e.* 1.6% of the average value). The average area obtained is in very good agreement with the most recently reported experimental values of 0.633 [41] and 0.640 nm^2 [42]. Even after equilibration, care must be taken of the large fluctuations of the area caused by the small lateral modulus of elasticity. These fluctuations may exhibit long periods since they result from collective motions of the lipid molecules. In order to discuss physical properties of the lipid bilayer and determine equilibrium structural parameters, average quantities must be calculated over a time that is much larger than these fluctuation periods. Although the exact values of the fluctuation periods are unknown, they can be evaluated from the simulation. A Discrete Fourier Transform (DFT) analysis performed on the time evolution of the area between 25 and 150 ns indicates three main periods of 9, 18, and 31 ns, as shown in Figure 4.11. Thus, a MD simulation of close to 100 ns may be desirable to investigate the structure and dynamics of the DPPC membrane at thermal equilibrium.

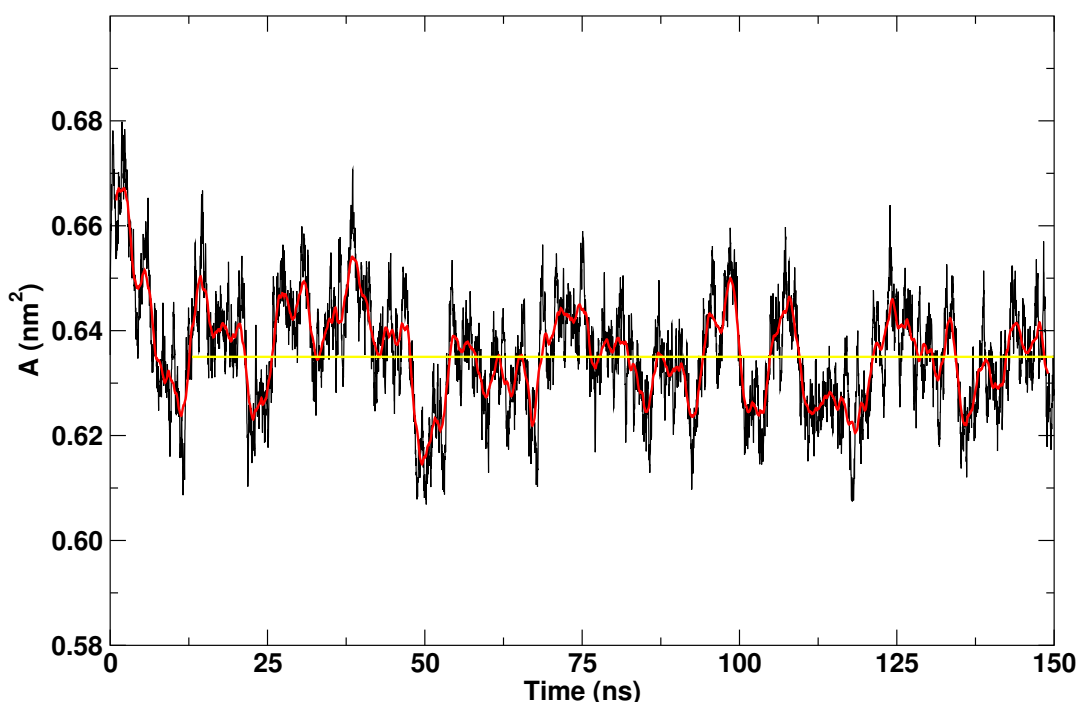


Figure 4.10: Time evolution of the area per DPPC: the red curve represents a running average, while the yellow line is a linear regression from 13 to 150 ns.

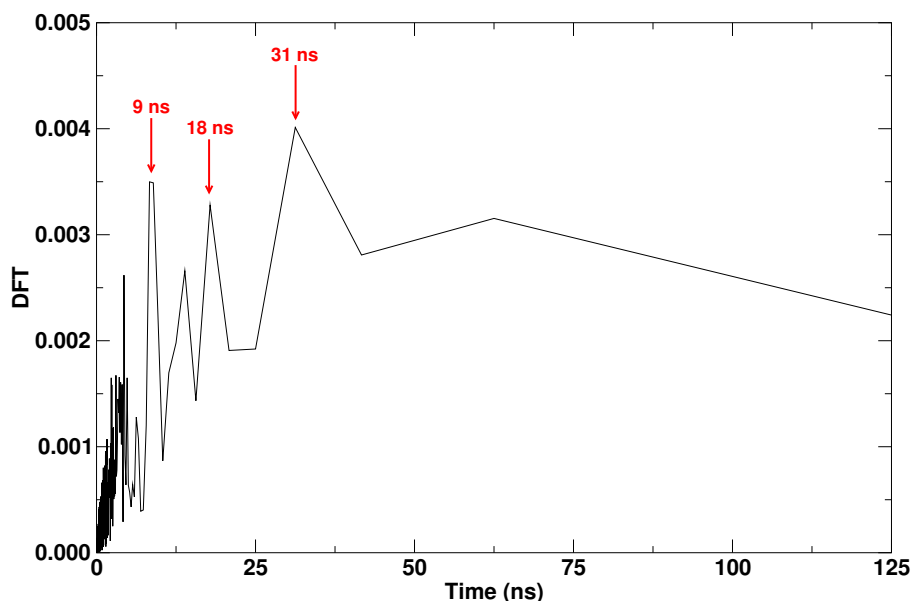


Figure 4.11: DFT analysis performed on the time evolution of the area per DPPC between 25 and 150 ns: three main peaks, corresponding to fluctuation periods of 9, 18, and 31 ns, are indicated by arrows.

Volume per lipid The volume per DPPC is calculated from Equation 4.2, page 80. The volume per water molecule V_W has first been determined from a separate simulation of pure water: a system consisting of 7161 SPC water molecules has been simulated for 500 ps under the appropriate conditions (*i.e.* $T = 323$ K, $P = 1$ bar, use of the PME algorithm for electrostatics) and a value of 0.0316 nm^3 has been found for V_W . As it can be observed from Figure 4.12, the volume per lipid V_L converges faster than the area does – within about 6 ns – and fluctuates around an average value of 1.219 nm^3 with small amplitudes, the standard deviation being of only 0.005 nm^3 (*i.e.* 0.4% of the average value). The calculated volume per DPPC is close to the experimental value of 1.232 nm^3 [134]. The smaller amplitudes registered in the volume fluctuations compared to those in the area fluctuations can be explained as follows. The stability of the membrane results from a balance between the hydrophobic effect on the exposure of lipid chains to water which favors a small area and intermolecular interactions inside the bilayer which favor a larger area. This balance leads to a free energy which varies only weakly with the area. Thus, it is one to two orders of magnitude easier to change the area of a bilayer at constant volume with an accompanying change in bilayer thickness than to change the volume of the bilayer [104].

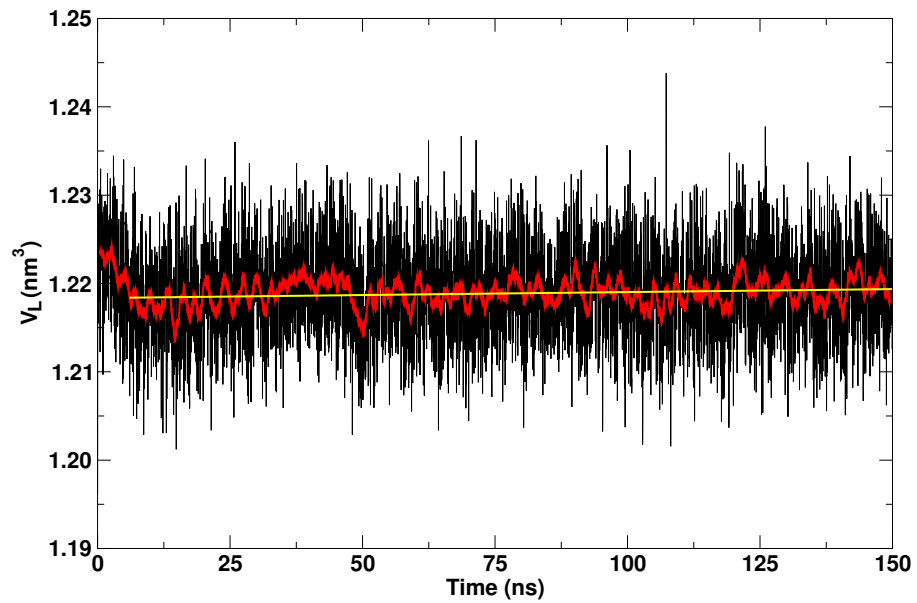


Figure 4.12: Time evolution of the volume per DPPC: the red curve represents a running average, while the yellow line is a linear regression from 6 to 150 ns.

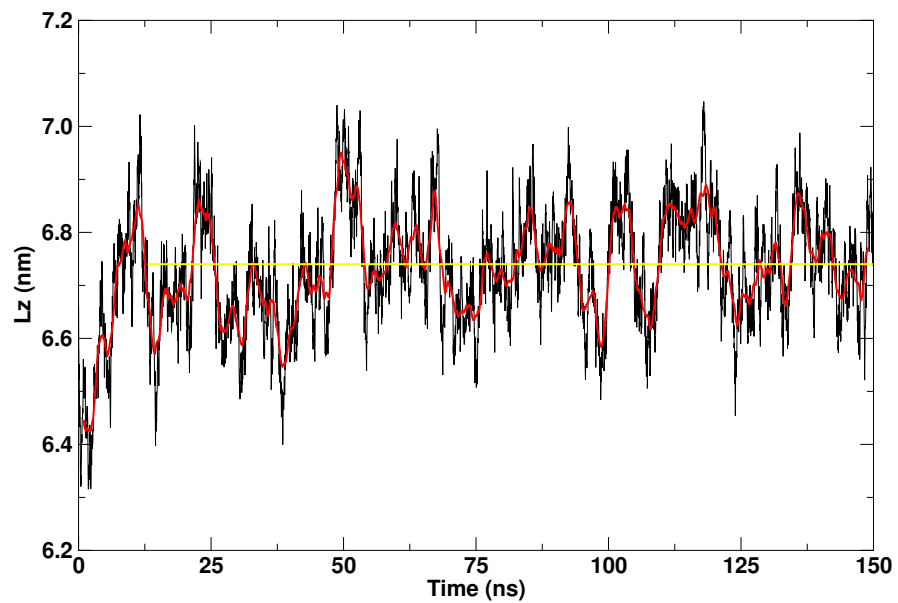


Figure 4.13: Time evolution of the bilayer repeat spacing: the red curve represents a running average, while the yellow line is a linear regression from 13 to 150 ns.

Bilayer repeat spacing The time evolution of the bilayer repeat spacing L_z is depicted in Figure 4.13. As for the area, an equilibration time of 13 ns is required for L_z . An average repeat spacing of 6.74 nm is obtained with a standard deviation of 0.10 nm (*i.e.* 1.5% of the average value). This spacing matches the experiment value of 6.72 nm, determined at the same hydration degree ($n_W = 29.1$) [117]. L_z , like the area, exhibits large fluctuations. Both fluctuations are anti-correlated since the volume remains approximately constant.

Given the slow convergence of the energy of the system, data were analyzed starting at 25 ns in the following sections.

4.3.2 Overall bilayer organization

The overall organization of the bilayer can be compared to that of a two-dimensional liquid. This is, however, a special liquid with an anisotropic and inhomogeneous character. A snapshot of the DPPC membrane after 150 ns simulation time is presented in Figure 4.14. This picture gives the distribution of the various parts of the lipid and water molecules at a specific time. The bilayer is a very stratified composite consisting of a layer of perturbed water, a heterogeneous layer mixing hydrophilic and hydrophobic components, including bound water, lipid headgroups, and upper end parts of the lipid acyl chains, and a layer of hydrocarbon segments. The interface between the water and lipid components of the membrane seems to be quite diffuse, and the lipid tails exhibit different packing, depending on the position along the membrane normal.

These assumptions on the transverse structure of the membrane, deduced from the atom distribution at a particular time, are confirmed by the time-averaged (from 25 to 150 ns) density distribution profiles of DPPC and water along the bilayer normal (*i.e.* the z -axis), shown in Figure 4.15. Since the position of all atoms is known at any time during the simulation, it is straightforward to extract density profiles for different atoms, molecules, or molecular subgroups from the MD trajectory. The simulation box is divided into slices of 0.1 Å thickness perpendicular to the bilayer normal and the time-averaged density is computed in each slice for a given component. From the large overlap between the DPPC and water density profiles observed in Figure 4.15, the existence of a diffuse interface becomes obvious. Water penetrates very deeply into the membrane, leaving a region of only 2 nm devoid of water, and the DPPC headgroups protrude into the middle of the water. Defining the interface as the region where the water density drops from 90% to 10% of its maximum value [135], an interfacial

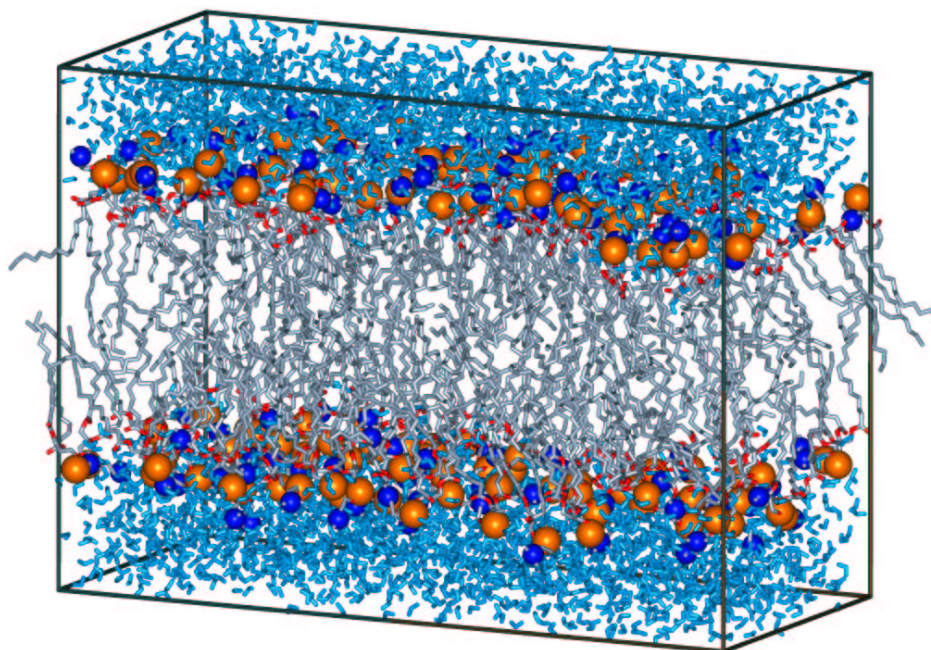


Figure 4.14: Snapshot of the DPPC membrane after 150 ns simulation time. The nitrogen (blue) and phosphorus (orange) atoms of DPPC are emphasized (space-filling format).

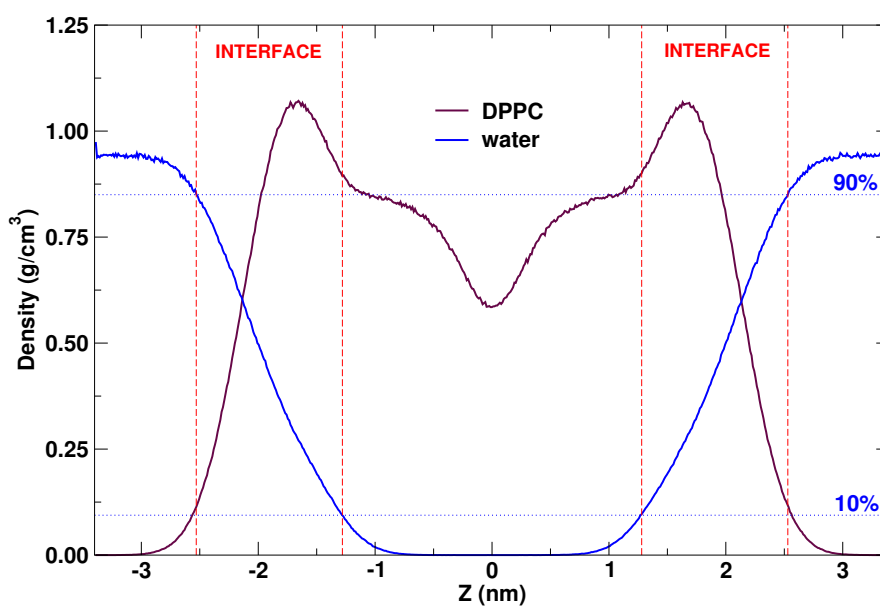


Figure 4.15: Trans-bilayer density profiles of DPPC and water. The center of the bilayer is located at $z = 0$ nm. The two horizontal dotted lines correspond to water densities equal to 90% and 10% of the maximal water density. Both interfaces are delimited by vertical dashed lines.

width of 1.24 nm is found. A similar value can be calculated from diffraction studies [134]. Taking twice this value to include both interfaces, this means that approximately 40% of the whole membrane belong to the interfacial region. The DPPC density reaches its maximum in the headgroup region and decreases in the middle of the bilayer by a factor of about two, in agreement with experimental results.

4.3.3 Headgroup region

4.3.3.1 Interfacial atom distributions

The time-averaged density distributions (along the bilayer normal) of a few interfacial DPPC subgroups (choline $\text{N}(\text{CH}_3)_3$ and phosphate PO_4 moieties, ester oxygens, and carbonyl groups) are plotted in Figure 4.16. The curves show a broad distribution of the headgroup atoms, which can be interpreted in term of lipid perpendicular motion. Although a bit noisy, the distribution curves can be reasonably well approximated by Gaussian distributions with a specific half-width. A half-width of about 10 Å is found for the distribution curve of the choline groups, and the distribution curves of the phosphate and ester groups are characterized by a half-width of about 6 Å. These values underline the high degree of perpendicular motion of individual lipids, with a strong tendency for single lipid molecules to protrude from the surface of the bilayer. Note that the choline groups exhibit the highest mobility. The roughness of the membrane surface is also reflected in the distribution of the water molecules (see Figure 4.16): rather than forming a sharp boundary, the water density drops continuously. The deepest penetration of the water molecules coincides with the position of the carbonyl groups.

Distances between particular atoms or groups along the bilayer normal can also be deduced from density distribution profiles. The average distance between the phosphate groups on both sides of the bilayer, for instance, is a characteristic structural feature and corresponds to the distance separating the density maxima found in both layers. For clarity, the density distribution of the phosphate groups along the bilayer normal is plotted again in Figure 4.17. A $\text{PO}_4\text{-PO}_4$ distance of 3.87 ± 0.10 nm between the two membrane faces is measured and is in good agreement with the experimental value of 3.7 ± 0.1 nm determined by analysis of continuous X-ray scattering data from DPPC vesicles at 317 K [136]. Mean distances between specific pairs of carbon atoms of the DPPC headgroup on both sides of the bilayer have been determined in the same way and are listed in Table 4.1. A close agreement is

found with neutron diffraction experiments done at 323 K on selectively deuterated DPPC lipids [137]. It should be however noted that the diffraction experiments were performed at a lower hydration level ($n_W = 13.6$). The half-widths of the distribution curves are also given in Table 4.1. The atoms are spread out over quite large regions: the methyl carbon atoms of the choline moiety are even more smeared out; the transversal mobility of the carbon atoms seems however to decline towards the glycerol backbone, as shown in the decrease registered of the half-widths.

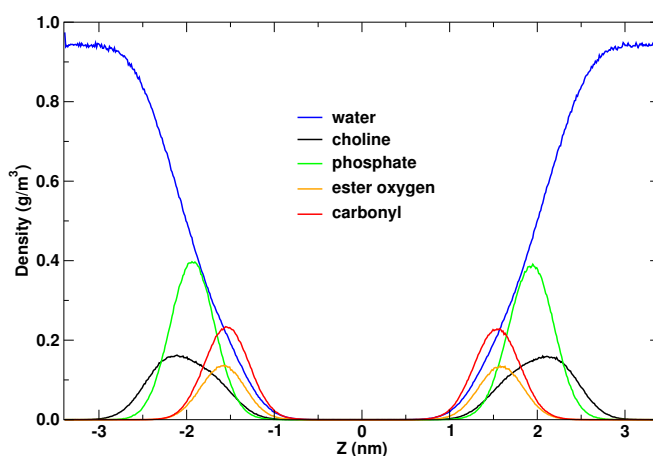


Figure 4.16: Time-averaged trans-bilayer density distribution profiles of water and interfacial DPPC subgroups.

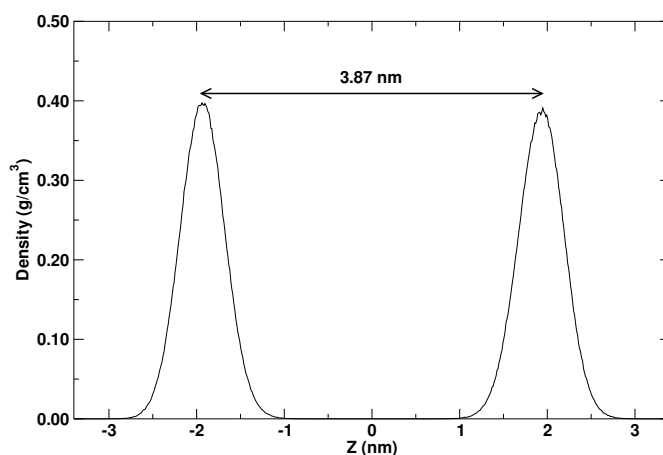
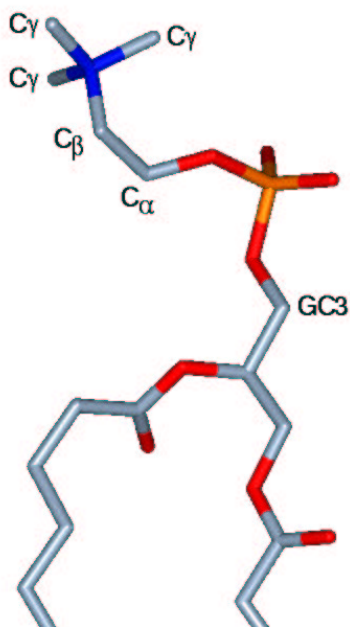


Figure 4.17: Time-averaged trans-bilayer density distribution profile of the phosphate groups.

Table 4.1: Trans-bilayer distances (in nm) between specific carbon atoms of the DPPC headgroup.

Carbon atom ^a	Simulation [half-width ^b]	Experiment
C _γ ^c	4.24±0.10 [1.0]	4.36±0.12
C _β	3.99±0.10 [0.8]	4.24±0.20
C _α	3.93±0.10 [0.7]	4.20±0.20
GC3	3.57±0.10 [0.6]	3.48±0.30

^aSee Figure 4.18 for the labeling of the carbon atoms. ^bThe density distribution curves are approximated by Gaussian curves whose half-widths are given in square brackets (in nm). ^cAverage over the three methyl groups.

**Figure 4.18:** Labeling of the carbon atoms of the DPPC headgroup.

4.3.3.2 Headgroup hydration and water ordering

The hydration degree of the DPPC lipids can be estimated from radial distribution functions (RDFs) of water molecules around the headgroups or parts of them. In an inhomogeneous system, the pair radial distribution function $g_{AB}(r)$ between particles of type A and B is computed from:

$$\begin{aligned} g_{AB}(r) &= \frac{\langle \rho_B(r) \rangle}{\langle \rho_B \rangle_{local}} \\ &= \frac{1}{\langle \rho_B \rangle_{local}} \cdot \frac{1}{N_A} \cdot \sum_{i=1}^{N_A} \sum_{j=1}^{N_B} \frac{\delta(r_{ij} - r)}{4\pi r^2} \end{aligned} \quad (4.9)$$

N_A and N_B correspond to the number of atoms of type A and B. $\langle \rho_B(r) \rangle$ represents the particle density of type B at a distance r around particles A, and $\langle \rho_B \rangle_{local}$ the particle density of type B averaged over all spheres around particles A with a maximal radius r_{max} equal to half the box length. In practice, the system is divided into spherical slices of radius r and of thickness dr , and the δ -function is replaced by a histogram. Figure 4.19 shows the RDF of the water oxygen atoms OW around the choline nitrogen atom N. The high peak corresponds to the first layer of water molecules hydrating the nitrogen atom. The first hydration shell is defined as the number of water molecules found inside the radius corresponding to the first minimum after the main peak in the RDF. The number of water molecules in the first hydration shell is thus obtained by integrating the RDF to the first minimum. On average, 18.8 water molecules are found in the first hydration shell of the nitrogen atom by integrating the RDF g_{N-OW} to the first minimum located at 0.63 nm. Table 4.2 includes the hydration numbers and the locations of the first minimum for a few headgroup atoms. The choline nitrogen atom exhibits the largest hydration shell since it has the greatest tendency to protrude into the water layer. The phosphate phosphorus atom P is buried somewhat deeper in the membrane and is hydrated by only 5 water molecules. The number of waters bound to a phosphate free oxygen Op is 1.7 on average. A slightly lower number is found for the carbonyl oxygen Oc (1.5 waters). Interesting to compare is the hydration degree of the carbonyl oxygen Oc2, belonging to the chain *sn*-2, and of the carbonyl oxygen Oc1, belonging to the chain *sn*-1. A higher hydration degree is found for Oc2, indicating that both carbonyl oxygens are not fully equivalent. This lack of equivalence can be explained by the relative position of both oxygens, Oc1 being located deeper within the non-polar region of the membrane and thus less exposed to water than Oc2. The non-equivalence may also result, to a lesser extent,

from the different partial charges carried by both oxygens, Oc1 being less negative (carrying a partial charge of -0.6) than Oc2 (-0.7). Another interesting feature is the ordering effect on water exerted by the phosphate free oxygens (Op's) and the carbonyl oxygens (Oc's) compared to that exerted by the ester phosphate oxygens (Ope's) and the glycerol oxygens (Og's). The corresponding RDFs are shown in Figure 4.21: a large ordering of water is observed around Op and Oc oxygens, whereas Ope and Og oxygens have practically no ordering effect on water. The largest ordering of water is found around Op's.

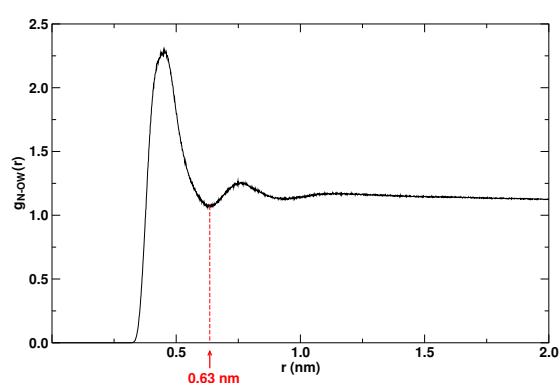


Figure 4.19: Radial distribution function of the water oxygen atoms around the choline nitrogen atom.

Table 4.2: Hydration of the choline nitrogen atom N, the phosphate phosphorus atom P, the phosphate free oxygen atom Op, the ester phosphate oxygen atom Ope, the glycerol oxygen atom Og, and the carbonyl oxygen atom Oc. Oc1 and Oc2 designate the carbonyl oxygens belonging to the chains *sn*-1 and *sn*-2, respectively (see Figure 4.20 for clarity). The given hydration number corresponds to the number of water molecules in the first hydration shell. The location of the first minimum in the RDF is also indicated. In all cases, a clear first minimum is observed.

Atom	Hydration number	First minimum (nm)
N	18.8	0.63
P	5.0	0.45
Op	1.7	0.32
Ope	0.6	0.32
Og	0.4	0.34
Oc	1.5	0.35
Oc1	0.8	0.34
Oc2	2.2	0.36

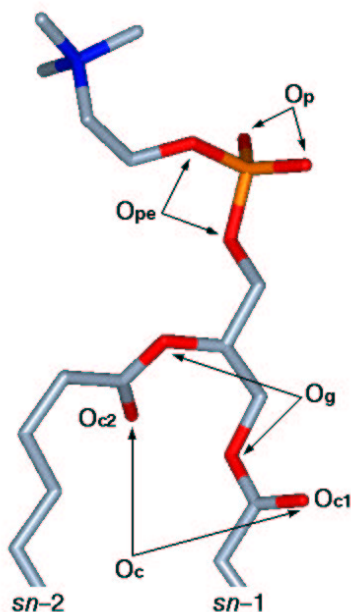


Figure 4.20: Labeling of the oxygen atoms of the DPPC headgroup.

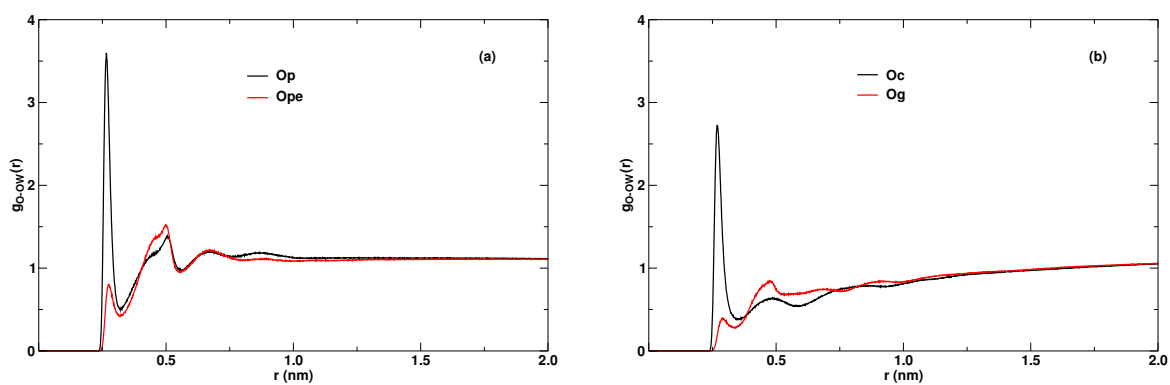


Figure 4.21: Radial distribution functions of the water oxygen atoms around (a): the phosphate free oxygen (Op) and the ester phosphate oxygen (Ope); (b): the carbonyl (Oc) and glycerol (Og) oxygens.

The stability of a phospholipid bilayer strongly depends on its hydration. A definite number of water molecules adhere tightly to the different residues of the lipid headgroups (6–9 waters in the case of DPPC [42, 117]) and are oriented by them, while a larger number of water molecules adhere more loosely, preserving their freedom of rotation but still contributing to the thermodynamic properties of the membrane. The structuring of the interfacial water can be clarified in terms of RDFs between headgroup atoms and water (previous paragraph) but also between water-water pairs. For comparison (see Figure 4.22), RDFs of water oxygen pairs have been calculated in the interfacial region (where the water density drops from 90% to 10% of its maximal value) and in the “actual” water layer (where the water density exceeds 90% of its maximum). In the water layer, the average number of nearest neighboring water molecules is 5, which is close to bulk SPC water (5.5 neighbors). In the interfacial region, this number drops to 3.4. In bulk water, because of the large number of neighboring water molecules, the water molecules do not need to orient themselves in a special manner to optimize the possibilities to form hydrogen bonds with surrounding water molecules. At the interface, the number of neighboring water molecules available for hydrogen bonding is smaller due to the competition with the lipid headgroups, so that the water molecules have to adopt a specific orientation to take optimal advantage of the hydrogen bonding possibilities. For instance, they are able to form hydrogen bonds to each other by creating a “clathrate-like” structure around the headgroups, which is illustrated in Figure 4.23.

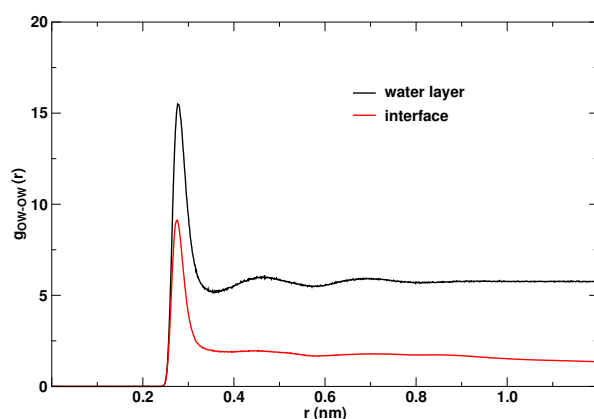


Figure 4.22: Radial distribution functions of water oxygen pairs in the water layer and in the interfacial region.

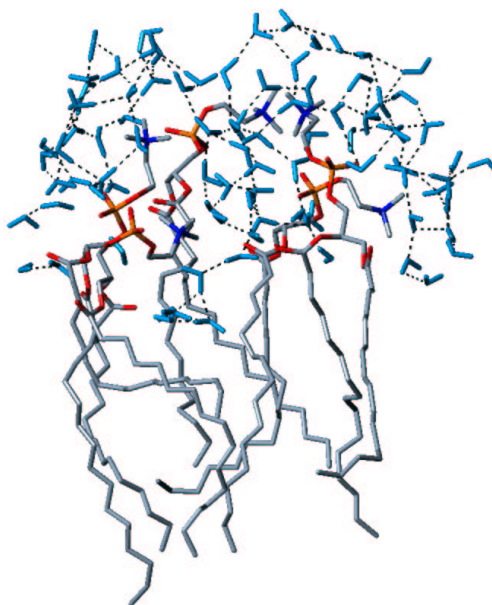


Figure 4.23: “Clathrate-like” structure of water around the DPPC headgroups. Only a patch of a few DPPC lipids is displayed for clarity. The dotted lines represent hydrogen bonds between the water molecules.

4.3.3.3 Headgroup orientation

Since the DPPC headgroup is a zwitterion, the properties of the membrane are strongly influenced by the orientation of the P–N dipole with respect to the bilayer surface. From the distribution curves plotted in Figure 4.16, page 99, it can be seen that the choline and phosphate groups lie at almost the same depth in the membrane, with the choline groups protruding, however, slightly further into the water layer. This means that the headgroups are oriented more parallel to the membrane plane than normal to it. The parallel orientation of the P–N dipoles is indeed favored in terms of free energy of electrostatic interactions. This preference for a parallel orientation is nevertheless thwarted by steric requirements and by the large degree of motional freedom in the water layer, which leads to a wide distribution of tilt angles. The average angle of tilt can be however characterized by the cosine of the angle θ between the P–N vector, pointing from the location of the phosphorus atom towards the location of the nitrogen atom, and the unit vector along the positive z -axis (see Figure 4.24):

$$\cos \theta = \frac{z_N - z_P}{\|\vec{PN}\|} \quad (4.10)$$

where z_N and z_P are the z -coordinates of the nitrogen N and phosphorus P atoms, and $\|\vec{PN}\|$ represents the norm of the vector \vec{PN} . The average depth difference $z_N - z_P$ (0.14 nm) can be deduced from the density distribution profiles of the N and P atoms along the z -axis, while the average intramolecular distance between N and P (0.41 nm) can be estimated from the intramolecular RDF between N and P and corresponds to the location of the first peak in the RDF. An average angle θ of about 70° is calculated this way. The P–N vector is thus inclined by about 20° on average from the membrane surface, pointing towards the water layer. This value agrees well with the experimentally determined one: an angle of 18° was indeed found at 332 K from ^2H -NMR combined with laser Raman studies [138].

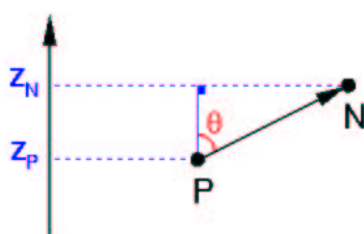


Figure 4.24: Definition of the angle θ characterizing the orientation of the vector \vec{PN} with respect to the bilayer normal.

4.3.3.4 Hydrogen bonding

The interfacial region is stabilized by networks of hydrogen bonds (H-bonds) between the DPPC headgroups and water. The DPPC molecule does not contain any donor but eight acceptors (*i.e.* eight oxygen atoms). The number of H-bonds formed between DPPC and water has been determined separately for each DPPC oxygen. The following geometric criteria for the H-bonds have been adopted (see also Figure 4.25): the distance r between the water oxygen OW (donor) and the DPPC oxygen (acceptor) has to be shorter than or equal to 0.35 nm (which corresponds to the position of the first minimum in the RDF of SPC water), and the angle α between the vector linking the water and DPPC oxygens and one of the OW–H bonds of the water (*i.e.* the hydrogen-donor-acceptor angle) has to be less than or equal to 60° . A relative large angle value is used since the deviation from linearity in H-bonding may be greater in the dense packing of the membrane than that in an unrestricted environment. The number of H-bonds made by a DPPC oxygen is obtained by determining the number of water molecules that satisfy these geometric criteria and by averaging over the

simulation time (125 ns) and over all the DPPC molecules present in the system (128). Each DPPC molecule makes 7.1 H-bonds with water: 4.2 H-bonds involve the phosphate group (*i.e.* 60% of the total number of H-bonds) and 2.9 the two ester groups (*i.e.* 40%). H-bonds on the phosphate free oxygens (Op's) account for 47% and on the carbonyl oxygens (Oc's) for 33% of the total number of H-bonds on DPPC. These together are responsible for 80% of the H-bonds formed between DPPC and water. The difference in the H-bonding capability of Op and Oc oxygens – the LJ parameters for the two oxygen types being the same – arise principally from the accessibility of water to the oxygen (*i.e.* from its location in the membrane) and, to a lesser extent, from the difference in partial charges on both types of atoms. The Op's are well hydrated, whereas the Oc's are located in a water-deficient region, and the partial charges on the Op's are a bit higher than on the Oc's. Thus, the number of accepted bonds may be greater for the Op's than those for the Oc's, and the H-bonding stronger. If both Op's are equivalent, it is not the case for the the Oc's. The carbonyl oxygen on the chain *sn*-2 (Oc2) exhibits a much higher level of H-bonding than the oxygen on the chain *sn*-1 (Oc1). This observation agrees with IR measurements on the water binding sites in diacylphospholipids like DPPE, DMPC, or DPPC, which indicated the lower capacity of Oc1 for hydrogen bonding than that of Oc2 [139]. The ester phosphate oxygens (Ope's) and glycerol oxygens (Og's) involve only 13% and 7% of the total number of H-bonds, respectively. The difference in H-bonding capability of Ope's and Og's can be explained by the same reasons as those mentioned above for Op's and Oc's. The numbers and percentages of H-bonds between DPPC and water molecules are listed in Table 4.3.

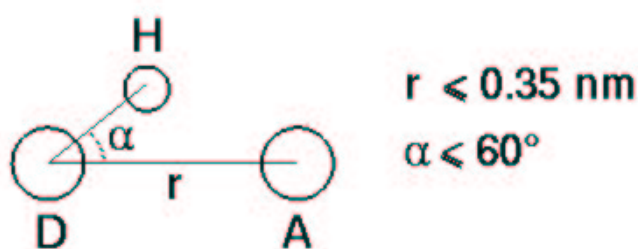


Figure 4.25: Geometric criteria for hydrogen bonding (H: hydrogen atom; D: donor atom; A: acceptor atom).

Table 4.3: Number and percentage of hydrogen bonds formed between water and each type of DPPC oxygen atom (see Figures 4.20 and 4.26 for the labeling of the oxygen atoms). Values are averaged over the 128 DPPC molecules and over 125 ns simulation time.

Atom or group	Number of H-bonds	%
DPPC	7.1	100%
PO ₄	4.2	60%
2×CO ₂	2 × 1.45 = 2.9	2 × 20% = 40%
Opa	1.6	23%
Opb	1.7	24%
2×Op	2 × 1.65 = 3.3	2 × 23.5% = 47%
Opea	0.5	7%
Opeb	0.4	6%
2×Ope	2 × 0.45 = 0.9	2 × 6.5% = 13%
Og1	0.1	1%
Og2	0.4	6%
2×Og	2 × 0.25 = 0.5	2 × 3.5% = 7%
Oc1	0.7	10%
Oc2	1.7	23%
2×Oc	2 × 1.2 = 2.4	2 × 16.5% = 33%

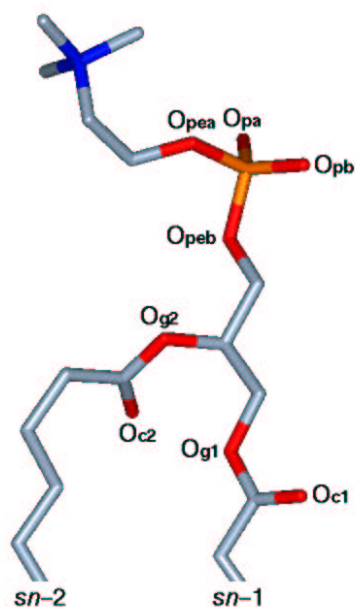


Figure 4.26: Labeling of the oxygen atoms of the DPPC headgroup.

4.3.3.5 Headgroup-headgroup interactions

Two major classes of short-distance interactions occur between the DPPC headgroups. The first class involves charge associations (charge pairs) formed when oppositely charged groups are located within 4 Å from one another, in analogy to salt bridges in proteins. To the second class of interactions belongs the formation of water cross-bridges between negatively charged groups in which two DPPC headgroups are bridged by one or two water molecules via hydrogen bonds.

Charge pairs In the interfacial region, the DPPC headgroups essentially interact via intermolecular charge pairs formed between positively charged choline methyl groups and negatively charged phosphate or carbonyl oxygen atoms. The radial distribution function of the phosphorus atoms relative to the nitrogen atom, g_{N-P} , depicted in Figure 4.27 (a) (intramolecular distances are not included), has a distinct maximum at 0.50 nm. The presence of this maximum indicates that the choline and phosphate groups stay in a close, preferred distance from one another in the membrane. For comparison, the RDFs of the phosphorus atom pairs and nitrogen atom pairs are also represented in Figure 4.27 (b) and (c), respectively. These functions exhibit broader peaks at longer distances (0.62 and 0.82 nm for g_{P-P} and g_{N-N} , respectively). The RDF of the phosphate free oxygen atoms (Op's) relative to a methyl group (Me) of the choline residue, g_{Me-Op} (Figure 4.28 (a)), presents three maxima located at 0.34, 0.55, and 0.75 nm, which reflects the presence of three methyl groups in a residue. The first minimum is located at 0.45 nm. The RDF of the carbonyl oxygen atoms (Oc's) relative to a choline methyl group, g_{Me-Oc} (Figure 4.28 (b)), is similar to g_{Me-Op} , with a first maximum located at 0.33 nm and a first minimum at 0.45 nm. Since the sum of the van der Waals radii of a phosphate or carbonyl oxygen and a choline methyl group is equal to 0.34 nm, the Op-Me and Oc-Me pairs that contribute to the peak at 0.33-0.34 nm in the RDFs must be strongly interacting with each other, forming thus very stable charge pairs. Figure 4.28 (c) compares the RDFs of the carbonyl oxygen atoms Oc1 and Oc2 relative to a choline methyl group. The two first peaks in g_{Me-Oc2} are more pronounced than those in g_{Me-Oc1} : charge pair interactions between the choline methyl groups and Oc2 occur thus with a higher probability and tend to be stronger than Me-Oc1 pair interactions. The RDFs of the phosphate and carbonyl oxygen atoms relative to a choline methyl group are very similar to that of the water oxygen atoms (OW's) relative to Me (see Figure 4.28 (d)), especially in the position of the first peak and the first minimum. The fact that the interaction

spheres around Me coincide for Op's/Oc's and OW's means there is a permanent competition between headgroup-headgroup and headgroup-water charge pair associations. Examples of Me-Op and Me-Oc charge pairs are given in Figure 4.29. The number of DPPC molecules linked via charge pairs represents about 90% of all molecules in the membrane.

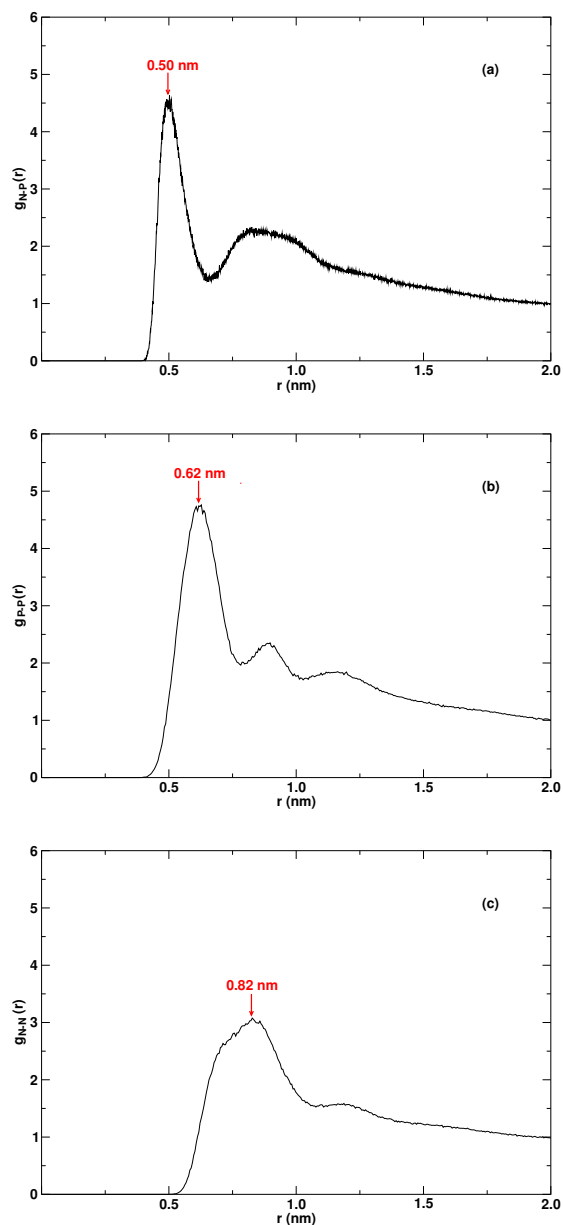


Figure 4.27: (a): RDF of the phosphorus atoms around the nitrogen atom. (b): RDF of the phosphorus atom pairs. (c): RDF of the nitrogen atom pairs.

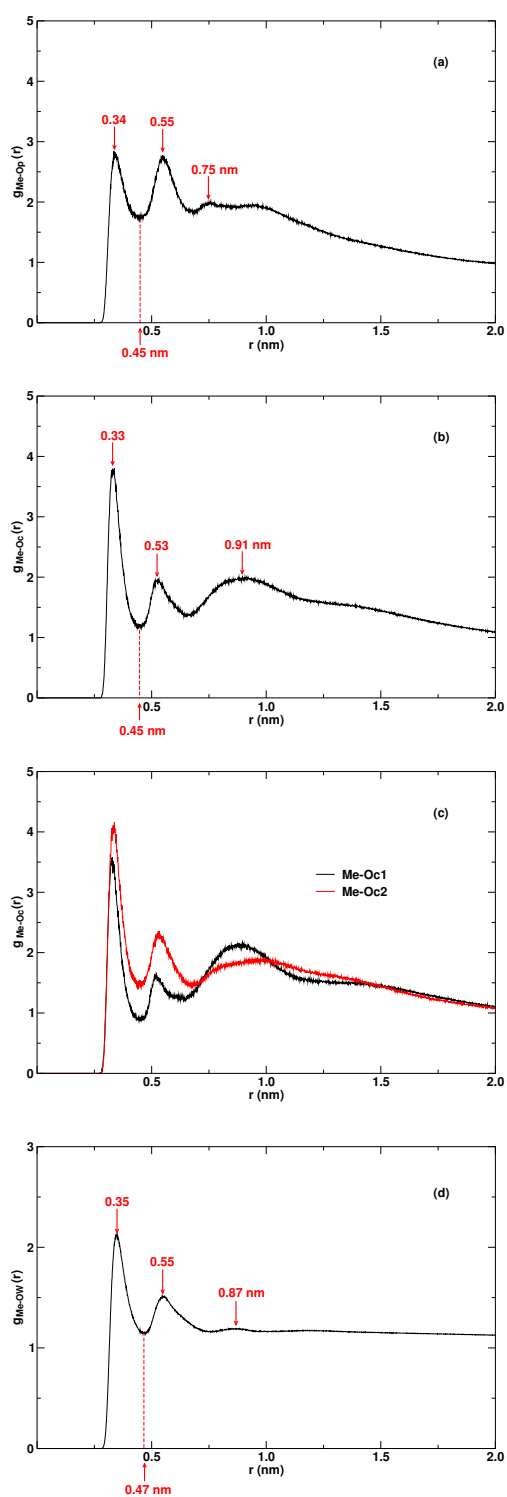


Figure 4.28: RDFs around a choline methyl group (Me) of : **(a)**: the phosphate free oxygens (Op's); **(b)**: the carbonyl oxygens (Oc's); **(c)**: the carbonyl oxygens Oc1 and Oc2; **(d)**: the water oxygens (OW's).

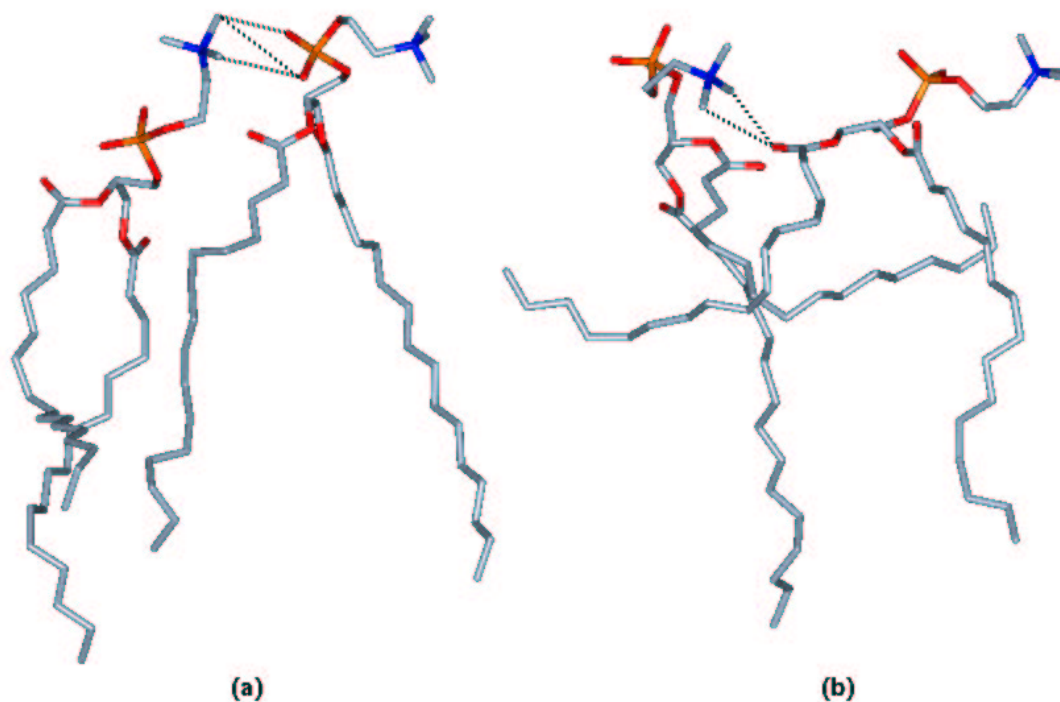


Figure 4.29: Representations of charge pairs between the DPPC headgroups. **(a):** Me-Op triple pair. **(b):** Me-Oc double pair.

Water bridges Approximately 70% of all DPPC molecules are cross-linked by either single or multiple water bridges. These bridges do not form networks as extended as in crystal structures, but give rise to local clusters of two to seven molecules. Representative conformations of single and double water bridges between the DPPC headgroups are shown in Figure 4.30.

Headgroup-headgroup interactions in the DPPC bilayer, both via Coulombic attraction (charge pairs) and via water bridges, reduce the headgroup mobility and largely contribute to the stability of the membrane in the liquid crystalline state. These interactions link about 98% of all DPPC molecules in the membrane.

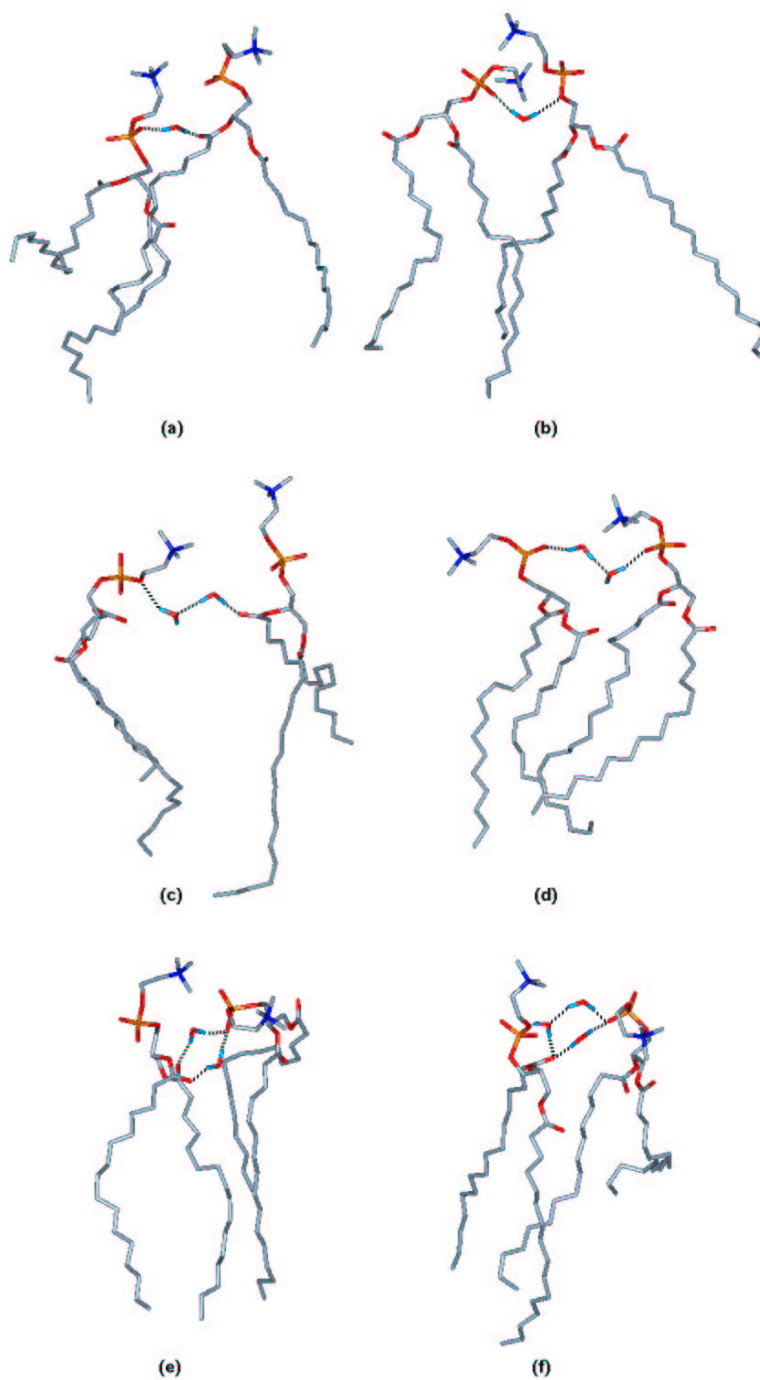


Figure 4.30: Representations of water bridges between the DPPC headgroups. (a): Op-Oc bridge via one water molecule. (b): Op-Ope bridge via one water molecule. (c): Ope-Oc bridge via two water molecules. (d): Op-Op bridge via two water molecules. (e): Oc1-Op and Oc2-Op bridges, both via one water molecule. (f): Two Oc-Op bridges, the first one via one water molecule, the second one via two water molecules.

4.3.4 Hydrocarbon region

4.3.4.1 Atom distributions

The time-averaged density distributions along the bilayer normal of the methylene and methyl groups of the DPPC hydrocarbon chains are plotted in Figure 4.31. The density distribution of water is also plotted as reference. The pronounced dip in the CH₂ distribution at the center of the bilayer shows that there is little overlap or interdigitation of the tails of the two monolayers. Another interesting feature is the broad width of the distribution of the CH₃ groups: the lipid tails are indeed able to fold back on themselves to give a noticeable CH₃ density over a range of about 2 nm in the middle of the bilayer. Figure 4.31 also gives the density distribution of the carbon atoms C2 located at the beginning of the chains, after the carbonyl groups (see also Figure 4.32). The distance between the two maxima in the C2 density profile defines the thickness of the hydrocarbon region or hydrophobic thickness $2D_C$, which is equal to 2.83 ± 0.20 nm. X-ray experiments on DPPC vesicles at 317 K give a value of 2.6 ± 0.1 nm [136], and ²H-NMR measurements on DPPC multilamellar dispersions at 323 K, a value of 2.84 nm [41].

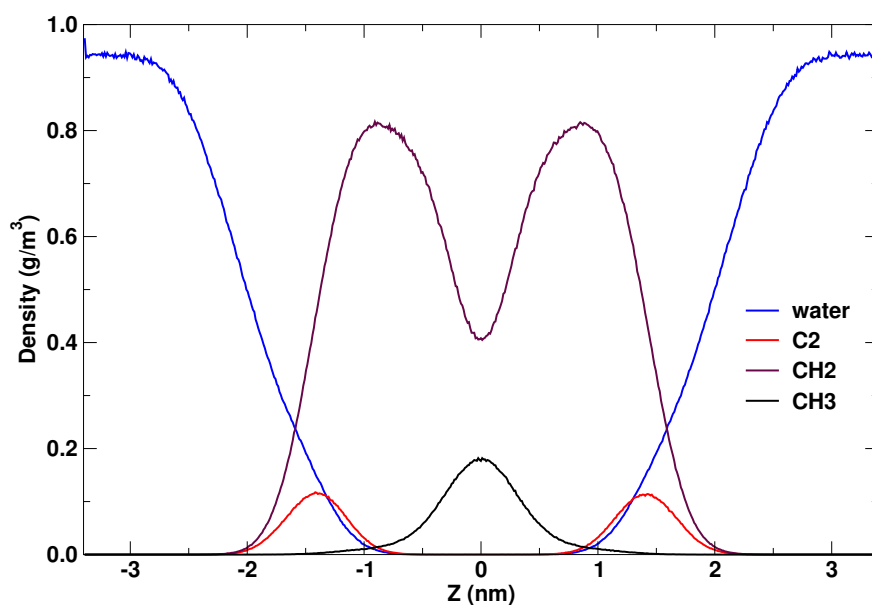


Figure 4.31: Time-averaged trans-bilayer density distribution profiles of the methylene and methyl groups as well as the carbon atoms C2 of the DPPC hydrocarbon chains. The density distribution of water is also plotted as reference.

Table 4.4 includes the mean distances between pairs of carbon atoms belonging to the lipid chains on both sides of the bilayer. These distances stem from density distribution profiles and can be compared with those obtained from neutron diffraction experiments performed at 323 K on DPPC multilayers at a hydration level of 13.6 waters per lipid [140]. The simulation results agree within 1.6 \AA with the experimental data. The distances determined experimentally present, however, some uncertainties, since the distance between C4 and C5 and that between C14 and C15 exceed the carbon-carbon bond length ($\sim 1.5 \text{ \AA}$) by 0.2 \AA .

Table 4.4: Trans-bilayer distances (in nm) between specific carbon atoms of the DPPC hydrocarbon chains (distances are averaged over both chains).

Carbon atom ^a	Simulation	Experiment
C4	2.44 ± 0.20	2.44 ± 0.30
C5	2.26 ± 0.20	2.10 ± 0.30
C9	1.50 ± 0.20	1.62 ± 0.20
C14	0.73 ± 0.20	0.72 ± 0.20
C15	0.43 ± 0.30	0.38 ± 0.20

^aSee Figure 4.32 for the labeling of the carbon atoms.

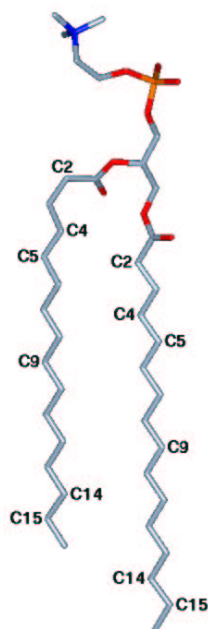


Figure 4.32: Labeling of the carbon atoms of the DPPC hydrocarbon chains.

4.3.4.2 *Trans-gauche* isomerization

The origin of the dynamic properties of lipid bilayers stems, for the most part, from rotations about the C–C single bonds in the lipid chains. The dihedral (or torsion) angles of hydrocarbon chains exhibit three minima: “*trans*” at 180° , “*gauche plus*” at approximately -60° , and “*gauche minus*” at approximately $+60^\circ$. The creation of *gauche* isomers is energetically unfavorable on enthalpic grounds, since the *gauche* conformers lie 2.1 kJ/mol per methylene group higher in energy than the *trans* conformers, but is favored on entropic grounds as a result of the increase in rotational disorder. Transitions between the *trans* and *gauche* states are among the fastest molecular motions in lipid bilayers. This rotational isomerism provides the basis for the membrane fluidity, being translated into rotational and translational mobility of the lipid molecules.

In a hexadecyl chain, about 4–6 *gauche* conformers are predicted at room temperature. In a lipid bilayer in the liquid crystalline state, however, the steric hindrance to rotations about C–C bonds varies throughout the length of the acyl chain. The number of bonds about which rotations can take place increases as one proceeds down the chain: near the interfacial region, indeed, the chains are quite efficiently packed, whereas the bilayer interior may be as disorganized as liquid hydrocarbons. Single *gauche* conformations induce large angular deviations of the chain axis, which can lead to energetically unfavorable interactions between the chains in a close-packed lattice. Hence, in the upper dense part of the hydrocarbon chains, only cooperative tilting and combinations of *gauche* conformations that minimize lateral displacements and preserve the lateral packing of the chains are allowed. Towards the methyl end of the chains, lateral displacements caused by single *gauche* conformations are much smaller and are, therefore, allowed. Bond rotations generate, furthermore, a shortening of the chains that tends, on average, to create more free volume towards the center of the bilayer: this allows a greater amplitude of oscillation away from the *trans* conformation and gives rise to an increased rotational isomerism in the center of the bilayer.

Experimentally, vibrational spectroscopies (infrared and Raman) can be used to probe the physical state of the lipid bilayer and determine the occurrence of *gauche* dihedrals in the acyl chains. Changes in lipid chain conformations can be monitored by the frequency shifts of the CH_2 absorption bands, which can in turn be interpreted in terms of changes in the number of *gauche* isomers in the chains. Quantitatively, 3 to 5 *gauche* rotamers per acyl chain are found on average for DPPC in the liquid crystalline phase [141–146]. This is equivalent to a fraction of *trans* dihedrals (or “*trans*-fraction”) ranging from 60 to 77%.

From the DPPC simulation, a *trans*-fraction of $76.6 \pm 1.1\%$ is calculated, which corresponds to the upper limit of the experimental range. Figure 4.33 gives the probabilities of *gauche* defects as a function of the dihedral position, separately for the chains *sn*-1 and *sn*-2. The probability of *gauche* defects along the chain *sn*-2 is almost constant, with a continuous increase towards the methyl end, whereas large fluctuations are observed in the chain *sn*-1, especially in the upper part where low probability values alternate with high values for consecutive dihedrals. A different behavior of the chains *sn*-1 and *sn*-2 was also observed by Smondyrev and Berkowitz [147]. They attributed this difference to a different orientation of the ester groups at the beginning of the chains. The plane of the ester group of the chain *sn*-2 has a tendency to orient parallel to the surface of the bilayer, while that of the chain *sn*-1 orients parallel to the bilayer normal. The different positioning of the ester groups relative to the surface of the membrane in *sn*-1 and *sn*-2 would have an influence on the rotational behavior of each chain. A greater conformational freedom, reflected by a higher probability of *gauche* defects, is for instance registered at the beginning of *sn*-2 compared to *sn*-1.

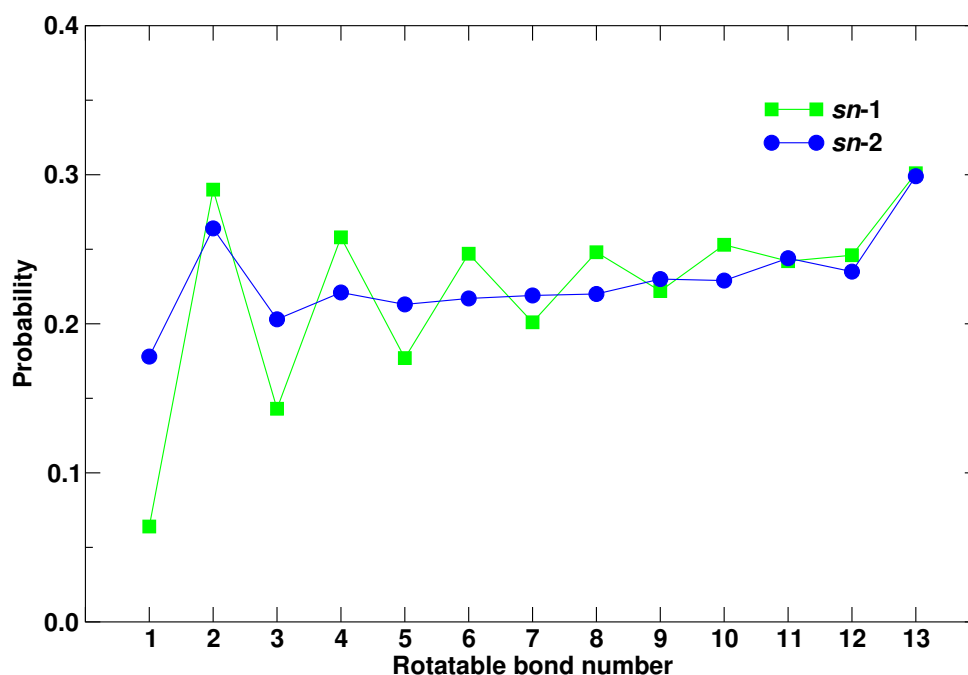


Figure 4.33: Probability of *gauche* defects as a function of the dihedral position for the chains *sn*-1 and *sn*-2 of DPPC.

Rotational isomerism occurring in the hydrocarbon chains plays a decisive role in determining the properties of the DPPC bilayer in the liquid crystalline phase. The cooperative

interaction of these chain rotations gives rise to the characteristic dynamic properties of the fluid bilayer, while the equilibrium population of *gauche* rotamers conditions its structural and thermodynamic properties.

4.3.4.3 Hydrocarbon chain order parameters

The average orientation of the lipid hydrocarbon chains with respect to the bilayer normal can be characterized by order parameters. Experimentally, ^2H -NMR yields, by far, the most detailed picture of the conformational state of the chains. Deuterium is substituted for hydrogen at specific positions along the acyl chains: the substitution of hydrogen by deuterium atoms is considered non-perturbing and causes no change in the structure. The corresponding deuterium quadrupole splitting $\Delta\nu_Q$ (*i.e.* the distance between the resonant absorption peaks) provides information on the orientation of the C–D bond with regard to the magnetic field of the NMR spectrometer. The quadrupole splitting is indeed related to the so-called deuterium order parameter S_{CD} by the following equation:

$$\Delta\nu_Q = \frac{3}{4} \cdot \frac{e^2qQ}{h} \cdot S_{CD} \quad (4.11)$$

where e^2qQ/h represents the quadrupole coupling constant of the C–D bond and is equal to approximately 170 kHz in the case of aliphatic chains. The deuterium order parameter gives a measure of the motional anisotropy of the particular C–D bond investigated:

$$S_{CD} = \frac{1}{2} \langle 3 \cos^2 \theta - 1 \rangle \quad (4.12)$$

θ is the instantaneous angle between the C–D bond and the direction of the bilayer normal, *i.e.* the z -axis (see Figure 4.34 for clarity), and the brackets denote an averaging over time and over all the lipid molecules. Only the absolute value of S_{CD} can be determined from Equation 4.11. It is however assumed that S_{CD} is negative, since the average orientation of the C–D bond is essentially perpendicular to the bilayer normal. Extreme cases of the order parameter are $-S_{CD} = 0.5$ if the chains are fixed in an all-*trans* conformation and are aligned along the bilayer normal, exhibiting rotation only around the long molecular axis (ordered state), and $-S_{CD} = 0$ if the chains do not show any preferred orientation and undergo isotropic rotation (complete disorder).

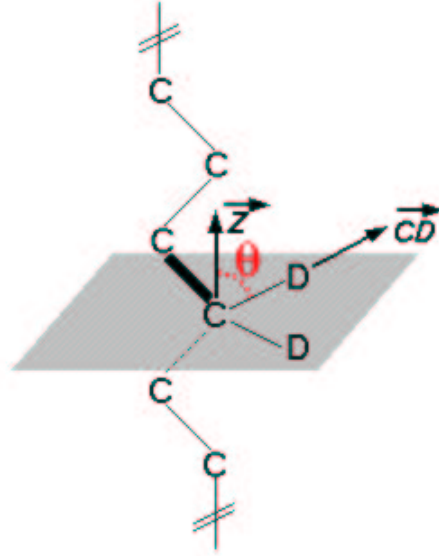


Figure 4.34: Definition of the angle θ between the molecular vector \vec{CD} and the bilayer normal \vec{z} .

The formal definition of the order parameter tensor S is given by:

$$S_{ij} = \frac{1}{2} \langle 3 \cos \theta_i \theta_j - \delta_{ij} \rangle \quad (4.13)$$

where θ_i (with $i \in \{x, y, z\}$) is the angle between the i th molecular axis and the bilayer normal, and δ_{ij} is the Kronecker delta ($\delta_{ij} = 0$ if $i \neq j$ and $\delta_{ij} = 1$ if $i = j$). For the carbon atom C_n of a methylene group, the molecular axes are defined as follows: x is along the H–H vector, y along the bisector of the H–C_n–H angle, and z along the vector from C_{n-1} to C_{n+1}. In a simulation, the “deuterium” order parameter for the carbon C_n can be calculated from the diagonal elements of the tensor S using the equation:

$$S_{CD}^n = \frac{2}{3} S_{xx}^n + \frac{1}{3} S_{yy}^n \quad (4.14)$$

When an all-atom force field is employed, S_{CD}^n can be evaluated directly and compared to the experimental deuterium order parameter derived from the quadrupole splitting. In the present simulation, non-polar hydrogens are not explicitly treated, so that their positions have to be reconstructed from the coordinates of the carbons along the acyl chains, assuming an ideal geometry of the C–H bond.

The order parameters S_{CD} provide a quantitative measure of the degree of order along the lipid hydrocarbon chains. They are related to the tilt angle of the chain and to the *trans-gauche* distribution of the dihedrals along the chains, but the relation is not direct. They are readily available from simulations and can be compared with the experimental order parameters, which are among the most accurately determined experimental properties. The deuterium order parameters along the DPPC hydrocarbon chains have been computed from the simulation and compared with experimental data [41, 146, 148]. Figure 4.35 (a) gives the order parameters averaged over both chains, Figure 4.35 (b) those for the chain *sn-2*. The overall form of the order parameter profiles is reproduced extremely well. The order parameters for the methylene segments C3-C8 decrease only slowly with chain position: this is conventionally referred to as the order parameter plateau. The plateau region is followed by a significant decrease in magnitude of the order parameter values towards the chain terminal methyl groups. The order gradient reflects a progressive loss of the regularity in chain packing from the interface towards the bilayer center. The plateau in the order profile is associated with the tethering of the acyl chains to the interface: the intermolecular restrictions on chain packing in this region leads to relatively high order parameter values ($-S_{CD} \approx 0.2$). Beyond the plateau region, the methylene segments are substantially more disordered to fill in the free volume that would otherwise be present due to the chain terminations: the methylene segments exhibit an almost isotropic behavior towards the chain extremities with order parameters approaching 0. The S_{CD} profiles determined separately for the chains *sn-1* and *sn-2* are plotted in Figure 4.36. The two tails exhibit slightly different behavior: in the upper part of the chain, *sn-1* is more ordered than *sn-2*, while the situation is reversed from the carbon C8 to the chain end. A similar behavior has been observed in a simulation of a DPPC bilayer performed by Smondyrev and Berkowitz [147].

The deuterium order parameters reflect thus the average orientation of the lipid hydrocarbon tails with respect to the bilayer normal and measure the ordering degree along the tails. They are characteristic of the physical state of the membrane and are very sensitive to physicochemical conditions such as temperature or hydration level. They say however little about the dynamics of the system or the range of motion. Disorder is indeed a static property and implies nothing about motion (one can have, for instance, a highly disordered structure, like window-glass, which displays little motion). The order parameters obtained from ^2H -NMR underline the increasing disorder of the lipid chains from the interface towards the bilayer interior. NMR relaxation data, for example, show that molecular motions are also maximized at the bilayer center.

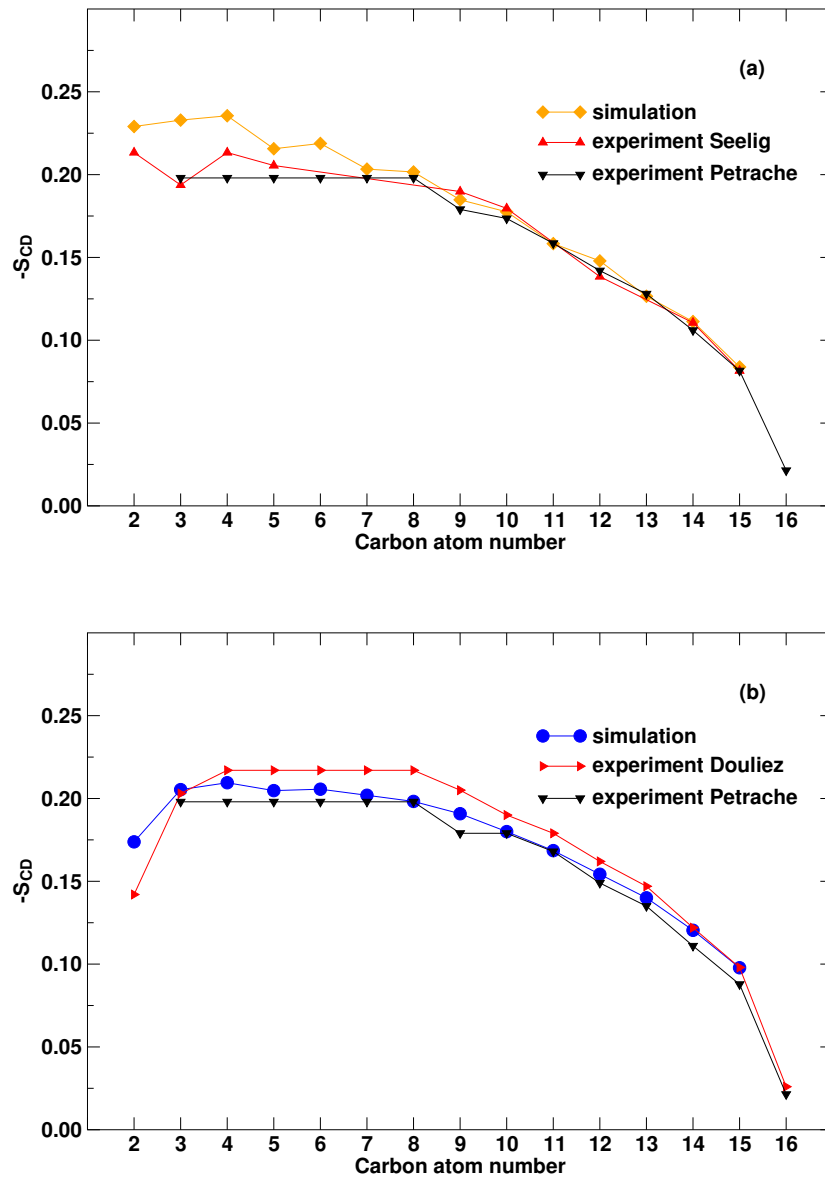


Figure 4.35: Deuterium order parameters for the hydrocarbon chains of DPPC as a function of the carbon atom number. **(a):** Comparison of the S_{CD} values averaged over both chains from the simulation with the experimental data of Seelig *et al.* [148] and of Petrache *et al.* [41]. **(b):** Comparison of the S_{CD} values for the chain *sn*-2 from the simulation with the experimental data of Douliez *et al.* [146] and of Petrache *et al.* [41].

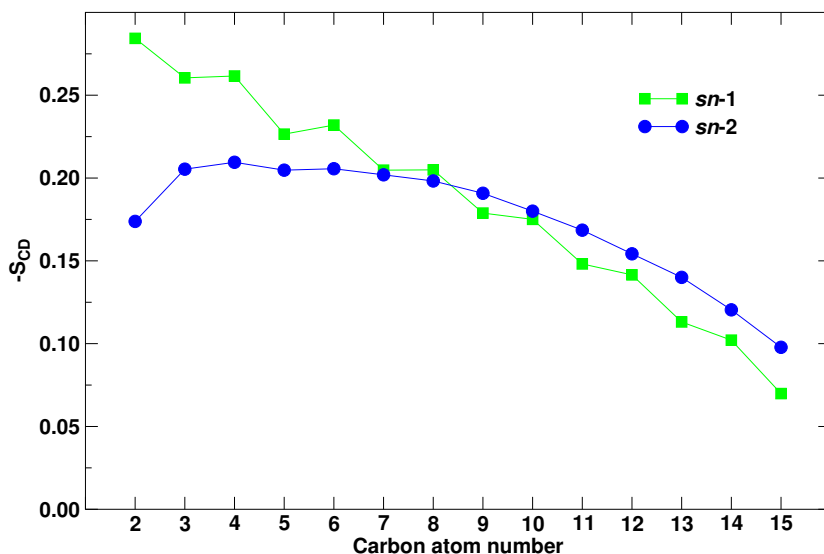


Figure 4.36: Deuterium order parameters obtained from the simulation for the chains *sn-1* and *sn-2* of DPPC.

4.3.5 Electron density distribution

The distribution of the electron density along the bilayer normal can be easily computed from the MD trajectory: since all atomic positions are known, the time-averaged z -distribution of electrons in the system can be evaluated with good accuracy. Experimentally, electron density profiles are usually obtained by Fourier reconstruction from bilayer form factors extracted from X-ray scattering data. Figure 4.37 shows the overall shape of the electron density profile: the profile computed from the simulation is in good agreement with the experimental profile of Nagle *et al.* determined by X-ray diffraction for multilamellar DPPC vesicles at 50°C [117]. The computed profile is symmetric, as it should be for a stable bilayer at equilibrium. It exhibits two maxima, essentially associated with the electron dense phosphate groups, and a minimum located in the middle of the bilayer, corresponding to the low density of the terminal methyl groups. The distance between the two peaks, also called “head-head spacing” X_{HH} , provides a good measure for the location of the phosphate groups. This distance corresponds to 3.62 nm in the computed profile, which is slightly lower than the distance between the phosphate groups previously determined from the atom density distribution (3.87 nm) and may be explained by the fact that the electron density maxima also include the electron density of the ester groups. The experimentally determined peak-

to-peak distance in the electron density profile ranges from 3.64 to 3.96 nm, depending on how the density was calculated.

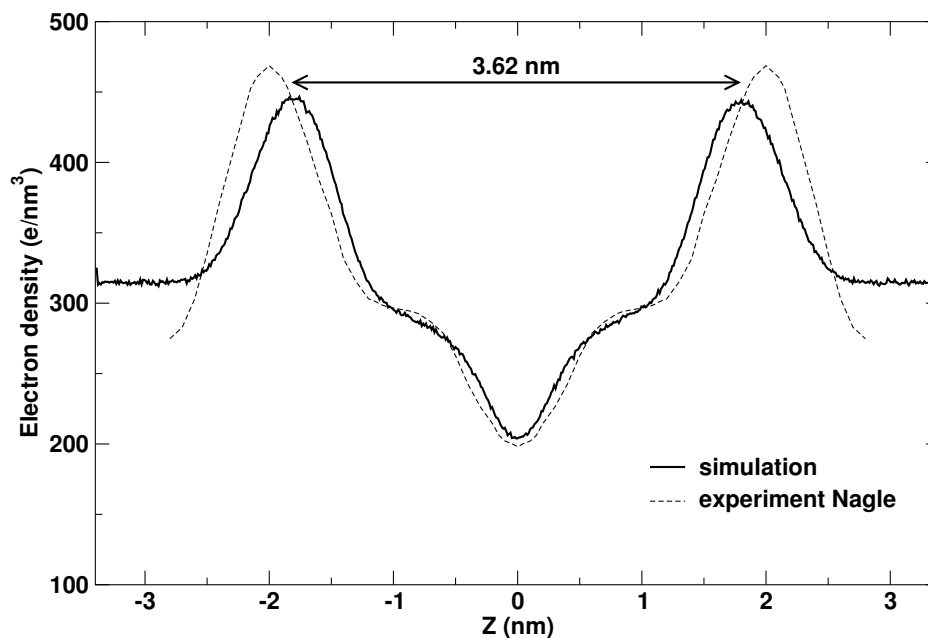


Figure 4.37: Electron density profile across the bilayer in absolute units of electrons per nm^3 . Simulation results (solid line) are compared with the experimental data (dashed line) of Nagle *et al.* [117].

4.3.6 Membrane dipole potential

The membrane potential is known to have a profound influence on the structure and function of the membrane: it is thought to play an important role in regulating not only the permeation of small molecules and ions, but even more complex processes such as the insertion of proteins or peptides and the adsorption of various membrane binding proteins. Three major sources contribute to the existence of the membrane potential: the transmembrane potential (or membrane voltage), the membrane surface potential, and the membrane dipole potential. The transmembrane potential is best understood with respect to its origin and magnitude. It is generated by ion gradients across the membrane and, hence, represents the potential difference between the aqueous phases partitioned by the membrane. It usually ranges from 10 to 100 mV with the inside aqueous compartment negative relative to the outside. The surface potential arises from the presence of charged groups (e.g. lipid headgroups) anchored

at the membrane surface but still exposed to the aqueous medium. These fixed charges attract counterions from the bulk aqueous phase to the membrane surface, which leads to a concentrating effect and to the creation of a diffusional flux of counterions away from the membrane surface. When these fluxes are equal in magnitude, the excess concentration of counterions and, hence, the electrical potential, decay to the bulk value over a distance of several nanometers. This surface potential is usually much smaller than the transmembrane potential, on the order of a few tens of millivolts [149]. Membranes also possess an internal potential, commonly referred to as the dipole potential. This potential is much larger than either the transmembrane or surface potentials, typically on the order of several hundred millivolts [150–152]. Its origin is more subtle and less understood, and is generally attributed to the non-random orientation of the electric dipoles in the lipid headgroups, the fatty acid carbonyl groups, and water. Experimentally, the membrane dipole potential is rather difficult to measure. Its existence was revealed by earlier experiments which showed that the passive permeability of lipid bilayers is orders of magnitude greater for organic anions than for organic cations. This observation led to the conclusion that a membrane dipole potential is responsible for the large disparity in membrane permeability of ionic species of opposite charges. More precisely, it was supposed that the internal membrane dipole potential in the hydrocarbon core of the bilayer must be positive relative to the water layer to explain the discrimination against cationic species.

The dipole potential across the DPPC bilayer was determined from the simulation as follows. The simulation box was divided into slices of 0.1 Å thickness perpendicular to the bilayer normal and the time-averaged charge density was computed in each slice. The dipole potential profile along the bilayer normal was estimated by integrating this charge distribution twice using Poisson's equation:

$$\psi(z) - \psi(0) = -\frac{1}{\epsilon_0} \int_0^z dz' \int_0^{z'} \rho(z'') \cdot dz'' \quad (4.15)$$

where $\psi(z)$ and $\rho(z)$ are the time-averaged dipole potential and charge density as a function of z , respectively, and ϵ_0 is the vacuum permittivity. The origin of the z -axis was fixed in the middle of the water layer, where the potential was chosen to be zero. The resulting membrane dipole potential is plotted in Figure 4.38 (a). The magnitude and overall shape of the potential profile are similar to those reported in previous simulations [94, 153]. A positive potential of about 640 ± 100 mV with respect to the water layer is found in the bilayer interior. The phosphatidylcholine headgroups have a large dipole moment. They tend to orient

their dipoles parallel to the bilayer surface for energetic reasons, but a completely parallel orientation is prevented for steric reasons: the free energy compromise results in a distribution of orientations averaging around a 20° tilt with respect to the bilayer surface (see Section 4.3.3.3, page 105). The average resulting z -component of the dipole generates a substantial dipole potential through the interfacial region which tends to make the inside of the bilayer negative. This dipole potential leads, in turn, to an ordering of adjacent water molecules. The observed water ordering is also caused by the steric constraints imposed by the optimization of hydrogen bonding between the water molecules intercalated between the lipid headgroups (see Section 4.3.3.2, page 101). In the interfacial region, the water molecules orient their dipoles preferentially towards the hydrocarbon region, in the direction opposite to that of the headgroup dipole, which tends to make the membrane interior positive relative to the water layer. In order to assess the contribution of the DPPC and water molecules to the total dipole potential, this one was split into components caused by both types of molecules (see Figure 4.38 (b)). The membrane dipole potential is due to a relatively small difference between two much larger and oppositely directed potentials, one produced by the orientation of the water dipoles and the other by the orientation of the headgroup dipoles. The net potential is positive because the net water polarization is larger in magnitude than the net phospholipid polarization. The overbalancing contribution of water to the dipole potential can be explained by the slowness of the motion of the phospholipid headgroups compared to the motion of the water molecules. The electrostatic potential of the headgroups fluctuates on the time scale of several nanoseconds. In response to these fluctuations, the water molecules reorient themselves and compensate for the fluctuating field. Since the reorientation of the water molecules happens on a much faster time scale, the contribution of the headgroups to the potential is overall overcompensated by that of water.

In addition to the net dipole potential, in which the hydrocarbon region is positive relative to the water phase, there is a positive potential peak in the interfacial region, at the position of the ester groups. The presence of this peak may play a role in the mechanism for the positive-inside rule of membrane protein folding [154]. This rule refers to the fact that positively charged amino-acids are disproportionately found in intracellular loops of membrane proteins, suggesting that it is particularly difficult for positive residues to cross the interface between the cytoplasm and the membrane interior.

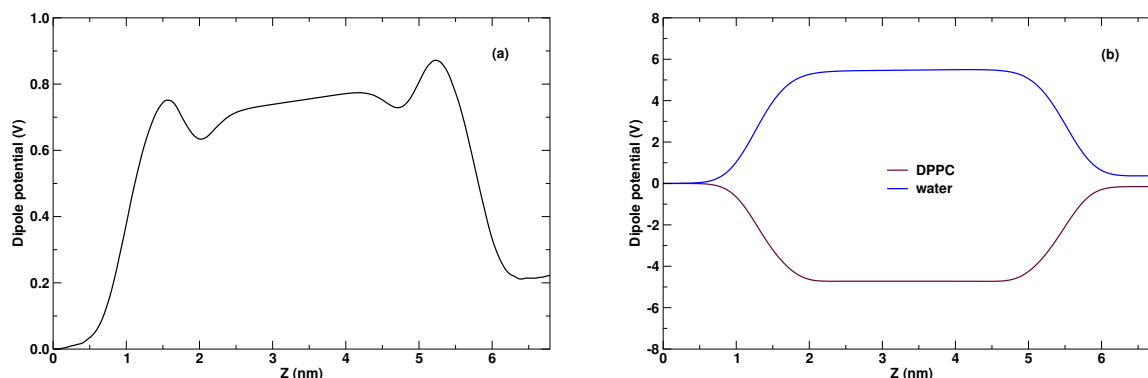


Figure 4.38: Dipole potential across the DPPC bilayer. The position $z = 0$ nm corresponds to the middle of the water layer and is taken as the zero of the potential. **(a):** Total potential. **(b):** Separate contributions due to DPPC and water.

4.3.7 Lipid mobility and lateral diffusion

The details of the dynamics of the lipid molecules are particularly important for determining the passive transport of small molecules across the membrane. Dynamic properties include *trans-gauche* isomerizations, dynamical fluctuations within the lipid moiety (rotation, reorientation, and relaxation), and lateral diffusion within the plane of the membrane.

To better understand the dynamics of the DPPC lipids, the motion of a single DPPC molecule within the bilayer was followed on different time scales (see Figure 4.39). On the 250 ps time scale, the only significant motions are rotation of the choline moiety and *trans-gauche* isomerizations in the lower part of the acyl chains. The glycerol backbone remains very stiff and the upper part of the acyl chains does not change its orientation. On the 1 ns time scale, the DPPC molecule exhibits a slight increase in the amplitude of motion, with a loosening of the glycerol backbone and additional rotations about the C–C bonds in the lipid tails. However, the headgroup has not moved very much and is still oriented in roughly the same direction. On the 10 ns time scale, the DPPC molecule starts to diffuse laterally and the headgroup undergoes significant rotation. The lipid tails show now a large amplitude of motion. On the 100 ns time scale, the DPPC molecule as a whole experiences additional rotational and translational motion. On this time scale only, the diffusional behavior of the lipids within the plane of the membrane can be really investigated. This is the main reason why the simulation was extended up to 150 ns.

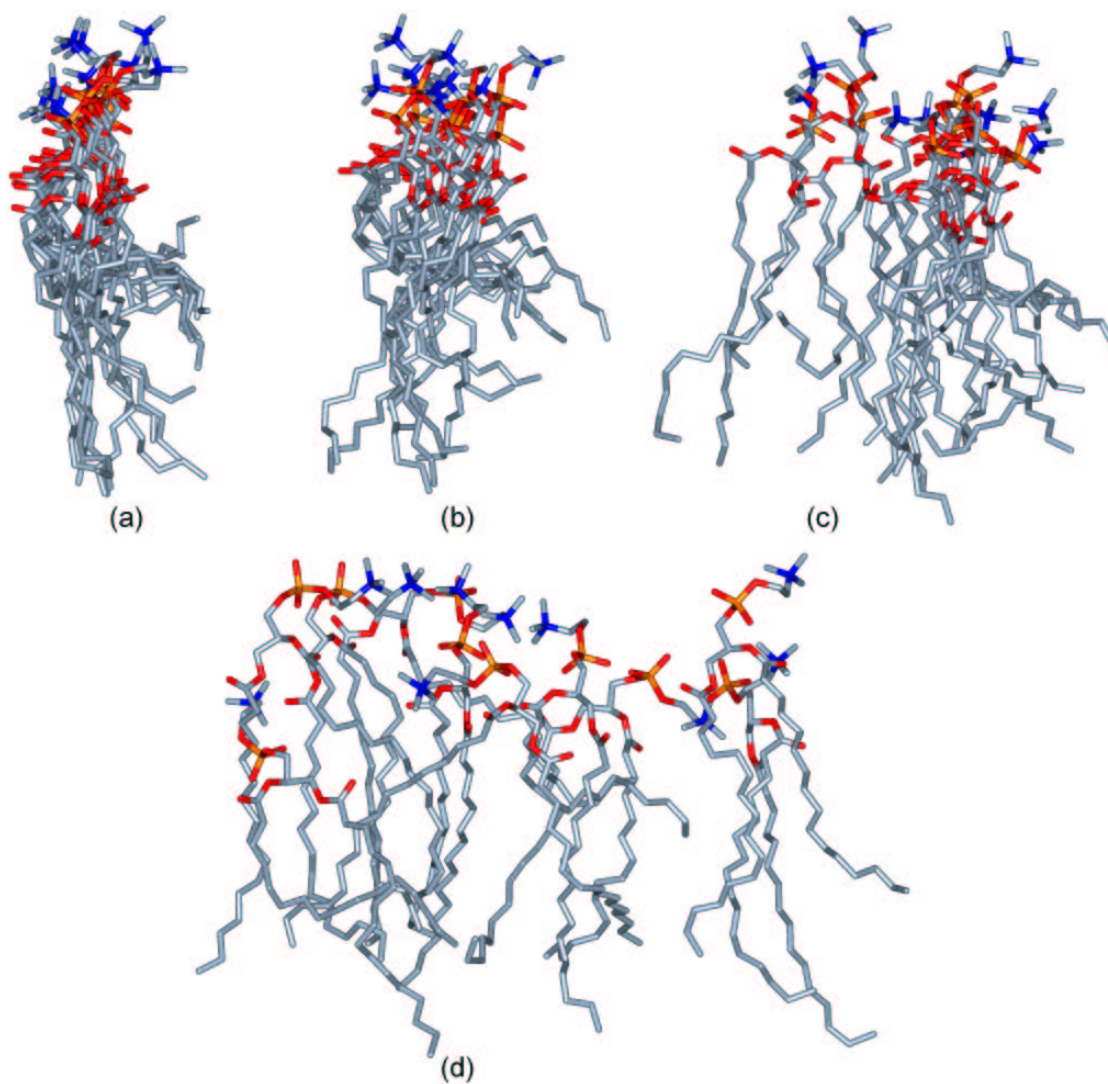


Figure 4.39: Four sets of ten evenly spaced configurations of a single DPPC molecule taken from the MD simulation of the DPPC membrane, spanning 250 ps (a), 1 ns (b), 10 ns (c), and 100 ns (d).

Although diffusion in lipid membranes has been studied for at least 40 years, the mechanism for lateral diffusion is still neither well characterized nor completely understood. Diffusion probably occurs by a combination of liquid-like 2D-diffusion and cage hopping between locally confined regions in the liquid crystalline lattice of the membrane, according to which a lipid “rattles” in a cage formed by its neighbors until a defect appears and it can jump to the next cage [155]. The lateral diffusion coefficient D_{lat} of the DPPC molecules within the membrane plane can be obtained from the slope of the lateral mean square displacement (MSD) versus time:

$$D_{lat} = \lim_{t \rightarrow \infty} \frac{1}{4} \frac{d}{dt} \left\langle [r(t+t_0) - r(t_0)]^2 \right\rangle_{t_0} \quad (4.16)$$

where r represents the center-of-mass (COM) positions. The MSDs were calculated for the COM of each DPPC molecule and averaged over time and over all the lipid molecules. r represents the COM positions. To improve statistics, the time origin t_0 was shifted every 25 ps. Before calculating MSDs, two corrections were introduced into the lipid coordinates. Although the COM of the whole system is reset after each step, both lipid layers can acquire some drift velocity and develop an opposite COM motion while the total COM motion for the system is still zero. The random relative motions of the two layers [156] give rise to an apparent supradiffusivity which is purely artificial and needs to be removed. For this reason, the DPPC coordinates were corrected by subtracting these monolayer COM motions. Because of the large box fluctuations observed in the x,y -plane with the anisotropic pressure coupling, the lipid coordinates were first calculated as fraction of the box dimensions and the MSD values were finally corrected for the average box dimensions. It turned out that this second correction did not introduce significant changes into the calculated diffusion coefficients, proving that the box anisotropy is not alarming. The lateral MSDs have been calculated over 62.5 ns, using data between 25 and 150 ns (see Figure 4.40 (a)). A linear regression of the MSD curve between 2.5 and 62.5 ns gives a lateral diffusion coefficient of $9 \times 10^{-8} \text{ cm}^2/\text{s}$, which is in good agreement with the coefficient of $12 \times 10^{-8} \text{ cm}^2/\text{s}$ reported by Lindahl and Edholm from a 100 ns DPPC simulation [156]. Experimentally, Sheats and McConnell, using a spin-label technique, measured a lateral diffusion coefficient ranging from 9.9 to $12 \times 10^{-8} \text{ cm}^2/\text{s}$ in planar DPPC multilayers at about $48 \text{ }^\circ\text{C}$ [157]. Kuo and Wade determined the lateral diffusion coefficient of DPPC in multilayers by pulsed NMR at various temperatures and hydration levels. Interpolation of their data at 323 K for $40 \text{ wt } \% \text{ water}$ results in a coefficient of about $9.5 \times 10^{-8} \text{ cm}^2/\text{s}$ [158]. Orädd and co-workers, also using pulsed NMR, found a lateral diffusion coefficient of about $28 \times 10^{-8} \text{ cm}^2/\text{s}$ for DMPC at 323

K using an Arrhenius temperature dependence with an activation energy of 49 kJ/mol [159]. Pace and Chan predicted a coefficient of about $15 \times 10^{-8} \text{ cm}^2/\text{s}$ from a jump-diffusion model for two- chains lipids at 323 K for a probability of jump success of 50% [160]. The type of diffusion regime reached in the simulation has also been investigated. Three regimes can be distinguished (see Figure 4.41). In a truly diffusive regime (Einstein diffusion), the lateral MSD is proportional to the time t ($\text{MSD} \sim t$), so that the slope S_l of $\ln(\text{MSD})$ versus $\ln(t)$ is equal to 1. This is a prerequisite to obtain a time-independent diffusion coefficient. In a subdiffusive regime, the MSD is proportional to $t^{1/n}$ ($\text{MSD} \sim t^{1/n}$ with $n > 1$), so that S_l is equal to $1/n$ and thus inferior to 1. For instance, if the lipid molecules are completely trapped, S_l is close to 0. For lipids diffusing around obstacles (*i.e.* neighboring lipids), S_l lies between 0 and 1. In a supradiffusive regime, the MSD is proportional to t^n ($\text{MSD} \sim t^n$), so that S_l is equal to n and superior to 1. For instance, over very short times, on the order of picoseconds, the displacement itself is linear with time and $\text{MSD} \sim t^2$, which corresponds to $S_l = 2$. A supradiffusive motion can also be found if the whole monolayer acquires a net velocity in a certain direction (the correction described previously on the DPPC coordinates was applied to avoid such phenomena). The time-dependent slope S_l of the curve $\ln(\text{MSD})$ vs $\ln(t)$ has been estimated using a centered different quotient approximation and is plotted in Figure 4.40 (b). Only after about 10 ns, the slope fluctuates around 1, which means that the truly diffusive regime is finally reached.

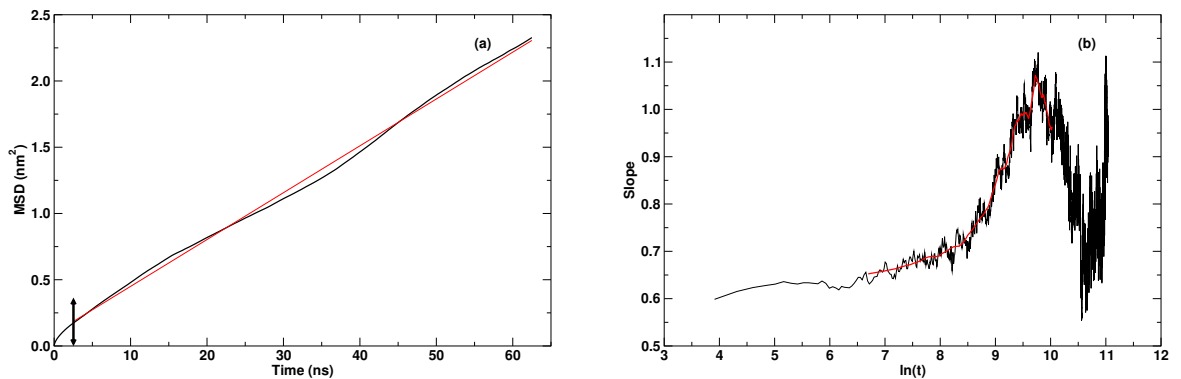


Figure 4.40: (a): Center-of-mass mean square displacement of the DPPC molecules versus time (black curve) and linear regression from 2.5 to 62.5 ns (red line). (b): Time-dependent slope of the curve $\ln(\text{MSD})$ vs $\ln(t)$. The red curve represents a running average.

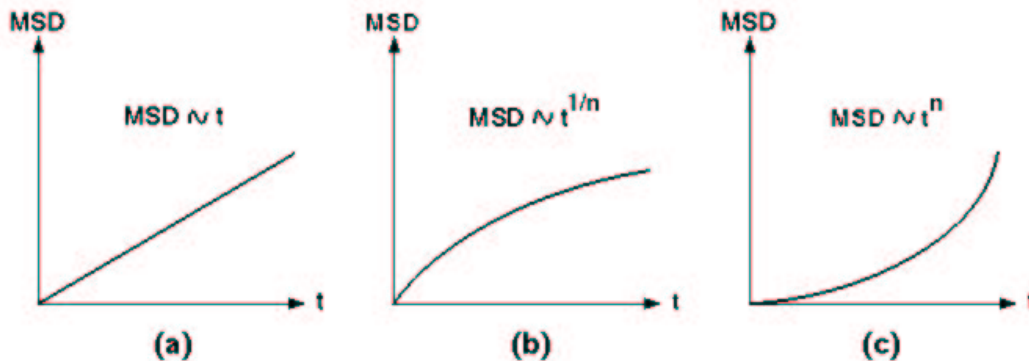


Figure 4.41: Types of diffusion regime. (a): Truly diffusive regime. (b): Subdiffusive regime. (c): Supradiffusive regime.

4.3.8 Summary

The main quantitative results obtained from the simulation of the DPPC membrane are listed in Table 4.5: the area per lipid (A), the volume per lipid (V_L), the density of the DPPC/water system (ρ), the bilayer repeat spacing (D), the hydrophobic thickness ($2D_C$), the distance between the phosphate groups on both sides of the bilayer ($\text{PO}_4\text{-PO}_4$), the average hydrocarbon chain order parameter found in the plateau region from the carbons C3 to C8 (S_{CD}^{plateau} : average value over both chains), the fraction of *trans* dihedrals in the hydrocarbon chains (*trans*-fraction), and the lateral diffusion coefficient of the DPPC molecules (D_{lat}). A satisfying agreement with experimental data is found for all these parameters.

Table 4.5: Comparison of the results from the simulation of the DPPC membrane with experimental data.

323 K	Simulation	Experiment
A (nm ²)	0.635	0.633 ^a / 0.640 ^b
V_L (nm ³)	1.219	1.232 ^c
ρ (g/cm ³)	0.977	0.991 ^d
D (nm)	6.74	6.72 ^e
$2D_C$ (nm)	2.83	2.84 ^a
$\text{PO}_4\text{-PO}_4$ (nm)	3.87	3.6–3.8 ^f
S_{CD}^{plateau} (C3–C8)	0.218	0.198 ^a / 0.202 ^g
<i>trans</i> -fraction (%)	76.6	60–77 ^h
D_{lat} (10 ⁻⁸ cm ² /s)	9	~ 10 ⁱ

^aSee reference [41]. ^bSee reference [42]. ^cSee reference [134]. ^dSee reference [161]. ^eSee reference [117].

^fSee reference [136]. ^gSee reference [148]. ^hSee references [141–146]. ⁱSee references [157–160].

4.4 Discussion

The most important result from the simulation of the DPPC membrane is that a phospholipid membrane is a very stratified and heterogeneous structure. Structural and dynamic studies of lipid bilayers which consider the membrane as a whole and only focus on “global” membrane properties fail into giving a realistic picture of the complex lipid/water system. The simulated DPPC/water bilayer differs indeed considerably from a two-phase alkane/water system. Instead of sharp interfaces, very diffuse interfaces between the PC headgroups and water are observed. The interfacial region (including both interfaces) represents about 40% of the whole membrane, so that the term of *interphase* would be actually more appropriate than *interface* to designate this broad region. The interphase is a polar, multicomponent region where specific headgroup-headgroup and headgroup-water interactions take place. The hydrocarbon interior of the membrane also shows an inhomogeneous and anisotropic character and cannot be compared to a bulk liquid alkane phase. The density and disorder degree vary significantly along the DPPC acyl chains: the density decreases towards the middle of the bilayer, while the chain disorder increases towards the terminal methyl groups. The bilayer is indeed a highly cooperative system. An acyl chain cannot change its direction without any compensating changes in the neighboring chains. Hence, groups of adjacent chain segments must move in a cooperative manner. Deviations in chain segment direction from the bilayer normal accumulate as one proceeds from the bilayer surface to the interior, so that the disorder is maximal at the center of the bilayer.

A robust framework to discuss the overall structure of the simulated DPPC bilayer is the model proposed by Marrink and Berendsen [135]. This model takes into account the stratification and the heterogeneous character of the lipid/water system and splits up the membrane into four distinct regions, each of them having its own characteristics. The location and extent of the four regions can be visualized in Figure 4.42, from the density distribution profile of the DPPC/water system along the bilayer normal, or in Figure 4.43, from a transversal section of the DPPC membrane. In this model, the exact location of the boundaries is not so important and may vary between different phospholipid membranes, but the characterization of four regions with specific features is essential to understand the complex properties of lipid membranes as well as their barrier functions. The characteristics of each region are described below. Note that the present definition of the regions 1 and 2 slightly differs from that reported by Marrink and Berendsen.

Region 1: perturbed water phase The first region starts at the point where the water molecules begin to be perturbed by the vicinity of the lipid headgroups, and goes to the point where the water density decreases to 90% of its maximal value. This region can be quite extensive, since the water molecules can feel the presence of the lipids over large distances. In the model of Marrink and Berendsen, region 1 ends where the water and DPPC densities are comparable and thus includes a part of the water/DPPC interface. In the present DPPC model, region 1 is 0.88 nm broad. The DPPC headgroups protrude into this region and substantially affect the water properties: the water molecules show an increasing orientational profile and a slowdown of their movement from the bulk water phase towards the interface. The protruding headgroups (especially the choline moieties) are particularly mobile in this region and exhibit large hydration shells.

This region is important for the understanding of membrane-membrane interactions. The strong repulsive hydration force between membranes [42], for instance, originates from the water ordering in this part of the membrane. This region is also involved in the initial step of membrane fusion processes and in membrane-protein binding.

Region 2: interphase Within this region, the water density drops from 90% to 10% of its maximal value over a distance of about 1.24 nm, whereas the DPPC headgroup density reaches its maximum. In this region, which constitutes the most polar part of the membrane, DPPC headgroups and water molecules are strongly organized. This organization is not only found along the bilayer normal, where the water molecules are polarized to counteract the effect of the headgroup dipoles, but also in the plane of the membrane, where the headgroups form a network of interacting moieties to optimize the electrostatic interactions via charge pairs. In this network, water molecules strongly interact with the headgroups and even form bridges among them. Bulk-like water is no longer present in this part of the membrane. This region has the highest density of the membrane and is extremely complex owing to its strong heterogeneity: it is populated by water, choline, phosphate, ester groups, and a part of the upper tail methylene groups. Wiener and White have called it “a region of tumultuous chemical heterogeneity” [162].

This region plays an important role in the polymorphic behavior of the lipids. The headgroup-headgroup and headgroup-water interactions strongly influence the surface tension and surface curvature of the membrane, which condition the phase transitions and phase separations. A solute entering this region will find tight quarters, slow diffusion rates, polar interactions, and many opportunities to form hydrogen bonds. The large, bulky headgroups

limit the volume available to solute molecules and, hence, present an entropic barrier to permeation.

Region 3: soft polymer phase The third region (~ 0.86 nm broad) starts just after the DPPC carbonyl groups (which is the limit for the penetration of water into the bilayer) and ends at the point where the density of the DPPC hydrocarbon chains has dropped to that of liquid hexadecane (~ 0.75 g/cm³ at 323 K [163]). The density and properties of this region are similar to those of a soft polymer. The density is still high: the hydrocarbon chains are relatively well ordered and closely packed, leaving little free volume. The chain order parameters are here at their plateau values.

Due to its high density and its hydrophobic character, this region constitutes the main barrier to the permeation of solutes through the membrane, especially in the case of polar solutes. The solute will experience some constriction due to the order and packing of the hydrocarbon chains.

Region 4: liquid alkane phase The middle and remaining part of the bilayer constitutes the fourth region (~ 0.84 nm broad). This region has the lowest density of the membrane and hence, exhibits the highest fraction of free volume. At the center of the bilayer, the tail density is comparable to that of liquid pentane. The tails are very disordered, with order parameters close to zero, and exhibit an almost isotropic behavior.

The hydrophobic environment and the presence of large free volume pockets in this region allow for the accommodation of relatively large apolar molecules. Closer to the bilayer center, owing to the increased free volume, a solute will experience a wider range of orientations. The increased rate of movement of the hydrocarbon chains will break up and move the voids, allowing more frequent jumps by small solutes.

According to the above description, lipid bilayers have thus a structure very different from that of bulk organic fluids. Lipid bilayers might be considered as a continuous interface in that their properties vary continuously from the bulk water through the ordered water layer, the headgroup region, the upper hydrocarbon chains, and the bilayer center. Understanding this makes it easier to rationalize the problems related to the prediction of permeation rates across membranes.

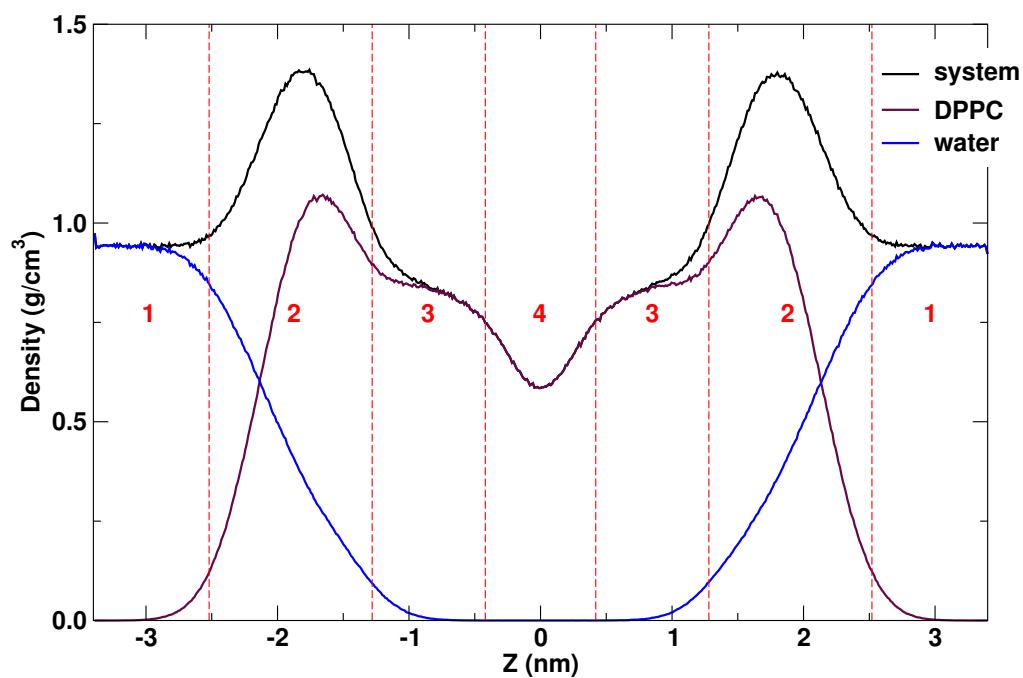


Figure 4.42: Trans-bilayer density distribution profiles of the whole system, DPPC, and water. The vertical dashed lines delimit the different regions of the membrane.

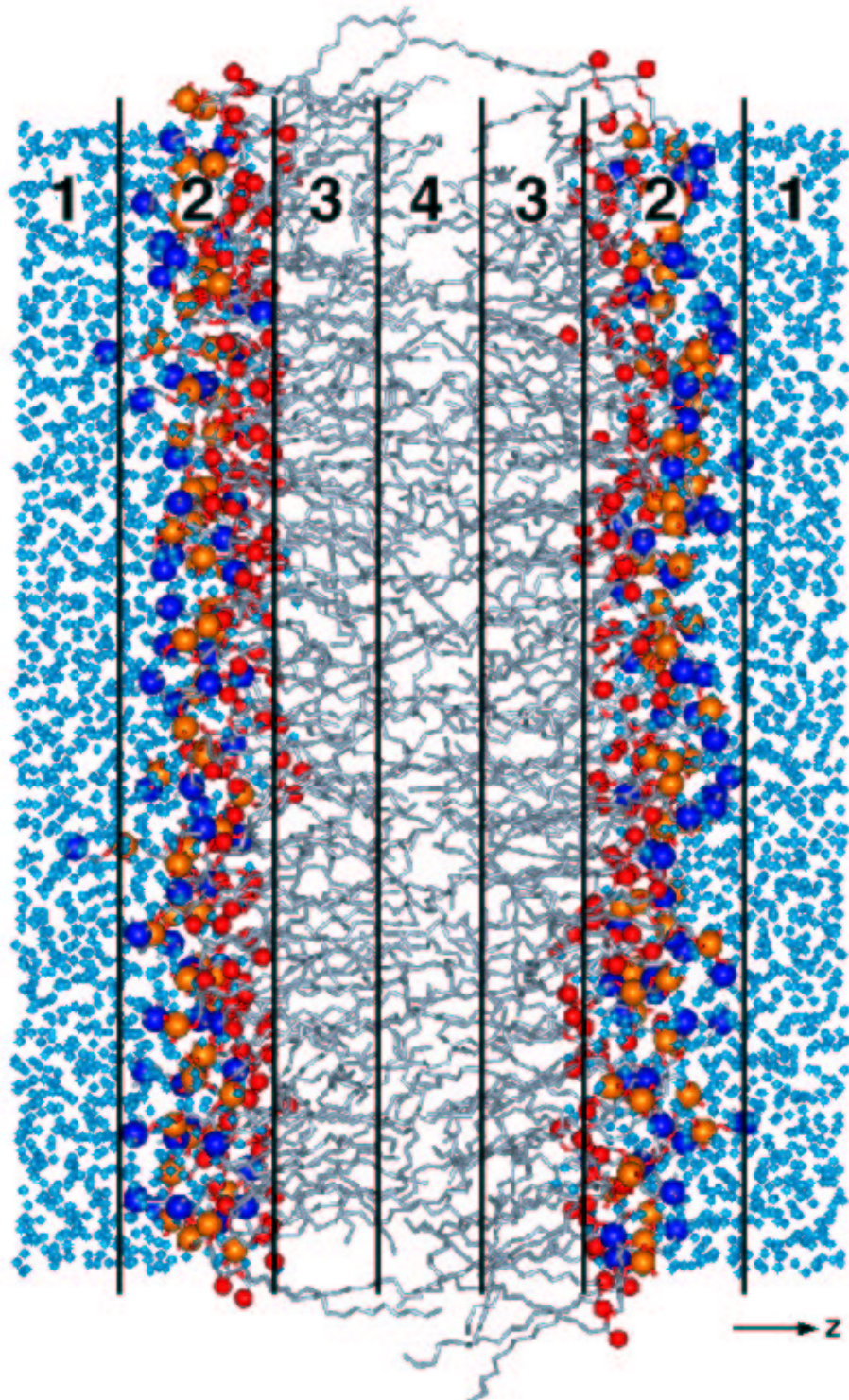


Figure 4.43: Transversal section of the simulated DPPC membrane. The nitrogen (blue), phosphorus (orange), and carbonyl oxygen (red) atoms of DPPC are emphasized (space-filling format). The vertical solid lines delimit the different regions of the membrane.

4.5 Conclusion

The results obtained in the present MD study suggest that the simulated DPPC membrane patch is well equilibrated, stable over a long period of time, and shows good agreement with experimental observations in many respects. This close agreement with experiments justifies the use of the obtained membrane model as starting structure for extended simulations incorporating solute molecules into the membrane and investigating their interactions with the lipid environment as well as their permeation through the membrane (see Chapter 5).

In particular, the MD simulation of the DPPC/water system yields a very insightful picture of the static arrangement and the dynamic properties of a phospholipid membrane on the atomic level. It must be underlined that *membrane structure* is different in many aspects from *protein structure*. In a protein, the position of a particular atom may fluctuate no more than tenths of an angstrom to a couple of angstroms during the entire lifetime of the molecule. In a fluid membrane, however, individual atoms commonly migrate very long distances. Hence, by contrast to protein structure, a fluid membrane structure is a set of statistical distributions for how different atom types and molecular groups dispose themselves relative to each other, averaged over time [115]. Contrary to common belief, phospholipid bilayers are highly structured fluids, both transversely and laterally. They can be divided into four distinct regions, each having its own specificities [135]. This type of organization is of particular importance for membrane function. A good understanding and appreciation of the subtleties of membrane structure are essential for the study of various membrane processes such as permeation processes.

Chapter 5

Solute permeation across a phospholipid bilayer

5.1 Introduction

Although the transport of many nutrients, waste products, and ions is facilitated by specialized molecules in the membrane, the most fundamental mechanism for translocating small molecules across membranes is unassisted transport (*i.e.* passive diffusion). Water, oxygen, carbon dioxide, most drugs, and some toxins are among the species transported via this mechanism. The absorption of orally administered drugs is largely determined by their ability to cross the mucosa of the gastrointestinal tract: unless they are analogs of physiological molecules, they are absorbed across the gastrointestinal mucosa by a passive diffusion mechanism. In drug research, around one third of development candidates is lost due to inappropriate pharmacokinetic properties. To increase the quality of potential drug compounds, methods are required in early drug discovery to dissect key factors influencing drug absorption. Despite extensive experimental research, the process, energetics, and kinetics of drug permeation is still not well understood, and the prediction of permeation rates, a quantity intensively desired by the pharmaceutical community, remains a very challenging area. A number of molecular properties influencing passive absorption of drugs has been identified and includes octanol/water or alkane/water partition and distribution coefficients ($\log P$ and $\log D$ coefficients), ionization state (pK_a), hydrogen-bonding capability, and molecular size. Although these parameters prove to be useful to predict passive absorption, their impact in early drug discovery is limited due to the amount of material, manpower, and time

needed to collect these data. Furthermore, semi-empirical relations linking octanol/water or alkane/water $\log P/D$ values to absorption rates, although successful in many cases, often collapse when non-congeneric structures are analyzed. The anisotropic structure of lipid membranes, in contrast to bulk phase solvents with invariant properties throughout, has indeed very different physical and chemical characteristics as a function of the position along the bilayer normal axis that affect drug-lipid interactions. Drug molecules exploit these local differences within the membrane to achieve an energetically favorable location, orientation, and conformation.

The MD technique can apprehend the subtle balance of solute-lipid interactions when the solute molecule is transferred from the aqueous environment to the hydrophobic core of the membrane and reveal the detailed motions of the solute within the membrane. Solute permeation across a lipid bilayer is thus an interesting topic for study with MD. Experimentally, the permeability coefficients measured for small penetrants in phospholipid bilayers vary by several orders of magnitude, ranging roughly from 10^1 cm/s for penetrants like hexanoic acid [164], toluic or naphthoic acid [40], to 10^{-10} – 10^{-11} cm/s for fructose or glucose [165]. These permeation rates are too slow on the time scale available to the MD technique, which limits simulations to several tens of nanoseconds at most. This means that, within the time scale of MD simulations, the permeation of solute molecules through a lipid bilayer cannot be observed directly, so that special techniques have to be used to simulate the permeation process and estimate the permeation rate. Standard procedures consist either in dragging the penetrant into the membrane or in immobilizing it at various depths within the membrane by applying some constraints.

In this chapter, permeation studies through the DPPC bilayer model developed in Chapter 4 are presented. The permeation process of a sugar molecule (methylglucose), a polyalcohol (mannitol) as well as a drug-like molecule (salicylic acid) has been investigated. As a first step, equilibrium MD simulations have been performed to examine the partitioning of these solutes into the membrane in a qualitative way. As a second step, series of extensive non-equilibrium MD simulations have been undertaken to quantify the energy barrier to be overcome by the solutes for their translocation from the water phase into the membrane interior (transfer free energy) as well as the rate by which they diffuse through the membrane (diffusion coefficient). Both quantities – transfer free energy and diffusion coefficient – should enable one to determine the permeability coefficient of the solute in the membrane and to compare it with available experimental data.

5.2 Theory

5.2.1 Permeation models

Two alternative models are commonly used to describe the molecular mechanisms of solute permeation through lipid membranes. One is referred as the *solubility-diffusion model*, in which the solute has to partition into and diffuse through the membrane. The other model, the *defect model*, involves the occurrence of transient pore-like defects such as water pores in the lipid bilayer which allow ions and small polar molecules to bypass the partitioning energy barrier.

5.2.1.1 Homogeneous solubility-diffusion model

The most generally accepted model to describe the permeation of small neutral permeants across lipid bilayer membranes is the homogeneous solubility-diffusion model [166–168], which was originally applied by Overton [13] to permeation across cell membranes. This model depicts the bilayer membrane as a thin static slab of bulk organic solvent, representing the permeation barrier and separating two aqueous phases. The bilayer is considered to be isotropic and homogeneous, and the water/membrane interface is treated as a sharp boundary between the two phases. The permeation process is described in three steps: the permeating molecule has first to partition into the membrane, then to diffuse through the membrane interior, and finally to dissolve again into the second aqueous phase. In this model, permeation through the membrane is assumed to be the rate-limiting step in the transport process and interfacial barriers for membrane entry or exit are neglected.

Thus, the permeation resistance R , which is equivalent to the inverse of the permeability coefficient P , can be expressed as follows:

$$R = \frac{1}{P} = \frac{d_b}{K_{b/w} \cdot D_b} \quad (5.1)$$

The permeation resistance is proportional to the bilayer thickness of the barrier d_b (which does not include the two interfaces and is assumed to be constant), and inversely proportional to the partition and diffusion coefficients of the permeant in the barrier, $K_{b/w}$ and D_b , respectively. In practice, $K_{b/w}$ is associated to the partition coefficient of the permeant between water and a bulk organic solvent resembling the membrane interior, such as octanol,

olive oil, or a liquid hydrocarbon like decane or hexadecane, and D_b is approximated by the diffusion coefficient of the permeant in a bulk hydrocarbon solvent.

The solubility-diffusion theory as typically employed (*i.e.* Equation 5.1) suffers from several weaknesses. It is quite obvious, both from experiment and simulation, that the membrane exhibits a structure that would not be expected at an interface between an organic solvent and water. The rough features of a lipid bilayer are clear: the polar headgroups of the lipids interface with water and the hydrocarbon interior. However, as shown in Chapter 4, the structure of a bilayer has a much finer detail than this: a bilayer is a very heterogeneous construct, with distinct regions that may have very different affinities for a solute. Experimental and theoretical analyses clearly show that solute partitioning into bilayers differs in many respects from that into bulk solvents. Specifically, the solute partition coefficients into bilayers exhibit a strong dependence on the local lipid microstructure, a feature that cannot be accounted for based on partition coefficients in bulk fluids. Neglecting in the permeation process the role of the water/membrane interfaces, which represent about 40% of the total membrane phase, is a particularly crude approximation that often leads to erroneous estimations of permeation rates. Alkane/water partitioning systems, for instance, can only model the hydrophobic contribution of solute-membrane interactions, whereas the interactions between the solute and the polar lipid headgroups are not taken into account. Finally, the diffusion process within the membrane is not homogeneous. The lipid chains are more ordered near the water/lipid interface and become progressively less ordered as the bilayer center is approached. However, even in the center, the order parameters do not suggest the complete disorder expected in fluid hydrocarbons.

To conclude, the oversimplifications made in this homogeneous model fail to take into account the diverse and complex properties of real membranes, so that the permeation mechanism cannot be properly described by this approach.

5.2.1.2 Inhomogeneous solubility-diffusion model

Considering the limitations of the homogeneous solubility-diffusion model to predict the permeation rates of solutes in lipid membranes, Marrink and Berendsen derived an inhomogeneous solubility-diffusion model [135]. In this model, the diffuse interfaces between the lipid headgroups and water are included in the description of the permeation process, and the anisotropic and inhomogeneous character of the membrane interior is now taken into consideration.

For a structurally heterogeneous membrane, both the partition and diffusion coefficients of the solute and, hence, its permeability coefficient exhibit spatial variations within the membrane. Equation 5.1 can be thus generalized to express the overall membrane resistance R as the integral over the local resistances across the membrane and to relate it to spatially-dependent solute partition and diffusion coefficients:

$$R = \frac{1}{P} = \int_0^d R(z) \cdot dz = \int_0^d \frac{dz}{K_{z/w}(z) \cdot D(z)} \quad (5.2)$$

$K_{z/w}$ and D_z are the depth-dependent partition coefficient of the solute between water and the membrane and the solute diffusion coefficient within the membrane, respectively, at a position z along the bilayer normal. d is now the entire membrane thickness, including the water/membrane interfaces. The critical parameter in Equation 5.2 is the partition coefficient $K_{z/w}$ which does not only reflect the solute distribution between the aqueous phase and the membrane, but also all possible molecular interactions between the solute and both environments. $K_{z/w}$ can be calculated from the Gibbs free energy ΔG required to transfer the solute from the aqueous to the hydrophobic phase as follows:

$$K_{z/w}(z) = \exp(-\Delta G(z)/R_c T) \quad (5.3)$$

where R_c is the ideal gas constant and T , the temperature. In essence, water/membrane partitioning cannot be predicted reliably and accurately without the ability to determine the associated free energy changes. Thus, the permeation resistance can be also expressed in terms of free energy:

$$R = \frac{1}{P} = \int_0^d \frac{\exp(\Delta G(z)/R_c T)}{D(z)} \cdot dz \quad (5.4)$$

Permeability is therefore a rate process that contains contributions from both an equilibrium (partitioning) and a non-equilibrium (transverse diffusion) step. Partitioning into the membrane can be well described by the free energy profile across the membrane, *i.e.* the free energy barrier to be overcome by the solute to permeate through the membrane. The challenge is thus to determine the free energy barrier as well as the local diffusion coefficient of the solute in the membrane. The permeability coefficient can be then obtained by numerical integration of Equation 5.4.

5.2.1.3 Defect model

The formation of transient aqueous pores produced by thermal fluctuation within the membrane has been shown to contribute to the permeability of the bilayer to ions, water, and small neutral molecules [169, 170]. As is known, the bilayer membrane represents a two-dimensional liquid crystal with a rather high lateral mobility of the lipid components; the large fluctuations in the bilayer structure may give rise to transient defects. Two types of through-going pores, namely, with hydrophilic or hydrophobic lateral surface (see Figure 5.1), can be distinguished [171]. During the formation of a transient hydrophobic defect, the lipid molecules are moved apart by thermal fluctuations, so that the membrane hydrophobic core is penetrated by the aqueous bulk phase, resulting in the formation of a pore. There are two possibilities for the development of such a pore. One of them is the collapse of the pore, with the simultaneous return of the lipid molecules to their original positions. The other possibility involves the reorientation of the lipid molecules resulting in the covering of the inner surface of the pore by the polar lipid headgroups, *i.e.* an inverted pore is formed. In both hydrophobic and hydrophilic defects, pore formation results from dynamic properties of the lipid bilayer, and the equilibrium pore distribution is relatively constant over time [172]. By passing through such hydrated defects, the permeating molecule can avoid the high-energy barrier associated with partitioning into the hydrophobic membrane interior. Transport through transient pores seems to be the dominant mechanism for the permeation of ions through lipid bilayers [173]. In the case of small polar molecules, it is plausible that both mechanisms, the partitioning and pore mechanisms, operate in parallel [170].

Water wires extending across a lipid bilayer are thermodynamically unstable, so that they form infrequently and their lifetime is limited. Owing to their transient character, they are particularly hard to detect experimentally, which makes their existence doubtful. However, it should be noted that the hydrophobic core of the membrane is not impenetrable to water and, just as organic liquids, has a measurable miscibility with water. Water is thought to exist at a millimolar concentration within the hydrocarbon core [174]. Subczynski and co-workers determined the hydrophobicity profile across PC bilayer membranes using an ESR spin-labeling method and showed that the water penetration into the membrane is extensive up to the depth of the carbon atom C8 [175]. Membrane permeability to hydrophilic solutes could be therefore facilitated by penetration of water into the hydrophobic region of the membrane.

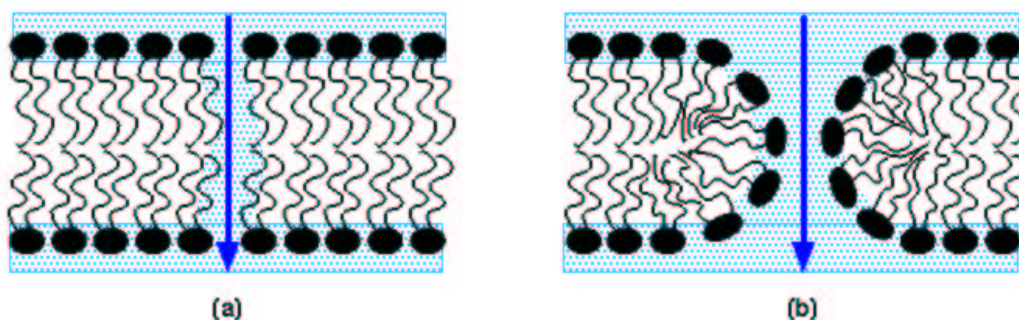


Figure 5.1: (a): Hydrophobic pore. (b): Hydrophilic pore.

5.2.2 Simulation of permeation processes

As already mentioned in the introduction, the time required for a penetrating molecule to permeate through the membrane is much longer than can be simulated. To get some statistical information on permeation processes, simulations on the order of microseconds are indeed necessary. Equilibrium MD simulations can still be performed to follow the trajectory of the penetrant in time within the membrane. But, in order to get a full description of the permeation process across the whole membrane, non-equilibrium MD simulations using indirect methods have to be carried out. In the present study, the *umbrella sampling method* as well as the *average force method on constrained particle* have been employed and are described below.

5.2.2.1 Equilibrium MD simulations

“Conventional” equilibrium MD simulations, starting with solute molecules located at various depths within the membrane (e.g. hydrophobic core, interface, water layer), directly provide the average distribution of the solute in the membrane. They also allow the direct analysis of a variety of properties, such as hydrogen bonding between the solutes and the water or lipid molecules, specific orientations or conformations of the solutes within the bilayer. Equilibrium MD simulations give thus information on the preferred location of the solutes within the membrane and enable one to get some idea of the shape of the free energy profile across the membrane. These issues are not only relevant to the transverse diffusion of drugs across membranes, but can also have a direct influence on the activity of drugs binding to receptors via the membrane bilayer. Indeed, the passive partitioning of drugs into membranes and their subsequent location and movement within membranes is thought to be important

for their interactions with membrane-bound receptors [176]. Some lipophilic drugs diffuse to hydrophobic, intramembranous receptor sites by first penetrating the membrane to a certain location and then laterally diffusing to the receptor, so that their preferred location in membranes is of particular importance. A drug that does not penetrate to the proper depth within the bilayer will be not as active as a drug which, at the proper depth within the bilayer, can diffuse to the receptor site and participate in a successful interaction. In addition, the conformations adopted by the drug in the membrane may influence its binding to the receptor site. The lipid bilayer may constrain flexible portions of the drug molecule, thus setting up different overall drug conformations that are dependent on the bilayer structure and composition. A “membrane bilayer pathway” has for instance been reported for the binding of lipophilic 1,4-dihydropyridine calcium channel blockers to voltage-dependent calcium channels in cardiac and smooth muscle sarcolemma [177].

The perturbations of the bilayer structure generated by the presence of solute molecules inside the membrane can also be observed from equilibrium MD simulations by comparison with the properties of the pure bilayer system simulated under the same conditions. This topic is also of pharmaceutical importance. For instance, general anesthetics are thought to produce anesthesia by a common mechanism involving perturbation of the structure of membranes in the neuronal tissue [178]. An other example is the perturbing effect of permeation enhancers on the membrane structure (see Chapter 1, Section 1.3.2.3, page 48).

Hence, equilibrium MD simulations of membranes including solute molecules can provide a wealth of information. However, the simulation time scale is simply not long enough to allow the solute molecules to explore the entire range of membrane environments. In the case of a hydrophilic solute molecule, not enough statistical data are collected in the hydrocarbon core of the bilayer, whereas the sampling is poor in the polar headgroup region for a hydrophobic solute. These regions where the probability to find the solute is low determine, however, the rate of permeation and, thus, need to be thoroughly sampled.

5.2.2.2 Non-equilibrium MD simulations

Umbrella sampling method Umbrella sampling is a special biased sampling technique which has been developed by Torrie and Valleau [179, 180]. In this approach, the system of interest is simulated in the presence of an artificial biasing potential (also called “umbrella” or “window” potential), introduced to enhance the sampling in the vicinity of a chosen region of configurational space and thus to confine the system around this region. A complete

calculation requires a number of separate simulations (or “windows”), each biasing the configurational sampling around a selected region. Ultimately, the information from the various windows must be unbiased and recombined together to obtain the final result.

Applied to the permeation process of a solute molecule across a lipid bilayer, the umbrella sampling method enables one to compute the free energy profile along the bilayer normal (taken as the z -direction). In a series of independent simulations, the solute molecule is restrained at various depths in the bilayer by means of a biasing potential, helping to achieve a more efficient sampling. The biasing umbrella potential (V_{umb}) is usually a harmonic potential of this form:

$$V_{umb}(z) = \frac{1}{2} \cdot k \cdot (z - z_0)^2 \quad (5.5)$$

where k is a force constant, z the z -coordinate of the center-of-mass (COM) of the solute, and z_0 the center of the umbrella potential. k defines the width of the umbrella potential: high values of k correspond to narrow potentials, *i.e.* to very restraining potentials. Note that only the z -coordinate of the solute COM is restrained, which means that the solute is free to rotate in all three directions around its COM and also free to diffuse in the plane perpendicular to the bilayer normal. For a given window, the free energy ΔG can be derived from the probability distribution ρ_{umb} of the solute in the membrane in the presence of the umbrella potential according to the relation:

$$\Delta G(z) = -R_c T \ln \rho_{umb}(z) + C - V_{umb}(z) \quad (5.6)$$

where C is an integration constant.

The procedure to obtain ΔG is illustrated in Figures 5.2 and 5.3. Figure 5.2 shows the qualitative free energy profile across a lipid bilayer for a polar solute. The large energy barrier present in the hydrocarbon core of the membrane would prevent an effective exploration of this region within the available computer time with “straight” MD simulations. This problem can be addressed by applying an umbrella potential which confines the solute within a narrow region in the bilayer and for which a correction is made subsequently (unbiasing) to obtain the “true” free energy. Figures 5.3 (a) and (b) summarize the different steps for the computation of ΔG in the case of a polar solute located in the bilayer at $z_0 = 0$ and $z_0 = -1$ nm, respectively.

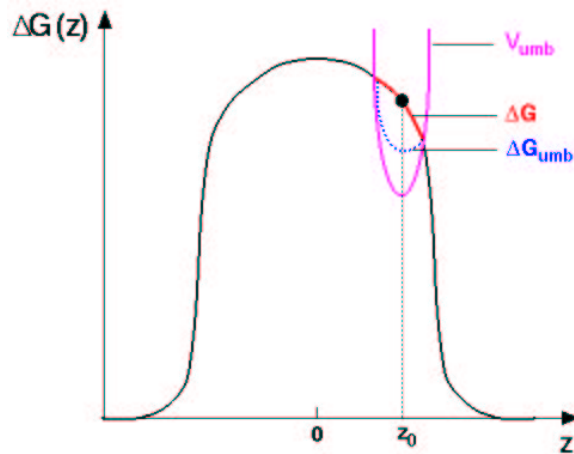
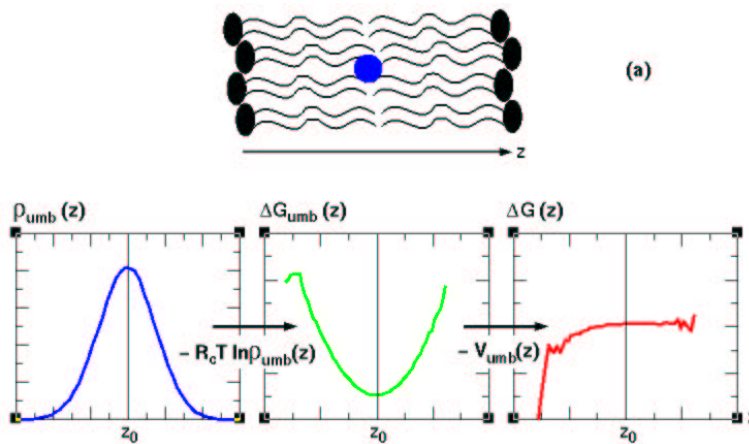


Figure 5.2: Qualitative free energy profile across a lipid bilayer for a polar solute ($z = 0$ corresponds to the center of the bilayer). By applying an umbrella potential V_{umb} (in magenta), the solute samples a local minimum (in blue: $\Delta G_{umb}(z) = -R_c T \ln \rho_{umb}(z)$). The “true” free energy ΔG (in red) can be deduced from ΔG_{umb} by subtracting the contribution of the umbrella potential.



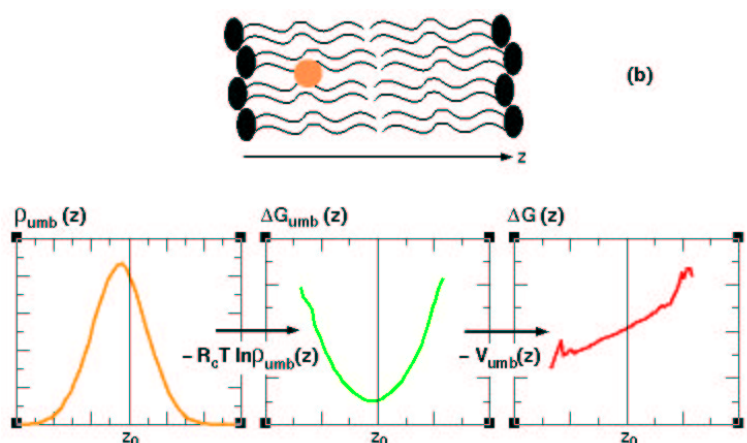


Figure 5.3: (a): For a polar solute located at the center of the bilayer ($z_0 = 0$ nm), the probabilities to reach the one or the other interface are equal, so that the resulting probability distribution profile (ρ_{umb}) is symmetric with respect to the center of the umbrella potential z_0 . After conversion of ρ_{umb} into an energy (ΔG_{umb}) and subtraction of the umbrella potential V_{umb} , a flat free energy profile ΔG is obtained. (b): For a polar solute located at $z_0 = -1$ nm, the probability distribution profile ρ_{umb} is slightly shifted towards the nearer interface and the corresponding free energy profile, after correction of the umbrella potential, exhibits a decreasing gradient towards the nearer interface.

Average force method on constrained particle An alternative method to compute the free energy profile across the membrane is the average force method on constrained particle. In this approach, the solute molecule is constrained at a given depth in the membrane and the force needed to keep the constraint is calculated. The norm of this force corresponds to the derivative (or slope) of the free energy at a given depth in the membrane (see Figure 5.4 for clarity). Repeating this constraining procedure at different depths in the membrane enables one to construct the free energy profile across the membrane. This method can be viewed as a limiting case of the umbrella sampling method, *i.e.* with an infinitely narrow restraining potential.

The free energy profile, also called potential of mean force, is obtained upon integration of the constraining force across the membrane:

$$\Delta G(z) = \int_0^z \langle F_z(z) \rangle \cdot dz \quad (5.7)$$

where $\langle F_z(z) \rangle$ is the mean force on the constraint (or, more precisely, the z -component of the force imposed on the solute, averaged over the constraint ensemble). This force can be

monitored during a constrained simulation as follows: the constraint is imposed by resetting the z -coordinate of the COM of the solute molecule each step to its initial, constrained value z_0 , and the force needed to keep the constraint on the solute is directly proportional to the distance over which the z -coordinate is reset. This procedure is schematically described in Figure 5.5. As in the umbrella sampling method, the solute molecule is free to rotate around its COM and free to diffuse in the plane of the membrane.

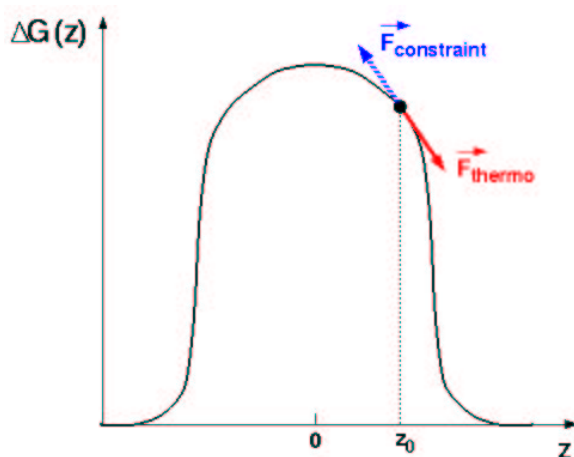


Figure 5.4: Qualitative free energy profile across a lipid bilayer for a polar solute. The force $\vec{F}_{constraint}$ to maintain the constraint on the solute at $z = z_0$ corresponds to the force opposite to the thermodynamic force \vec{F}_{thermo} acting on the solute. \vec{F}_{thermo} is the derivative or slope of the free energy at $z = z_0$.

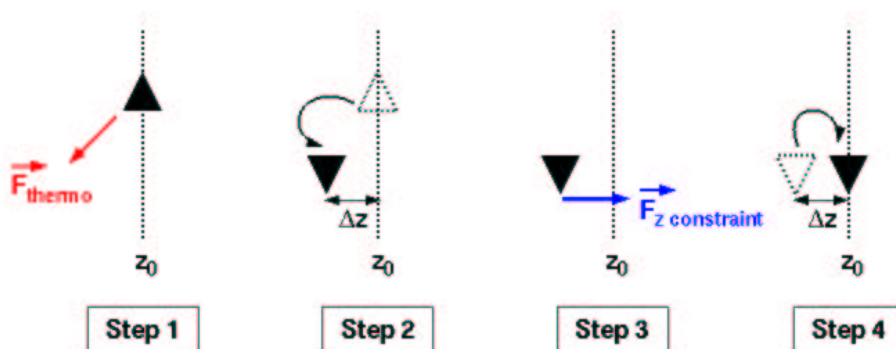


Figure 5.5: Constraining procedure. In step 1, the thermodynamic force \vec{F}_{thermo} is computed, which results, in step 2, in a displacement Δz of the solute molecule. In step 3, a constraining force $\vec{F}_{z\,constraint}$ is imposed on the z -coordinate of the solute COM to put it back to its initial constrained position $z = z_0$ (step 4).

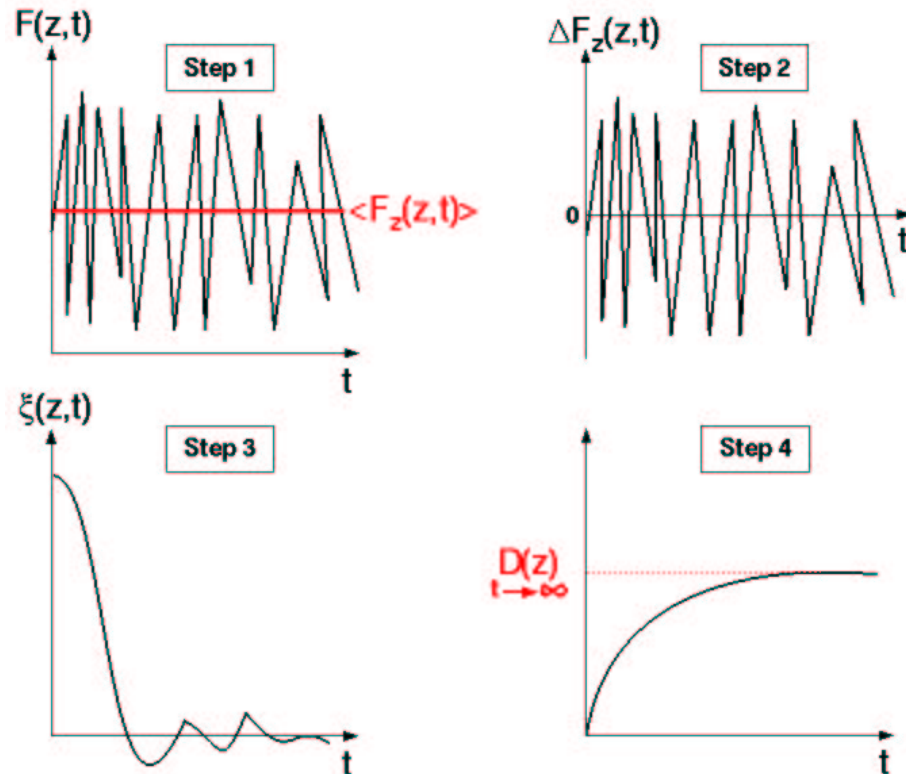


Figure 5.6: Computation of the local diffusion coefficient $D(z)$ of the solute at a depth z in the membrane. **Step 1:** Computation of the instantaneous force $F_z(z,t)$ imposed on the constrained solute. Note that this force fluctuates heavily, but long simulations should provide an accurate average. **Step 2:** Computation of $\Delta F_z(z,t)$ (deviation of the instantaneous force $F_z(z,t)$ from its average $\langle F_z(z,t) \rangle$). **Step 3:** Computation of the local time-dependent friction coefficient $\xi(z,t)$ using Equation 5.10. **Step 4:** Determination of the local diffusion coefficient applying Einstein's relation (Equation 5.11). The plateau value corresponds to $D(z)$.

The advantage of the average force method over the umbrella sampling approach is that the local diffusion coefficient of the solute in the bilayer can be computed simultaneously by applying the force autocorrelation method. This method, generally used to study diffusion over free energy barriers [181], is based on the fluctuation-dissipation theorem [182]. This theorem relates a time-dependent friction function $\xi(t)$ to the autocorrelation function of a Gaussian random force $f(t)$ with zero average:

$$\xi(t) = \frac{\langle f(t) \cdot f(0) \rangle}{R_c T} \quad (5.8)$$

The random force $f(t)$ can be identified with $\Delta F_z(z, t)$, the deviation of the instantaneous force from the average force acting on the constrained solute at a position z along the bilayer normal:

$$\Delta F_z(z, t) = F_z(z, t) - \langle F_z(z, t) \rangle \quad (5.9)$$

This approximation enables one to extract the local time-dependent friction coefficient $\xi(z, t)$ from the constrained MD trajectory:

$$\xi(z, t) = \frac{\langle \Delta F_z(z, t) \cdot \Delta F_z(z, 0) \rangle}{R_c T} \quad (5.10)$$

Time integration of this equation gives the local static friction coefficient $\xi^s(z)$. Assuming that, during the decay time of the local time-dependent friction coefficient $\xi(z, t)$, the solute remains in a region of constant free energy (*i.e.* in the limit of overdamped Markovian diffusion), the local diffusion coefficient $D(z)$ of the solute in the membrane can be related to $\xi^s(z)$ via Einstein's relation:

$$D(z) = \frac{R_c T}{\xi^s(z)} = \frac{(R_c T)^2}{\int_0^\infty \langle \Delta F_z(z, t) \cdot \Delta F_z(z, 0) \rangle \cdot dt} \quad (5.11)$$

The computation of the diffusion coefficient is summarized in four steps in Figure 5.6 (only qualitative curves are represented).

5.3 Review

The aim of this section is to highlight the main MD studies of membrane-solute interactions reported in the last decade to show the rapidly increasing possibilities in this field.

Owing to the large amount of computer time needed to describe the full permeation process of a solute across a membrane, most MD studies focused their efforts on the diffusion process only and/or on the effects of penetrants on the bilayer structure and lipid behavior. Stouch and co-workers reported in 1993 the first simulation of diffusion across a realistic membrane, in which they studied the diffusion process of benzene through a DMPC bilayer [183]. In a subsequent paper, they investigated the effect of temperature on the diffusion rate and mechanism of benzene [184]. They studied then the orientation and diffusion of a drug analog, nifedipine, in the same membrane [65]. Finally, they carried out comparative simulations with methane and adamantane molecules to observe the size dependence on the diffusion rates of non-polar molecules [185]. Jin and Hopfinger determined the diffusion rates of two moderately polar molecules, methanol and propanol, in a DPPC membrane [186]. López Cascales *et al.* reported the rotational and translational diffusion coefficients of a dye molecule (1,6-diphenyl-1,3,5-hexatriene) in a DPPC membrane and also evaluated the structural changes in the membrane as a consequence of the presence of the dye molecule [67]. The introduction of fluorescent probes into a membrane is indeed a widely used experimental technique for studying dynamic and stationary properties of supra-molecular assemblies like lipid bilayers. However, little is known about the effect of the presence of these probes on the microenvironment in which they reside. Aiello *et al.* studied the interaction of two calcium channel antagonists, lacidipine and nifedipine, with a DMPC bilayer, as well as the local perturbations induced in the membrane in the vicinity of the dihydropyridine molecules [68]. More recently, Söderhäll and Loaksonen performed a series of multianosecond MD simulations of a DPPC membrane with ubiquinone molecules freely moving inside the bilayer [72]. The focus was on the mobility and the preferential positions of the quinone molecule in the membrane. Ubiquinone, or co-enzyme Q, plays a role in photosynthetic processes in plasma membranes, so that the position and dynamics of membrane embedded quinones are of biological importance. Finally, a series of studies [66, 69–71] have examined the interactions of anesthetics such as trichloroethylene, halothane, or hexafluoroethane with phospholipid bilayers to probe the hypothesis of a lipid-mediated mechanism of general anesthetic action on a molecular level.

In all the studies mentioned above, equilibrium MD simulations were performed to qualitatively determine the distribution or orientation of a given penetrant in the membrane, to observe its effects on the lipid behavior, and/or to calculate its transverse or lateral diffusion coefficient from its mean square displacement. Few studies focusing on the computation of free energy profiles or permeation rates have been reported so far. In 1994, Paci and Marchi

investigated the passing of dimethylsulfoxide (DMSO) through a model bilayer composed of glycerolmonooleate by non-equilibrium MD [187]. The DMSO molecule was pulled by constraints through the bilayer, allowing equilibration at different depths. They interestingly observed that DMSO, upon entering the membrane, tries to drag a water molecule inside. However, the too short simulation time (300 ps) did not allow for the calculation of the mean force acting on DMSO, due to convergence problems, so that no free energy profile could be obtained from the constrained simulation. Pohorille and co-workers [188,189] have calculated free energies of anesthetic analogs at water-glycerolmonooleate and water-hexane interfaces, either using equilibrium MD or the particle insertion method [190,191]. Recently, Xiang and Anderson, combining thermodynamic integration and perturbation methods, have evaluated the contribution of various functional groups in p-toluic acid to the transfer free energy of the acid from water into the ordered-chain interior of a DPPC bilayer [192]. Grossfield and Woolf have performed umbrella sampling simulations to construct the free energy profiles of two tryptophan analogs (indole and N-methylindole) across a POPC bilayer [73]. This year, MacCallum *et al.* have published a series of equilibrium and non-equilibrium MD simulations focusing on the distribution of various molecules within phospholipid bilayers of different types [193]. Using an umbrella sampling procedure, free energy profiles of hexane, halothane, and pentachlorophenol (PCP, a biopollutant) have been calculated. The orientation and dynamics of PCP and methylindole within the bilayer have also been investigated.

One of the first, but still the most detailed and systematic study of the permeation process of small molecules across a DPPC bilayer, was reported by Marrink and Berendsen [135, 194]. This study differs from those mentioned above in that both the solubility (free energy) and diffusion contributions were determined in order to calculate overall permeation rates across the membrane. The permeability coefficients of water, oxygen, and ammonia were calculated: free energy profiles were computed either by the particle insertion method or by the average force method on constrained particle, while local diffusion coefficients were determined by the force autocorrelation method. The obtained permeability coefficients were in good agreement with experimental data.

Processes of solute permeation across lipid membranes are thus difficult to simulate and, despite their considerable biological and pharmaceutical relevance, have attracted little interest so far. This can be explained by the problems encountered in performing simulations of events that need considerable time and are out of reach with standard MD methods.

5.4 Method of simulation

5.4.1 Choice of penetrants

3-O-Methyl- α -D-glucose and D-mannitol The passive transport through a DPPC bilayer membrane of a sugar, 3-O-methyl- α -D-glucose, and an acyclic sugar alcohol, D-mannitol, has been investigated. Their chemical 2D and 3D-structures are depicted in Figure 5.7. The 3D-structure of 3-O-methyl- α -D-glucose was derived from the crystal structure of α -D-glucose reported by Mostad [195]: a methoxy group was substituted for the hydroxyl group on carbon 3 in glucose. The 3D-structure of D-mannitol corresponds to the crystal structure reported by Kaminsky [196]. Both structures were energy minimized using a steepest descent procedure prior to MD simulations. These two molecules present different hydrophilic properties, mannitol being more hydrophilic than methylglucose. The octanol/water partition coefficients of methylglucose and mannitol are around -2.5 and -3.1, respectively [197–199]. Both molecules are furthermore relatively small and do not present too much complexity from a conformational viewpoint, so that their parameterization should pose no problem for MD simulations. In addition, some experimental permeation data of sugars in different lipid membranes are available from the literature [165, 199, 200]. Glucose, galactose, and 3-O-methylglucose are thought to share a common intestinal carrier-mediated transport mechanism [201]. However, as facilitated transport is a saturable process, the contribution of passive permeation becomes an important consideration at high concentrations. Mannitol is commonly used as an intestinal permeability probe. Indeed, to assess intestinal permeability in clinical study, poorly absorbed probes which are not metabolized in the body are given orally, and their penetration of the intestinal barrier is calculated from their appearance in the urine in the following hours. The passage of a monosaccharide is frequently decreased in patients with mucosal pathology of the small intestine [202]. Although the paracellular route appears to be the largest component of the passive transport of mannitol [203, 204], the transcellular lipoidal pathway is not negligible [205].

Salicylic acid The third investigated penetrant is salicylic acid, the metabolite of acetyl-salicylic acid (aspirin). The 2D and 3D-structures of the acid can be seen in Figure 5.7. The crystal structure reported by Bacon and Jude [206] has been adopted and energy minimized. Salicylic acid has amphiphilic properties, with its hydrophilic carboxyl and hydroxyl functions on the one hand, and its hydrophobic benzene ring on the other. For comparison

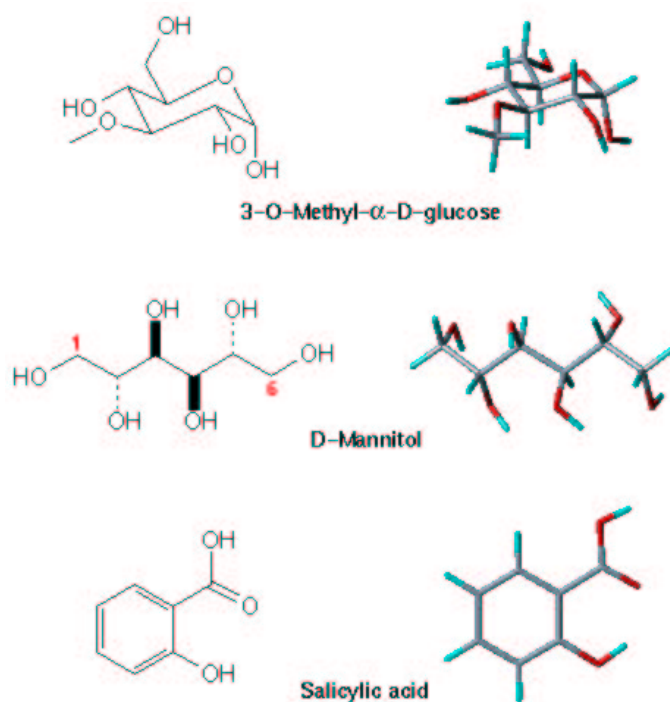


Figure 5.7: 2D and 3D-structures of 3-O-methyl- α -D-glucose, D-mannitol, and salicylic acid.

with the two more polar compounds, its octanol/water partition coefficient is of 2.2 [198]. During and following its absorption from the gastrointestinal tract, acetylsalicylic acid is rapidly hydrolyzed to form salicylic acid. After oral administration, salicylic acid is quickly absorbed from the small intestine, which indicates a rapid diffusion across the enterocytes. Since the acid (with a pK_a equal to 3) is ionized almost completely in the intestinal tract, the pH-partition theory [33], according to which a dissociable substance permeates through a cell membrane in the unionized form, cannot explain its extensive absorption. Tagaki and co-workers examined the transport of salicylic acid across a liposomal membrane with an inward proton gradient and proposed a new interpretation of the permeation mechanism of the acid [207]. Protonated salicylic acid (SAH) in the extraliposomal solution of pH 5.8 (at this pH, 0.14% of salicylic acid is expected to be protonated) was taken up rapidly by the liposomes: the permeability of the acid SAH is indeed 7 orders of magnitude higher than that of the salicylate anion SA^- [208]. Permeation of SAH was followed by a redissociation to the anion SA^- according to the intraliposomal pH of 7.5. As illustrated in Figure 5.8, the most important point in this mechanism is that the uptake rate of SAH must be faster than the inward diffusion of protons into the liposome. In such a situation, protons are supplied into

the liposome mainly by the dissociation of SAH, and the uptake of SAH can last until the pH gradient is eliminated. *In vivo*, the vicinity of the luminal surface of enterocytes is kept acidic (pH=5.5–6), so that the initial conditions in the liposomal uptake experiment described above give almost the same pH gradient as that under normal conditions in the intestine. Moreover, it is thought that, *in vivo*, the absorption of salicylic acid is facilitated by the proton gradient across the apical membrane of enterocytes generated by the proton/sodium antiporter [207].

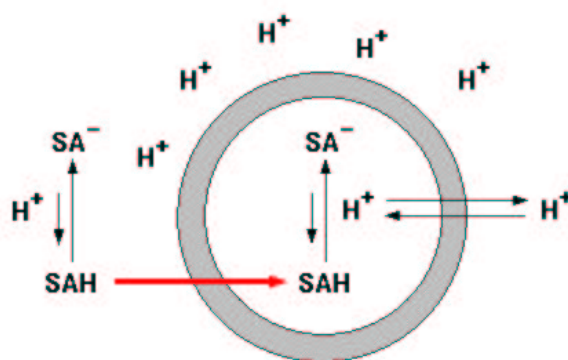


Figure 5.8: Possible mechanism of the pH-dependent uptake of salicylic acid by liposomes in the presence of an inward proton gradient. SAH and SA⁻ correspond to the protonated and ionized forms of salicylic acid, respectively.

5.4.2 Force field parameters and partial atomic charges

Methylglucose The force field parameters and partial atomic charges for methylglucose are described in the article of Damm *et al.* [209]. In this article, they extended the OPLS all-atom force field [210] to treat carbohydrates. In contrast to the development of other carbohydrate force fields based on model compounds, the parameters were obtained from fitting *ab initio* results for complete hexopyranoses. Note that the OPLS all-atom parameters for bond stretching and angle bending were largely taken from the AMBER all-atom force field [211].

Mannitol and salicylic acid The force field parameters and partial atomic charges for mannitol and salicylic acid are taken from the OPLS all-atom force field [210, 212–215]. Parameters and charges for both standard alcohols and polyols are used for mannitol, while parameters and charges for benzene, phenol, and benzoic acid are adopted for salicylic acid.

DPPC The force field parameters and partial atomic charges for DPPC are those described in Chapter 4, Section 4.2.4, page 84.

1,4 LJ and electrostatic interactions are scaled by a factor of 2 for the three permeants, whereas they are scaled by factors of 8 and 2, respectively, for DPPC.

5.4.3 Equilibrium MD simulations

Equilibrium MD simulations are first performed to determine the preferred locations of the solute molecules in the DPPC membrane.

Twelve solute molecules are homogeneously incorporated into the DPPC bilayer model developed in Chapter 3. Starting structures contain four solute molecules in the membrane interior, four in the interfacial regions, and four in the water layers (see Figure 5.9, page 160, for clarity). To avoid repulsive contacts between the solute and lipid molecules, the introduction of the solute molecules is achieved using a free energy perturbation or “growing” method in a 100 ps simulation. At the beginning of the simulation, the solute molecules are treated as point masses with zero LJ parameters and charges, so that they do not interact with the lipid environment. Step by step, the LJ parameters and charges are rescaled, so that the solute molecules fully interact with the lipids at the end of the simulation. LJ and electrostatic interactions from the initial state (state A) to the final state (state B) are computed in the following way (see Chapter 3, Section 3.1.3, page 56, for the notations):

$$\begin{aligned}
 V_{nb}(r_{ij}) &= V_{LJ}(r_{ij}) + V_C(r_{ij}) \\
 &= \frac{(1-\lambda)C_{ij}^{A(12)} + \lambda C_{ij}^{B(12)}}{r_{ij}^{12}} - \frac{(1-\lambda)C_{ij}^{A(6)} + \lambda C_{ij}^{B(6)}}{r_{ij}^6} \\
 &\quad + \frac{f}{\epsilon_r r_{ij}} \left[\left((1-\lambda)q_i^A + \lambda q_i^B \right) \cdot \left((1-\lambda)q_j^A + \lambda q_j^B \right) \right] \quad (5.12)
 \end{aligned}$$

where $\lambda = 0$ corresponds to the initial state (*i.e.* no interaction between the solute and the membrane) and $\lambda = 1$, to the final state (*i.e.* full interaction). The parameter λ is incremented each time step, so that the solute molecules are progressively “grown” in size. This procedure allows one to incorporate the solute molecules without having first to create free volume, which would induce large perturbations in the bilayer structure. Note that the solute coordinates are “frozen” during the whole procedure to maintain the initial solute distribution throughout the bilayer.

Three equilibrium MD simulations of 30 ns are carried out with each type of solute in the DPPC membrane. Simulation conditions are the same as those for the pure DPPC system (see Chapter 4, Section 4.2, page 78), *i.e.* NPT ensemble with $T = 323$ K and $P_{xx} = P_{yy} = P_{zz} = 1$ bar, choice of PME for the computation of electrostatics, and periodic boundary conditions. All bond lengths in the solute molecules are kept constant using the LINCS algorithm [109]. The time step is decreased from 5 to 2 fs, however, to ensure a more accurate description of solute dynamics. An equilibration time of 2 ns was required for the simulations with methylglucose and mannitol, and 5 ns with salicylic acid, so that trajectories are analyzed over 28 and 25 ns simulation time, respectively.

5.4.4 Umbrella sampling MD simulations

To construct the free energy profile along the membrane normal (z-direction) corresponding to the transfer of the solute from the water layer into the membrane hydrocarbon core, a series of biased simulations is carried out, where an umbrella potential is added to the system to maintain the solute molecules at different positions in the DPPC membrane.

In order to follow the complete permeation pathway across the membrane, initial configurations for the umbrella sampling windows are generated by introducing the solute molecules at different depths into the membrane, applying the growing procedure described in the previous section. 67 positions along the bilayer normal, 1 Å apart, are investigated from $z_0 = -3.3$ to $z_0 = 3.3$ nm (the position of the solute COM is defined relative to the position of the DPPC bilayer COM, taken as reference). The solute COM is restrained in the z-direction by a harmonic umbrella potential with a force constant k of 3000 kJ/mol.nm² (see Equation 5.5), which allows sufficient overlap between adjacent windows. To limit the computational cost, four solute molecules (two per leaflet) are incorporated into the membrane in each starting structure, which reduces the number of simulations from 67 to 17.

Simulation conditions are identical to those for the equilibrium MD simulations, with the exception of the type of pressure coupling. Indeed, constant surface area (in the x,y-plane) is maintained in each simulation to avoid having to sample over slow fluctuations in the area per lipid, which would give rise to convergence problems. Each window is equilibrated for 2.5 ns, after which a production trajectory of 12.5 ns is generated for the umbrella sampling calculations. Each simulation of 15 ns requiring about 45 days of CPU time on a single Pentium III 1 GHz processor, the total computer time amounts to approximately 6 years for the umbrella sampling study of the three solutes.

5.4.5 Constrained MD simulations

Constrained simulations allow for the computation of free energy profiles and local diffusion coefficients at the same time, so that permeability coefficients of the solutes in the membrane should be obtained.

Concerning the generation of starting structure, the same procedure as described in the previous sections is applied. However, as the constrained method is more time consuming than the umbrella sampling method, only 43 positions in the membrane from $z_0 = -3$ to $z_0 = 3$ nm are investigated (the points are spaced out by about 2 Å in the hydrocarbon part of the membrane and in the water layers, and by 1 Å in the interfacial regions). A tolerance of constraint equal to 1×10^{-6} nm is used, which corresponds to very small displacements Δz (see Figure 5.5, page 148) from one step to the other. To monitor these small displacements, the double precision of GROMACS, which calculates atom coordinates with 12 digits instead of 6, is needed. Unfortunately, double precision slows down the simulations by a factor of about 2.

Simulation conditions and times are the same as for the umbrella sampling procedure. 15 ns production run requires about 100 days of CPU time with double precision and on the same type of processor as described before. This method was only applied to methylglucose and mannitol (see Section 5.5.3, page 180, for explanations) and required around 6 years of computer time for both solutes.

5.5 Results

5.5.1 Equilibrium MD simulations

5.5.1.1 Time course of solute position

Figure 5.9 shows the distribution of the twelve solute molecules in the DPPC membrane at the start (uniform distribution) and after 30 ns MD simulation for each type of solute. In the final ensemble, the polar methylglucose and mannitol molecules are not found in the hydrophobic membrane core anymore and are essentially located in the water layers and at the water/membrane interfaces. At first sight, however, mannitol seems to penetrate somewhat deeper into the membrane than methylglucose does. The salicylic acid molecules leave the aqueous phase and the membrane interior to adsorb, owing to their amphiphilic

character, at the water/membrane interface, with the polar carboxyl and hydroxyl groups of the molecule interacting with the DPPC headgroups and the hydrophobic benzene ring protruding into the bilayer core.

In order to follow the trajectory of the solute molecules over the course of the simulation from their initial position, the perpendicular motions of the solute COM (z -coordinate) have been monitored as a function of time and are depicted in Figures 5.10, 5.11, and 5.12. The four methylglucose molecules initially located in the hydrocarbon part of the membrane essentially sample the interfacial region (region 2 and limit between regions 2 and 3). One of the four molecules reaches the water phase after about 15 ns MD. The methylglucose molecules initially located in the water layer or at the interface are principally found in the water phase (region 1) during the simulation. Some of them, however, occasionally migrate to the interfacial region (region 2). A similar behavior is registered for mannitol. Nonetheless, the mannitol molecules seem to sample more frequently the region 2 as well as the beginning of the region 3 than the methylglucose molecules (see the trajectories of two mannitol molecules from the interface in Figure 5.11). The salicylic acid molecules, independent on their initial position, all sample the frontier zone between regions 2 and 3. The water phase (region 1) is only rarely sampled.

Interesting is to compare, for each type of solute, how long the four molecules remain in the hydrophobic core of the membrane. The solute trajectories from the hydrocarbon part of the membrane are displayed over the first 1.5 ns of simulation in Figure 5.13. According to their increasing hydrophobicity, the residence times of mannitol, methylglucose, and salicylic acid in region 4 are about 150 ps, 300 ps, and 1 ns, respectively.

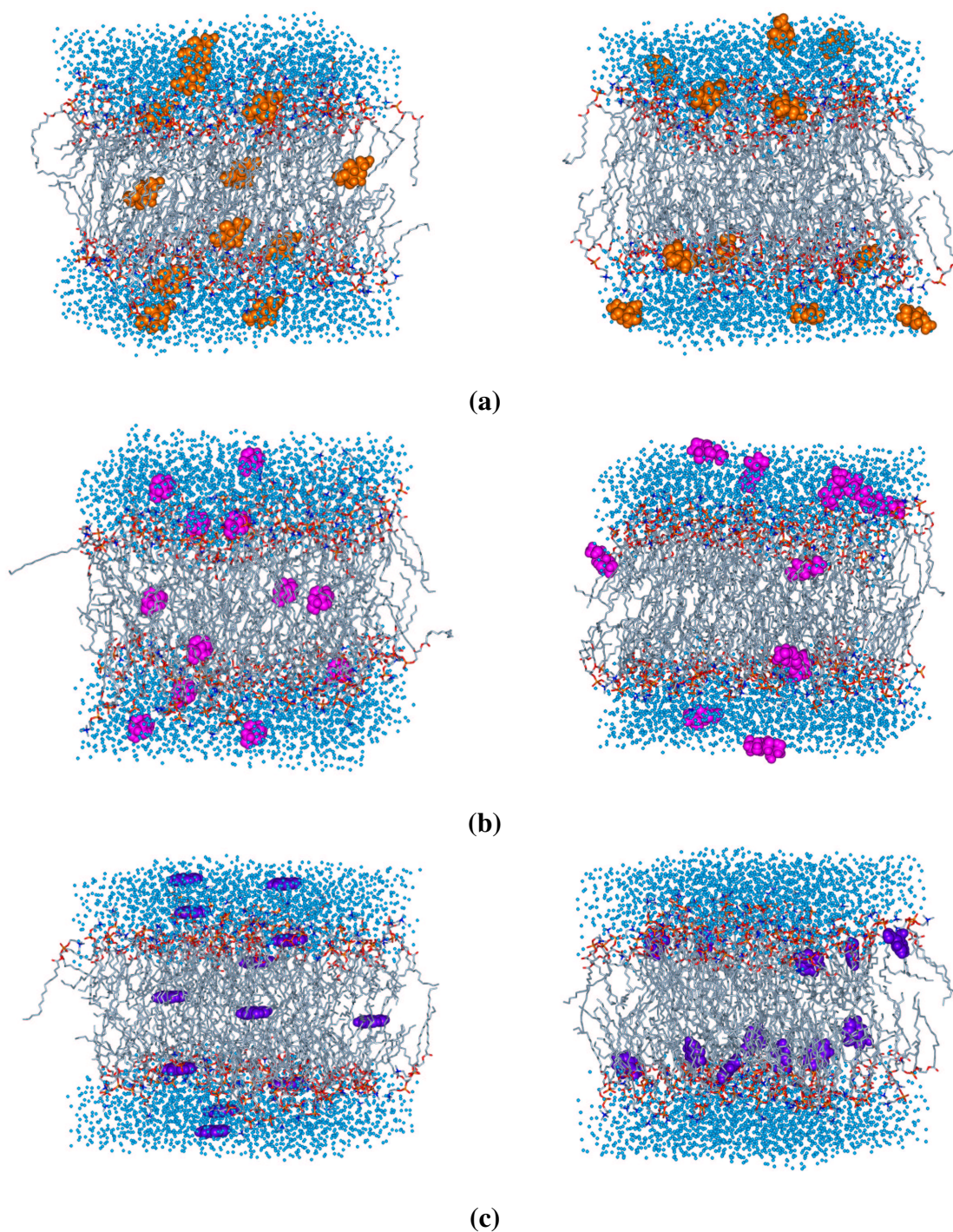


Figure 5.9: Solute distribution in the DPPC membrane at the start (left) and after 30 ns MD simulation (right) for **(a)**: methylglucose (space fill, orange), **(b)**: mannitol (space fill, magenta), and **(c)**: salicylic acid (space fill, violet).

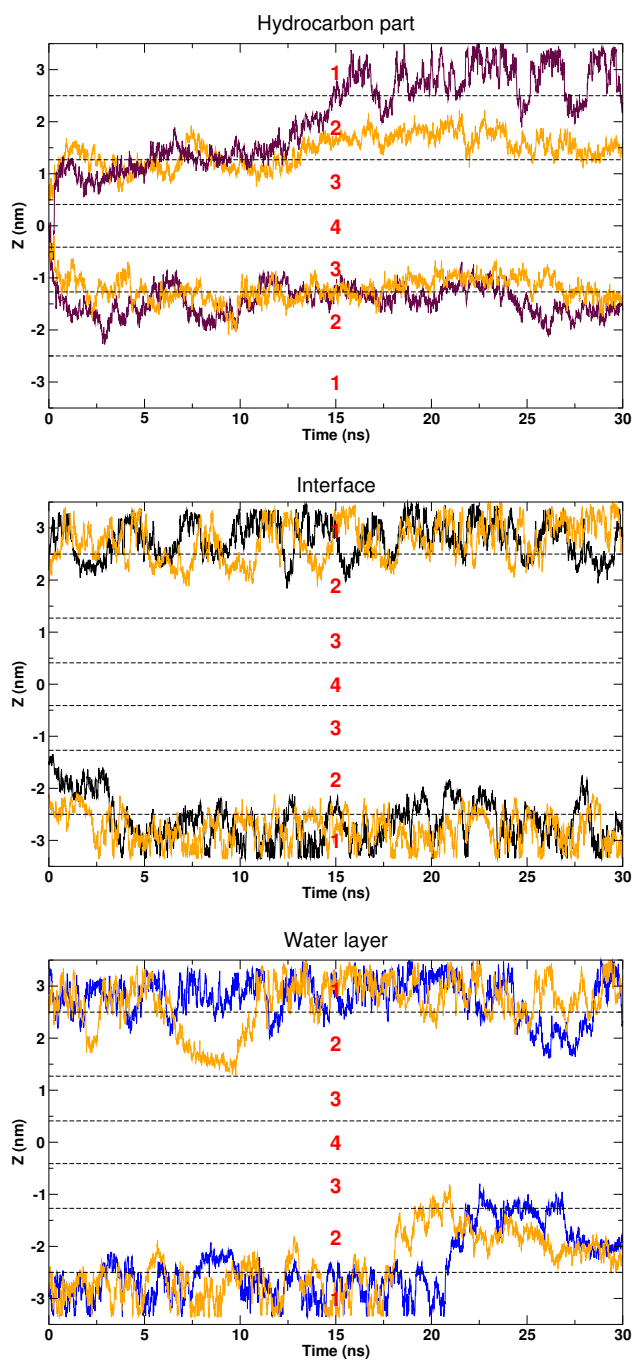


Figure 5.10: z -coordinate of the COM of the twelve methylglucose molecules as a function of time ($z = 0$ is the membrane center). “Hydrocarbon part”, “interface”, and “water layer” refer to the initial environment of the methylglucose molecules. The four regions within the membrane are delimited by dashed lines.

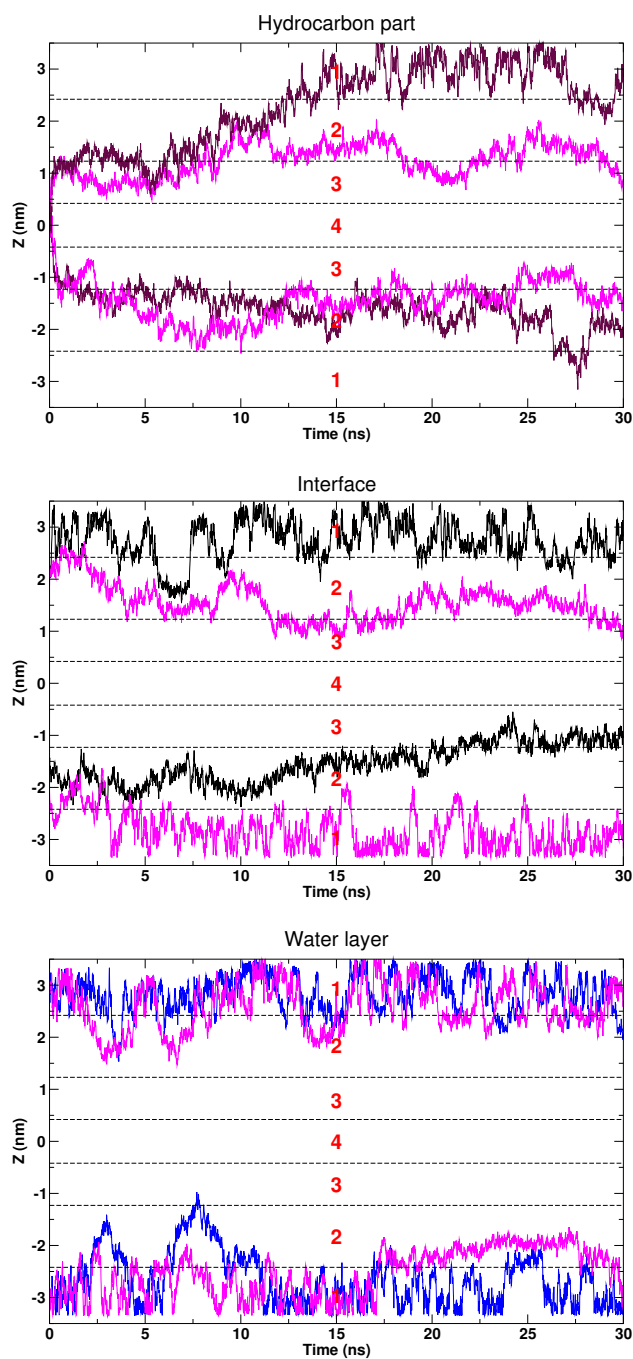


Figure 5.11: z -coordinate of the COM of the twelve mannitol molecules as a function of time.

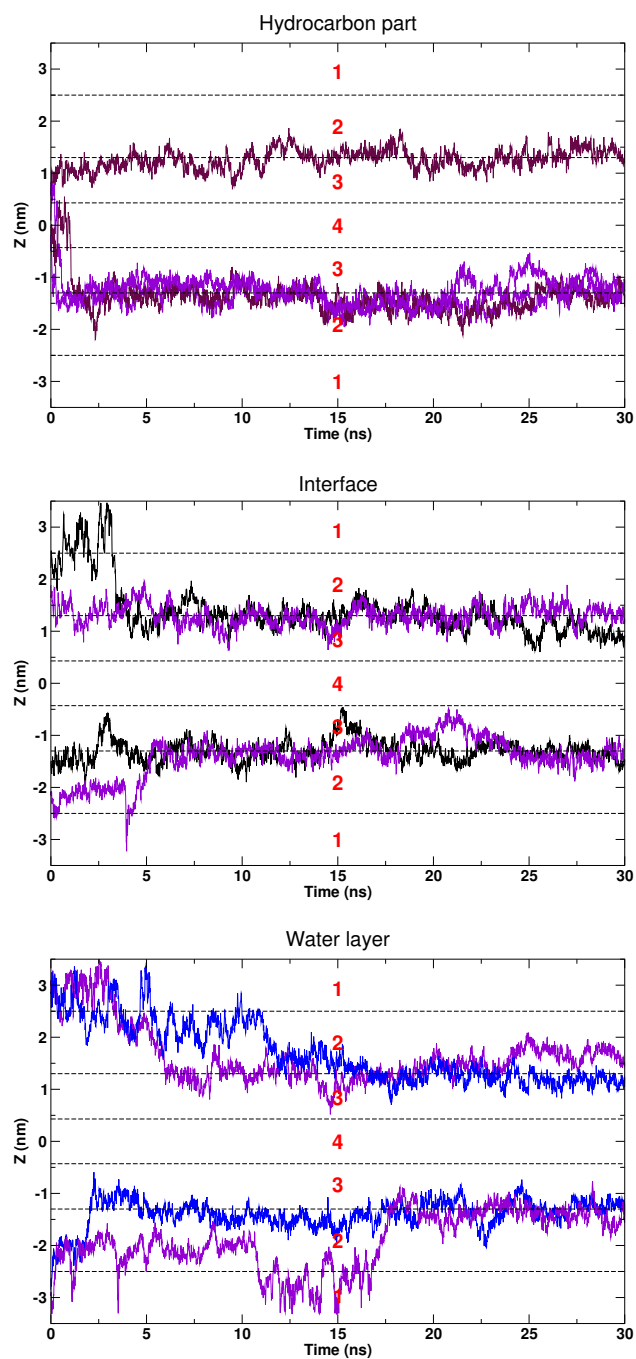


Figure 5.12: z -coordinate of the COM of the twelve salicylic acid molecules as a function of time.

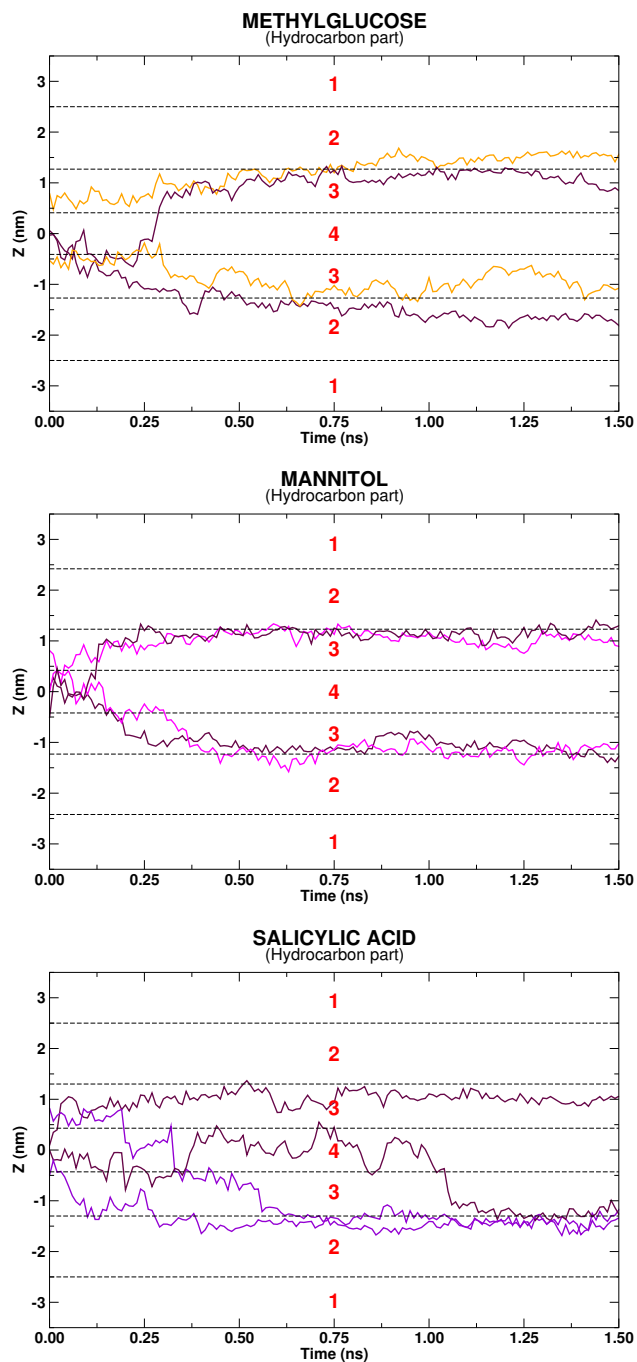


Figure 5.13: Time course of the z-COM of each type of solute from the hydrocarbon part of the membrane during the first 1.5 ns of the simulation.

5.5.1.2 Solute distribution

The density distribution profiles along the bilayer normal of the three solute types at the start and during the simulation can be compared in Figure 5.14. The DPPC and water density profiles are also plotted as reference. From these profiles, it can be observed that the density distribution of methylglucose and mannitol exhibits two maxima: one is located in the water phase (region 1), the other one at the interface, at the limit between regions 2 and 3. The density distribution of salicylic acid exhibits only one maximum, also located at the limit between regions 2 and 3. Methylglucose and mannitol penetrate into the membrane as long as water is present. Due to its partial hydrophobicity, the penetration of salicylic acid into the hydrocarbon region of the bilayer is somewhat deeper than that of water.

The solute density distribution profiles are plotted again in Figure 5.15 and compared to those of the choline, phosphate, and carboxyl moieties of the DPPC headgroups. For the three solutes, the origin of the density maximum located at the border of regions 2 and 3 is a strong interaction between the polar moieties of the solute molecules and the phosphate and carboxyl groups of DPPC. In the case of salicylic acid, the maximum is slightly shifted towards the carboxyl groups, which reflects a stronger interaction of salicylic acid with the carboxyl than the phosphate groups of DPPC. Figure 5.16 shows the preferred location and orientation of salicylic acid in the membrane. The carboxyl and hydroxyl groups of the acid are hydrogen bonded to the DPPC headgroups, essentially to the DPPC carbonyl oxygens (see next section), while the benzene ring is roughly aligned with the nearby DPPC hydrocarbon chains to optimize van der Waals interactions.

Figure 5.17 is a close-up shot of the solute density distribution profiles which allows for a better comparison of the three profiles. Qualitatively, the probability to find methylglucose in the water layer is greater than that to find mannitol and mannitol seems to interact stronger than methylglucose with the DPPC headgroups in the interfacial region. It can be also noticed from Figure 5.17 that the obtained distribution profiles are not completely symmetric with respect to the bilayer center, despite the relative long simulation time (30 ns). A thorough investigation of solute distribution in the membrane requires intensive statistical sampling, which involves simulation times beyond the reach of equilibrium MD.

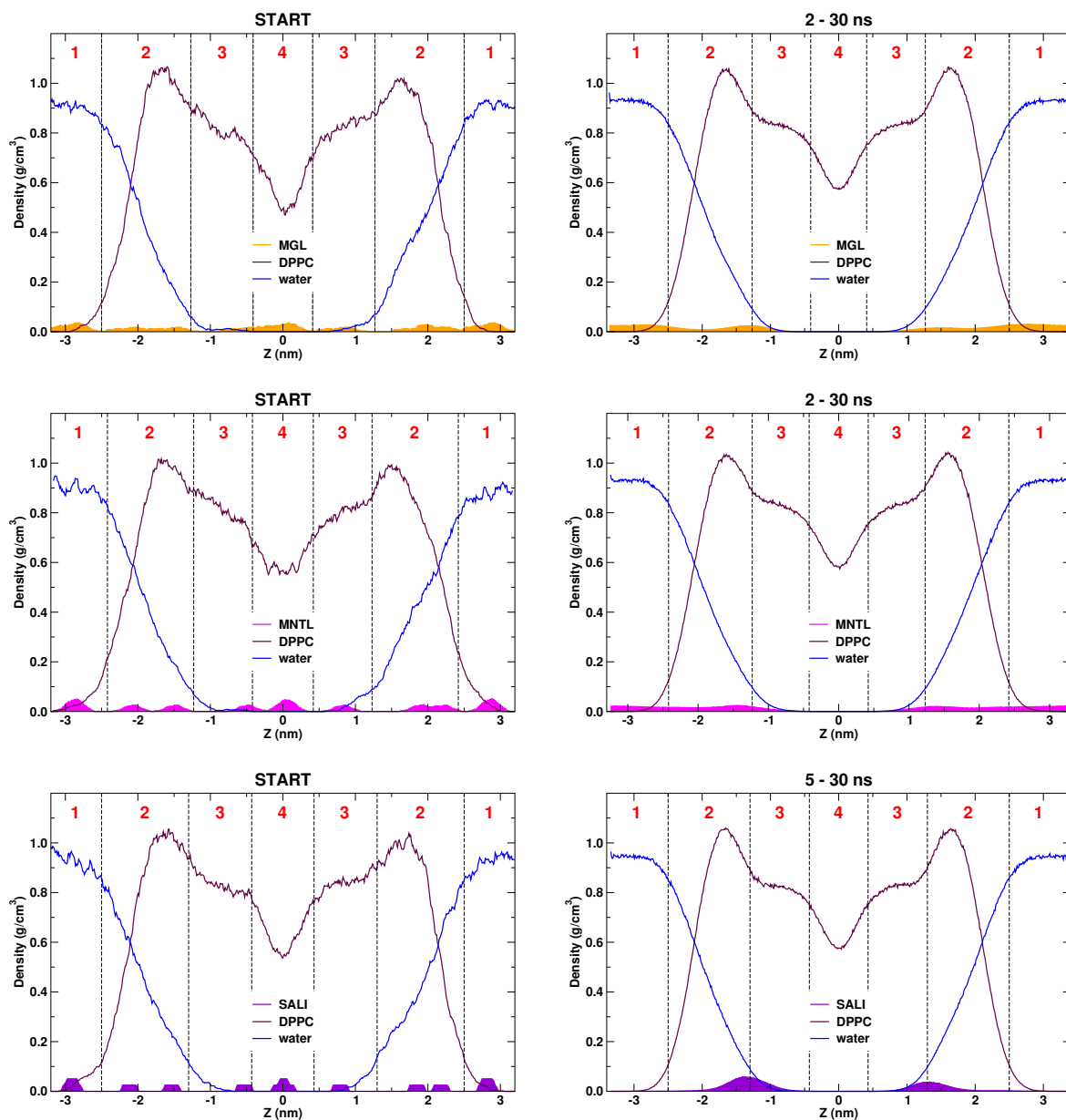


Figure 5.14: Density distribution profiles along the bilayer normal of the solute (MGL: methylglucose; MNTL: mannitol; SALI: salicylic acid), DPPC, and water molecules at the start and during the simulation.

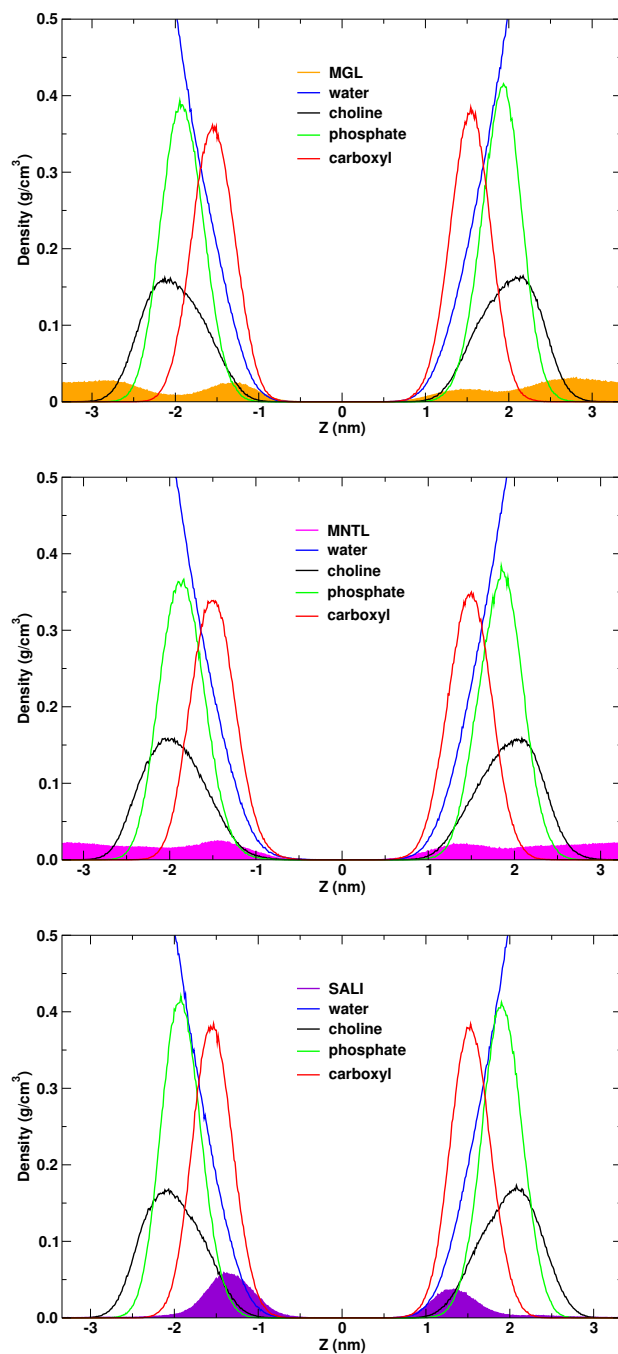


Figure 5.15: Density distribution profiles along the bilayer normal of the solute molecules as well as water and the choline, phosphate, and carboxyl groups of DPPC during the simulation.

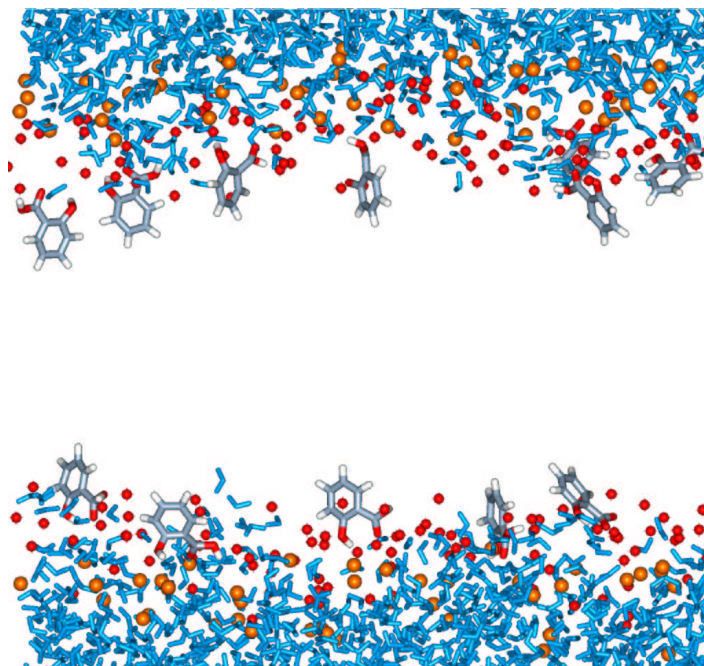


Figure 5.16: Snapshot of the DPPC membrane including twelve salicylic acid molecules. For clarity, the DPPC molecules are undisplayed. Only the phosphorus (orange) and carbonyl oxygens (red) atoms of DPPC are represented in space-filling format.

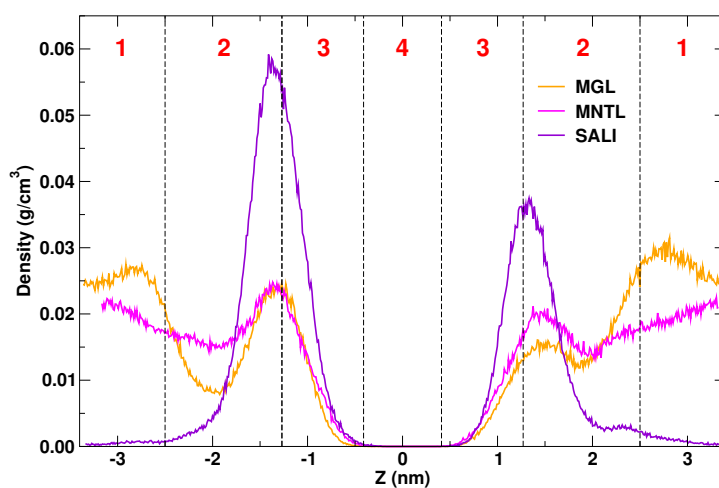


Figure 5.17: Density distribution profiles along the bilayer normal of methylglucose, mannitol, and salicylic acid during the simulation.

5.5.1.3 Hydrogen bonding

In order to better understand the location of the preferred sites for solute-membrane interactions, hydrogen bonding between the solute molecules and the water and lipid components of the membrane are investigated. Table 5.1 reports the percentages of hydrogen bonds (H-bonds) formed with DPPC and water. For DPPC, the contribution of the different headgroup parts is also given. The large majority of H-bonds formed between the polar molecules and the membrane involves water (84 and 89% of the total number of H-bonds for mannitol and methylglucose, respectively). Mannitol forms 5% more H-bonds with DPPC than methylglucose does (16% vs 11%): mannitol contains indeed two more hydroxyl groups (H-donors) than methylglucose. This can explain why mannitol interacts stronger with the DPPC headgroups at the interface than methylglucose. Concerning the H-bonds formed with DPPC, about 40% of them involve the phosphate groups and 60% the carboxyl groups, for both polar molecules. It should be noted that the carbonyl oxygen is the principal acceptor atom in the DPPC carboxyl group and accounts for 86-88% of the H-bonds between the solute and the carboxyl group. Salicylic acid forms a number of H-bonds equal in percentage with DPPC and water. The DPPC carboxyl group accounts now for 72% of the H-bonds between the acid and DPPC, reflecting the deeper penetration of the acid into the bilayer compared to that of the polar molecules.

Table 5.1: Percentages of hydrogen bonds formed between the solute molecules and the water/DPPC system, averaged over the simulation time.

	Methylglucose	Mannitol	Salicylic acid
Water	89%	84%	49%
DPPC	11%	16%	51%
PO ₄	42%	43%	28%
CO ₂	58%	57%	72%

From this series of equilibrium MD simulations, a qualitative idea of the solute distribution inside the DPPC membrane could be gained. However, the absence of sampling in the hydrophobic membrane interior precludes the estimation of the free energy barrier associated to the transfer of the solute from the water phase into the center of the bilayer. Furthermore, even in the headgroup region, massive sampling would be required to yield uniform unbiased distribution probabilities and, hence, reach convergence of the free energy.

5.5.2 Umbrella sampling MD simulations

5.5.2.1 Free energy profiles

The series of biased simulations, where an umbrella potential is added to the system to restrain the solute molecule at different positions from the water layer through the interface to the membrane center, allows for the computation of the free energy $\Delta G(z)$ to bring the solute molecule from the aqueous phase to a depth z in the membrane. The free energy profile along the bilayer normal is calculated from the equilibrium probability distributions $\rho_{umb}(z)$ obtained from the biased simulations. The probability distributions $\rho_{umb}(z)$ from the 67 windows are unbiased and recombined using the weighted histogram analysis method (WHAM) [216, 217]. The WHAM procedure consists in constructing an optimal estimate of the unbiased probability distribution $\rho(z)$, using all the available data extracted from the umbrella sampling windows.

The resulting free energy profiles, symmetrized over both membrane leaflets, are depicted in Figure 5.18 for all three solutes. Note that only relative energy values are calculated: the center of the bilayer ($z = 0$) is chosen as reference, where the energy is arbitrarily set to zero. The profiles of methylglucose and mannitol are very similar, as expected from the equilibrium MD simulations, and exhibit a minimum in the water layer (region 1). In the case of methylglucose, the energy remains roughly constant at the interface (region 2), while a slight energy increase by about 7 kJ/mol is observed through region 2 for mannitol. For both polar molecules, the energy goes up with a steep slope through regions 3 and 4 to reach its maximum in the middle of the bilayer. A free energy barrier of $+42 \pm 1$ kJ/mol from the water phase to the bilayer center is obtained for methylglucose, and of $+49 \pm 2$ kJ/mol for mannitol. A higher energy barrier for mannitol makes sense, since mannitol is more hydrophilic than methylglucose. The free energy profile of salicylic acid exhibits a local minimum at the border between regions 2 and 3, in agreement with the results obtained from the equilibrium MD simulations. The energy increases then through regions 3 and 4 towards

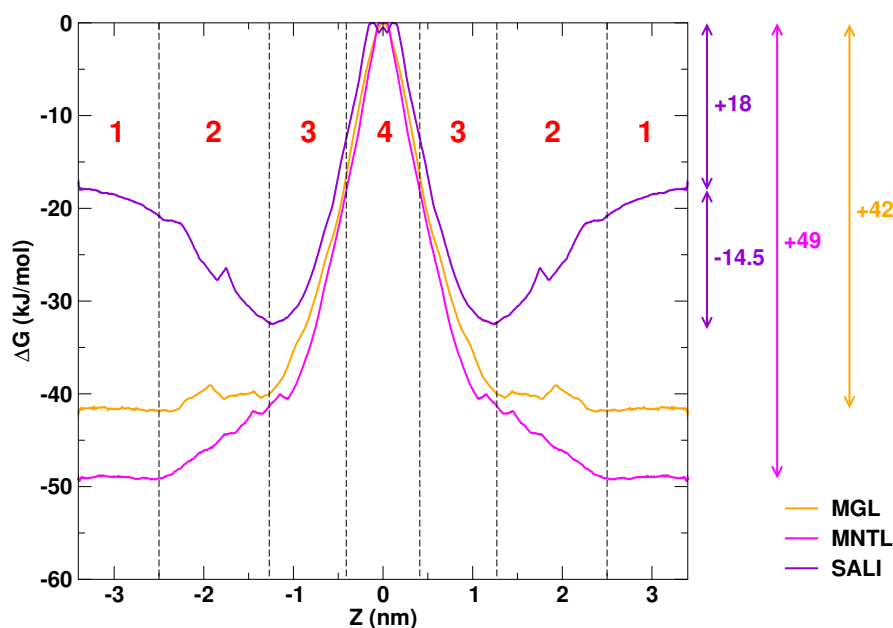


Figure 5.18: Free energy profiles along the bilayer normal and related free energy barriers for the three solutes. The center of the bilayer is taken as reference ($\Delta G(z = 0 \text{ nm}) = 0 \text{ kJ/mol}$).

the bilayer center with the same slope as that observed for the polar molecules. For salicylic acid, a free energy barrier of $+18 \pm 3 \text{ kJ/mol}$ is computed from the water phase to the bilayer center, and an energy decrease of $-14.5 \pm 2 \text{ kJ/mol}$ is found between the water phase and the interfacial energy minimum.

From the density distribution profiles obtained from the equilibrium MD simulations, free energy profiles can be calculated, at least in the water and interfacial regions, using the relation $\Delta G(z) = -R_c T \ln \rho(z)$, where $\rho(z)$ represents the density distribution of the solute in the water/DPPC system. These profiles are compared to those obtained from the umbrella sampling simulations in Figure 5.19. A good agreement is generally found between both methods. In particular, a similar energy gradient is registered towards the bilayer interior.

Validation of the calculated free energy barriers is difficult, since few experimental data about solute partitioning at water/membrane interfaces are available from the literature. Recently, water/dodecane partition coefficients have been determined by Bas *et al.* [218], using the shake flask method, for a series of drug and drug-like molecules, including α -D-glucose. This method requires, however, that the aqueous concentrations measured before and after partition are significantly different and, hence, fails for very polar solutes like glu-

cose. To estimate the $\log P$ value of glucose at the water/dodecane interface, they postulated that partition coefficients between dodecane and water ($\log P_{\text{dod/wat}}$) are necessarily related to those between octanol and water ($\log P_{\text{Oct/wat}}$). The partition coefficients in these two environments were thus measured for a series of prototypical compounds and differences between both types of partition coefficients (*i.e.* $\log P_{\text{dod/wat}} - \log P_{\text{Oct/wat}}$) were correlated with structural molecular descriptors. From an extrapolation of the behavior of $\log P_{\text{dod/wat}} - \log P_{\text{Oct/wat}}$, they deduced $\log P_{\text{dod/wat}}$ values from their experimentally measured $\log P_{\text{Oct/wat}}$ values. For glucose, the $\log P_{\text{dod/wat}}$ value was inferred between -11.1 and -7.6 , which corresponds to a transfer free energy barrier from water to dodecane between 47 and 68 kJ/mol at 50°C. Although the water/DPPC and water/dodecane interfaces cannot be directly compared, water/alkane partition coefficients give relatively good estimates of solute partitioning between water and the membrane hydrocarbon interior. The hydrophilicity of glucose is intermediate between that of methylglucose and mannitol, so that the experimental range found for the free energy barrier of glucose at the water/dodecane interface (47–68 kJ/mol) can give a rough estimate of the free energy barrier of the polar molecules at the water/DPPC interface. The free energy barriers of 42 and 49 kJ/mol obtained from the umbrella sampling procedure for methylglucose and mannitol, respectively, lie close to the experimental estimates, although rather at the lower limit. For salicylic acid, only experimental partition coefficients at the water/hexadecane and water/octanol interfaces have been reported and are equal to 6.1×10^{-2} [164] and 1.7×10^2 [198], respectively, which corresponds to transfer free energies of +7.5 and -14 kJ/mol at 50°C. The calculated energy barrier of +18 kJ/mol between water and the DPPC bilayer interior is significantly higher than +7.5 kJ/mol. This difference may be attributed to weaknesses in the OPLS force field parameters used for salicylic acid, which tend to underestimate the solubility of aromatic compounds in the membrane interior. The computed free energy difference of -14.5 kJ/mol between water and the interfacial local minimum can be compared to the experimental transfer free energy of -14 kJ/mol from water to octanol. Indeed, the energy minimum is located at the border between regions 2 and 3, in an environment containing the polar carbonyl groups of DPPC and the beginning of the lipid hydrocarbon chains which presents a degree of polarity similar to that of octanol.

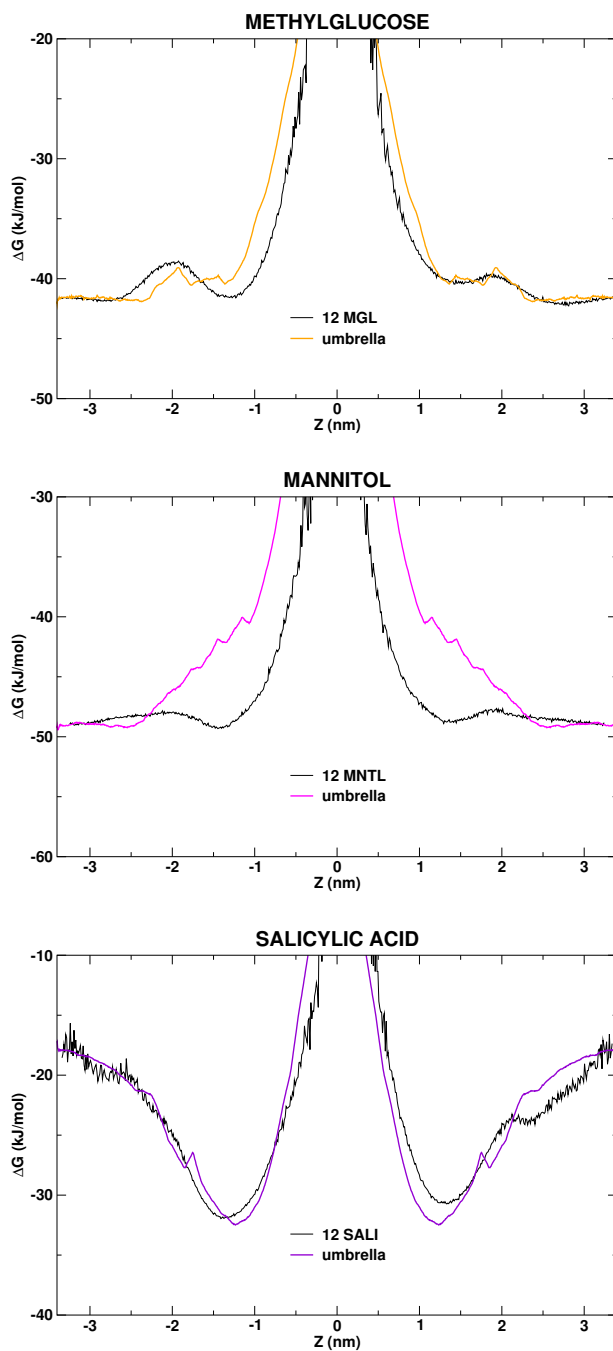


Figure 5.19: Comparison of the free energy profiles obtained from the equilibrium and umbrella sampling MD simulations in the aqueous and interfacial regions of the DPPC membrane.

5.5.2.2 Hydrogen bonding

The biased simulations can be further used to characterize the propensity of a solute molecule to form hydrogen bonds either with its environment or intramolecularly, as a function of its location in the membrane. Figure 5.20 shows the average number of H-bonds present. The striking feature is the occurrence of occasional H-bonds between the solute and water in the bilayer center, which indicates that the membrane hydrocarbon core is not entirely hydrophobic (see next section). Another interesting point is the net increase in solute intramolecular H-bonds towards the bilayer center, which makes the solute less hydrophilic and thus facilitates its permeation through the hydrophobic core of the membrane.

5.5.2.3 Water penetration

A rather surprising observation is the penetration of water molecules into the hydrophobic core of the membrane in simulations where methylglucose or mannitol is restrained in the bilayer interior. Figures 5.21 (a) and (b) show the massive water penetration from the lower bilayer leaflet in the case of a methylglucose and mannitol molecule restrained at respectively 1 and 2 Å from the bilayer center. In each case, the bilayer interior is devoid of water at the beginning of the simulation and, in the course of the simulation, water molecules progressively enter the hydrocarbon region of the membrane from one side to hydrate the polar molecule. To point out the water penetration into the membrane, density distribution profiles of water along the bilayer normal are computed in both simulation windows and are compared with the water density profile in the pure DPPC membrane (see Figure 5.21). In a few windows, the formation of transient water wires extending through the bilayer is even observed, as shown in Figure 5.22.

5.5.2.4 Solute orientation

Inside the membrane, the solute molecules are able to rotate and explore a wide range of orientations with respect to the bilayer normal. Their motions are, however, not as free as in the water phase and, depending on the region of the membrane they sample, they may exhibit preferred orientations. The numerous possibilities of hydrogen bonds with the DPPC headgroups in the interfacial region (region 2) and the high lipid chain density in region 3 tend to slow down their motions, while the lower density and higher degree of chain disorder in region 4 tend to promote the rotation of the whole solute molecules.

The mannitol molecule has rather the tendency to align its end-to-end molecular axis roughly parallel to the bilayer normal in the hydrocarbon core of the membrane, likely to orient parallel to the neighboring lipid chains and, this way, optimize van der Waals contacts. At the interface, in contrast, mannitol tends to orient its long molecular axis more or less parallel to the plane of the membrane to increase the number of possible H-bonds with the DPPC headgroups and avoid to protrude into the hydrophobic core of the membrane. These orientations are depicted in Figure 5.23.

Salicylic acid tends to orient the plane of its benzene ring roughly parallel to the bilayer normal in most cases, as already shown in Figure 5.16. Methylglucose experiences no favored orientation.

The series of umbrella sampling simulations allowed thus for the construction of free energy profiles across the DPPC membrane and for the determination of a variety of solute properties that are dependent on the location of the solute in the membrane (such as hydrogen-bonding capability or orientation) and that could be extracted from the different windows. It should be however kept in mind that these free energy calculations do not fully address the permeation process since they do not yield the solute diffusion coefficients.

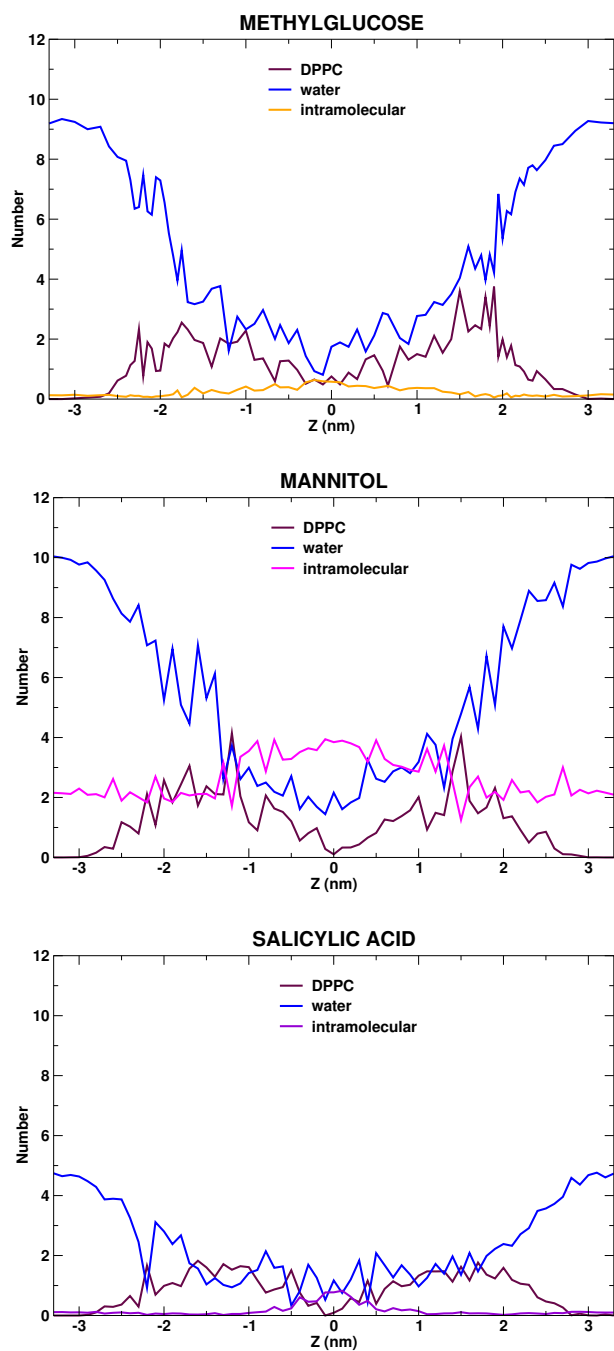


Figure 5.20: Average number of hydrogen bonds made by the solute molecules as a function of their depth in the DPPC membrane. H-bonds between the solute and DPPC or water are depicted, as well as intramolecular H-bonds within the solute molecule.

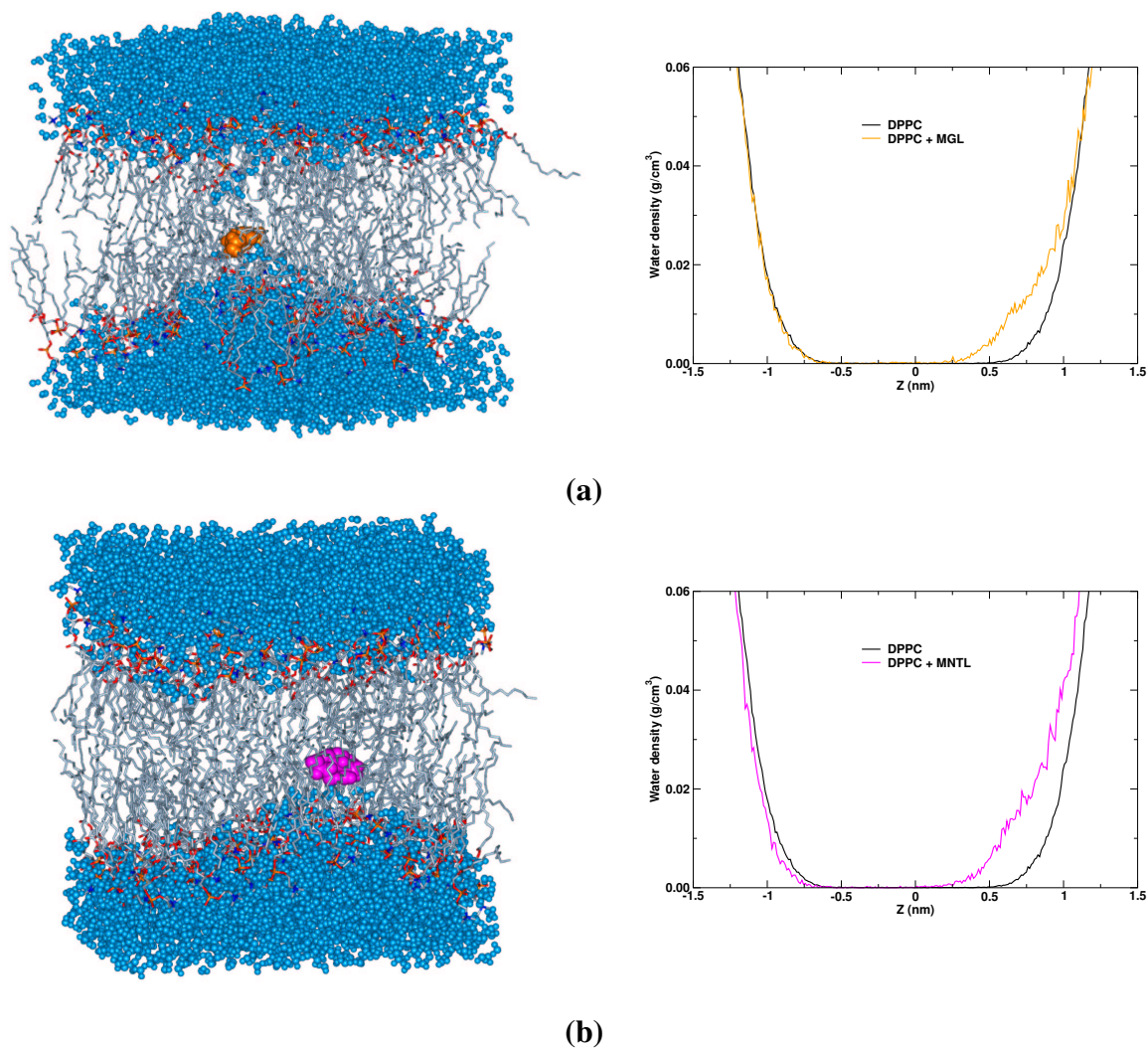


Figure 5.21: Water penetration into the hydrocarbon region of the membrane. **(a):** Simulation window with a methylglucose molecule restrained at $z = +0.1$ nm from the bilayer center. **(b):** Simulation window with a mannitol molecule restrained at $z = +0.2$ nm from the bilayer center. The corresponding trans-bilayer water density profiles are depicted and compared with that of water in a pure DPPC membrane.

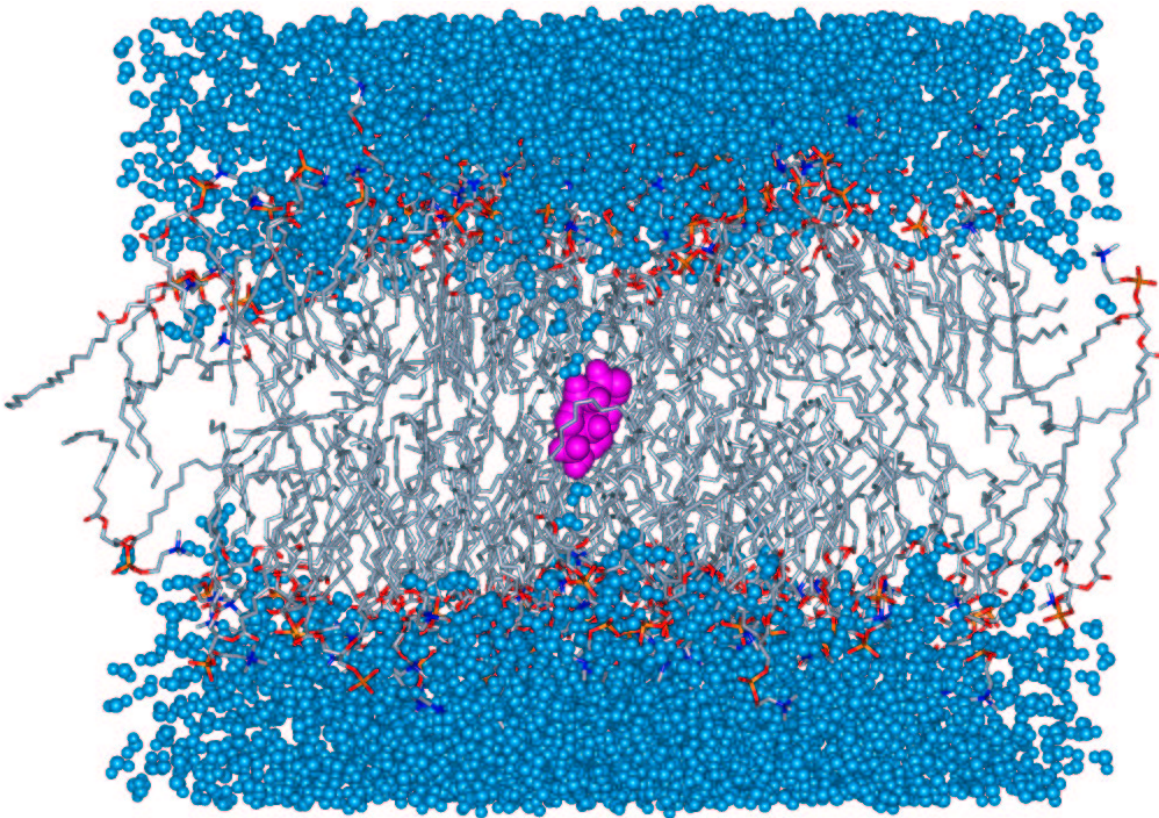


Figure 5.22: Formation of a transient water pore observed in a simulation window with a mannitol molecule restrained at $z = 0$ nm.

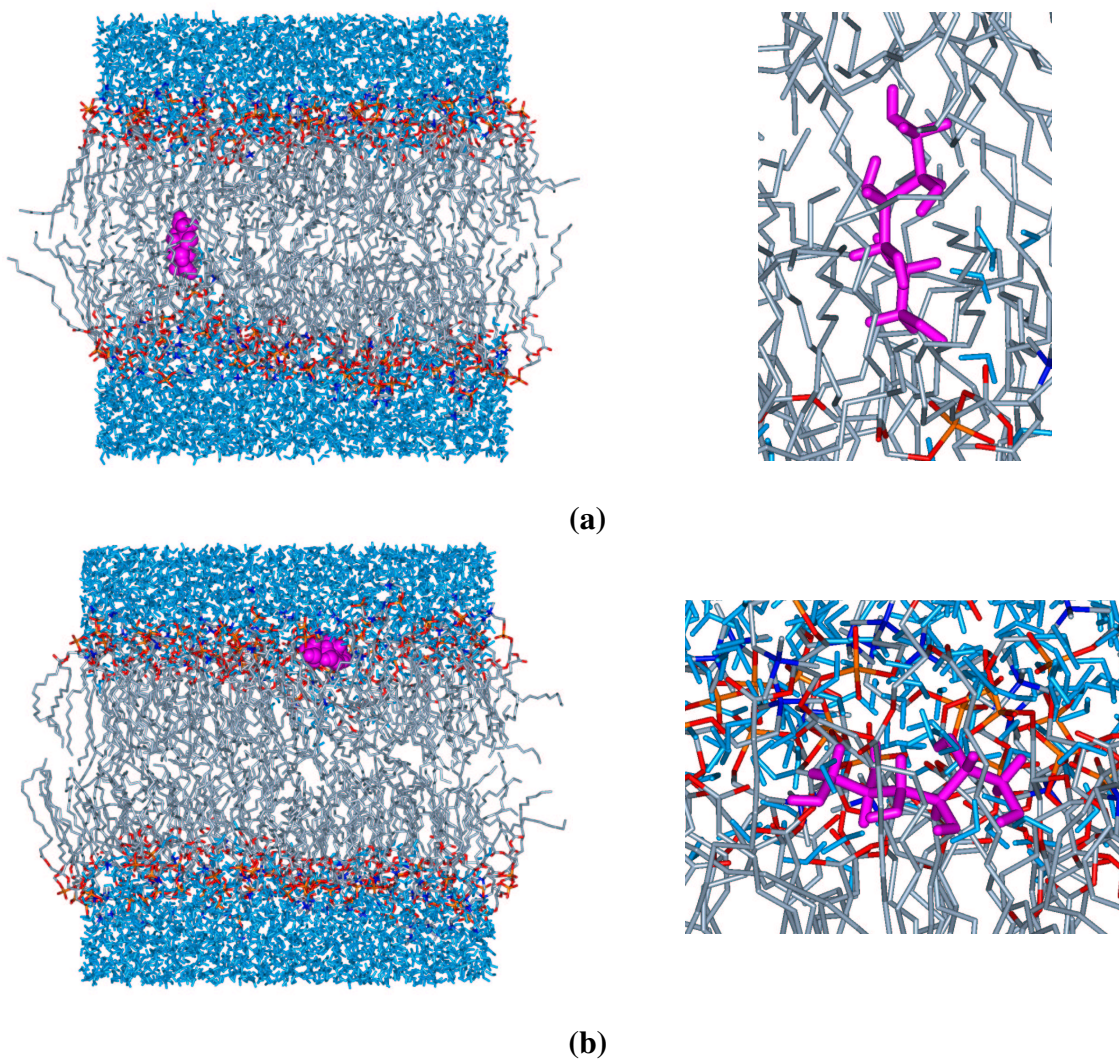


Figure 5.23: (a): Parallel orientation of mannitol with respect to the bilayer normal in the hydrocarbon region of the membrane. (b): Parallel orientation of mannitol with respect to the bilayer plane in the interfacial region of the membrane. For each orientation, a close-up shot is juxtaposed.

5.5.3 Constrained MD simulations

Constrained MD simulations, aimed at calculating the solute permeability coefficients, are performed. The average force acting on the constrained solute is computed for methylglucose and mannitol, and is displayed in Figure 5.24 as a function of the position z of the solute along the bilayer normal. From the free energy profiles of methylglucose and mannitol obtained by the umbrella sampling technique, the thermodynamic force acting on the solute can be derived using a centered difference procedure (to obtain the slope) and be compared to the force issued from the constrained method. Both force profiles exhibit a similar shape (see Figure 5.24). The force profile obtained from the constrained simulations is however less accurate owing to the reduced number of points compared with the umbrella sampling procedure. Integration of the force profile yields the potential of mean force (PMF), which can also be compared to the free energy profile from the umbrella sampling (see Figure 5.25). The PMF profiles obtained for methylglucose and mannitol from the constrained procedure are compared in Figure 5.26. An energy barrier of about +36 kJ/mol is found for both solutes. This method yields thus a lower transfer free energy than the umbrella sampling method and does not enable one to distinguish both solutes.

The force autocorrelation method is applied to deduce the local diffusion coefficients along the bilayer normal. The corresponding diffusion curves are very noisy, so that the determination of the plateau value (see Figure 5.6, page 149) is particularly difficult. The local diffusion coefficients have been nonetheless roughly estimated and range between 1×10^{-7} and 10×10^{-7} cm²/s. Equation 5.4, page 141, has finally been applied to determine the permeability coefficients (taking the values issued from the umbrella sampling for the energy). $P \approx 3 \times 10^{-6}$ cm/s and $P \approx 4 \times 10^{-8}$ cm/s have been calculated for methylglucose and mannitol, respectively, at 50°C. Experimentally, permeability coefficients of 0.3×10^{-10} and 1.1×10^{-10} cm/s have been measured by Brunner *et al.* for glucose in vesicular (at 25°C) and planar (at 26°C) egg lecithin bilayers, respectively [165]. In stratum corneum lipid liposomes, permeability coefficients of 5.8×10^{-11} and 5.8×10^{-12} cm/s have been determined by Yoneto *et al.* for methylglucose and mannitol, respectively, at 37°C [199]. The computed permeability coefficients are thus much too high, by at least two or three orders of magnitude (taking into account a correction for the temperature), compared with the experimental coefficients.

Since the constrained method does not seem to be valid for penetrants of the size of the studied molecules (see next section), this method was not further applied to salicylic acid.

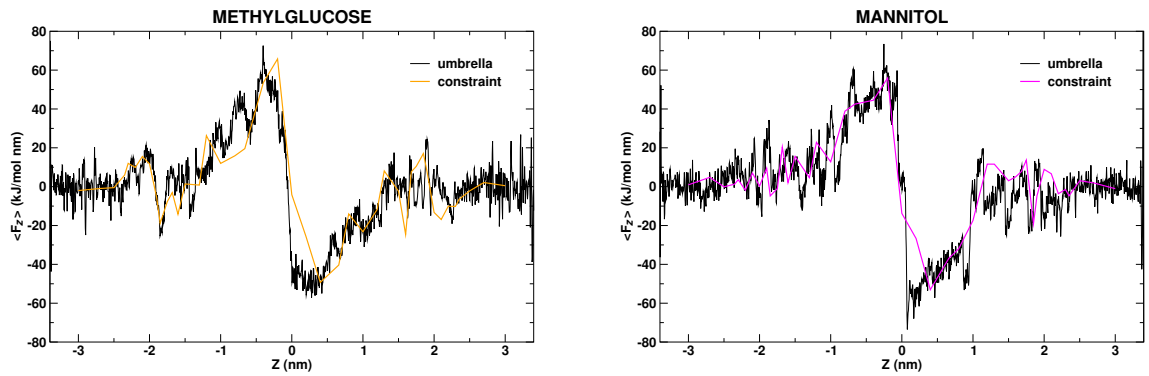


Figure 5.24: Comparison of the force profiles along the bilayer normal obtained from the umbrella sampling and constrained simulations for methylglucose and mannitol.

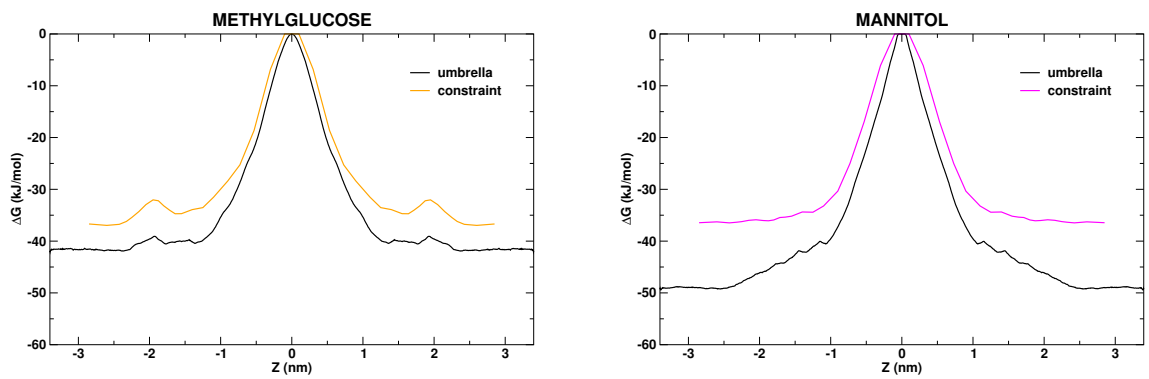


Figure 5.25: Comparison of the free energy profiles along the bilayer normal obtained from the umbrella sampling and constrained simulations for methylglucose and mannitol.

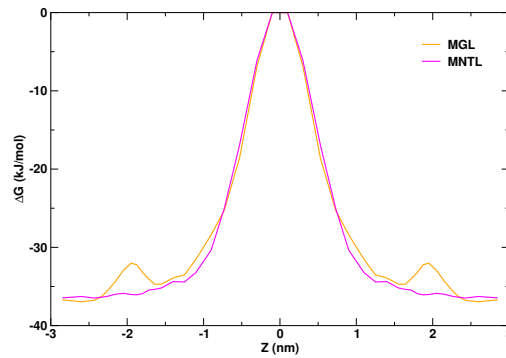


Figure 5.26: Free energy profiles (or PMF) of methylglucose (MGL) and mannitol (MNTL) obtained from the constrained method.

5.6 Discussion

The simulations performed show that the permeation process of polar solutes through a phospholipid membrane is essentially determined by the free energy barrier that results from the breakage of H-bonds between the solutes and water and between the solutes and the polar lipid headgroups and from the loss of electrostatic interactions. In the DPPC membrane, the carbonyl groups of the glycerol-ester linkages seem to play an important role in the permeation process: they have the polar and hydrogen-bonding function closest to the bilayer center and attract water as well as polar solutes close to the hydrophobic hydrocarbon region of the bilayer. They also play a determinant role in the adsorption of amphiphilic solutes, as shown in the simulations with salicylic acid.

The umbrella sampling calculations yield an estimation of the free energy barrier associated to the solute permeation through the DPPC membrane. The energy barriers obtained for methylglucose and mannitol are in relatively good agreement with experimental partition coefficients of glucose at a water/dodecane interface, although a slightly higher solubility of the polar molecules inside the membrane seems to be found in the simulations. A direct comparison with the experimental results is, however, difficult, since the water/DPPC system cannot be completely identified with the water/dodecane interface and glucose is more hydrophilic than methylglucose but less hydrophilic than mannitol. Nonetheless, the higher solubility of the polar molecules observed in the DPPC membrane is likely due to their stabilization by water molecules. Indeed, an extensive penetration of water into the hydrocarbon core of the membrane as well as the formation of transient water wires are observed in simulation windows where the polar molecule is restrained in the bilayer interior. These observations lend credit to the pore pathway model according to which small polar molecules may permeate across membranes through transient water pores. At least, it could mean that polar solutes do not necessarily get rid of their hydration shell, which would require a great amount of energy, before entering the membrane. In the case of salicylic acid, the energy barrier calculated between the water layer and the bilayer center seems to be too high compared to the partition coefficient of the acid in a water/hexadecane system, which means that a lower solubility of the acid in the hydrocarbon core of the membrane is predicted by the simulations. However, the umbrella sampling method must not necessarily be called into question. The discrepancy can probably be attributed to the parameters adopted for salicylic acid, issued from the standard OPLS force field, which may be not optimal in the context of free energy calculations to properly describe the interactions between the aromatic ring of the acid and

the hydrocarbon chains of DPPC. But, again, comparison with experiments is not without ambiguity, since the water/hexadecane interface exhibits properties very different from those of a water/DPPC interface. The energy difference computed between the water layer and the interfacial local minimum is, however, very well described by the partition coefficient of the acid between water and octanol. This may also show that octanol/water partition coefficients cannot always be identified with the whole energy barrier through the membrane and, in some cases, depending on the chemical nature of the penetrant and/or the membrane, may only describe one part of the permeation process. Despite some possible uncertainties related to the choice of the force field parameters or to the sampling time, the free energy profiles obtained from the umbrella sampling procedure provide more insight on solute partitioning into lipid bilayers and detailed information about solute-membrane interactions.

The full description of permeation processes requires not only the knowledge of the underlying free energy behavior, but also of the local diffusion coefficient, both quantities contributing to the global permeation rate. Unfortunately, the simulations based on the average force method on constrained particle, aimed at calculating permeability coefficients, were not successful. The theoretical derivation of the permeability coefficient described in Section 5.2.2.2, page 144, rests on the assumption that the thermodynamic gradient can be considered constant over the correlation distance of the particle. In the strict sense, this method is only valid for permeants of relative small size and for energy barriers which do not exhibit too steep slopes [135, 194]. The molecules, on which the method was experimented, are probably too big for this method, and their permeation cannot be treated as an equilibrium process. A permeant of the size of the molecules studied does not get to the top of the energy barrier slowly and in constant equilibrium, but is driven over it quickly by its momentum, inertia effects becoming important in the case of a large permeant. The transport of a sugar through membranes will be thus an activated and essentially non-equilibrium process, for which the activation energy will be probably higher than the transfer energy calculated in the presence of water molecules in the membrane.

5.7 Conclusion

Hence, MD simulations can test theoretical notions and complement experimental techniques to further the conceptual understanding of the solute distribution and dynamics in lipid membranes. The free energy computations described in this chapter offer more than a

simple estimation of the height of the energy barrier associated to the permeation process. By constructing the complete free energy profile across the membrane, details of the solute-membrane interactions are brought in light and help to rationalize the mechanisms of transport. The computational effort that warrants accurate, converged free energies is, however, prohibitive and remains, in large measure, incompatible with the investigation of large sets of compounds. In the present study, a compromise had to be found between the computational cost and the need for adequate sampling. The constrained method tested for the description of the full permeation process, including both the partitioning and diffusion contributions, was not successful. Nonetheless, the realization of the limits of the method, *i.e.* the difficulty to extract a permeability coefficient from the data, proved to be very informative, helping to better understand the permeation process.

Chapter 6

Summary

The aim of this thesis was to investigate the permeation of small drug-like molecules through a membrane computer model at a molecular level by means of molecular dynamics (MD) simulations.

As a first step, a realistic model for a typical biological membrane was developed. As phospholipid bilayers provide simple but very informative model systems, a pure phospholipid bilayer system, containing a single type of phospholipid (dipalmitoylphosphatidylcholine or DPPC), was simulated in the biologically relevant liquid crystalline state. DPPC was chosen in reason of its prevalence in mammalian plasma membranes and of the large amount of experimental data available on phosphatidylcholine membranes. The simulated DPPC membrane patch consists of 128 lipids (64 per leaflet) and about 4000 water molecules. A series of extensive MD simulations of the DPPC bilayer was first performed, in which the methodology of simulation was systematically varied. Methodological issues in MD simulations, such as the treatment of long-range electrostatic interactions, the type of pressure coupling, or the size of the integration time step, have, indeed, major consequences for the equilibrium properties observed. Benefits and artifacts of various methods were pointed out and optimal simulation conditions for phosphatidylcholine bilayer systems were inferred. A well equilibrated system, stable over a long period of time, was finally generated, and structural as well as dynamic properties were determined and compared to experiments for validation of the model. Emphasis was laid on properties that are thought to play an important role in permeation processes, such as membrane density, ordering degree of the lipid acyl chains, or lipid mobility. A close agreement with experimental observations was found in many respects.

As a second step, the permeation process of a sugar (methylglucose), a polyalcohol (mannitol), and a drug-like molecule (salicylic acid) through the DPPC membrane model was studied. As permeation processes are too slow on the time scale accessible to the MD technique, they cannot be directly followed. Equilibrium MD simulations were first carried out to gain insight into the solute partitioning behavior within the membrane. Non-equilibrium simulations, based on the umbrella sampling approach, were then undertaken to quantify the free energy barrier to be overcome by the permeants for their translocation from the water phase into the membrane interior.

Bibliography

- [1] J. L. W. Thudichum. *A Treatise on the Chemical Constitution of the Brain*. Baillière, Tindall & Cox, London, 1884.
- [2] P. L. Yeagle. *The Membranes of Cells*. Academic Press, San Diego, second edition, 1993.
- [3] G. A. Jamieson and D. M. Robinson. *Mammalian Cell Membranes*, volume 2. Butterworth, London, 1977.
- [4] M. K. Jain. *Introduction to Biological Membranes*. John Wiley & Sons, New York, second edition, 1988.
- [5] T. E. Redelmeier, M. J. Hope, and P. R. Cullis. *Biochemistry*, 29:3046–3053, 1990.
- [6] J. E. Rothman and J. Lenard. *Science*, 195:743–753, 1977.
- [7] P. F. Devaux and A. Zachowski. *Chem. Phys. Lipids*, 73:107–120, 1994.
- [8] P. Williamson and R. A. Schlegel. *Mol. Membr. Biol.*, 11:199–216, 1994.
- [9] K. Boesze-Battaglia and A. D. Albert. *J. Biol. Chem.*, 265:20727–20730, 1990.
- [10] Y. A. Isaacson, P. W. Deroo, A. F. Rosenthal, R. Bittman, J. O. McIntyre, H. G. Bock, P. Gazzoti, and S. Fleischer. *J. Biol. Chem.*, 254:117–126, 1979.
- [11] K. Beyer and M. Klingenberg. *Biochemistry*, 24:3821–3826, 1985.
- [12] R. A. Anderson and V. T. Marchesi. *Nature*, 318:295–298, 1985.
- [13] E. Overton. *Vierteljahrsschr. Naturforsch. Ges. Zürich*, 44:88–135, 1899.
- [14] E. Gorter and F. Grendel. *J. Exp. Med.*, 41:439–443, 1925.
- [15] J. F. Danielli and H. Davson. *J. Cell. Comp. Physiol.*, 5:495–508, 1935.
- [16] D. E. Green and J. Perdue. *Proc. Natl. Acad. Sci. USA*, 55:1295–1302, 1966.
- [17] L. D. Frye and M. Edidin. *J. Cell. Sci.*, 7:319–335, 1970.
- [18] S. J. Singer and G. L. Nicolson. *Science*, 175:720–731, 1972.

- [19] R. B. Gennis. *Biomembranes: Molecular Structure and Function*. Springer-Verlag, C. R. Cantor (Ed.), Berlin, 1989.
- [20] J. M. Seddon and R. H. Templer. Polymorphism of Lipid-Water Systems. *In: Handbook of Biological Physics - Structure and Dynamics of Membranes: From Cells to Vesicles*, volume 1A. Elsevier Science, R. Lipowsky and E. Sackmann (Eds.), Amsterdam, 1995.
- [21] J. M. Seddon. *Biochim. Biophys. Acta*, 1031:1–69, 1990.
- [22] T. Landh. *FEBS Lett.*, 369:13–17, 1995.
- [23] V. Luzzati. *Curr. Opin. Struct. Biol.*, 7:661–668, 1997.
- [24] P. G. Barton and F. D. Gunstone. *J. Biol. Chem.*, 250:4470–4476, 1975.
- [25] G. Cevc. *Chem. Phys. Lipids*, 57:293–307, 1991.
- [26] H. Ohvo-Rekilä, B. Ramstedt, P. Leppimäki, and J. P. Slotte. *Prog. Lipid Res.*, 41:66–97, 2002.
- [27] G. Cevc. *Biochemistry*, 30:7186–7193, 1991.
- [28] E. Sackmann. Physical Basis of Self-Organization and Function of Membranes. *In: Handbook of Biological Physics - Structure and Dynamics of Membranes: From Cells to Vesicles*, volume 1A. Elsevier Science, R. Lipowsky and E. Sackmann (Eds.), Amsterdam, 1995.
- [29] A. Blume. Dynamic Properties. *In: Phospholipids Handbook*. G. Cevc (Ed.), Marcel Dekker, New York, 1993.
- [30] M. Schinitzky. *Physiology of Membrane Fluidity*. CRC Press, Boca Raton, 1984.
- [31] P. Artursson and J. Karlsson. *Biochem. Biophys. Res. Commun.*, 175:880–885, 1991.
- [32] K. Balon, B. U. Riebesehl, and B. W. Müller. *Pharm. Res.*, 16:882–888, 1999.
- [33] H. M. Jacobs. *Cold Spring Harbor Symp. Quant. Biol.*, 8:30–39, 1940.
- [34] J. K. Seydel, E. A. Coats, H. P. Cordes, and M. Wiese. *Arch. Pharm.*, 327:601–610, 1994.
- [35] U. Hellwich and R. Schubert. *Biochem. Pharmacol.*, 49:511–517, 1995.
- [36] A. Pagliara, M. Reist, S. Geinoz, P.-A. Carrupt, and B. Testa. *J. Pharm. Pharmacol.*, 51:1339–1357, 1999.
- [37] O. A. Raevsky, K.-J. Schaper, and J. K. Seydel. *Quant. Struct.-Act. Relat.*, 14:433–436, 1995.

- [38] H. van de Waterbeemd, G. Camenisch, G. Folkers, and O. A. Raevsky. *Quant. Struct.-Act. Relat.*, 15:480–490, 1996.
- [39] A. Walter and J. Gutknecht. *J. Membr. Biol.*, 90:207–217, 1986.
- [40] T.-X. Xiang and B. D. Anderson. *J. Membr. Biol.*, 140:111–122, 1994.
- [41] H. I. Petrache, S. W. Dodd, and M. F. Brown. *Biophys. J.*, 79:3172–3192, 2000.
- [42] J. F. Nagle and S. Tristram-Nagle. *Biochim. Biophys. Acta*, 1469:159–195, 2000.
- [43] K. Gawrisch, N. V. Eldho, and I. V. Polozov. *Chem. Phys. Lipids*, 116:135–151, 2002.
- [44] M. Wiese. Computer Simulation of Phospholipids and Drug-Phospholipid Interactions. In: *Drug-Membrane Interactions*. J. K. Seydel and M. Wiese (Eds.), Wiley-VCH Verlag GmbH, Weinheim, 2002.
- [45] P. La Rocca, Y. Shai, and M. S. P. Sansom. *Biophys. Chem.*, 76:145–159, 1999.
- [46] K. Binder. *Applications of the Monte Carlo Method in Statistical Physics*. Springer-Verlag, Heidelberg, 1984.
- [47] S.-W. Chiu, M. M. Clark, E. Jakobsson, S. Subramaniam, and H. L. Scott. *J. Comput. Chem.*, 20:1153–1164, 1999.
- [48] J. I. Siepmann and D. Frenkel. *Mol. Phys.*, 75:59–70, 1992.
- [49] D. Frenkel and B. Smit. *Comput. Phys.*, 11:246–255, 1997.
- [50] J. C. Shelley, M. Y. Shelley, R. C. Reeder, S. Bandyopadhyay, and M. L. Klein. *J. Phys. Chem. B*, 105:4464–4470, 2001.
- [51] C. F. Lopez, P. B. Moore, J. C. Shelley, M. Y. Shelley, and M. L. Klein. *Comput. Phys. Commun.*, 147:1–6, 2002.
- [52] A. J. Kox, J. P. J. Michels, and F. W. Wiegel. *Nature*, 287:317–319, 1980.
- [53] P. van der Ploeg and H. J. C. Berendsen. *J. Chem. Phys.*, 76:3271–3276, 1982.
- [54] E. Egberts and H. J. C. Berendsen. *J. Chem. Phys.*, 89:3718–3732, 1988.
- [55] E. Egberts. *Molecular Dynamics Simulations of Multibilayer Membranes*. Ph. D. thesis, University of Groningen, The Netherlands, 1988.
- [56] E. Egberts, S. J. Marrink, and H. J. C. Berendsen. *Eur. Biophys. J. with Biophys. Lett.*, 22:423–436, 1994.
- [57] A. H. de Vries, A. E. Mark, and S. J. Marrink. *J. Phys. Chem. B*, 2003. In press.
- [58] A. J. Robinson, W. G. Richards, P. J. Thomas, and M. M. Hann. *Biophys. J.*, 68:164–170, 1995.

- [59] K. Tu, M. L. Klein, and D. J. Tobias. *Biophys. J.*, 75:2147–2156, 1998.
- [60] A. M. Smondyrev and M. L. Berkowitz. *Biophys. J.*, 77:2075–2089, 1999.
- [61] M. Pasenkiewicz-Gierula, K. Murzyn, T. Róg, and C. Czaplewski. *Acta Biochim. Pol.*, 47:601–611, 2000.
- [62] M. Pasenkiewicz-Gierula, T. Róg, K. Kitamura, and A. Kusumi. *Biophys. J.*, 78:1376–1389, 2000.
- [63] A. Léonard, C. Escrive, M. Laguerre, E. Pebay-Peyroula, W. Néri, T. Pott, J. Katsaras, and E. J. Dufourc. *Langmuir*, 17:2019–2030, 2001.
- [64] A. M. Smondyrev and M. L. Berkowitz. *Biophys. J.*, 80:1649–1658, 2001.
- [65] H. E. Alper and T. R. Stouch. *J. Phys. Chem.*, 99:5724–5731, 1995.
- [66] P. Huang, E. Bertaccini, and G. H. Loew. *J. Biomol. Struct. Dyn.*, 12:725–754, 1995.
- [67] J. J. López Cascales, M. L. Huertas, and J. García de la Torre. *Biophys. Chem.*, 69:1–8, 1997.
- [68] M. Aiello, O. Moran, M. Pisciotta, and F. Gambale. *Eur. Biophys. J.*, 27:211–218, 1998.
- [69] K. Tu, M. Tarek, M. L. Klein, and D. Scharf. *Biophys. J.*, 75:2123–2134, 1998.
- [70] L. Koubi, M. Tarek, M. L. Klein, and D. Scharf. *Biophys. J.*, 78:800–811, 2000.
- [71] L. Koubi, M. Tarek, S. Bandyopadhyay, M. L. Klein, and D. Scharf. *Biophys. J.*, 81:3339–3345, 2001.
- [72] J. A. Söderhäll and A. Laaksonen. *J. Phys. Chem. B*, 105:9308–9315, 2001.
- [73] A. Grossfield and T. B. Woolf. *Langmuir*, 18:198–210, 2002.
- [74] D. P. Tieleman and H. J. C. Berendsen. *Biophys. J.*, 74:2786–2801, 1998.
- [75] D. P. Tieleman, H. J. C. Berendsen, and M. S. P. Sansom. *Biophys. J.*, 76:1757–1769, 1999.
- [76] S.-W. Chiu, S. Subramaniam, and E. Jakobsson. *Biophys. J.*, 76:1929–1938, 1999.
- [77] S.-W. Chiu, S. Subramaniam, and E. Jakobsson. *Biophys. J.*, 76:1939–1950, 1999.
- [78] Y. Z. Tang, W. Z. Chen, C. X. Wang, and Y. Y. Shi. *Eur. Biophys. J.*, 28:478–488, 1999.
- [79] M. Nina, S. Bernecke, and B. Roux. *Eur. Biophys. J.*, 29:439–454, 2000.

- [80] R. J. Law, L. R. Forrest, K. M. Ranatunga, P. La Rocca, D. P. Tieleman, and M. S. P. Sansom. *Proteins: Struct. Func. Genet.*, 39:47–55, 2000.
- [81] L. R. Forrest, A. Kukol, I. T. Arkin, D. P. Tieleman, and M. S. P. Samson. *Biophys. J.*, 78:55–69, 2000.
- [82] D. P. Tieleman and M. S. P. Sansom. *Int. J. Quant. Chem.*, 83:166–179, 2001.
- [83] J. Baudry, E. Tajkhorshid, F. Molnar, J. Phillips, and K. Schulten. *J. Phys. Chem. B*, 105:905–918, 2001.
- [84] D. E. Elmore and D. A. Dougherty. *Biophys. J.*, 81:1345–1359, 2001.
- [85] C. M. Shepherd, H. J. Vogel, and D. J. Tieleman. *Biochim. J.*, 370:233–243, 2003.
- [86] S. J. Weiner, P. A. Kollman, D. A. Case, U. C. Singh, C. Ghio, G. Alagona, S. Profeta, and P. Weiner. *J. Am. Chem. Soc.*, 106:765–784, 1984.
- [87] B. R. Brooks, R. E. Bruccoleri, B. D. Olafson, D. J. States, S. Swaminathan, and M. Karplus. *J. Comput. Chem.*, 4:187–217, 1983.
- [88] W. F. van Gunsteren and H. J. C. Berendsen. *Groningen Molecular Simulation (GROMOS) Library manual*. Biomos, Nijenborgh 4, 9747 AG Groningen, The Netherlands, 1987.
- [89] W. Jorgensen and J. Tirado-Rives. *J. Am. Chem. Soc.*, 110:1666–1671, 1988.
- [90] M. Schlenkrich, J. Brickmann, A. D. MacKerell Jr., and M. Karplus. An Empirical Potential Energy Function for Phospholipids: Criteria for Parameter Optimization and Applications. *In: Biological Membranes: A Molecular Perspective from Computation and Experiment*. K. M. Merz Jr. and B. Roux (Eds.), Birhäuser, Boston, 1996.
- [91] S. E. Feller, D. Yin, R. W. Pastor, and A. D. MacKerell Jr. *Biophys. J.*, 73:2269–2279, 1997.
- [92] S. E. Feller and A. D. MacKerell Jr. *J. Phys. Chem. B*, 104:7510–7515, 2000.
- [93] O. Berger, O. Edholm, and F. Jähnig. *Biophys. J.*, 72:2002–2013, 1997.
- [94] A. M. Smondyrev and M. L. Berkowitz. *J. Comp. Chem.*, 20:531–545, 1999.
- [95] M. P. Allen and D. J. Tildesley. *Computer Simulation of Liquids*. Clarendon Press, Oxford, 1996.
- [96] E. Jakobsson, S. Subramaniam, and H. L. Scott. Strategic Issues in Molecular Dynamics Simulations of Membranes. *In: Biological Membranes: A Molecular Perspective from Computation and Experiment*. K. M. Merz Jr. and B. Roux (Eds.), Birhäuser, Boston, 1996.

- [97] S.-W. Chiu, M. M. Clark, V. Balaji, S. Subramaniam, H. L. Scott, and E. Jakobsson. *Biophys. J.*, 69:1230–1245, 1995.
- [98] D. P. Tieleman and H. J. C. Berendsen. *J. Chem. Phys.*, 105:4871–4880, 1996.
- [99] S. E. Feller and R. W. Pastor. *J. Chem. Phys.*, 111:1281–1287, 1999.
- [100] U. Essmann, L. Perera, and M. L. Berkowitz. *Langmuir*, 11:4519–4531, 1995.
- [101] U. Essmann and M. L. Berkowitz. *Biophys. J.*, 76:2081–2089, 1999.
- [102] F. Jähnig. *Biophys. J.*, 71:1348–1349, 1996.
- [103] S. J. Marrink and A. E. Mark. *J. Phys. Chem. B*, 105:6122–6127, 2001.
- [104] E. Lindahl and O. Edholm. *J. Chem. Phys.*, 113:3882–3893, 2000.
- [105] R. M. Venable, Y. Zhang, B. J. Hardy, and R. W. Pastor. *Science*, 262:223–226, 1993.
- [106] H. J. C. Berendsen and D. P. Tieleman. Molecular Dynamics Studies of Lipid Bilayers. *In: Encyclopedia of Computational Chemistry*, volume 3. P. von Rague Schleyer (Ed.), John Wiley & Sons, 1998.
- [107] W. Shinoda, N. Namiki, and S. Okazaki. *J. Chem. Phys.*, 106:5731–5743, 1997.
- [108] J. P. Ryckaert, G. Ciccotti, and H. J. C. Berendsen. *J. Comput. Phys.*, 23:327–341, 1977.
- [109] B. Hess, H. Bekker, H. J. C. Berendsen, and J. G. E. M. Fraaije. *J. Comput. Chem.*, 18:1463–1472, 1997.
- [110] A. Cheng and K. M. Merz Jr. *J. Phys. Chem. B*, 103:5396–5405, 1999.
- [111] R. W. Hockney and J. W. Eastwood. *Computer Simulation using Particles*. McGraw-Hill, New York, 1981.
- [112] T. Darden, D. York, and L. Pedersen. *J. Chem. Phys.*, 98:10089–10092, 1993.
- [113] U. Essmann, L. Perera, M. L. Berkowitz, T. Darden, H. Lee, and L. G. Pedersen. *J. Chem. Phys.*, 103:8577–8593, 1995.
- [114] I. G. Tironi, R. Sperb, P. E. Smith, and W. F. van Gunsteren. *J. Chem. Phys.*, 102:5451–5459, 1995.
- [115] E. Jakobsson. *Trends Biochem. Sci.*, 22:339–344, 1997.
- [116] D. P. Tieleman, S. J. Marrink, and H. J. C. Berendsen. *Biochem. Biophys. Acta*, 1331:235–270, 1997.
- [117] J. F. Nagle, R. Zhang, S. Tristram-Nagle, W. Sun, H. I. Petrache, and R. M. Suter. *Biophys. J.*, 70:1419–1431, 1996.

- [118] R. S. Armen, O. D. Uitto, and S. E. Feller. *Biophys. J.*, 75:734–744, 1998.
- [119] R. H. Pearson and I. Pascher. *Nature*, 281:499–501, 1979.
- [120] G. Vanderkooi. *Biochemistry*, 30:10760–10768, 1991.
- [121] E. J. Dufourc, C. Mayer, J. Stohrer, G. Althoff, and G. Kothe. *Biophys. J.*, 61:42–57, 1992.
- [122] J. P. Ryckaert and A. Bellemans. *Chem. Phys. Lett.*, 30:123–125, 1975.
- [123] H. J. C. Berendsen, J. P. M. Postma, W. F. van Gunsteren, and J. Hermans. Interaction Models for Water in Relation to Protein Hydration. *In: Intermolecular Forces*. B. Pullman (Ed.), Reidel, Dordrecht, 1981.
- [124] H. J. C. Berendsen, J. R. Grigera, and T. P. Straatsma. *J. Phys. Chem.*, 91:6269–6271, 1987.
- [125] W. L. Jorgensen, J. Chandrasekhar, J. D. Madura, R. W. Impey, and M. L. Klein. *J. Chem. Phys.*, 79:926–935, 1983.
- [126] H. J. C. Berendsen, D. van der Spoel, and R. van Drunen. *Comput. Phys. Commun.*, 91:43–56, 1995.
- [127] A. R. van Buuren, S. J. Marrink, and H. J. C. Berendsen. *J. Phys. Chem.*, 97:9206–9212, 1993.
- [128] S. Miyamoto and P. A. Kollman. *J. Comput. Chem.*, 13:952–962, 1992.
- [129] Y. H. Zhang, S. E. Feller, B. R. Brooks, and R. W. Pastor. *J. Chem. Phys.*, 103:10252–10266, 1995.
- [130] P. Ewald. *Ann. Phys.*, 64:253, 1921.
- [131] A. Y. Toukmaji and J. A. Board Jr. *Comput. Phys. Commun.*, 95:73–92, 1996.
- [132] K. A. Feenstra, B. Hess, and H. J.C Berendsen. *J. Comput. Chem.*, 20:786–798, 1999.
- [133] H. J. C. Berendsen, J. P. M. Postma, W. F. van Gunsteren, A. DiNola, and J. R. Haak. *J. Chem. Phys.*, 81:3684–3690, 1984.
- [134] J. F. Nagle and M. C. Wiener. *Biochim. Biophys. Acta*, 942:1–10, 1988.
- [135] S. J. Marrink and H. J. C. Berendsen. *J. Phys. Chem.*, 98:4155–4168, 1994.
- [136] B. A. Lewis and D. M. Engelman. *J. Mol. Biol.*, 166:211–217, 1983.
- [137] G. Büldt, H. U. Gally, J. Seelig, and G. Zaccai. *J. Mol. Biol.*, 134:673–691, 1979.
- [138] H. Akutsu and T. Nagamori. *Biochemistry*, 30:4510–4516, 1991.

- [139] P. T. T. Wong and H. H. Mantsch. *Chem. Phys. Lipids*, 46:213–224, 1988.
- [140] G. Zaccai, G. Büldt, A. Seelig, and J. Seelig. *J. Mol. Biol.*, 134:693–706, 1979.
- [141] D. Marsh. *J. Membr. Biol.*, 18:145–162, 1974.
- [142] J. F. Nagle and D. A. Wilkinson. *Biophys. J.*, 23:159–175, 1978.
- [143] D. A. Pink, T. J. Green, and D. Chapman. *Biochemistry*, 19:349–356, 1980.
- [144] R. Mendelsohn, M. A. Davies, J. W. Brauner, H. F. Schuster, and R. A. Dluhy. *Biochemistry*, 28:8934–8939, 1989.
- [145] R. Mendelsohn, M. A. Davies, H. F. Schuster, Z. C. Xu, and R. Bittman. *Biochemistry*, 30:8558–8563, 1991.
- [146] J.-P. Douliez, A. Léonard, and E. J. Dufourc. *Biophys. J.*, 68:1727–1739, 1995.
- [147] A. M. Smondyrev and M. L. Berkowitz. *J. Chem. Phys.*, 110:3981–3985, 1999.
- [148] A. Seelig and J. Seelig. *Biochemistry*, 13:4839–4845, 1974.
- [149] H. Brockman. *Chem. Phys. Lipids*, 73:57–79, 1994.
- [150] S. A. Simon and T. J. McIntosh. *Proc. Natl. Acad. Sci. USA*, 86:9263–9267, 1989.
- [151] K. Gawrisch, D. Ruston, J. Zimmerberg, V. A. Parsegian, R. P. Rand, and N. Fuller. *Biophys. J.*, 61:1213–1223, 1992.
- [152] J. C. Franklin and D. S. Cafiso. *Biophys. J.*, 65:289–299, 1993.
- [153] A. M. Smondyrev and M. L. Berkowitz. *Biophys. J.*, 78:1672–1680, 2000.
- [154] G. von Heijne. *Annu. Rev. Biophys. Biomol. Struct.*, 23:167–192, 1994.
- [155] S. König, T. M. Bayerl, G. Coddens, D. Richter, and E. Sackmann. *Biophys. J.*, 68:1871–1880, 1995.
- [156] E. Lindahl and O. Edholm. *J. Chem. Phys.*, 115:4938–4950, 2001.
- [157] J. R. Sheats and H. M. McConnell. *Proc. Natl. Acad. Sci. USA*, 75:4661–4663, 1978.
- [158] A.-L. Kuo and C. G. Wade. *Biochemistry*, 18:2300–2308, 1979.
- [159] G. Orädd, G. Lindblom, and P. W. Westerman. *Biophys. J.*, 83:2702–2704, 2002.
- [160] R. J. Pace and S. I. Chan. *J. Chem. Phys.*, 76:4241–4247, 1982.
- [161] D. L. Melchior, F. J. Scavitto, and J. M. Steim. *Biochemistry*, 19:4828–4834, 1980.
- [162] M. C. Wiener and S. H. White. *Biophys. J.*, 61:434–447, 1992.

- [163] A. Bondi. *J. Phys. Chem.*, 58:929–939, 1954.
- [164] A. Walter and J. Gutknecht. *J. Membr. Biol.*, 77:255–264, 1984.
- [165] J. Brunner, D. E. Graham, H. Hauser, and G. Semenza. *J. Membr. Biol.*, 57:133–141, 1980.
- [166] T. Hanai and D. A. Haydon. *J. Theor. Biol.*, 11:370–382, 1966.
- [167] J. B. Reeves and R. M. Dowben. *J. Membr. Biol.*, 3:123–141, 1970.
- [168] A. Finkelstein. *J. Gen. Physiol.*, 68:127–135, 1976.
- [169] J. F. Nagle and H. L. Scott. *Biochim. Biophys. Acta*, 513:236–243, 1978.
- [170] J. C. Weaver, K. T. Powell, and R. A. Mintzer. *Bioelectrochem. Bioenerg.*, 12:405–412, 1984.
- [171] I. G. Abidor, V. B. Arakelyan, L. V. Chernomordik, Yu. A. Chizmadzhev, V. F. Pastushenko, and M. R. Tarasevich. *Bioelectrochem. Bioenerg.*, 6:37–52, 1979.
- [172] A. G. Volkov, S. Paula, and D. W. Deamer. *Bioelectrochem. Bioenerg.*, 42:153–160, 1997.
- [173] S. Paula, A. G. Volkov, A. N. van Hoek, T. H. Haines, and D. W. Deamer. *Biophys. J.*, 70:339–348, 1996.
- [174] T. R. Stouch. *Prog. Colloid. Polym. Sci.*, 103:116–120, 1997.
- [175] W. K. Subczynski, A. Wisniewska, J.-J. Yin, J. S. Hyde, and A. Kusumi. *Biochemistry*, 33:7670–7681, 1994.
- [176] R. P. Mason, D. G. Rhodes, and L. G. Herbetette. *J. Med. Chem.*, 34:869–877, 1991.
- [177] D. G. Rhodes, J. G. Sarmiento, and L. G. Herbetette. *Mol. Pharmacol.*, 27:612–623, 1985.
- [178] A. S. Janoff and K. W. Miller. A Critical Assessment of the Lipid Theories of General Anaesthetic Action. *In: Biological Membranes*, volume 4. D. Chapman (Ed.), Academic Press, New York, 1982.
- [179] G. M. Torrie and J. P. Valleau. *Chem. Phys. Lett.*, 28:578–581, 1974.
- [180] G. M. Torrie and J. P. Valleau. *J. Comput. Phys.*, 23:187–199, 1977.
- [181] B. Roux and M. Karplus. *J. Phys. Chem.*, 95:4856–4868, 1991.
- [182] R. Kubo. *Rev. Mod. Phys.*, 29:255–284, 1966.
- [183] D. Bassolino-Klimas, H. E. Alper, and T. R. Stouch. *Biochemistry*, 32:12624–12637, 1993.

- [184] D. Bassolino-Klimas, H. E. Alper, and T. R. Stouch. *J. Am. Chem. Soc.*, 117:4118–4129, 1995.
- [185] D. Bassolino, H. E. Alper, and T. R. Stouch. *Drug. Des. Discov.*, 13:135–141, 1996.
- [186] B. Jin and A. J. Hopfinger. *Pharm. Res.*, 13:1786–1794, 1996.
- [187] E. Paci and M. Marchi. *Mol. Simulat.*, 14:1–10, 1994.
- [188] A. Pohorille and M. A. Wilson. *J. Chem. Phys.*, 104:3760–3773, 1996.
- [189] A. Pohorille, M. A. Wilson, M. H. New, and C. Chipot. *Toxicol. Lett.*, 100–101:421–430, 1998.
- [190] B. Widom. *J. Chem. Phys.*, 39:2808, 1963.
- [191] B. Widom. *J. Chem. Phys.*, 86:869–872, 1982.
- [192] T.-X. Xiang and B. D. Anderson. *Biophys. J.*, 82:2052–2066, 2002.
- [193] J. L. MacCallum, P. Mukhopadhyay, H. Luo, and D. P. Tieleman. Large Scale Molecular Dynamics Simulations of Lipid-Drug Interactions. *In: Proceedings of the 17th Annual International Symposium on High Performance Computing Systems and Applications and the OSCAR Symposium*. D. Senechal (Ed.), NRC Research Press, Ottawa, 2003.
- [194] S. J. Marrink and H. J. C. Berendsen. *J. Phys. Chem.*, 100:16729–16738, 1996.
- [195] A. Mostad. *Acta Chem. Scand.*, 48:276–278, 1994.
- [196] W. Kaminsky. *Z. Kristallogr.*, 212:283–296, 1997.
- [197] R. Collander. *Acta Chem. Scand.*, 4:1085–1098, 1950.
- [198] A. Leo, C. Hansch, and D. Elkins. *Chem. Rev.*, 71:525–616, 1971.
- [199] K. Yoneto, S. K. Li, A.-H. Ghanen, D. J. A. Crommelin, and W. I. Higuchi. *J. Pharm. Sci.*, 84:853–861, 1995.
- [200] S. G. Clerc and T. E. Thompson. *Biophys. J.*, 68:2333–2341, 1995.
- [201] A. B. R. Thomson. *J. Membr. Biol.*, 50:141–163, 1979.
- [202] M. Elia, R. Behrens, C. Northrop, P. Wraight, and G. Neagle. *Clin. Sci.*, 73:197–204, 1987.
- [203] M.-C. Grès, B. Julian, M. Bourrié, V. Meunier, C. Roques, M. Berger, X. Boulenc, Y. Berger, and G. Fabre. *Pharm. Res.*, 15:726–733, 1998.
- [204] C. Hilgendorf, H. Spahn-Langguth, C. G. Regardh, E. Lipka, G. L. Amidon, and P. Langguth. *J. Pharm. Sci.*, 89:63–75, 2000.

- [205] P. Krugliak, D. Hollander, C. C. Schlaepfer, H. Nguyen, and T. Y. Ma. *Dig. Dis. Sci.*, 39:796–801, 1994.
- [206] G. E. Bacon and R. J. Jude. *Z. Kristallogr.*, 138:19–40, 1973.
- [207] M. Takagi, Y. Taki, T. Sakane, T. Nadai, H. Sezaki, N. Oku, and S. Yamashita. *J. Pharmacol. Exp. Ther.*, 285:1175–1180, 1998.
- [208] J. Gutknecht. *Mol. Cell. Biochem.*, 114:3–8, 1992.
- [209] W. Damm, A. Frontera, J. Tirado-Rives, and W. L. Jorgensen. *J. Comput. Chem.*, 18:1955–1970, 1997.
- [210] W. L. Jorgensen, D. S. Maxwell, and J. Tirado-Rives. *J. Am. Chem. Soc.*, 118:11225–11236, 1996.
- [211] W. D. Cornell, P. Cieplak, C. I. Bayly, I. R. Gould, K. M. Merz, D. M. Ferguson, D. C. Spellmeyer, T. Fox, J. W. Caldwell, and P. A. Kollman. *J. Am. Chem. Soc.*, 117:5179–5197, 1995.
- [212] W. L. Jorgensen and N. A. McDonald. *Theochem.*, 424:145–155, 1998.
- [213] W. L. Jorgensen and N. A. McDonald. *J. Phys. Chem. B*, 102:8049–8059, 1998.
- [214] R. C. Rizzo and W. L. Jorgensen. *J. Am. Chem. Soc.*, 121:4827–4836, 1999.
- [215] M. L. P. Price, D. Ostrovsky, and W. L. Jorgensen. *J. Comput. Chem.*, 22:1340–1352, 2001.
- [216] S. Kumar, D. Bouzida, R. H. Swendsen, P. A. Kollman, and J. M. Rosenberg. *J. Comput. Chem.*, 13:1011–1021, 1992.
- [217] B. Roux. *Comput. Phys. Commun.*, 91:275–282, 1995.
- [218] D. Bas, D. Dorison-Duval, S. Moreau, P. Bruneau, and C. Chipot. *J. Med. Chem.*, 45:151–159, 2002.
- [219] C. Anézo, A. H. de Vries, H.-D. Höltje, D. P. Tieleman, and S. J. Marrink. *J. Phys. Chem. B*, 2003. In press.
- [220] S. E. Feller, D. Huster, and K. Gawrisch. *J. Am. Chem. Soc.*, 121:8963–8964, 1999.
- [221] P. B. Moore, C. F. Lopez, and M. L. Klein. *Biophys. J.*, 81:2484–2494, 2001.
- [222] R. W. Pastor, R. M. Venable, and S. E. Feller. *Acc. Chem. Res.*, 35:438–446, 2002.
- [223] E. Lindahl and O. Edholm. *Biophys. J.*, 79:426–433, 2000.
- [224] J. Norberg and L. Nilsson. *Biophys. J.*, 79:1537–1553, 2000.
- [225] B. Hess. *J. Chem. Phys.*, 116:209–217, 2002.

- [226] S. E. Feller, R. W. Pastor, A. Rojnuckarin, S. Bogusz, and B.R. Brooks. *J. Phys. Chem.*, 100:17011–17020, 1996.
- [227] P. H. Hünenberger and W. F. van Gunsteren. *J. Chem. Phys.*, 108:6117–6134, 1998.
- [228] P. Mark and L. Nilsson. *J. Comput. Chem.*, 23:1211, 2002.
- [229] H. E. Alper, D. Bassolino, and T. R. Stouch. *J. Chem. Phys.*, 98:9798–9807, 1993.
- [230] C. L. Brooks III, B. M. Pettitt, and M. Karplus. *J. Chem. Phys.*, 83:5897–5908, 1985.
- [231] P. E. Smith and B. M. Pettitt. *J. Chem. Phys.*, 105:4289–4293, 1996.
- [232] P. E. Smith, H. D. Blatt, and B. M. Pettitt. *J. Phys. Chem. B*, 101:3886–3890, 1997.
- [233] W. Weber, P. H. Hünenberger, and J. A. McCammon. *J. Phys. Chem. B*, 104:3668–3675, 2000.
- [234] R. M. Venable, B. R. Brooks, and R. W. Pastor. *J. Chem. Phys.*, 112:4822–4832, 2000.
- [235] I.-C. Yeh and M. L. Berkowitz. *J. Chem. Phys.*, 111:3155–3162, 1999.
- [236] J. de Joannis, A. Arnold, and C. Holm. *J. Chem. Phys.*, 117:2503–2512, 2002.
- [237] D. Bostick and M. L. Berkowitz. *Biophys. J.*, 85:97–107, 2003.
- [238] D. P. Tieleman, B. Hess, and M. S. P. Sansom. *Biophys. J.*, 83:2393–2407, 2002.
- [239] D. van der Spoel, A. R. van Buuren, E. Apol, P. J. Meulenhoff, D. P. Tieleman, A. L. T. M. Sijbers, B. Hess, K. A. Feenstra, E. Lindahl, R. van Drunen, and H. J. C. Berendsen. *Gromacs User Manual version 3.0*. Nijenborgh 4, 9747 AG Groningen, The Netherlands, 2001.
- [240] M. Parrinello and A. Rahman. *J. Appl. Phys.*, 52:7182–7190, 1981.

Appendix A

List of abbreviations

COM	Center-of-mass
DFT	Discrete Fourier Transform
DLPE	Dilauroylphosphatidylethanolamine
DMPC	Dimyristoylphosphatidylcholine
DPPC	Dipalmitoylphosphatidylcholine
DPPE	Dipalmitoylphosphatidylethanolamine
ESR	Electron Spin Resonance
FFT	Fast Fourier Transform
GMO	Glycerolmonoolein
GROMACS	Groningen Machine for Chemical Simulations
GROMOS	Groningen Molecular Simulations
LINCS	Linear Constraint Solver
LJ	Lennard-Jones
MAS	Magic Angle Spinning
MC	Monte Carlo
MD	Molecular Dynamics

MSD	Mean Square Displacement
NMR	Nuclear Magnetic Resonance
OPLS	Optimized Potentials for Liquid Simulations
PBC	Periodic Boundary Conditions
PC	Phosphatidylcholine
PE	Phosphatidylethanolamine
PME	Particle-Mesh Ewald
POPC	Palmitoyl-oleoylphosphatidylcholine
QSAR	Quantitative Structure-Activity Relationships
SPC	Simple Point Charge

Appendix B

Methodological issues in lipid bilayer simulations

The results described in this appendix have already been reported in [219].

B.1 Introduction

On the one hand, MD simulations are primarily limited by the system size, the accessible time scale, and the accuracy of the force field that describes the interactions in the system. Currently, simulations typically involve a few hundreds of lipids and are confined to a few nanoseconds [101, 220–222]. Recently, Lindahl and Edholm reported the first 100 ns simulation of a bilayer consisting of 64 DPPC molecules, and a larger system containing 1024 lipids, with a linear size of 20 nm, was simulated for 10 ns [156, 223]. Marrink and Mark carried out a series of glycerolmonoolein (GMO) bilayer simulations, reaching system sizes up to 20 nm and time scales up to 40 ns [103]. This order of time scale is required to adequately follow lateral diffusion of individual lipids, whereas simulation of large patches allows one to discern collective phenomena like undulation motions. On the other hand, methodological issues in MD simulations, such as the treatment of the long-range electrostatic interactions, the type of pressure coupling, or the size of the integration time step, have important consequences for the equilibrium properties observed.

Truncation of the long-range electrostatic interactions is a common practice in biomolecular simulations to speed up the calculations. These so-called cutoff methods are also widely used in membrane simulations, including some of the studies mentioned above. The abrupt

truncation of the electrostatic forces can, however, have a significant influence on the system properties. To avoid the drastic effects of straight cutoffs, some kind of smoothing schemes (like “shift” or “switch” functions) can be applied, either within the whole cutoff range or over a limited region. Two widespread alternative methods that include the effect of long-range electrostatic interactions are Particle-Mesh Ewald (PME) [112, 113] and moving boundary reaction field (RF) [114]. In PME, the central simulation cell is replicated by the periodic boundary conditions and all the electrostatic interactions in this periodically replicated system are summed. PME is a well-established method for a rigorous treatment of long-range electrostatics in periodic systems [224, 225]. In the RF approach, the electrostatic interactions are corrected for the effect of the polarizable surroundings beyond the cutoff radius.

A number of studies compare the methods of treating long-range electrostatics. In bulk water, for instance, several studies show an artificial ordering of water when using a Coulomb cutoff method, resulting in a higher viscosity [225–228]. The artifacts induced by the Coulomb cutoff are particularly clear in the analysis of the water dipole correlations: the water dipoles are anti-correlated slightly below the cutoff and correlated slightly above the cutoff. A significant decrease of the long-range dipole correlation is observed with the RF approach and especially with PME. However, short- and intermediate-range correlation is still stronger with RF than with PME. The use of electrostatic cutoffs has similar effects on the water structure in interfacial systems, including the water/lipid interface [226, 229]. Furthermore, cutoff induced ordering strongly affects the structure of ionic solutions [114, 230].

The Ewald technique may induce artificial effects due to the infinite periodicity implied by this technique. Ewald-enhanced stability of peptides, for instance, has been observed in a number of simulations [231–233]. Periodicity artifacts were found to be particularly important in systems involving a solvent of low dielectric permittivity, a small size of the unit cell, or a solute with a net charge or a large dipole. Venable and co-workers carried out a series of MD simulations of a DPPC bilayer in the gel state, applying the Ewald summation and spherical cutoff methods [234]. Better agreement with experiment was found for the lamellar spacing and the chain tilt in simulations using the Ewald summation, while the molecular area was better reproduced by spherical cutoff methods. Simulation times were between 0.2 and 2.5 ns, which might not be sufficient to be conclusive about these methods. Instead of 3D Ewald summation methods one can also use 2D versions which contain correction terms for slab geometries [235, 236]. These methods are shown to be faster and more accurate than previous versions of 2D Ewald, yet not as fast as 3D methods. A pseudo 2D system can

be generated by including a large vacuum layer separating the slab from its periodic image. Recent simulations of a water channel inside a lipid bilayer show that the ordering of water inside the channel is strongly enhanced when using 3D Ewald compared to the pseudo 2D method [237]. Erroneous results using 3D Ewald for interfacial systems were also reported by Yeh and Berkowitz [235]. Tieleman *et al.* simulated alamethicin channels embedded in a lipid bilayer, comparing the effects of twin-range cutoff, PME, and RF methods on the water orientation inside the channels [238]. The ordering degree of water within the pore was found to be significantly lower in PME and RF simulations than in cutoff ones. The water orientation was, however, better reproduced with PME than with the RF approach, making Ewald treatment the method of choice for this system and thus suggesting that the periodicity artifacts are minor.

A priori, none of the electrostatic methods mentioned above seem to be very well suited for membrane simulations. The cutoff method induces artificial ordering, the PME method enhances periodicity, and the RF method ignores the heterogeneous nature of the membrane.

The effect of the way of handling the long-range electrostatic interactions on membrane properties has never been systematically investigated in long-time simulations. In this appendix, an extensive series of simulations of a DPPC bilayer, in the biologically relevant liquid crystalline state, is reported, in which the methodology of simulation is systematically varied. Four methods for the treatment of electrostatics are compared: a standard group-based truncation method, the PME summation method, the RF method, and the use of shift functions. The size of cutoff radii is tested in the truncation and shift function methods. Different groupings of the partial charges in the phospholipids are also experimented.

The choice of macroscopic boundary conditions [98, 99] and pressure coupling algorithms can significantly influence the system characteristics as well. Therefore, different pressure coupling types and algorithms are also tested. Finally, the effect of an increased integration time step is evaluated.

An accurate comparison of simulation procedures requires long simulation times to be able to unambiguously distinguish differences in equilibrium quantities – too short sampling times often leading to erroneous conclusions. Simulation time was thus extended up to 150 ns in some cases to cover a broad spectrum of modes of motion. Special attention was devoted to the response of the membrane area to the simulation conditions. This structural quantity not only describes the molecular packing of the bilayer but also provides informa-

tion on the degree of membrane fluidity. The area per lipid is very sensitive to simulation details and generally considered a reliable criterion to compare and validate calculations.

B.2 Method of simulation

B.2.1 Simulated systems

The membrane system is the same as that described in Chapter 4 and consists of 128 DPPC molecules surrounded by 3726 water molecules, corresponding to 29 waters per lipid and to a fully hydrated state of the bilayer. Two additional simulations (H and I) are carried out at a lower degree of hydration at a water to lipid ratio of 6, reducing the total number of water molecules to 776.

B.2.2 Force field

Force field parameters and partial atomic charges used for DPPC have already been described in Chapter 4, Section 4.2.4, page 84. A different set of bonded parameters, based on the standard GROMOS-87 force field [88], is experimented in two simulations (C and F). In simulation B2b, a long-range dispersion correction is applied.

B.2.3 Electrostatics

The sensitivity of results to the treatment of electrostatics treatments is investigated, using different methods for computing long-range interactions.

A twin-range cutoff scheme is employed in simulations A, B1-3, and C1,2. Short-range electrostatic interactions are calculated every time step within a sphere of 1 nm radius, whereas long-range electrostatic interactions are calculated within the long-range cutoff sphere only every 20 fs and then kept constant until the next update. The standard long-range electrostatic cutoff, R_C , is 1.8 nm (A, B1, and C1,2). Two additional values for R_C are tested – a smaller one of 1.4 nm (B2a) and a larger one of 2.4 nm (B3) – to observe any influence on the membrane behavior. The spherical truncation technique selected here is based on charge groups (see Chapter 3, Section 3.2.2.6, page 70). Ideally, charge groups should be both small and electrically neutral. In the case of the DPPC headgroup this is not possible. To test the influence of the definition of the charge groups, two different charge group distributions are

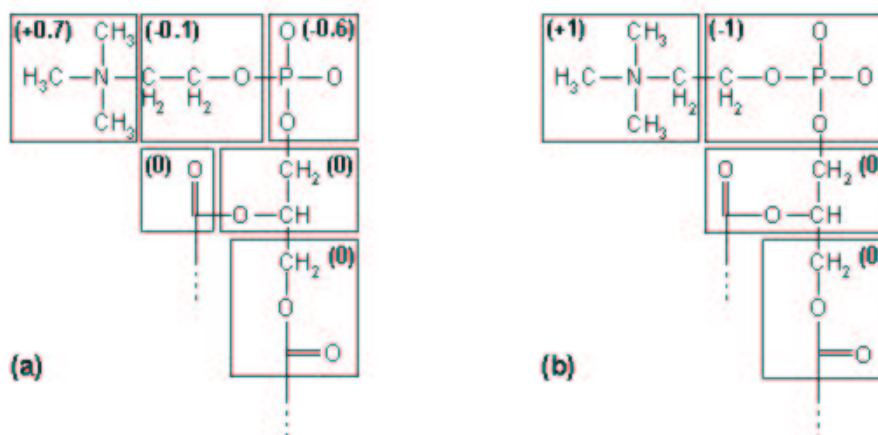


Figure B.1: Charge group definition in the DPPC headgroup part, with net charge per group indicated in parentheses. (a): Six charge groups. (b): Four charge groups.

experimented. One consists of six small groups possessing net charges as small as possible (see Figure B.1 (a)), whereas the other defines four big groups with integer charges (see Figure B.1 (b)). The latter is tested in simulations A and F, all other simulations use the distribution with six small groups.

The PME method is tested in simulations D, E1-3, F, and I. A cutoff of 1 nm is applied in the direct space sum for short-range interactions. For the calculation of long-range interactions in the reciprocal space, the charges are projected onto a grid using cardinal B-spline interpolation. This grid is then Fourier transformed with a 3D-FFT algorithm, using a maximum spacing of 1.2 Å for the FFT grid.

Moving boundary reaction field conditions are tested in simulation G. A relative dielectric constant of 1 is applied within the spherical cutoff region (with $R_C = 1.8$ nm), while the region beyond the cutoff is assumed to have a dielectric constant of 80, corresponding to the experimental value for water. Tironi *et al.* [114] simulated their system consisting of sodium and chloride ions immersed in SPC water molecules with a dielectric constant of 80, while Hünenberger and van Gunsteren [227], in pure SPC water simulations, set the dielectric constant to 54, corresponding to the self-consistent value reported for SPC water. Both values were tested (simulations not shown) and no effect on the membrane properties was observed.

Finally, the effect of a shift function [239] is tested (J1,2). Coulomb interactions are modified so that both energy and force vanish at the cutoff distance R_C , using a smooth shift

function Φ from 0 nm to R_C :

$$\Phi(r) = \frac{1}{r} - \frac{5}{3R_C} + \frac{5r^3}{3R_C^4} + \frac{r^4}{R_C^5} \quad (\text{B.1})$$

R_C is varied between 1.8 nm (J1) and 2.4 nm (J2).

B.2.4 Macroscopic boundary conditions and pressure coupling

All simulations are done under constant pressure conditions, so that the size and the shape of the simulation box are free to adjust, allowing membrane area and thickness to fluctuate. This offers the possibility to compare and validate the simulations by examining their ability to reproduce the projected area per lipid, the most important structural quantity. In the simulations, the pressure is controlled either anisotropically or semi-isotropically (E3). In the former case, the three unit cell dimensions fluctuate independently from each other, while the total pressure remains constant. This corresponds to an $NP_xP_yP_zT$ ensemble. The semi-isotropic case corresponds to NP_NP_LT , with P_N and P_L the normal and lateral pressures, respectively. In both cases, the pressure components are kept at 1 bar on average. The only difference is that the simulation box fluctuates independently in the x - and y -directions in the anisotropic case, whereas the interface maintains a square in the semi-isotropic case.

A weak pressure coupling scheme [133] is adopted in most of the simulations. Because the Berendsen algorithm does not produce a perfect NPT ensemble, the Parrinello-Rahman barostat [240] is also tested in simulation E2. This algorithm better reproduces pressure fluctuations and may also affect equilibrium properties such as the membrane area.

B.2.5 Simulation conditions

Simulation conditions are the same as those described in Chapter 4, Section 4.2.7, page 91, *i.e.* PBC, $P = 1$ bar, $T = 323$ K, and a time step of 5 fs with the use of LINCS to maintain the bond lengths constant in DPPC. One system (C1) was simulated for 50 additional nanoseconds with a time step of 2 fs (simulation C2), without any change in equilibrium properties, demonstrating that a time step of 5 fs provides enough accuracy.

Table B.1 gives a summary of the calculations performed.

Table B.1: Overview of the MD simulations.

Label	Electrostatics ^a	Charge groups	Pressure coupling		n_W^b	Simulation time (ns)	Time step (fs)	Speed ^c (h/ns)
			Algorithm	Type				
A	cutoff (1.8 nm)	4	Berendsen	anisotropic	29	150	5	20
B1	cutoff (1.8 nm)	6	Berendsen	anisotropic	29	150	5	20
B2a	cutoff (1.4 nm)	6	Berendsen	anisotropic	29	150	5	15
B2b ^d	cutoff (1.4 nm)	6	Berendsen	anisotropic	29	100	5	15
B3	cutoff (2.4 nm)	6	Berendsen	anisotropic	29	150	5	35
C1 ^e	cutoff (1.8 nm)	6	Berendsen	anisotropic	29	150	5	30
C2 ^{e,g}	cutoff (1.8 nm)	6	Berendsen	anisotropic	29	50	2	20
D	PME	4	Berendsen	anisotropic	29	150	5	20
E1	PME	6	Berendsen	anisotropic	29	150	5	20
E2	PME	6	Parrinello	anisotropic	29	150	5	20
E3	PME	6	Berendsen	semiisotropic	29	150	5	20
F ^e	PME	6	Berendsen	anisotropic	29	150	5	20
G	RF (1.8 nm)	6	Berendsen	anisotropic	29	150	5	20
H	cutoff (1.8 nm)	6	Berendsen	anisotropic	6	150	5	10
I	PME	6	Berendsen	anisotropic	6	150	5	10
J1	shift (1.8 nm)	6	Berendsen	anisotropic	29	50	5	20
J2	shift (2.4 nm)	6	Berendsen	anisotropic	29	50	5	35

^aThe long-range Coulomb cutoff is given in parentheses. ^b n_W corresponds to the number of water molecules per DPPC molecule. ^cThe simulation rate is that reached with the GROMACS package, versions 2.1 and 3.0, on a dual processor Pentium PIII 1 GHz node. ^dA long-range dispersion correction is applied in simulation B2b. ^eSimulations C1,2 and F are carried out with bonded parameters based on the standard GROMOS-87 force field for DPPC. ^gSimulation C2 is a prolongation of simulation C1, with a time step of 2 instead of 5 fs.

B.3 Results

B.3.1 Equilibration and fluctuations of structural properties

Depending on the simulation, the instantaneous projected area per lipid shows rather slow convergence. Figure B.2 displays the time evolution of the area per DPPC for three selected simulations. In simulation D, the equilibration of the area requires only a couple of nanoseconds, but in simulation A the area continues to decrease until 25 ns of simulation time. Simulation E2 represents an intermediate case, where convergence is reached after 10 ns. The time needed for equilibration does not appear to depend strongly on the method used, however, but rather on the difference between the initial and final area per lipid. This is not always true – sometimes equilibration is reached after a few nanoseconds, although the difference between the initial and final area per lipid is considerable. Because of this slow relaxation, data are analyzed starting at 25 ns. In the shorter simulations B2b and J1,2, analysis is started at 10 ns. Large thermal fluctuations of the lipid area around its average value are observed after equilibrium has been reached. Table B.2 gives the average area A per DPPC obtained for each simulation, with standard error (SE) and correlation time (τ_A). An estimate of the error in the calculated area per lipid is obtained using a block average procedure. Data are divided into n blocks, over which subaverages are calculated. The block averages are considered independent of the number of blocks when the block length is much longer than the correlation time. By dividing the standard deviation of these block averages by \sqrt{n} , a standard error estimate can be calculated. The function of the standard error estimate as a function of block size is then fitted to a single exponential function. The best estimate of the standard error of the data is then given by the limit to large block size of the fitted curve. The correlation time is also obtained from this fit [225]. Correlation times from 1 to 10 ns are found. However, even slower motions exist. A DFT analysis indicates two main periods in the range of 15–20 ns and 30–40 ns. Visual inspection of Figure B.2 also shows the presence of such modes, independent of simulation conditions. Even 100 ns simulation times are not sufficient to statistically sample these modes. The volume V_L per lipid converges faster than the area per lipid, within about 5 ns, after which it fluctuates around 1.2 nm^3 with small amplitudes. The bilayer repeat spacing L_z , like the area, exhibits large fluctuations. Both fluctuations are anti-correlated since the volume remains approximately constant. Average values for the volume and the bilayer repeat spacing are also listed in Table B.2.

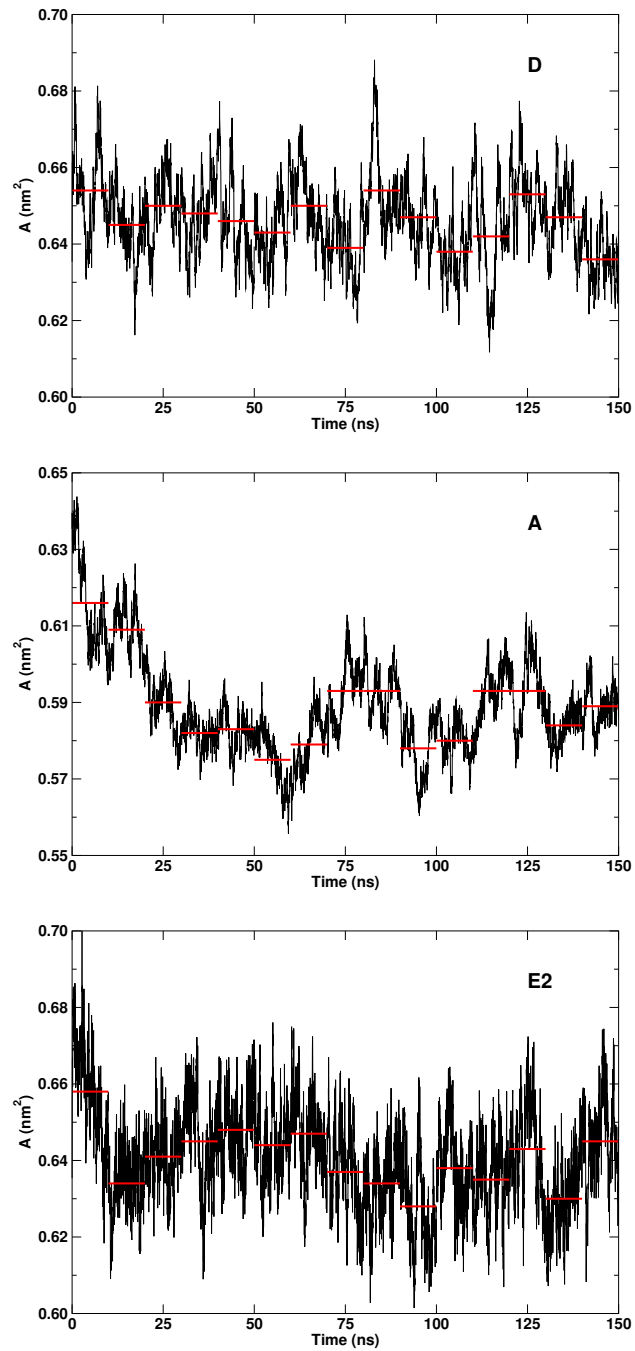


Figure B.2: Time evolution of the area per lipid in simulations D, A, and E2. The horizontal bars (in red) represent subaverages calculated over blocks of 10 ns each.

Table B.2: Equilibrium properties.

Label	$V_L \pm \text{SE}$ (nm ³)	$L_z \pm \text{SE}$ (nm)	$A \pm \text{SE}$ (nm ²)	σ_A (nm ²)	τ_A (ns)	$K_A \pm \text{SE}$ (mN/m)
A	1.2225 ± 0.0005	7.28 ± 0.03	0.585 ± 0.002	0.009	3	500 ± 100
B1	1.2204 ± 0.0005	7.14 ± 0.03	0.597 ± 0.003	0.011	5	350 ± 100
B2a	1.2225 ± 0.0006	6.87 ± 0.02	0.621 ± 0.002	0.010	2	450 ± 100
B2b	1.1717 ± 0.0004	6.79 ± 0.02	0.610 ± 0.002	0.011	1.5	350 ± 100
B3	1.2199 ± 0.0010	7.31 ± 0.06	0.583 ± 0.005	0.014	10	200 ± 50
C1	1.2254 ± 0.0004	7.15 ± 0.02	0.597 ± 0.002	0.010	2	400 ± 100
C2	1.2245 ± 0.0005	7.12 ± 0.03	0.599 ± 0.003	0.009	2.5	500 ± 100
D	1.2208 ± 0.0005	6.63 ± 0.02	0.646 ± 0.002	0.011	1	400 ± 100
E1	1.2190 ± 0.0005	6.74 ± 0.02	0.635 ± 0.002	0.010	1.5	450 ± 100
E2	1.2200 ± 0.0006	6.69 ± 0.02	0.640 ± 0.002	0.013	1.5	250 ± 50
E3	1.2200 ± 0.0005	6.71 ± 0.01	0.638 ± 0.001	0.010	1	450 ± 100
F	1.2226 ± 0.0005	6.80 ± 0.02	0.631 ± 0.002	0.010	1.5	450 ± 100
G	1.2180 ± 0.0004	6.62 ± 0.02	0.647 ± 0.002	0.011	3	400 ± 100
H	1.2200 ± 0.0006	4.85 ± 0.03	0.582 ± 0.003	0.010	7	400 ± 100
I	1.2221 ± 0.0004	4.72 ± 0.01	0.599 ± 0.001	0.007	2	850 ± 200
J1	1.2185 ± 0.0004	7.09 ± 0.01	0.600 ± 0.001	0.007	1	850 ± 200
J2	1.2235 ± 0.0004	7.08 ± 0.01	0.602 ± 0.001	0.007	1	850 ± 200
Experiments ^a	1.232	6.7	0.633 ^b / 0.64			231 ± 20

^aSee reference [42]. ^bSee reference [41].

B.3.2 Area per lipid

Of all different simulation conditions tested, the treatment of electrostatics has the largest impact on the area. Differences are especially found when applying the Particle-Mesh Ewald summation instead of a simple cutoff (runs D, E1, and F versus A, B1, and C1). Lipid areas obtained with PME are significantly higher than those obtained with abrupt truncation of the electrostatic interactions. Taking the best standard error estimates as the standard error of an infinitely large sample, a difference in reported areas of 0.006 nm^2 (or 1%) is considered significant. In a two-tailed student's t-test such a difference corresponds to a significance level of 0.05 when taking the standard errors in both area means as 0.002 nm^2 . Two additional simulations (H and I) were performed at reduced water content, corresponding to 6 water molecules per DPPC, to investigate if this increase in the area depends on the hydration level. At low hydration, the area increases by 3% from cutoff to PME, demonstrating that the response of the area to PME is not related to the amount of water, but rather governed by a different balance of forces in the lipid assembly itself. The difference between the truncation method and PME becomes larger as the cutoff radius increases. Three values of 1.4, 1.8, and 2.4 nm for the Coulomb cutoff were applied (B1-3). The smallest cutoff leads to the largest average area. The area drops by about 4% from $R_C = 1.4$ (B2a) to $R_C = 1.8$ nm (B1) and by about 2.5% from $R_C = 1.8$ (B1) to $R_C = 2.4$ nm (B3), which demonstrates the sensitivity of the area to the choice of the truncation radius. The evolution of the area per lipid is shown for the different cutoff radii in Figure B.3.

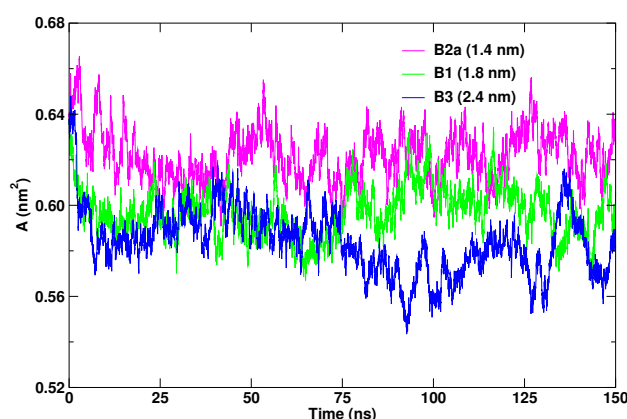


Figure B.3: Time evolution of the area per lipid in simulations using different cutoff radii.

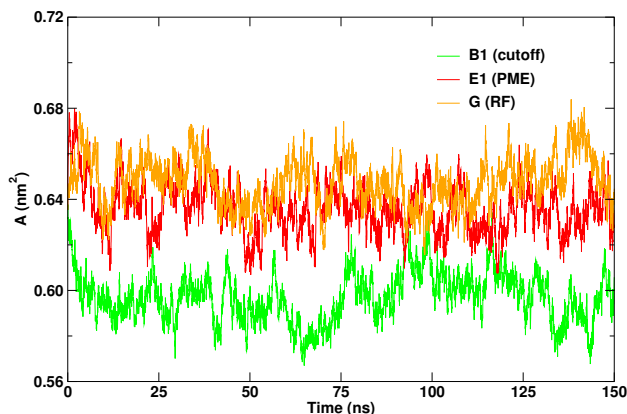


Figure B.4: Time evolution of the area per lipid in simulations with either a Coulomb cutoff, PME, or a reaction field.

Figure B.4 shows a comparison between straight cutoff (B1), PME (E1), and reaction field (G) approaches. The order of the area per lipid as a function of electrostatic treatment is straight cutoff < PME < RF. The difference in the area is less between PME and RF than between PME and cutoff. Applying the reaction field correction with the same cutoff as that in run B1 ($R_C = 1.8$ nm) leads to an increase by about 8% of the area per lipid (G vs B1). Apparently, the removal of the artificial favorable interactions just inside the cutoff sphere by the reaction field method results in a significant loosening of the system. In this context, the results of using a shift function (J1,2), which also avoids unrealistic favorable interactions just inside the cutoff sphere, but does not contain an energy term which stabilizes the dipole inside the cutoff sphere, are interesting. The use of a shift function does not have as dramatic an influence on the area per lipid as does the use of the reaction field method. The area per lipid is slightly superior to the one obtained with the middle Coulomb cutoff (B1). Increasing the cutoff radius from 1.8 nm to 2.4 nm with the shift function appears to (slightly) increase the area per lipid, an effect opposite to that observed with the straight cutoff approach.

The size of the charge groups has a significant effect on the area. The change from larger to smaller charge groups results in an increase of the area per lipid by 2% with a Coulomb cutoff (A vs B1) and in a decrease by 2% with PME (D vs E1). The effect seen with PME can be attributed to the effect of changing the effective cutoff for the Lennard-Jones interactions, since the electrostatic cutoff in PME serves only as a numerical device to separate direct and reciprocal space sums.

The introduction of a correction term into the Lennard-Jones potential to account for the long-range dispersion forces (B2b vs B2a) leads to a global compression of the bilayer system: a decrease of 2% in the area per lipid is observed and a decrease of 4% of the volume per lipid is registered.

The effect of pressure coupling on the area per lipid is deduced from a comparison of simulations E1-3. The anisotropic pressure coupling tends to generate a net deformation of the unit cell in the membrane plane. This anisotropy tends to be more pronounced in the PME than in the cutoff or RF runs. A simulation with semi-isotropic pressure coupling (E3) was added to avoid this large anisotropy in box sizes and to make sure that it does not alter structural membrane properties. Simulations E1 and E3, differing by the type of pressure coupling, lead to statistically indistinguishable average lipid areas. Furthermore, the type of barostat used (Berendsen or Parrinello-Rahman) did not affect the equilibrium properties significantly (compare runs E1 and E2).

The choice of the bonded parameters does not have any significant influence on the area per lipid. Simulations B1 and C1 on the one hand, or simulations E1 and F on the other hand, which only differ by the set of bonded parameters, lead, respectively, to the same average lipid area or to very close values.

Figure B.5 shows the time evolution of the area per lipid between 0 and 150 ns with a time step of 5 fs (C1) and between 150 and 200 ns with a time step of 2 fs (C2). The decrease in the size of the time step has no noticeable effect on the area per lipid, which proves that a relative large time step of 5 fs can be safely used.

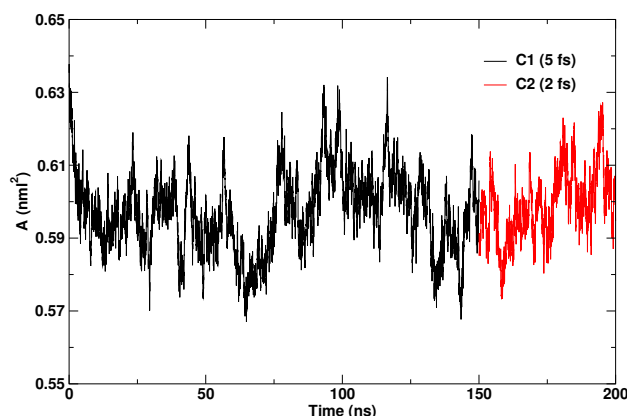


Figure B.5: Time evolution of the area per lipid in simulations C1 (with a time step of 5 fs) and C2 (with a time step of 2 fs).

B.3.3 Area compressibility

Elastic properties of lipid bilayers not only determine the response to external mechanical stress but are also important indicators of the internal state of the membrane, which can be directly associated to the dynamic molecular properties of the constituent lipids. The area compressibility modulus K_A describes an elastic property of the membrane and can be related to the variance of the lipid area σ_A^2 :

$$K_A = \frac{k_B T A}{N \sigma_A^2} \quad (\text{B.2})$$

where A denotes the average area per lipid, N the number of lipid molecules in one layer, T the temperature, and k_B the Boltzmann's constant. Area compressibility moduli have been calculated for all the simulations and are listed in Table B.2, together with the standard deviations (σ_A) in the lipid area. At full hydration of the membrane, they range between 200 and 850 mN/m and are rather above the experimental value of 231 ± 20 mN/m [42]. This is due to suppression of undulatory modes in a system of limited size [103]. There appears to be no direct relation between the average areas and the calculated compressibility moduli. A looser membrane packing, characterized by a larger area per lipid, does not systematically lead to a lower compressibility modulus, as would be expected due to the greater flexibility of membranes with a larger surface area. However, given the large standard errors, the differences observed are not highly significant. In particular, the compressibility moduli calculated for simulations E1 (450 ± 100 mN/m) and E2 (250 ± 50 mN/m) with, respectively, the Parrinello-Rahman and Berendsen barostats are not statistically different. The two-tailed student's t-test p-value for a difference of 200 mN/m is indeed 0.08.

B.3.4 Hydrocarbon chain order parameters

Deuterium order parameters of the DPPC hydrocarbon chains (see Chapter 4, Section 4.3.4.3, page 118) have been computed for all simulations. For clarity, order parameters obtained for only three selected simulations (B1, E1, and G) are displayed in Figure B.6. Order parameters are very sensitive to changes in the area: an increase in the area per lipid leads to an enhanced disordering of the acyl chains and, thus, to a decrease of the order parameters S_{CD} . From B1 to E1, the increase by about 6% in the area per lipid results in a decrease by about 14% in the order parameters. Even an increase by less than 2% in the area per lipid (e.g. from E1 to G) is perceptible in the order parameter profile.

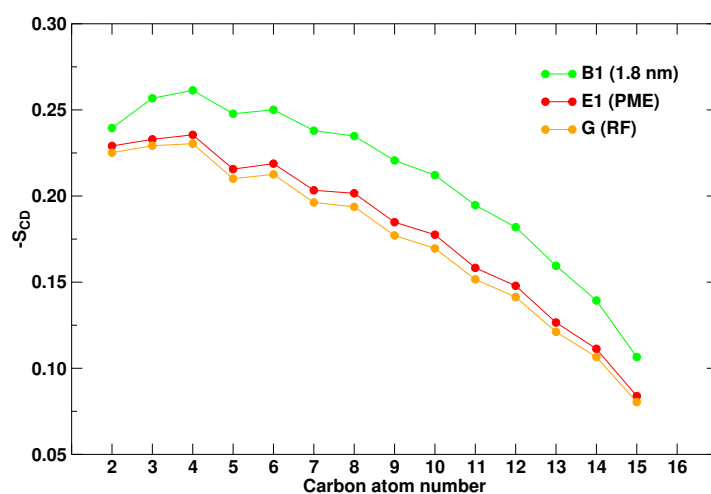


Figure B.6: Deuterium order parameters of DPPC, averaged over both chains, obtained in simulations B1 (cutoff 1.8 nm), E1 (PME), and G (RF).

B.3.5 Dipole potential and dipole moments

The dipole potential profile along the bilayer normal was estimated for the different simulations by integrating the charge distribution twice using Poisson's equation (see Equation 4.15 in Chapter 4, Section 4.3.6, page 124). A positive potential of several hundred millivolts with respect to the water region is found in the bilayer interior. A potential difference of 620 ± 20 mV is generated with PME (average value over runs D, E1-3, and F), 740 ± 100 mV with a cutoff of 1.8 nm (average value over runs A, B1, and C1), and 830 ± 50 mV with RF (run G). The potential curves obtained for simulations B1, E1, and G are plotted in Figure B.7. The most striking difference between the three types of simulation is the shape of the potential in the aqueous phase. The potential is flat with PME and RF, whereas a potential drop within the water layer can be observed when a cutoff is applied. This can be explained by a significant long-range ordering of the water dipoles, a known artifact of truncation methods. Despite the long simulation time, the potential in the two halves of the bilayer is not completely symmetrical. This asymmetry is particularly pronounced in simulations using a cutoff, which might be another artifact of this technique.

The average overall dipole moments in the lateral (x, y) and perpendicular (z) directions in the box and their fluctuations are shown in Figure B.8 for straight cutoff (1.4 nm) (B2a), RF (G), and PME (E1). As the area per lipid in these three runs is comparable, the differences in dipole moments should be indicative of the effects of the electrostatics methods. The most

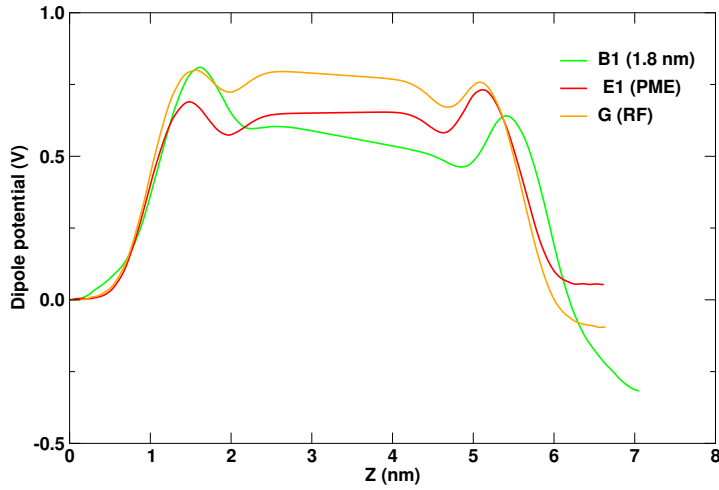


Figure B.7: Dipole potential across the DPPC bilayer in simulations using either a Coulomb cutoff of 1.8 nm (B1), PME (E1), or RF (G). The position $z = 0$ nm corresponds to the middle of the water layer and is taken as the zero of the potential.

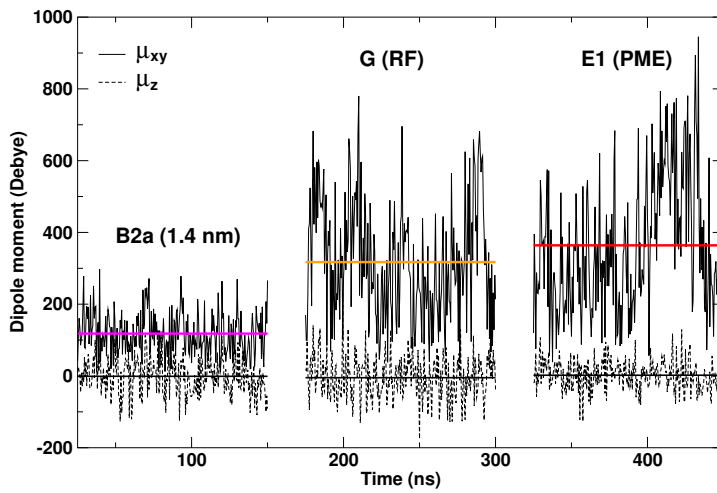


Figure B.8: Lateral (solid line curves) and perpendicular (dashed line curves) box dipole moments as a function of time in simulations using either a Coulomb cutoff of 1.4 nm (B2a), RF (G), or PME (E1). Averages are indicated by the horizontal lines. The lateral dipole moment μ_{xy} was calculated as $\sqrt{\mu_x^2 + \mu_y^2}$, μ_x and μ_y being the dipole moment components in the x - and y -directions, respectively.

striking feature observed in Figure B.8 is the difference in lateral dipole moment between straight cutoff and RF or PME. Both the average lateral dipole moment and its fluctuations are much smaller in the straight cutoff method. The difference between RF and PME is not very large. The average values of and fluctuations in the dipole moments appear to be somewhat larger in the PME approach.

B.3.6 Radial distribution functions

The radial distribution functions (RDFs) of the phosphorus atom pairs (g_{P-P}), the nitrogen atom pairs (g_{N-N}), and the phosphorus-nitrogen atom pairs (g_{N-P} , intermolecular) have been determined. The RDFs of P–P pairs are compared in Figure B.9 for a series of simulations. The application of PME and RF (E1 and G) yields a RDF which has a narrow peak around 0.6 nm and essentially no structure beyond 1 nm. Such a behavior is expected in a membrane in the liquid crystalline state, since no translational order should be present in the bilayer plane at long distances. The RDFs from simulations using a straight cutoff are dramatically different. An oscillating long-range component is observed and exhibits a local maximum exactly at the cutoff distance. Moreover, the oscillations seem to persist at distances beyond R_C . The use of a shift function with the same value for R_C allows one to avoid this structural artifact. Although the details are slightly different for N–N and N–P pairs (RDFs not shown), similar conclusions on artificial ordering can be drawn. Hence, truncation of the electrostatic interactions by a straight cutoff gives rise to artificial order in the membrane plane, which implies that the membrane is no longer in a truly fluid-like state.

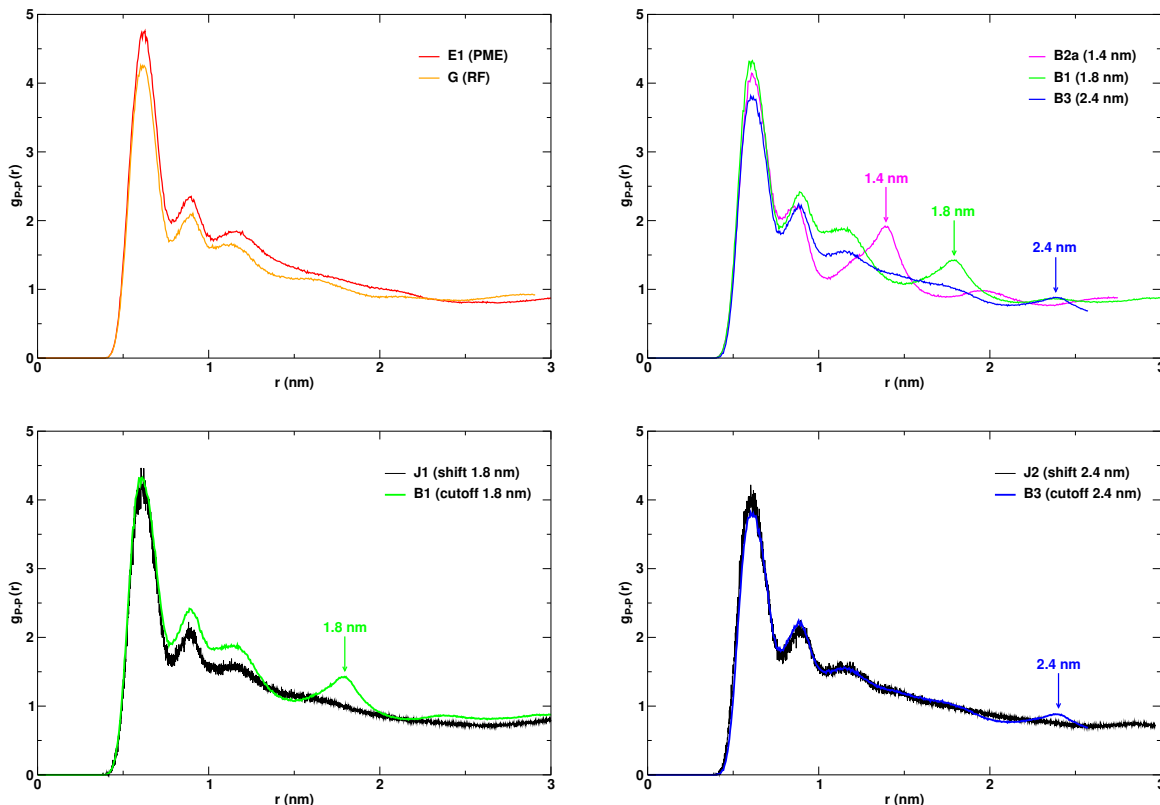


Figure B.9: Radial distribution functions of phosphorus atom pairs computed in simulations: E1 and G (PME and RF); B2a, B1, and B3 (cutoffs of 1.4, 1.8, and 2.4 nm); J1 and B1 (shift function and straight cutoff with $R_C = 1.8$ nm); J2 and B3 (shift function and straight cutoff with $R_C = 2.4$ nm).

B.3.7 Diffusion coefficients

To determine whether the dynamic properties of the bilayer are sensitive to the different simulation conditions, the lateral diffusion coefficient D_{lat} of the DPPC molecules within the membrane plane has been determined for various simulations (see Chapter 4, Section 4.3.7, page 126, for the details of the calculations). The uncorrected and corrected lateral diffusion coefficients were calculated over 62.5 ns, using data between 25 and 150 ns, and are given in Table B.3. A correlation between the area per lipid and the lateral diffusion coefficient is intuitively expected, as larger areas would lead to an increased mobility of the lipid molecules and thus to higher diffusion coefficients. Although the diffusion coefficients obtained with PME or RF tend to be slightly above those obtained with a Coulomb cutoff

(D vs A, E1 vs B1, F vs B1, or G vs B1), the differences observed are rather small and statistically not significant.

Table B.3: Lateral diffusion coefficients.

Label	$D_{lat} \pm SE$ (10^{-8} cm ² /s)	
	uncorrected	corrected
A	350 ± 150	3.4 ± 0.4
B1	150 ± 50	8.4 ± 1.3
C1	70 ± 15	9.9 ± 0.6
D	30 ± 3	12.0 ± 0.4
E1	40 ± 15	8.8 ± 0.5
E2	35 ± 5	8.2 ± 0.6
E3	15 ± 5	6.7 ± 0.7
F	25 ± 5	14.2 ± 1.8
G	150 ± 50	9.9 ± 0.7

B.4 Discussion

A number of important conclusions can be drawn based on the simulations reported in this appendix. Although the simulations only consider one type of lipid and one force field with two similar sets of bonded parameters, the effects observed are expected to be more generally valid.

Equilibration times of the order of 10–20 ns are required for phospholipid simulations

Clearly, long simulations are required to accurately calculate basic equilibrium properties such as the area per lipid. In the present simulations of the DPPC bilayer, the equilibration of the area per lipid requires on average 5 to 10 ns and even up to 25 ns in some cases. The slow convergence observed demonstrates that the generation of sufficient equilibrium sampling cannot definitely be obtained in simulations covering only a couple of nanoseconds. As was previously found by Lindahl and Edholm [223] and Marrink and Mark [103], large fluctuations of the membrane area with long correlation times (up to 10 ns) occur. These large area fluctuations can be attributed to the contribution from a hierarchy of motions, including isomerization, rotation, and diffusion of individual lipids, as well as collective motions of the bilayer itself, like the appearance of undulations. Owing to this slow process of area

fluctuations, simulations of multiple tens of nanoseconds are needed to trust the calculated average areas.

Area: poor judge of methodology or force field Reproducing experimental values for the lipid area with care is particularly important because a large number of both structural and dynamic quantities is strongly connected to the area. Naturally, larger areas allow more disorder in the lipid tails, leading to enhanced gauche population and decreased order parameters. The only exception seems to be the area compressibility, for which a clear correlation with the area was not observed.

Comparing the areas per lipid obtained for the DPPC system using different methodological approaches (see Table B.2), it appears that almost any area per lipid can be reproduced. Areas as small as 0.58 nm^2 or as large as 0.65 nm^2 can be obtained with the same force field. In contrast to the area, the volume per lipid does not appear very sensitive to methodological changes. For the area, the exact balance of forces between the headgroups and between the tails is crucial. The important question now is: is it possible, based on the areas obtained, to judge the quality of the different algorithms and parameters? Clearly, the simulations corresponding to the extreme values for the area are wrong in the sense that they do not properly model a DPPC membrane, but DPPC bilayers with an area per lipid in the range $0.62\text{--}0.65 \text{ nm}^2$, within a few percents of the experimental value of $0.63\text{--}0.64 \text{ nm}^2$, are very similar in their properties. Interestingly, areas per lipid in this range can be obtained using significantly different methods. Whether using cutoffs, reaction field, or PME, a reasonable area can be obtained. Therefore, the area per lipid is not a good judge of the quality of force field nor of methodology – the right combination of force field and methodology can always reproduce the proper area. As stated above, once the area is correct most other properties appear reasonable, and this is why the large number of DPPC simulations available in the literature, using very different force fields and simulation methodologies, results in bilayers with very similar properties.

Effect of long-range interactions In the series of simulations performed, the area proved to be very sensitive to the details of the simulation and especially to the treatment of long-range electrostatic interactions. The effects observed can be explained by examining the properties of the electrostatics methods in conjunction with a simple model of a phospholipid bilayer. In a simple picture, the phospholipid bilayer system may be viewed as two constrained dipole layers, with the zwitterionic headgroups as the basic dipoles constituting

the layers. The lipid dipoles in a layer will generally be aligned roughly parallel to each other and the bilayer normal because of the shape of the lipid molecule and headgroup hydration, thereby having a direct repulsive Coulomb interaction with each other. The dipole-dipole repulsion can be relieved by the tilting of the dipoles with respect to each other. Dipoles ideally adopt head-tail arrangements or align anti-parallel to each other. In a bilayer, tilting of the lipid headgroups towards parallel to the membrane plane is possible to a limited extent. Once tilted into the lateral directions, the headgroups have more freedom to adopt favorable orientations. The energetic costs for this tilting are various. First, tilting the headgroup requires a larger projected area of the lipid. The cost for this is loss of attractive interactions in the tail region. Second, tilting the headgroup at the same area per lipid will reduce the hydration of the headgroup since a tilted headgroup is less exposed to water. This can be remedied by pulling the lipid out of the bilayer somewhat, which will again be at the cost of attractive interactions in the tail region. Third, condensing the headgroups into the plane of the membrane results in a loss of entropy.

In straight cutoff techniques, only short-range interactions are minimized. Tilting of the headgroup is seen to a limited extent, reflected in a relatively small lateral dipole moment of the simulation box (see Figure B.8). In contrast, both PME and RF show a large lateral box dipole moment due to strong tilting of the headgroup dipoles into the lateral directions. Tilting of headgroups into the bilayer plane is the cheapest way of building up dipole moments and is rewarded energetically in both Ewald and RF methods. Ewald methods may thus induce artifacts by building up large simulation cell dipoles which are being replicated into infinity and interact favorably with each other. The reaction field model stabilizes local dipole moments. This results in a lateral expansion of the bilayers compared to straight cutoff methods (compare B1 to G). The difference between RF and PME for the area per lipid depends on the balance of forces within the bilayer. The RF approach seems to converge to the PME result if the cutoff radius is increased [219], which is expected since the “local” dipole moment within the cutoff sphere approaches the box dipole moment with increasing cutoff. Unfortunately, with large cutoffs the RF method becomes impracticable because of loss of computational speed.

Another possible artifact for bilayer systems in Ewald methods is the arrangement of dipoles parallel to an axis at half the axis-size. In this particular arrangement, the forces between parallel dipoles are zero, introducing strong spatial correlation into the system [227]. The tendency of the unit cell to become rather asymmetric (runs D, E1,2 and F) may find its origin in the fact that two charges do not exert a force on each other at a distance $L/2$,

where L is the dimension of the unit cell. For bilayer systems of not too small size, Ewald techniques appear, however, to be more appropriate than straight cutoff methods to simulate fluid phase bilayers.

The effects on the area of the bilayer observed with increased cutoff distance with the straight cutoff technique is reminiscent of the contraction of dipolar systems on increasing the electrostatic cutoff described for pure liquids [225, 230]. The contraction is explained by the build-up of favorable interactions just inside the cutoff sphere, reducing the outward pressure of the system. The non-neutrality of the charge groups gives rise to the creation of artificial charges which causes an even stronger lateral long-range attraction in the bilayer, analogous to the effects observed in ionic systems [114, 230]. Increasing the cutoff only makes things worse (compare runs B1-3). The effect increases with increasing cutoff distance because the number of these favorable interactions grows faster (scaling with r^2) than the strength of the interaction diminishes (which goes as $1/r$ due to the non-neutral charge groups).

As an alternative method, one could use a shift function, with or without a reaction field correction to the energy. It avoids the artifacts arising from cutting through dipoles as in straight cutoff methods and it also avoids dipole correlations across the simulation cell possible with Ewald methods. The RF method was already discussed. The GROMACS shift function appears to be intermediate between straight cutoff and RF. On the one hand, it does not suffer from the dipole-dipole correlation artifact associated with straight cutoff and, on the other hand, it avoids a large lateral dipole moment as seen with RF.

Apart from the long-range electrostatic interactions, also the long-range dispersion interactions can have a significant effect on the membrane properties through modulation of the system density. Including a long-range dispersion correction for the Lennard-Jones interactions (run B2b) shows a slight but significant decrease of the area and a net decrease of the volume per lipid, resulting in a clear contraction of the membrane. The LJ interactions also account for small but significant changes in area observed upon increasing the number of charge groups with PME, as can be seen from the comparison of runs D and E1.

Effect of pressure coupling and time step The type of pressure coupling scheme appears to have no significant effect on the equilibrium properties of the bilayer (compare E1 vs E2). Although the Parrinello-Rahman method is to be preferred on theoretical grounds (in contrast to the Berendsen method, it generates a well defined ensemble), the Berendsen scheme is

more practical as it damps large oscillations in box dimensions which may occur especially during the equilibration stage. Caution is needed when coupling anisotropically. If one of the lateral dimensions becomes too small, periodic ordering effects appear, especially when using PME. For systems of not too small size, the anisotropy is not worrying, as it does not seem to influence any of the system properties. Finally, the current constraining algorithms allow a time step of 5 fs, which can be safely used in phosphatidylcholine bilayer simulations (compare C1 vs C2).

B.5 Conclusion

The series of simulations presented in this appendix show that 10 to 20 ns equilibration time is required for MD studies of phospholipid bilayers. The area per lipid is observed to be very sensitive to the simulation conditions, especially to the treatment of long-range electrostatics. As long as the area remains within the experimental range, reasonable lipid properties are observed. With the right combination of methodology and force field, lipid bilayers with areas close to the experimentally determined one can be obtained with any approach of treating the long-range electrostatics. Benefits and artifacts of each method can be pointed out, demonstrating that none of these methods is perfect for the simulation of interfacial systems. Straight cutoff methods, however, most clearly show some unwanted ordering effects and should be avoided in pure bilayer simulations. In the present simulations of the DPPC bilayer system, PME and RF approaches seem to be the most reasonable options, leading to stable runs and alleviating severe artifacts. It is further shown that time steps in combination with proper constraining algorithms and a united-atom model can be taken up to 5 fs. Details of the pressure scaling method appear unimportant for the observed bilayer properties.

Lebenslauf

Name Céline Anézo
geboren am 24. März 1975
in Guérande (Frankreich)

Schulbildung

1981–1986 Ecole primaire Alain Boutlé, Batz-sur-Mer
1986–1990 Collège Jules Verne, Le Pouliguen
1990–1993 Lycée Grand air, La Baule
Juni 1993 Baccalauréat C (Mathematik, Physik und Chemie)

Studium

1993–1995 Naturwissenschaftliches Grundstudium an der
Ecole Nationale Supérieure de Chimie (ENSCR), Rennes

1995–1998 Hauptstudium an der Ecole Européenne de
Chimie, Polymères et Matériaux (ECPM), Strassburg

April–Sept. 1998 Externe Diplomarbeit in dem Arbeitskreis von Herrn Prof. Dr. Wamhoff
am Kekulé-Institut für Organische Chemie und Biochemie der
Rheinischen Friedrich-Wilhelms-Universität, Bonn

Sept. 1998 Abschluss: Diplom Ingenieur

Promotion

Februar 1999 Beginn der vorliegenden Dissertation am Institut für Pharmazeutische
Chemie der Heinrich-Heine-Universität Düsseldorf unter der Anleitung
von Herrn Prof. Dr. Höltje

Seit Februar 1999 Wissenschaftliche Mitarbeiterin am Institut für Pharmazeutische Chemie
der Heinrich-Heine-Universität Düsseldorf

Feb.–März 2001 Forschungsaufenthalt in dem Arbeitskreis von Herrn Dr. D. P. Tieleman,
Department of Biological Sciences, University of Calgary

April 2001 und
Juni–Juli 2002 Forschungsaufenthalte in dem Arbeitskreis von Herrn Prof. Dr. A. E. Mark,
Departement of Biophysical Chemistry, University of Groningen